

University of Warwick institutional repository: <http://go.warwick.ac.uk/wrap>

A Thesis Submitted for the Degree of PhD at the University of Warwick

<http://go.warwick.ac.uk/wrap/63808>

This thesis is made available online and is protected by original copyright.

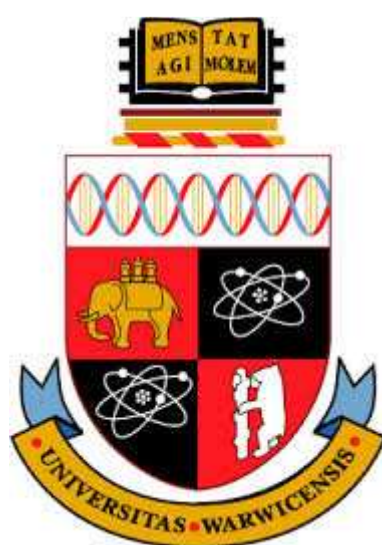
Please scroll down to view the document itself.

Please refer to the repository record for this item for information to help you to cite it. Our policy information is available from the repository home page.

Design of catalytic organometallic anti-cancer drugs

A thesis submitted for the degree of

Doctor of Philosophy



by

Joan Josep Soldevila Barreda

University of Warwick

Department of Chemistry

To my dad and my mom

To my grandparents, Pino i Pina

Contents

Acknowledgments	i
Declaration	iv
Abstract	v
Abbreviations	vi
Complexes	xii
1. Introduction	1
1.1. Metals in medicine	2
1.1.1. Platinum-based anti-cancer drugs	3
1.1.2. Ruthenium-based anti-cancer drugs	5
1.1.3. Other metal-based anti-cancer drugs	7
1.1.4. Organometallic anti-cancer complexes	9
1.1.4.1. Metallocenes	9
1.1.4.2. Half-sandwich organometallic complexes	13
1.2. Catalytic drugs	18
1.2.2. The particular case of $[(\eta^6\text{-arene})\text{Ru}(\text{en})\text{Cl}]^+$	24
1.2.3. The role of formate	24

1.3. Transfer hydrogenation reactions	25
1.3.1. Monotosylate diamine chelating ligands: Noyori-type catalysts	27
1.4. Nicotinamide adenine dinucleotide (NAD⁺/NADH)	37
1.4.1. Functions	38
1.4.2. Metabolism of nicotinamide adenine dinucleotide in cancer cells	41
1.5. Previous work on transfer hydrogenation reactions with NAD⁺	43
1.6. Aims	44
1.7. References	45
2. Materials, methods and instrumentation	61
2.1. Materials	62
2.1.1. Preparation of Cp ^X ligands	63
2.1.2. Preparations of Rh(III) dimers	64
2.1.3. Preparation of Ru(II) dimers	64
2.1.4. Preparation of the ligands	65
2.2. Methods and instrumentation	67
2.2.1. pH measurements	67
2.2.2. Nuclear magnetic resonance spectroscopy (NMR)	68
2.2.2.1. pKa determination	68

2.2.2.2. Kinetics of reactions	69
2.2.3. Elemental analysis	73
2.2.4. Electrospray ionization mass spectrometry (ESI-MS)	73
2.2.5. High resolution mass spectrometry (HR-MS)	73
2.2.6. Electronic absorption spectroscopy (UV-Vis)	74
2.2.6.1. Thermal denaturalization of DNA	74
2.2.7. X-ray crystallography	74
2.2.8. Circular dichroism (CD)	75
2.2.9. Flow linear dichroism (LD)	75
2.2.10. High performance liquid chromatography (HPLC)	76
2.2.11. Liquid chromatography – mass spectrometry (LC-MS)	76
2.2.12. Liquid chromatography – MAXIS (LC-HRMS)	77
2.2.13. Inductively coupled plasma mass spectrometry (ICP-MS)	77
2.2.14. Computational details	78
2.2.15. Biological studies	78
2.2.15.1. Cell maintenance	78
2.2.15.2. In vitro growth inhibition assay	79
2.2.15.3. Cell viability modulation experiments	80
2.3. References	81

3. Ruthenium(II) arene complexes for the catalytic reduction of NAD⁺	83
3.1. Introduction	84
3.2. Experimental	89
3.2.1. Materials	89
3.2.2. Synthesis and characterisation of the complexes	89
3.2.3. X-ray crystallography	96
3.2.4. Aqueous solution chemistry	97
3.2.5. Reduction of NAD ⁺ by $[(\eta^6\text{-arene})\text{Ru}(\text{XEn})\text{Cl}]$ and sodium formate	98
3.2.6. Mechanistic studies	98
3.3. Results	100
3.3.1. Synthesis and characterization	100
3.3.2. X-ray crystal structures	102
3.3.3. Aqueous solution chemistry	110
3.3.4. Kinetics of transfer hydrogenation reactions	112
3.3.5. Mechanistic studies	117
3.4. Discussion	127
3.4.1. Structures of the complexes	127
3.4.2. Hydrolysis of the chlorido complexes and acidity of the aqua complexes	129
3.4.3. Mechanism of the catalytic reduction of NAD ⁺	130

3.4.4. Hydride adduct formation	134
3.4.5. Kinetics of transfer hydrogenation reactions	135
3.5. Conclusions	136
3.6. References	137
4. Performing transfer hydrogenation reactions in cancer cells	142
4.1. Introduction	143
4.2. Experimental	145
4.2.1. Materials	145
4.2.2. Cell maintenance	147
4.2.3. In vitro growth inhibition assay	147
4.2.4. Cell viability modulation experiments	147
4.2.5. IC ₅₀ Modulation experiments of complex 2 by co-administration with sodium formate	148
4.2.6. Metal accumulation in cancer cells	148
4.2.7. Hydrophobicity	148
4.2.8. NAD ⁺ /NADH determination	149
4.2.9. Time-dependence of the NAD ⁺ /NADH ratio	149
4.2.10. ROS Determination	150
4.3. Results	151

4.3.1. In vitro growth inhibition	151
4.3.2. In vitro experiments with co-administration of a hydride source	153
4.3.3. Modulation of NAD ⁺ /NADH in cells	158
4.3.4. ROS detection	160
4.4. Discussion	161
4.4.1. In vitro growth inhibition	161
4.4.2. In vitro experiments with co-administration of an hydride source	161
4.4.3. Modulation of NAD ⁺ /NADH in cells	166
4.4.4. ROS detection	168
4.5. Conclusions	169
4.6. References	170
5. Interactions of half sandwich Ru(II) monotosylate complexes with DNA and GSH	173
5.1. DNA	174
5.1.1. Experimental	176
5.1.1.1. Materials	176
5.1.1.2. Interaction with nucleobases	177
5.1.1.3. CT-DNA binding kinetics	178

5.1.1.4.CT-DNA melting temperature	179
5.1.1.5.Conformational changes of CT-DNA	179
5.1.2. Results	180
5.1.2.1.Interaction with nucleobases	180
5.1.2.2.Interactions with calf thymus DNA	186
5.1.3. Discussion	194
5.1.3.1.Interactions with nucleobases	195
5.1.3.2.Interaction with CT-DNA	196
5.1.4. Conclusions	200
5.2. Glutathione (GSH)	202
5.2.1. Introduction	202
5.2.2. Experimental	204
5.2.2.1.Materials	204
5.2.2.2.Interaction with GSH	204
5.2.2.3.Identification of species	205
5.2.3. Results	207
5.2.3.1.Interaction with glutathione	207
5.2.3.2.Identification of species by LC-MS	211
5.2.4. Discussion	218

5.2.5. Conclusions	222
5.3. References	223
6. Rhodium(III) half-sandwich complexes for the catalytic reduction of NAD⁺	227
6.1. Introduction	228
6.2. Experimental	231
6.2.1. Materials	231
6.2.2. Synthesis and characterisation of the complexes	231
6.2.3. Aqueous solution chemistry	233
6.2.4. Reduction of NAD ⁺ by complexes	234
6.2.5. Mechanistic studies	234
6.2.5.1. Rate-limiting step	234
6.2.5.2. Dependence on NAD ⁺ and formate concentrations	234
6.2.5.3. Transfer hydrogenation reaction with 1,4-NADH as hydride source	235
6.2.5.4. pH dependence	235
6.2.6. Antiproliferative activity of complex	235
6.3. Results	236
6.3.1. Synthesis and characterization	236

6.3.2. Aqueous solution chemistry	236
6.3.3. Kinetics of transfer hydrogenation reactions	238
6.3.4. Mechanistic studies	240
6.3.5. Cancer cell growth inhibition	244
6.4. Discussion	246
6.4.1. Structures of the complexes	246
6.4.2. Hydrolysis of chlorido complexes and acidity of the aqua complexes	248
6.4.3. Kinetics of transfer hydrogenation reactions	249
6.4.4. Mechanism of the catalytic reduction of NAD ⁺	251
6.4.5. Cancer cell growth inhibition	255
6.5. Conclusions	257
6.6. References	258
7. Conclusions and future work	262
7.1. Conclusions	263
7.1.1. Chapter 3: Ruthenium(II) arene complexes for the catalytic reduction of NAD ⁺	263
7.1.2. Chapter 4: Performing transfer hydrogenation reactions in cancer cells	264
7.1.3. Chapter 5: Interactions of half sandwich Ru(II) monotosilate complexes with DNA and GSH	265

7.1.4. Chapter 6: Rhodium(III) half-sandwich complexes for the catalytic reduction of NAD ⁺	266
7.2. Conclusions and future work	266
7.2.1. New ligand for increased solubility	266
7.2.2. Increasing the stability of the catalysts	267
7.2.3. Controlling the hydrolysis and selectivity of the complexes	268
7.2.4. Cell Studies	269
7.2.5. Reactions with GSH	269
7.2.6. Reactions between Rh(III) complexes and GSH	270
7.3. References	270
Conferences and meetings attended	273
Publications	274
Patent	274

Acknowledgments

I would like to thank my supervisor Professor Peter J. Sadler for giving me the opportunity to do a PhD, for helping me to achieve my aim with his kind advice and dedication. I'm especially grateful for all the time and patience invested in training me, it might have been hard in several occasions.

This PhD would have been a very different experience if it was not for the help of Dr Abraha Habtemariam, to whom I must thank not only for the support, advice and help during the long three years of research, but also for being a great moral support. There are many things I would like to thank him for, but even if I keep writing about it I will not have enough space. Three years have been enough time for him to become a very close friend of mine, who I will miss to chat to every day once I leave the group.

Thank also to Dr Pieter Bruijninx for his guidance during the first year.

To my friends Dr Sarah J. Farley and Dr Soledad Betanzos Lara, I thank all the support and friendship and all the late nights at work. To them more than anybody I will thank for showing me how an amazing experience is to do a PhD, for making me realize I wanted to do a PhD. And even though they left early after my arrival in 2010 they have been supporting me, and giving me advice for 3 years.

A big big thank to my cool cypriot girl (Dr Evyenia Shaili), she has been one of my main support, the person that has always been there, even when I could not talk to anybody else. I really thank her for everything; she has become one of those people that will always be in my heart.

A big thank to Homer Simpson (soon Dr Nichola Smith), another of my main supports in the group. A person who made my life easier only by being there, talking, giving advice

and making me laugh even when the moment was bad enough to cry. Probably one of the people I will miss more.

Thank to the moody man sitting next to me for the last 2 years (Dr Nicolas Barry). Thank you for all the fun (especially with the spray), all the advice and all the patient discussions. I really appreciate your friendship. I can only say one thing to you....You are a MOOK!!!!

Thank to my friends Adam (HPLC man), Khatija and Maria. Thank you for your kindness, your friendship, for the talks, the dinners and the gossiping, for all the help when I have been in crisis... (Maria, thank you, also, for all your help with the CD, LD... and honestly, for all your help with the DNA).

Thank you to P. Socorro Murdoch, even though it has been short, I had a very nice time with you with our talk in the HPLC room. But more important, thank you for all your help with the HPLC.

I also thank Dr Ana M. Pizarro and Dr Isolda Romero for all your help in biology. I'm very sorry for all the extra work I gave you both. I need to say I could not have done everything without your help.

Thanks to all the PJS group which has become kind of a little family to me.

Thanks to Dr. Ivan Prokes for all your help and patience. I know it might have been difficult to deal with me sometimes, so thank you very much. Thanks to Phil Aston, that never shouted at me even though I kept asking him, annoying him often with questions and experiments. Thanks to Dr Lijiang Song for the help with the MS equipment. Thanks to Dr Guy Clarkson for solving the X-Ray structures. Thanks to Nikola Chmel and Alison Rodger

for their help and advice. Finally, thanks to Dr Robert J. Deeth for the help with computational work.

I would also like to thank Mayte Ramos, my teacher of chemistry in “Batxillerat”. If it would have not been by her introduction to chemistry, I would probably not have realized how wonderful the chemistry world is. She has been, until now, one of the more motivating persons I met and an excellent teacher.

I would also like to thank my friends in Spain. I left in 2010 for my PhD, and I know I’m not very good at keeping in touch, but even with the distance they have always been there. I can only say that I love all of you, for not being mad at me even when I forget to call, for being always there when I need you (even when my problems are stupid, tiring and repetitive because I can’t learn from previous mistakes), for worrying about me constantly, for making me feel like Spain will always be my house even if I’m not living there. Karen, Pau, Laura, Nerea, Eva, Nereita, Ari, Marck Balanger, Abel, Anna Argenter, Ruben Betes, Montse Bayo, many many thanks to all of you.

I also would like to thank my friends Masha, David Hill, Ayan, Shomanka, Jit, Amir, Ken, Ziga (zizi), Teena and Radhika Sarin I really appreciate your friendship and support during the PhD.

I also thank my family, for their unconditional support and their big efforts to help me both, economically and emotionally. I thank my mum who has been one of my biggest emotional supports. Also my step dad for his support and advises. I especially want to thank my dad and my stepmother, I would really not have reach this point without them. And I know it has been very difficult (because I’m too stubborn), they have sacrificed a lot, but they never complained and they have always been there.

Declaration

I hereby declare that except where specific reference is made to other sources, the work contained in this thesis is the original work of the author. It has been composed by myself and has not been submitted, in the whole or in part, for any other degree, diploma or other qualification.

Some of the work presented in this thesis has been published:

1. Improved Catalytic Activity of Ruthenium–Arene Complexes in the Reduction of NAD⁺

Soldevila-Barreda, J. J.; Bruijninx, P. C. A.; Habtemariam, A.; Clarkson, G. J.; Deeth, R. J.;

Sadler, P. J. *Organometallics* **2012**, *31*, 5958-5967.

Joan Josep Soldevila Barreda

April 2014

Abstract

This thesis is concerned with the design of organometallic half sandwich complexes which can catalyse the conversion of oxidised coenzyme nicotinamide adenine dinucleotide to its reduced form. The coenzyme pair NAD^+/NADH is involved in many biological processes, such as regulation of the redox balance, and DNA repair. Disturbance of the NAD^+/NADH ratio can lead to cell death. In particular, cancer cells are under constant oxidative stress and therefore might be more susceptible to changes in the NAD^+/NADH levels.

A series of neutral Ru(II) complexes of the type $[(\eta^6\text{-arene})\text{Ru}(\text{N},\text{N}')(\text{L})]$ (arene = *p*-cymene (*p*-cym), hexamethylbenzene (hmb), biphenyl (bip), benzene (bn); *N,N'* = *N*-(2-aminoethyl)-4-(trifluoromethyl)benzenesulfonamide (TfEn), *N*-(2-aminoethyl)-toluenesulfonamide (TsEn), or *N*-(2-aminoethyl)-4-methylsulfonamide (MsEn)) were synthesized and fully characterized. The complexes were shown by $^1\text{H-NMR}$ to catalyse region-selectively the transfer hydrogenation of NAD^+ to 1,4-NADH. Comparison of the turnover frequencies (TOF) for the complexes show a trend in which a decrease in catalytic activity with the arene ligand follows the order $\text{bn} > \text{bip} > \text{p-cym} > \text{hmb}$ and $\text{TfEn} > \text{TsEn} > \text{MsEn}$. Complex $[(\eta^6\text{-bn})\text{Ru}(\text{TfEn})\text{Cl}]$ (**12**) was found to be the most active with a TOF of 10.4 h^{-1} . The catalytic cycle for the transfer hydrogenation reaction was studied for complex $[(\text{p-cym})\text{Ru}(\text{TsEn})\text{Cl}]$ (**2**).

The monotosylate ethylenediamine Ru(II) complexes were used to carry out, for the first time, transfer hydrogenation reactions *in cellulo* (A2780 ovarian cancer cells) using formate as a hydride source. The antiproliferative activity of six complexes on co-administration with non-toxic doses of sodium formate were studied. A significant potentiation of the antiproliferative activity by formate was observed. The concentrations of NAD^+ and NADH in cells showed an important reduction in the NAD^+/NADH ratio. This study demonstrates that it may be possible to use catalytic transfer hydrogenation as a strategy for multi-targeted redox mechanisms of action for anticancer drugs.

In order to compare the anticancer mechanism of the monotosylate ethylenediamine Ru(II) complexes with the corresponding ethylenediamine (en) complexes, DNA binding studies were carried out. The complexes were shown to bind to nucleobases only moderately strongly and no direct coordination to calf thymus DNA was observed. The complexes can destabilize DNA, but they display low affinity towards DNA, which suggests that DNA is probably not involved in the mechanism of these family of compounds.

Interaction of complex [(*p*-cym)Ru(TsEn)] (**2**) with glutathione (GSH) was also studied. The complex undergoes ligand substitution. Two Ru(II) dimers were formed as the main products of the reaction: $[(p\text{-cym)Ru}_2(\mu\text{-GS})_3]$ and $[(p\text{-cym)Ru}_2(\mu\text{-GS})_2]$. These dimers share structural similitudes with other reported Ru(II) arene anticancer drugs, which suggests that they could be responsible for the moderate antiproliferative activity of complex **2**.

A series of Cp^XRh(III) (Cp^X = Cp^XPhPh, Cp^XPh or Cp^{*}) complexes containing en or TfEn were synthesised and fully characterised. The complexes were shown to catalyse regioselectively the transfer hydrogenation of NAD⁺ to 1,4-NADH with higher TOF than their Ru(II) analogues. Rh(III)-en compounds were shown to be more active than the Rh(III)-TfEn analogues. The nature of the Cp^X ring was shown to influence significantly the catalytic activity of the complexes following the trend: Cp^XPhPh > Cp^XPh > Cp^{*}. Complex $[(\text{Cp}^{\text{X}}\text{PhPh})\text{Rh}(\text{en})\text{Cl}]^+$ (**19**) was the most active, with a TOF of 24.2 h⁻¹. The catalytic cycle for the transfer hydrogenation reaction was studied using complex $[(\text{Cp}^*)\text{Rh}(\text{en})\text{Cl}]^+$ (**17**) and compared to that of the Ru(II) analogues, and was found to be similar. Antiproliferative activity of the complexes in combination with formate, in A2780 cells, was investigated, but the potentiation due to the transfer hydrogenation was much lower than that obtained with Ru(II) compounds.

Abbreviations

9-EtG 9-Ethylguanine

9-MetA 9-Methyladenine

Å Angstrom

bip Biphenyl

bipy Bipyridine

bn Benzene

°C Degree celsius

ca. *Circa*

CD Circular dichroism

Cp Cyclopentadienyl

Cp* Pentamethylcyclopentadienyl

Cp^xPh 3-Phenyl-1,2,4,5-tetramethyl-1,3-cyclopentadienyl

Cp^xPhPh 3-Biphenyl-1,2,4,5-tetramethyl-1,3-cyclopentadienyl

CT Calf Timus

d Doublet

dd Doublet of doublets

ddw doubly distilled water

DFT	Density functional theory
DMSO	Dimethyl sulfoxide
DNA	Deoxyribonucleic acid
EDTA	Ethylenediaminetetraacetic acid
en	Ethylenediamine
ESI-MS	Electrospray ionisation mass spectrometry
FDA	Food and drug administration (U.S.)
GSH	Glutathione
GSSG	Glutathione disulfide
h	Hour
hmb	Hexamethylbenzene
HPLC	High performance liquid chromatography
HR-MS	High resolution mass spectrometry
IC ₅₀	50 % inhibitory concentration
ICP-MS	Inductively coupled plasma mass spectrometry
ie.	In essence
J	Coupling constant
k	Kinetic constant

K	Kelvin
K_a	Association constant
K_{cat}	Catalyst constant
KIE	Kinetic isotope effect
K_M	Michaelis-Menten constant
L-BSO	L-Buthionine sulfoximine
LC-MS	Liquid chromatography-mass spectrometry
LD	Linear dichroism
m	Multiplet
min	Minutes
MsEn	<i>N</i> -(2-Aminoethyl)methylsulfonamide
m/z	Mass-to-charge ratio
NAC	N-acetyl-L-cysteine
NAD^+	Nicotinamide adenine dinucleotide
NADH	Nicotinamide adenine dinucleotide reduced
NbEn	<i>N</i> -(2-Aminoethyl)-4-nitrobenzenesulfonamide
<i>o</i> -terp	<i>ortho</i> -terphenyl
PBS	Phosphate buffer saline

<i>p</i> -cym	<i>para</i> -cymene
PDT	Photodynamic therapy
Ph	Phenyl
phen	Phenanthroline
ppm	Parts per million
q	Quadruplet
redox	Reduction-oxidation
RNS	Reactive nitrogen species
ROS	Reactive oxygen species
s	Second
s	Singlet
sept	Septuplet
SOD	Superoxide dismutase
SRB	Sulforhodamine B
t	Time
t	triplet
T	Temperature
TFA	Trifluoroacetic acid

TfEn	N-(2-Aminoethyl)-4-(trifluoromethyl)benzenesulfonamide
TH	Transfer hydrogenation
T _m	Melting temperature
TON	Turnover number
TOF	Turnover frequency
TOF _{max}	Maximum turnover frequency
TsEn	N-(2-Aminoethyl)-4-toluensulfonamide
TsDPEN	(1S,2S)-N-(<i>p</i> -toluensulfonyl)-1,2-diphenylethylenediamine
TsCYDN	(1S,2S)-N-(<i>p</i> -toluensulfonyl)-1,2-diaminocyclohexane
V	velocity
v/v	volume for volume
δ	Chemical shift
λ	Wavelength

Complexes

[(bip)Ru(en)Cl]⁺ (RM175)

[(*p*-cym)Ru(MsEn)Cl] (1)

[(*p*-cym)Ru(TsEn)Cl] (2)

[(*p*-cym)Ru(TfEn)Cl] (3)

[(hmb)Ru(MsEn)Cl] (4)

[(hmb)Ru(TsEn)Cl] (5)

[(hmb)Ru(TfEn)Cl] (6)

[(bip)Ru(MsEn)Cl] (7)

[(bip)Ru(TsEn)Cl] (8)

[(bip)Ru(TfEn)Cl] (9)

[(bn)Ru(MsEn)Cl] (10)

[(bn)Ru(TsEn)Cl] (11)

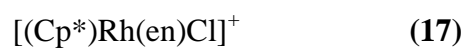
[(bn)Ru(TfEn)Cl] (12)

[(*o*-terp)Ru(MsEn)Cl] (13)

[(*o*-terp)Ru(TsEn)Cl] (14)

[(*o*-terp)Ru(TfEn)Cl] (15)

[(*p*-cym)Ru(NbEn)Cl] (16)



Chapter 1

Introduction



1. Introduction

This thesis is concerned with the design of catalytic drugs which can reduce nicotinamide adenine dinucleotide by transfer hydrogenation using Noyori-type catalysts. In this chapter, a brief introduction will be given to metals in medicine, followed by catalytic metallodrugs and transfer hydrogenation reactions, catalysis and mechanism, focusing on water-soluble Noyori-type complexes. Finally, the introduction will focus on NAD^+ and its functions, as well as the different chemical strategies to reduce NAD^+ .

1.1. Metals in medicine

It is generally accepted that many metals are toxic to humans. However, it is wise to remember the words of Paracelsus, "*Alle Ding' sind Gift, und nichts ohn' Gift; allein die Dosis macht, daß ein Ding kein Gift ist*" (All things are poison, and nothing is without poison; only the dose permits something not to be poisonous). For example, sugar, salt or water are essential nutrients, but when taken in excess either of them can result in disease as hyperactivity, hypertension or intoxication.¹ Consequently, and despite the fact that metals can be extremely toxic at high concentrations, some are essential for life. Currently 24 elements are thought to be essential for life, 14 of them being metals (Na, Mg, K, Ca, V, Mn, Fe, Co, Ni, Cu, Zn, Se, Mo and Sn).²

For many years, the use of metals in medicine has been a *taboo*. Nevertheless, we can find countless examples of metals and metal complexes that have been used in medicine since ancient times. In the 3000 BC the Egyptians used copper to sterilize water; around 1500 BC various iron remedies were used in Egypt and zinc was used to heal wounds; three thousand five hundred years ago gold was used in a variety of medicines in Arabia and during the renaissance era mercurous chloride was administered as a diuretic in Europe.² More recently,

arsenic based drugs (*salvarsan*, for syphilis treatment), gold based drugs ($K[Au(CN)_2]$ for tuberculosis treatment, and Auranofin for arthritis), and more recently, platinum drugs like cisplatin (which is now widely used in cancer treatment) were developed and commercialized.² All of these examples provide evidence of the potential of metal-based drugs in modern medicine. These examples, also demonstrate the possibility of structurally tuning the metallodrugs to modulate their properties. The structure can be altered by changing the ligands that surround the metal, or by changing the coordination number/oxidation state of the metal. In this way, we can begin to overcome the toxicity, and control the reactivity and selectivity of the metal complex towards specific targets or diseases.³

1.1.1. Platinum-based anti-cancer drugs

The history of modern metal-based chemotherapy begins in 1965 with the discovery of the antiproliferative and cytotoxic activity of cisplatin by B. Rosenberg.^{4, 5} The medical success of cisplatin opened the doors to a large research area focused on understanding its mechanism of action. It is currently accepted that cisplatin cytotoxicity is mainly, due to interactions with DNA.⁶⁻⁸

Even though cisplatin has been a clinical success, the drug has severe drawbacks.

- Severe side effects are due to high toxicity. The most common side-effects include nephrotoxicity (kidney damage), neurotoxicity (nerve damage), nausea and vomiting, ototoxicity (hearing loss), electrolyte disturbance, myelotoxicity (bone marrow suppression) and haemolytic anaemia.^{9, 10}
- Development of cisplatin-resistant by some cancer cell lines.¹¹
- Only a limited range of tumours is sensitive to cisplatin intervention.

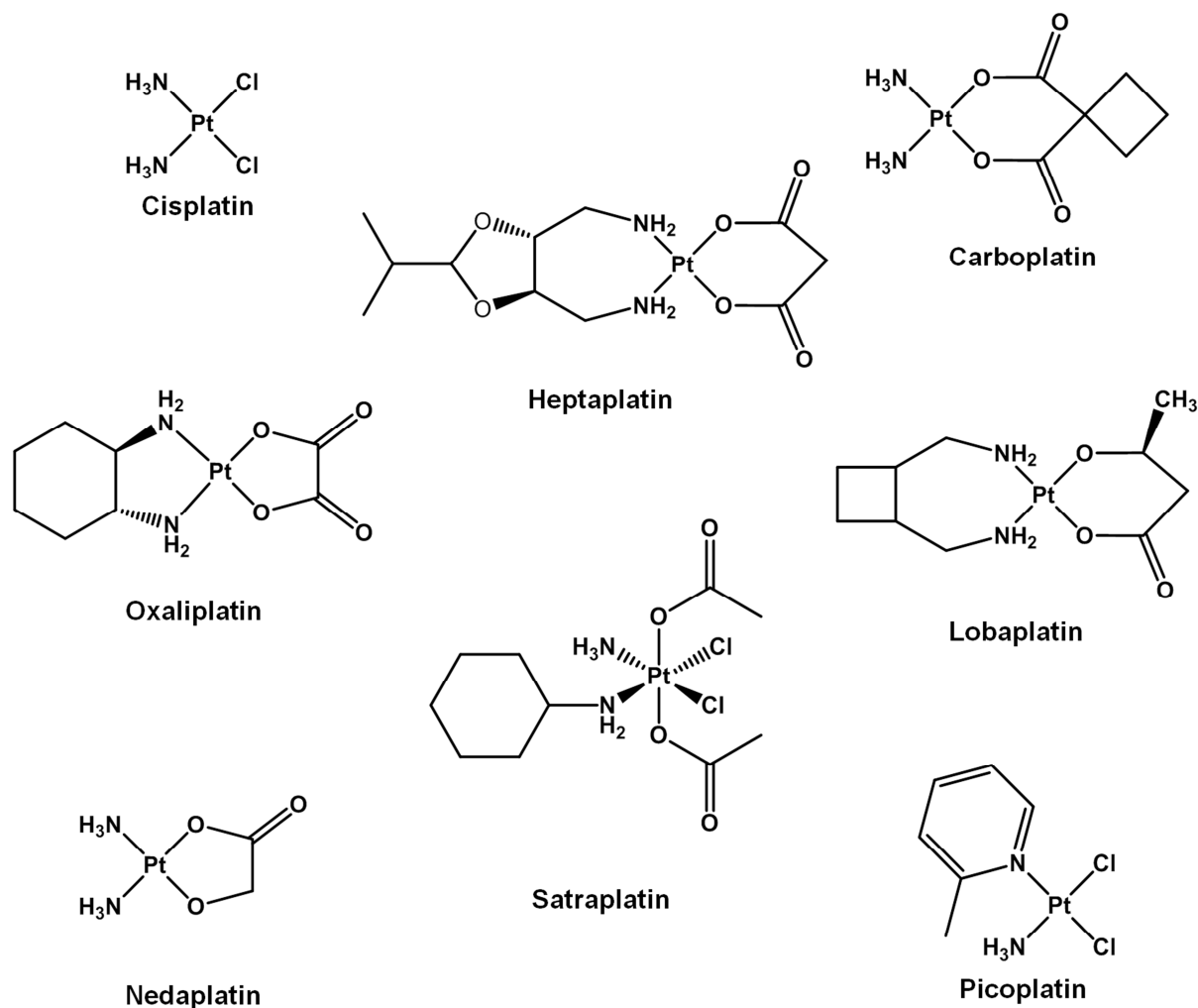


Figure 1.1. Structures of platinum anticancer drugs: cisplatin, carboplatin, oxaliplatin, nedaplatin, lobaplatin, heptaplatin, picoplatin and the Pt(IV) drug, satraplatin.

Many efforts have been focussed on the structure-activity relationships of platinum amino complexes in order to overcome toxicity and resistance. More than 3,000 platinum complexes have been studied for anticancer applications. However, only few of these have reached clinical trials, and currently only six platinum-based drugs have been approved and are in use (cisplatin, carboplatin, oxaliplatin, nedaplatin (Japan), heptaplatin (Korea) and Lobaplatin (China), (Figure 1.1)).¹²⁻¹⁴ There are currently five platinum-based drugs in various stages of clinical trials, with two being close to approval (satraplatin and picoplatin).¹²⁻¹⁴

More recently research on the platinum-based anticancer drugs has been focussed on the synthesis of platinum(IV) analogues.^{15, 16} Changing the oxidation state of the platinum centre, from +2 to +4, was a strategy developed in order to generate more stable and water-soluble complexes which could be administered orally. Furthermore, the platinum(VI) drugs are inactive, and only become active once they have been reduced to platinum(II). This reduction can either occur once the complex has been activated through an external source such as light, or by intracellular reduction pathways.¹⁷ This could be a useful strategy to reduce the toxicity and side effects associated with platinum (II) drugs.

1.1.2. Ruthenium-based anti-cancer drugs

Ruthenium complexes have been shown to be amongst the most promising metal-based compounds for use in cancer treatment, partly because of the slower ligand exchange rate compared to platinum and the wide availability of oxidation states.¹⁸ Furthermore, many ruthenium compounds have shown low toxicity, which could be due to the capability of ruthenium to mimic iron in binding biological molecules.¹⁸

In his initial reports, Rosenberg observed that disruption of DNA replication was achieved not only by cisplatin, but also by $[(\text{NH}_3)_4\text{RuCl}(\text{OH})]\text{Cl}$.⁵ In 1976, the first studies on amino-Ru(III) complexes, analogous to the successful cisplatin, were reported.¹⁹ Studies with complex $[fac\text{-}[(\text{NH}_3)_3\text{RuCl}_3]]$ in *E. coli* suggested that the cellular target of Ru(III) complexes was probably DNA. The research was, since then, focussed on the mode of action and the interactions of the amine-Ru(III) complexes with DNA. Clarke *et al.* demonstrated the ability of this type of complex to bind to nucleobases and inhibit DNA synthesis, as well as protein synthesis to a lesser extent.^{20, 21} In their work, Clarke *et al.* also reported that inert Ru(III) is reduced in cells by glutathione or other reducing agents to form more reactive Ru(II) species.²⁰⁻²⁴ The hypothesis was based on the fact that the Ru(II) π -acceptor property is lower than in

the case of Ru(III), leading to more labile bonds with π -donating ligands such as chlorides, facilitating hydrolysis.²⁰⁻²⁴

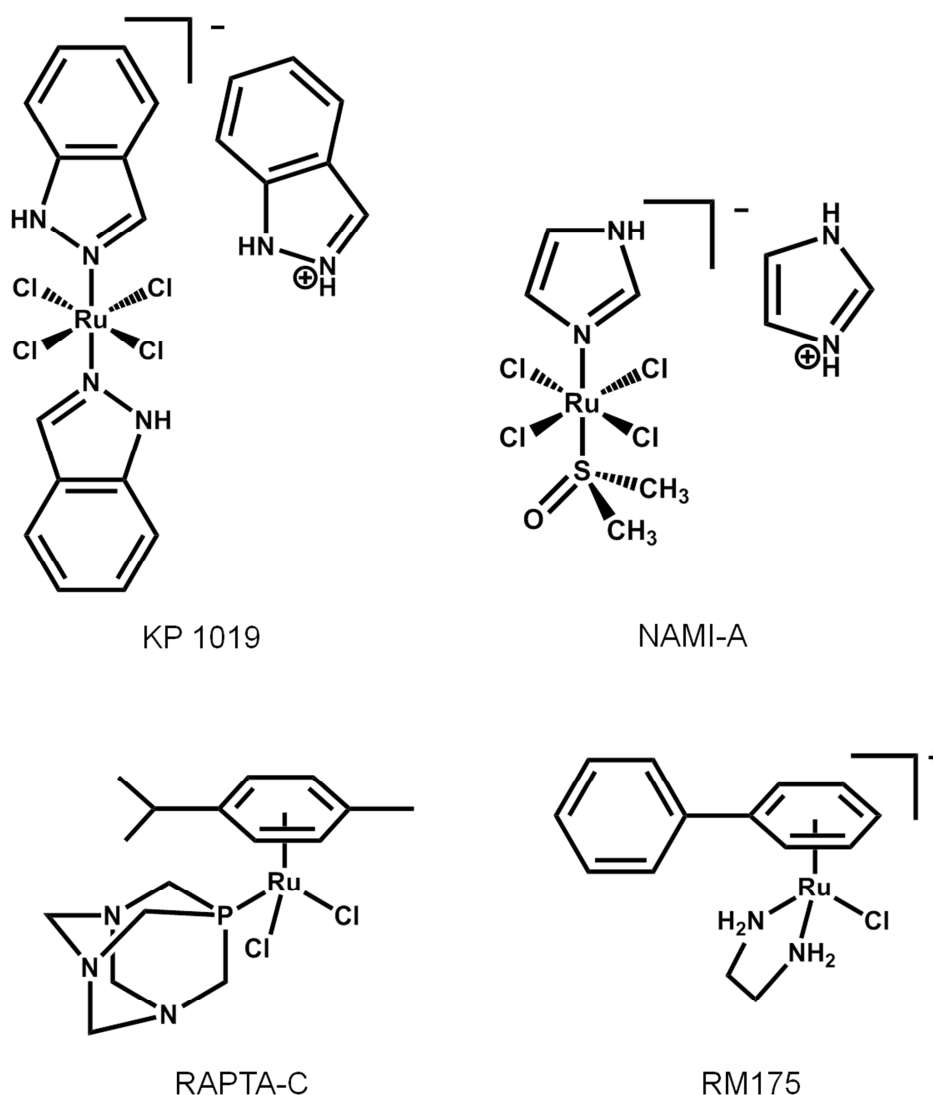


Figure 1.2. Structures of NAMI-A, KP1019, RM175 and RAPTA-C.

Currently, there are two Ru(III) coordination complexes undergoing clinical trials, NAMI-A and KP1019/NKP1339 (Figure 1.2). KP1019/NKP1339 was shown to have good activity against a wide variety of cancer cells including some platinum resistant cell lines (NCT01415297).^{25, 26} On the other hand, NAMI-A does not show high anticancer activity, but displays high selectivity for solid tumour metastatic cells and low toxicity at pharmacologically active doses.^{27, 28}

Proceeding the work of Clarke *et al*, a large number of Ru(II) complexes were developed. Initially, they were shown to have stability problems due to fast ligand substitution.²⁹ The first stable and active Ru(II) complex reported was $[\text{Ru}^{\text{II}}(\text{azpy})_2\text{Cl}_2]$, (azpy = 2-phenylazopyridine) by Reedijk *et al*.^{30,31} Unfortunately, despite the *in cellulo* activity, the complex was not tested *in vivo* due to low solubility.²⁹ Later, a series of organometallic compounds containing η^6 -arene moiety, which occupies three coordination sites, showed very promising results.³² Currently, the ruthenium(II) drugs which displayed the most promising anticancer activity are the half-sandwich organometallic complexes, in particular RM175. Another promising anticancer drug is the Ru(II) half sandwich compound RAPTA-C, which is not very active but demonstrated interesting anti-metastatic properties. (Figure 1.2).^{28,32}

1.1.3. Other metal-based anti-cancer drugs

Compounds of nearly all the metals of the periodic table have been investigated as chemotherapeutical anticancer agents, although, few of those have shown promising *in vivo* activities or entered clinical trials. Some of the most promising metals are arsenic, iron, tin, copper, gallium, titanium, gold, manganese, vanadium, bismuth and osmium.³³⁻³⁶

Table 1.1. Some metal complexes which show the most promising anticancer activity. The table does not include Ru or Pt complexes.

Metal	Drug	
Arsenic	Trisenox	Approved for acute promyelocytic leukaemia Currently in clinical trials for lung cancer and others
	Darinaparsin	Currently in clinical trials for solid tumours Approved in some countries for the treatment of T-cell lymphoma.
	GSAO	Currently in clinical trials for solid tumours
Iron	Ferrocenes and derivatives	See section 1.1.4.1.
Titanium	Budotitane	First non-platinum metal-based coordination compound entering clinical trials. Abandoned
	Titanocene dichloride	See section 1.1.4.1
Gold	Auranofin	Currently undergoing clinical trials for chronic lymphocytic leukaemia, small lymphocytic lymphoma and prolymphocytic leukaemia
Gallium	Gallium maltolate	Currently in clinical trials for liver cancer and lymphoma.
	Gallium nitrate	Currently in clinical use for the treatment of cancer-associated hypocalcaemia
	NKP-2235	Clinical trials for cancers with high incidence of bone metastases

1.1.4. Organometallic anti-cancer complexes

In general, the variety of oxidation states of metals allows the synthesis of complexes with a great diversity of structures, containing up to six different ligands (in octahedral complexes). The rational design of those ligands provides control over the reactivity and properties of the complexes. Organometallic complexes are a family of metal compounds containing at least one metal-carbon bond. Organometallic complexes in particular, can stabilize low oxidation states of the metal, and have recently shown promising results as anticancer agents.

1.1.4.1. Metallocenes

Metallocenes or sandwich complexes are organometallic complexes which contain two π -bonded cyclopentadienyl groups (Cp) bound to the metal centre. There are two main structures: a classical metallocene, where the metal atom is at the centre of two parallel Cp rings, and a bent structure where the metal centre is bound to two Cp rings and two halogens forming a tetrahedral type structure (Figure 1.3). The cytotoxicity of many metallocenes has been studied. However, the most promising results have been obtained with ferrocenes and titanocenes.

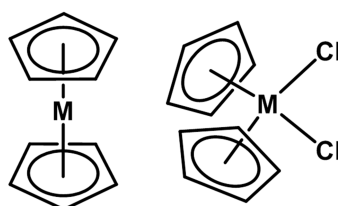


Figure 1.3. General structure of metallocenes.

Ferrocene and derivatives

Iron is an abundant metal in biology, it can be found in traces in nearly all living organisms. Due to the natural occurrence of iron in the body, the relative non-toxicity of the iron ions in high quantities and the capability of the body to metabolize it, the use of iron in medicine has been studied intensively. Furthermore, the iron transport system of the body represents an advantage for the distribution and accumulation of iron-based drugs.

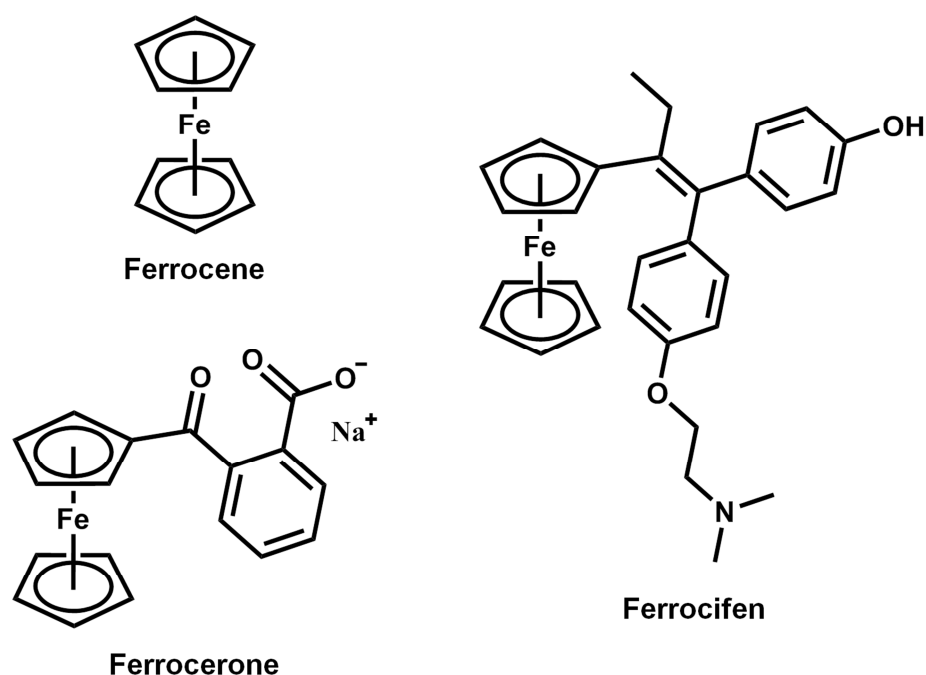


Figure 1.4. Structure of ferrocene, ferrocerone and ferrocifen.

Ferrocene (Figure 1.4) is the first organometallic compound for which antiproliferative activity was reported.³⁷ Initial reports by Köpf *et al.* confirm that anti-proliferative activity is associated with the ferrocenium salts and that neutral ferrocene is relatively non-toxic.³⁷ The mechanism of action of these compounds was also studied, showing that ferrocene derivatives can induce DNA damage, via generation of hydroxyl radicals.³⁸ However, other targets have been proposed and the mechanism of ferrocene and its derivatives is still uncertain.³⁹ Ferrocene is readily hydroxylated in the liver and excreted in the urine.⁴⁰ The newly formed hydroxyferrocene, is unstable, and easily decomposes liberating iron ions

which can be utilized by the body. On this basis, ferrocenone (Figure 1.4), a ferrocene cation, has been used for the treatment of anemia in Russia.⁴¹ Ferrocenone is the first organometallic compound commercialized for medicinal purposes. Numerous ferrocene derivatives have been tested for anti-proliferative purposes.

One of the most successful approaches for the development of anti-cancer ferrocene type drugs has been the addition of organic drugs to the Cp moiety, such as anti-cancer commercialized drugs (tamoxifen, or resveratrol), flavonoids (aurones, flavones or chalcones), hormones (testosterone), natural products (curcuma or illudins). Currently, the most promising compounds are ferrocifens.^{41, 42} Ferrocifen is a tamoxifen-containing ferrocene compound that has been synthesized for the treatment of hormone dependent breast cancer, (Figure 1.4). The complex has shown significant anti-proliferative activity towards non-hormone dependent as well as hormone dependent breast cancers.^{43, 44} These compounds are believed to have a dual mode of action, through the tamoxifen moiety binding to estrogens receptors of hormone dependent breast cancer cells, and through the formation of cytotoxic glutathione and nucleobases ferrocifen compounds.^{43, 44}

Titanocenes

In the family of bent metallocenes, the titanium(IV) compounds (titanocenes) have displayed higher cytotoxicity.⁴⁵ Titanocene dichloride (Figure 1.5) was the first titanium organometallic complex to enter clinical trials. Titanocene dichloride showed very promising results in animal testing, but the poor response displayed in humans led to the termination of the clinical trials. Furthermore, this compound also showed problems due to solubility and stability under biological conditions. Titanocenes containing different halides, with either mono- and bi-dentate ligands were also synthesized and tested for their anti-proliferative activity, leading to results similar to titanocene dichloride.⁴⁶ Lotz *et al.* published a series of

titanocenes containing one or two heteroaromatic molecules instead of chlorine (benzothiophene or dibenzothiophene, Figure 1.5).

In order to overcome the solubility issue, a series of ionic titanocenes ($[\text{Cp}_2\text{TiXL}]^+$ and $[\text{Cp}_2\text{TiL}_2]^{2+}$) containing neutral L ligands were also synthesized, however the activities were lower than those obtained for the neutral compounds.⁴⁶

Similarly in the case of ferrocenes, compounds with functionalized Cp rings have been studied, with the aim to overcome the drawbacks of $[(\text{Cp})_2\text{TiCl}_2]$. McGowan *et al.* synthesized a series of ionic titanocenes containing amino pendant arms attached to the Cp ring, which increased their solubility (Figure 1.5). These compounds showed an increased cytotoxicity compared to the neutral titanocene dichloride. Furthermore, some of the compounds synthesised were shown to be cytotoxic towards cisplatin resistant cell lines.^{47, 48}

Tacke *et al.* has also developed a versatile synthetic route to functionalized-Cp titanocenes via the fulvene route.⁴⁹ With this method, a series of *ansa*-titanocenes (titanocenes containing an interanular bridge between the Cp rings, Figure 1.5), with increased stability, have been synthesized, which have a greater cytotoxic activity when compared to titanocene dichloride. However, they are still 100 fold less active than cisplatin. Another series of titanocenes containing benzyl-substituted and heteroaryl-substituted Cp, were also synthesized (Figure 1.5) showing an important increase in the antiproliferative activity, some compounds displaying IC_{50} values in a similar range to cisplatin.⁴⁹

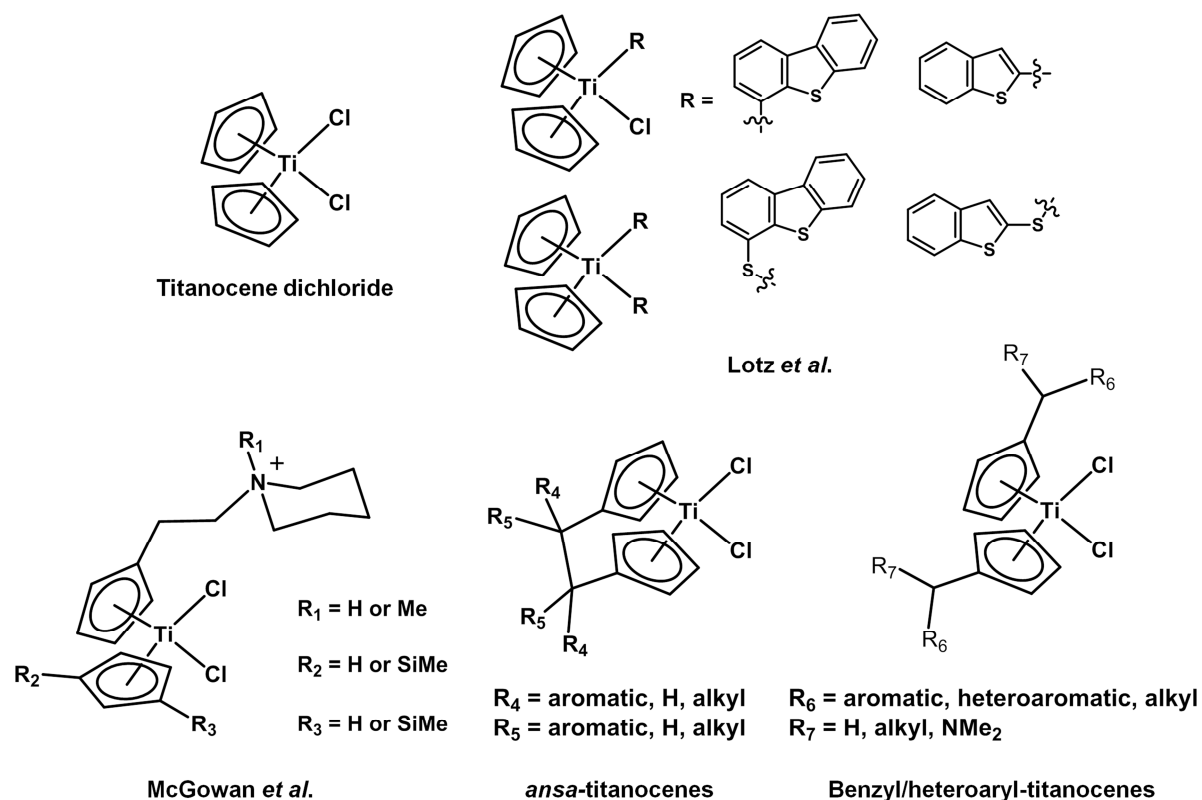


Figure 1.5. Structures of some titanocenes

1.1.4.2. Half-sandwich organometallic complexes

Half-sandwich or piano stool complexes are organometallic complexes that contain a cyclic polyhaptoligand bound to a metal centre and three other ligands either mono-, bi- or tridentate (Figure 1.6). The properties and behaviour of the complexes can be optimized by changing any of the ligands.^{18, 50-52}

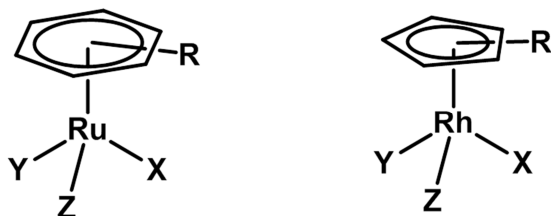


Figure 1.6. Typical structure of half-sandwich complexes $[(\eta^6\text{-arene})\text{Ru}(\text{X})(\text{Y})(\text{Z})]^{n+}$ and $[(\eta^5\text{-Cp ring})\text{Rh}(\text{X})(\text{Y})(\text{Z})]^{n+}$ where X, Y and Z can be mono-, bi- or tridentate ligands

Function of the aromatic ring

The arene unit in complexes of the type $[(\eta^6\text{-arene})M((X)(Y)(Z))]^{n+}$ can stabilize a low oxidation state of metals such as Ru(II) and Os(II), while the Cp aromatic rings are more suited to stabilize metals in a higher oxidation state such as Rh(III) or Ir(III). The nature of the arene or Cp ring is also an important factor to take into account; more electron-rich arenes or Cp rings will stabilise the complex better.

The arene and or the Cp ring does not only have an effect on the stability of the complex, but also plays an important role by adding a hydrophobic moiety that will facilitate the cellular uptake.^{52, 53}

It has also been observed that the cytotoxicity of some half sandwich Ru(II) complexes is closely related to the size of the arene. Complexes that target DNA, for example, display better anti-proliferative activity when containing extended arenes. The increase in the cytotoxicity is assumed to arise from the ability of the arenes to intercalate DNA.^{51, 54-56}

Function of the X, Y and Z ligands

The ligands X, Y and Z give metal complexes a wide versatility, for example, we can synthesize complexes containing three monodentate ligands (RAPTA-C), a monodentate ligand and a bidentate ligand (RM175), or in some cases complexes with a tridentate ligand. By changing those X, Y and Z ligands, the chemical reactivity, the physical properties, the stability, the affinity for determined targets or even the mechanism of action of the complex can be tuned. Linking the X,Y ligand in a chelating ligand, seems to be advantageous for anticancer activity.⁵²

In general, a monodentate ligand provides the metal complex with potential binding sites *via* ligand substitution. Changes on those monodentate ligands will, mainly, influence the rate of ligand exchange and the stability of the complex.^{51, 54} In a few cases, however, the

monodentate ligand does not play the role of a leaving group, but is part of an inert general structure with a similar roles as the bidentate ligands.⁵⁷

The bidentate ligand of a half sandwich organometallic complex provides the compound with stability. Furthermore, the nature of the chelating ligand allows the fine tuning of the electronic structure and reactivity of the complex. The nature of the chelating ligand can influence the rate and extent of hydrolysis or ligand substitution. The extent of DNA binding or the selectivity for different nucleobases can also be controlled by modifying the chelating ligand.⁵⁸⁻⁶¹ For example, comparing the complexes of the type $[(\eta^6\text{-arene})\text{Ru}(\text{en})\text{Cl}]^+$ and $[(\eta^6\text{-arene})\text{Ru}(\text{acac})\text{Cl}]$ (en = ethylenediamine, acac = acetoacetate), the complex containing the N,N' chelating ligand shows a higher affinity for N7 guanine, whereas the complexes containing acac have a preference for N7 adenine nucleobases.^{56, 62} Finally, the chelating ligand can also influence the target and the mechanism of action of the drug.⁶³

Anti-cancer complexes

In this area of organometallic complexes, ruthenium(II) complexes have been promising. However, osmium, rhodium and iridium complexes are currently being intensively studied.⁶³⁻⁶⁶ Nowadays, there is an immense library of half sandwich organometallic compounds displaying promising results. However, for the purpose of this introduction, only a few representative compounds will be discussed.

Initially, half-sandwich ruthenium complexes were synthesized with the aim of targeting DNA. Many Ru(II) compounds were shown to interact with DNA, although the binding, in various cases, was shown to be weaker than with platinum drugs.^{41, 52, 67-69} On the contrary, various Ru complexes have shown a strong affinity for protein binding, and it is currently believed that some complexes like RAPTA have preference for proteins instead of DNA.⁷⁰⁻⁷⁴

$[(\text{bip})\text{Ru}(\text{en})\text{Cl}]^+$ (RM175) is an inactive drug in its chlorido form. At low chloride concentrations (cell nucleus) the complex hydrolyses to form $[(\text{bip})\text{Ru}(\text{en})\text{H}_2\text{O}]^{2+}$. The active aqua complex binds strongly to DNA, binding preferentially to N7 of guanine. The binding of this type of complex generates unwinding of the DNA helix which results in the inhibition of DNA replication. RM175 possesses an interesting biological mode of action since in addition to the ruthenium-guanine binding, it also interacts with DNA through the intercalation of the extended arene (biphenyl) between nucleobases, the so-called dual mode interaction. Such a double interaction results in a DNA with extra degree of distortion.^{52, 53, 62, 74-78} It has also been shown that RM175 reacts with glutathione (GSH) to form *S*-coordinated GSH-Ru(II) adducts. However, this thiolato adduct is then oxidised to the sulfenato adduct, which weakens the ruthenium-sulfur bond. Then, substitution of the sulfenato group by N7 guanine occurs. GSH does not act as a detoxification system for this type of complex.^{77, 78}

RAPTA complexes are believed to bind DNA.⁶⁸ However, *in vivo* studies demonstrated that those compounds were not active against healthy cells or primary tumours, but to metastatic cells.⁷⁹ Those results suggested that DNA is not the primary target for this complex. It is currently believed that the mechanisms of action involve protein binding and enzyme inactivation.^{70-72, 80} Currently, it is believed that RAPTA-C treatment leads to the increase of p53 (tumour suppressor protein) and apoptosis.⁸¹

Similarly in the case of ferrocenes, complexes containing biomolecules or active organic compounds have also been synthesized.⁸² For example, Ru(II) arene compounds containing paullone (organic drug capable of inhibiting cyclin-dependent kinase) type chelating ligands displayed high cytotoxicity, as well as, inhibition of cyclin-dependent kinases (regulate cell division and apoptosis).^{83, 84} RAPTA analogues containing ethacrynic acid have been synthesized to inhibit glutathione transferase. Two of those complexes have shown higher affinity for the enzyme than the ethacrynic acid itself.⁸⁵ Ru(II) compounds

containing chloroquine (anti-parasitic) have been shown to be active against malaria, and some cancer cell lines.⁸⁶ Cp*Ru(II) complexes containing staurosporin (kinase inhibitor that competitively binds to the ATP binding site) have also been synthesised and shown to selectively inhibit specific kinases.^{87, 88} Sulphonamide containing compounds, capable of inhibiting carbonic anhydrases have also been reported.⁸⁹

Sheldrick *et al.* reported a series of Cp* Ir(III) and Rh(III) compounds containing polypyridyl chelating ligands. These compounds were shown to intercalate DNA, and over time, covalently bind and deform the DNA. However, DNA does not seem to be the main target for these type of complexes. IC₅₀ values achieved with some of the complexes were as low as that of cisplatin, and in some cases an order of magnitude lower.^{90, 91}

A library of Ir(III) compounds of the type [(Cp^x)Ir(XY)Cl] (Cp^x = petamethylcyclopentadienyl (Cp*), 3-Phenyl-1,2,4,5-tetramethyl-1,3-cyclopentadiene (Cp^xPh) or 3-biphenyl-1,2,4,5-tetramethyl-1,3-cyclopentadiene (Cp^xPhPh); XY = *N,N'*; *N,O* or *O,O'* ligands) was synthesised.⁵⁸ Cp* compounds were the less active complexes from the series, while Cp^xPhPh were 1 to 2 orders of magnitude more active, achieving μM and sub μM IC₅₀ values in some cases. The anti-proliferative activity of these Cp series was correlated with hydrophobicity and DNA-binding.⁵⁸ A series of phenylpyridyl Ir(III) Cp complexes also displayed significant cytotoxic activity towards A2780 cancer cell lines. The high activity of those complexes was attributed to the high nucleobase binding ability.^{92, 93}

McGowan *et al.* reported a series of Ir(III) compounds containing picolinamide ligands, ketoiminates or naphthoquinone chelating ligands. The ketoiminate complexes exhibited high activity against some cancer cell lines, comparable to cisplatin.⁹⁴ More recently, the same group reported Rh(III) and Ir(III) picolinamide complexes which inhibited thioredoxin

reductase I (an enzyme that can reduce thioredoxin) and displayed high cytotoxicity against HT-29, MCF-7 and A2780 cancer cell lines.⁶⁶

In the search for new mechanisms of action, a series of compounds has also been studied with the aim of targeting the redox system, and induce cell death by oxidative stress.⁹⁵ Some examples are the azopyridine ruthenium(II) complexes. The chlorido analogues are able to catalytically oxidize glutathione to form glutathione disulfide in cells. The iodide adducts, however, do not hydrolyze or react with GSH but still increased levels of ROS.^{96,107} Amouri *et al.* presented a series of Cp*-Ir compounds containing 2-methyl-1,4-naphthoquinone derivatives which are believed to target cytochrome P450 reductase triggering the formation of ROS.⁹⁷

1.2. Catalytic drugs

For many years the development of metal-based drugs was focussed on cytotoxic compounds which can react stoichiometrically with some biologically relevant molecules. Therefore, the concentration of the complex necessary to display cytotoxic activity is relatively high. The downfall of using high concentrations of metal drugs relies on their lack of specificity towards their targets. Metal-based drugs might show significant preference towards some targets, but they might also be reactive towards other biomolecules. The same principle applies to the selectivity towards cells. Some drugs might preferentially target malignant cells, however, at a higher concentration also healthy cells will be affected.

In recent years, a number of compounds with catalytic properties, have been synthesized and tested *in vitro* or *in vivo*, showing promising results.⁹⁸⁻¹⁰¹ This novel approach decreases the metallodrug concentration necessary to achieve the desired antitumoural effect. Nevertheless, catalytic drugs require specific substrates and conditions,

which might translate with reduce side reactions and general toxicity. So far the applications of catalytic drugs have been mainly focused on the regulation of redox levels in cells, depletion or transformation of specific biomolecules, functional group transformations and *in situ* synthesis of compounds. However, catalytic drugs are still a recent research area and many other applications can be found. Here some of the most promising metal-based catalytic drugs are discussed.

Redox regulation

Porphyrins are well known photosynthesizers which can be used in photodynamic therapy (PDT) when coordinated to transition metals and lanthanides. PDT consists on the administration of non-cytotoxic compound which can be excited by light irradiation, at a specific wavelength. The excited compound promotes the formation of singlet oxygen ($^1\text{O}_2$). Singlet oxygen, like other reactive oxygen species (ROS), is known to cause damage by oxidative stress when in high concentrations.¹⁰² PDT has also been achieved with non-porphyrin containing complexes.¹⁰³

Some Mn(II) and Fe(III) porphyrins have also been shown to catalyse decomposition of peroxinitriles and act as scavengers for other reactive oxygen species (ROS) and reactive nitrogen species (RNS).^{104, 105}

Manganese(II) compounds have been studied as mimics of superoxide dismutase enzymes. These enzymes, and the Mn(II) mimics, are capable of dismutating superoxide to oxygen and hydrogen peroxide. Superoxides are strong oxidizing agents that can cause cellular damage by oxidative stress.^{105, 106} This strategy allows control of the levels of oxidative species, and can be used to treat many illnesses caused by oxidative stress damage. The most successful Mn(II) SOD mimic is M40403 (Figure 1.7), which was in Phase II clinical trials (NCT00101621, NCT 00033956).

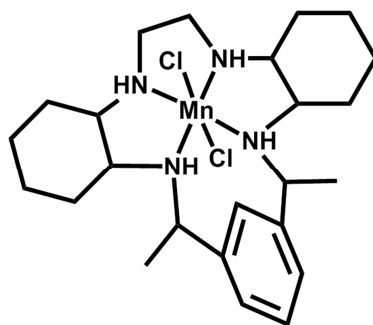


Figure 1.7. Structure of Mn40403.

Depletion or transformation of bimolecules

Sadler *et al.* have developed a series of Ru(II) complexes with potential catalytic activity which can be utilised for cancer therapy. For example, [(bip)Ru(2(*p*-*N,N*-diethylaminophenylazo)pyridine)I], has been shown to catalyse the oxidation of glutathione (GSH) to glutathione disulphide (GSSG).¹⁰⁷ This process depletes the GSH pool and disrupts the redox balance of the cell. [(bip)Ru(en)Cl]⁺ (en = ethylenediamine) has also been shown to react with GSH at pH 7 in the presence of oxygen to give the sulfenato-GSH adduct.^{77,78}

More recently, The possibility of performing transfer hydrogenation reactions *in vitro* has been published. Initially, [(bip)Ru(en)Cl]⁺ was used to regenerate NADH from NAD⁺ using sodium formate as a hydride source (see section 1.2.2.).¹⁰⁸ Later, a series of Ru(II) and Ir(III) complexes of the type [(η⁶-arene)Ru(bpm)Cl]⁺, [(Cp^x)Ir(phen)OH₂]²⁺ and [(Cp^x)Ir(PhPy)Py]⁺ (bpm = bipyrimidine, phen = phenantroline, PhPy = 2-phenylpyridine, Py = pyridine), which can use NADH as a hydride donor, were studied.^{109,110}

The development of catalytic drugs for the hydrolytic cleavage of peptide/proteins has been investigated for several years. However, few of those catalysts can be used as therapeutic agents. In 2000, Suh *et al.* reported the first Co(III) compound capable of catalysing the cleavage of peptide deformylase at physiologically relevant conditions, which

might be attractive as antibiotic agents.¹¹¹ In 2002, a Co(III) compound capable of catalysing the cleavage of myoglobin was developed, however the compound was not fit for therapeutic applications.^{112, 113} More recently, the same group has reported the synthesis and catalytic applications of a series of Co(III) complexes capable of performing hydrolytic cleavage of amyloids at 310 K and pH 7.4.¹¹⁴⁻¹¹⁶ Amyloids are insoluble aggregations of peptides or proteins, and are present in some conditions such as Alzheimer's disease, Parkinson's disease and Type II diabetes.^{117, 118}

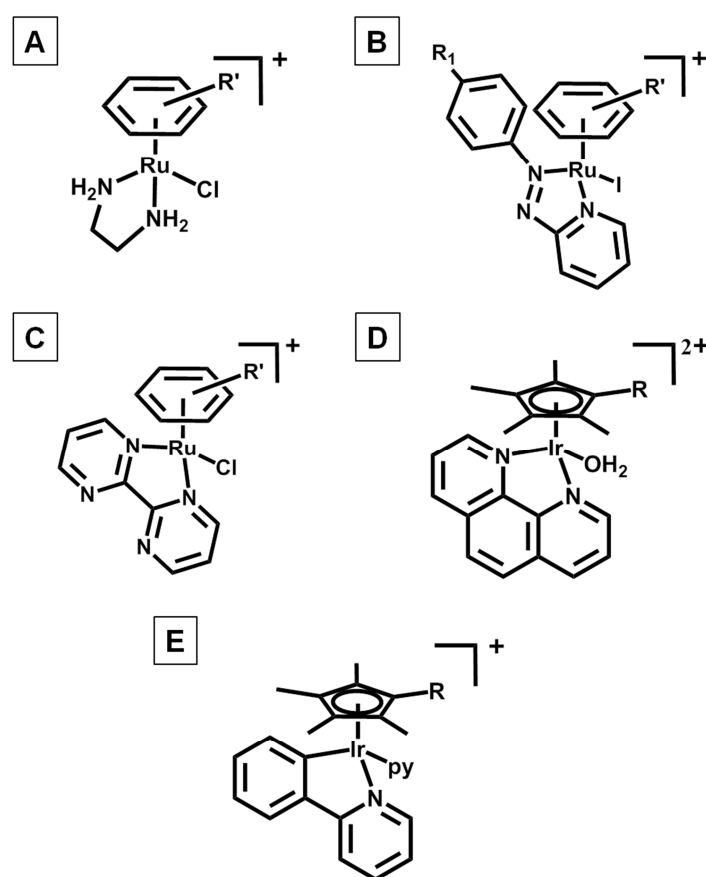


Figure 1.8. Structures of $[(\eta^6\text{-arene})\text{Ru}(\text{en})\text{Cl}]^+$ (A), $[(\eta^6\text{-arene})\text{Ru}(2(p\text{-}N,N\text{-diethylaminophenylazo)pyridine})\text{I}]^+$ (B), $[(\eta^6\text{-arene})\text{Ru}(\text{bpm})\text{Cl}]^+$ (C), $[(\text{Cp}^x)\text{Ir}(\text{phen})\text{OH}_2]^{2+}$ (D) and $[(\text{Cp}^x)\text{Ir}(\text{Phpy})\text{py}]^+$ (E). $R' = p\text{-cym, bip, hmb, bn, indane}$ or others arenes. $R = \text{methyl, phenyl}$ or biphenyl.

Cowan *et. al.* have developed copper and nickel compounds containing the ATCUN moiety (Figure 1.9) which can be coupled to enzyme recognizing peptides.⁹⁸ In such a strategy, the compound binds to the enzyme sequence and catalyses its degradation in the presence of H₂O₂ and ascorbic acid. In a similar approach, binding and degradation of RNA, have been used by Cowan and co-workers as a method to target Stern Loop IIb in hepatitis C.¹¹⁹

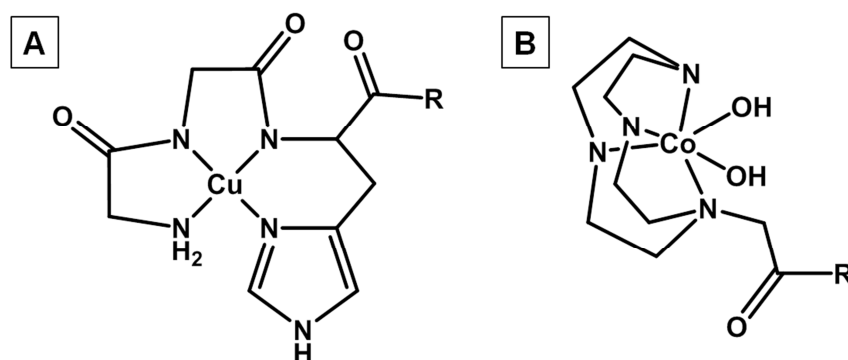


Figure 1.9. Structures of [Cu(ATCUN-R)] (A) and [Co(cyclen-R)(OH)₂]. R = peptides, biotine and other molecules which can be recognised by specific targets.

Functional group transformations

[(Cp*)Ru(COD)Cl], is a Ru(II) complex which has been shown to catalyse the cleavage of allylcarbamates, to give the corresponding primary amine.¹²⁰ In a similar manner, the complex [(Cp*)Ru(η⁶-pyrene)]PF₆ can catalyse the same reaction after irradiation with light (λ = 330, or UV light) and further release of the pyrene moiety. Both reactions require the presence of thiols, preferably aromatic. This reaction allows the activation of fluorescent or cytotoxic compounds containing protected amines, which in their protected form are inactive.¹²¹

Organic azides have been shown to be inert towards any cell components and can be hydrolysed to amines. This property makes azides ideal candidates for the delivery of active

amine containing fluorophores or cytotoxic compounds into living organism.¹²² After hydrolysis of the azide, the amine can display its fluorescence or activity. A series of metal porphyrine has been studied by Meggers *et al.*, which can catalyse the hydrolysis of azides. The complex $[\text{Fe}(\text{TPP})\text{Cl}]$ (TPP = 5,10,15,20-tetraphenylporphyrine) displayed the best catalytic activity. This strategy has been shown *in vivo* for the activation of an azide caged rhodamine 110 which after reaction with an Fe(III) compound becomes rhodamine 110 and displays fluorescence.¹²³

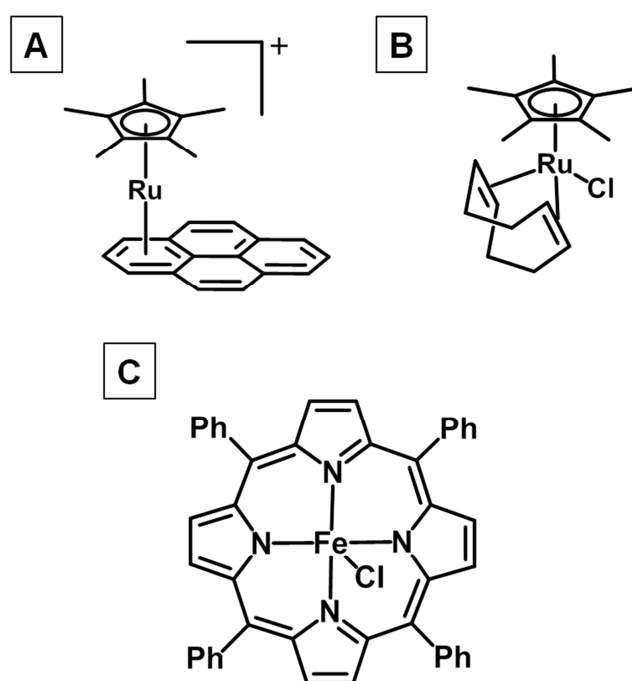


Figure 1.10. Structures of $[(\text{Cp}^*)\text{Ru}(\text{COD})\text{Cl}]$ (A), $[(\text{Cp}^*)\text{Ru}(\eta^6\text{-pyrene})]^+$ (B) and $[\text{Fe}(\text{TPP})\text{Cl}]$ (C)

In situ synthesis

Click chemistry, or azide-alkynyl cycloadditions, has been studied as an *in vitro* synthetic method for C-C bond formation. However the process requires the presence of cytotoxic Cu(I) as a catalyst.¹²⁴

Bradley *et al.* carried out Suzuki-Miyaura cross-coupling reactions and allylcarbamate cleavage inside HeLa cells using Pd(0) nanoparticles.¹²⁵ Suzuki-Miyaura cross coupling

reactions, using the palladium(II) catalyst $[\text{Pd}(\text{OAc})_2(\text{ADHP})_2]$ (ADHP = 2-amino-4,6-dihydropyrimidine), have also been performed to label I-containing modified proteins with fluorescent tags bearing boronic acid.¹²⁶⁻¹²⁸ In 2012, Davis *et al.* demonstrated the application of such catalytic reaction on the membrane surface of *E. coli*.^{127, 128}

Sonogashira reactions, using $[\text{Pd}(\text{OAc})_2(\text{N,N-dimethylADHP})_2]$, were also achieved. Homopropargylglycine modified ubiquinone and peptides were labelled with a fluorescent tag.¹²⁹

1.2.1. $[(\eta^6\text{-arene})\text{Ru}(\text{en})\text{Cl}]^+$

Ruthenium(II) arene complexes of the type $[(\eta^6\text{-arene})\text{Ru}(\text{en})\text{Cl}]\text{PF}_6$ where the arene is hexamethylbenzene, *p*-cymene, indane and en is ethylenediamine have been shown to catalyse the regioselective reduction of NAD^+ , using formate as a hydride source, *via* a transfer hydrogenation process. The catalytic reactions can be carried out in water at physiological relevant conditions (pH* 7.2, 310 K). Complex $[(\text{hmb})\text{Ru}(\text{en})\text{Cl}]\text{PF}_6$ displayed the higher catalytic activity with a turnover frequency (TOF) of 0.85 h^{-1} . The complex shows typical Michaelis-Menten type kinetics behaviour. The Michaelis constant (K_M) calculated was 58 mM and a maximum TOF (TOF_{max}) was 1.46 h^{-1} .

Human lung A549 cancer cells were treated with concentrated sodium formate solutions and exposed to the complex $[(\text{hmb})\text{Ru}(\text{en})\text{Cl}]\text{PF}_6$. However, no significant effect on cell growth in the presence of these ruthenium complexes, and formate, was observed.¹⁰⁸ In order to catalyze the reduction of NAD^+ *in vivo*, more active catalysts are required.

1.2.2. The role of formate

In order to perform transfer hydrogenation reactions to reduce NAD^+ *in cellulo* and *in vivo*, a hydride source must be co-administrated with the catalyst. For that purpose, formate has been selected amongst other hydride sources for various reasons: formate salts

are mild hydride adducts with very good water solubility, which allow good absorption and distribution of complexes in the body. Many formate salts are easily available and very cheap. Finally, mammalian cells display high tolerance for formate.

Formic acid and formate salts are natural constituents of many foods. They are intermediary metabolites in normal metabolism, for example formate is generated in the catabolism of several amino acids like glycine or tryptophan, and they are precursor in the biosynthesis of several body constituents. Under normal conditions the concentration of formate in human blood serum is between 0.02-0.25 mM. Furthermore formate is a product from the metabolism of methanol, which is ingested in low quantities through fruit juices and fermented beverages. High doses of methanol have been shown to be toxic in humans and primates, including blindness, kidney damage, acidosis and death. Excessive concentrations of formate (10-20 mM in human blood plasma) have also been shown to be toxic. However, clinical reports suggest that irreversible damage occurs when concentration of formate in plasma is 7 mM or higher for at least 24 h. In general, the tolerance of the body to large amounts of formate is relatively high.¹³⁰

Calcium formate, for example have been patented (US 5248818 A) and is currently used as a calcium supplement.¹³⁰ Sodium and calcium formate salts have also been approved by the FDA as additives in preserved food.¹³¹

1.3. Transfer hydrogenation reactions

Transfer hydrogenation reactions are usually defined as the reduction process by which a metal complex catalyses the transfer of a hydride ion from a donor to a molecule containing a multiple bond. Double bonds such as C=C, C=N and C=O can be successfully reduced affording high yields with excellent enantioselectivity. Transfer hydrogenation reactions have

been studied extensively during the last few years as an alternative to hydrogenation and hydroboration reactions. In general, transfer hydrogenation reactions provide an inexpensive method for the reduction of substrates under mild conditions, without the toxicity and flammable nature of borane or hydrogen.

The study of transfer hydrogenation reactions has primarily focused on the reduction of ketones and imines. Initially, metal catalysts containing phosphine,¹³²⁻¹³⁶ pyridine,^{132, 137, 138} oxazole,^{139, 140} diamines,^{141, 142} diimines¹⁴³ or carbonate¹⁴⁴ as the chelating ligands have been studied. The discovery of the catalytic properties of half-sandwich organometallic complexes, containing either β -amino-alcohols or mono-tosylated diamines, has been a new paradigm.¹⁴⁵ These two types of complexes allowed transfer hydrogenation reactions to be performed under mild conditions, and with turnover frequencies (TOF) of up to *c.a.* 30 x to 70 x times higher than with previous catalysts.¹⁴⁵ Turnover frequency is the number of catalytic cycles per catalytic site per unit of time for a fixed set of reaction conditions. Higher turnover frequencies indicate a better catalytic activity.¹⁴⁵

Complexes containing β -amino alcohols chelating ligands are amongst the most successful catalysts for transfer hydrogenation reactions, leading to high yield and enantioselectivity. However, transfer hydrogenation reactions are performed using secondary alcohols as hydride donor, and in organic solvents.¹⁴⁶⁻¹⁵¹ The reactions were not successful in aqueous media until recently. Catalytic reactions using formic acid/triethylamine in water have been achieved under basic pH or using sodium formate.¹⁵²⁻¹⁵⁵

The catalysts containing mono-tosylate diamine chelating ligands have been shown to carry out the asymmetric reduction of ketones and imines with high yield in organic solvents, using secondary alcohols as hydride donors. However, the complexes were less active than those containing β -amino alcohols as chelating ligands.¹⁴⁵ Interestingly, transfer

hydrogenation reactions in aqueous media were achieved successfully, and with higher conversions and enantioselectivities than catalysts containing β -amino alcohols.¹⁵⁴

1.3.1. Mono-tosylate diamine chelating ligands: Noyori-type catalysts

In 1995 Noyori *et al.* discovered the transfer hydrogenation properties of the ruthenium catalyst containing (1*S*,2*S*)-*N*-(*p*-toluensulfonyl)-1,2-diphenylethylenediamine (TsDPEN) (Figure 1.11).¹⁵⁶ In the first report, Noyori's catalyst was prepared *in situ* by reacting the $[\text{RuCl}_2(\eta^6\text{-mesitylen})]_2$ dimer with the TsDPEN ligand immediately before the reaction, without further purification.¹⁵⁶ The complex was synthesized in isopropanol at 80° C for 20 min. The catalysis was activated in the presence of KOH base. The reduction of acetophenone was achieved with 95 % yield and 97 % enantiomeric excess after 15 h. The catalytic activity of Ru(II) complexes containing R-DPEN chelating ligand were, later, studied using different η^6 -arenes, with $[(p\text{-cym})\text{Ru}(\text{TsDPEN})\text{Cl}]$ displaying more promising results.

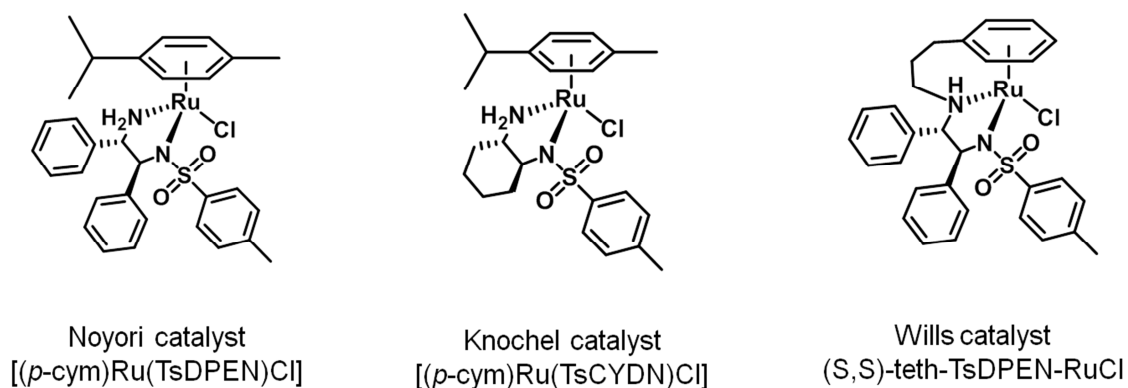


Figure 1.11. Structures of Ru(II) complexes containing Noyori's catalyst, TsCYDN and a tethered compound from Wills *et al.*

Transfer hydrogenation reactions with Noyori's catalysts are generally carried out in organic solvents, and using isopropanol/KOH or formic acid/triethylamine as a hydride source.

The reduction of ketones with the *p*-cym Ru(II) compounds containing TsDPEN was achieved at room temperature and in the presence of air, with high conversions and enantioselectivities. In many cases, the conversion time was shorter than with other catalysts except for β -amino alcohol containing complexes.¹⁴⁵ Cp*Rh(III) and Cp*Ir(III) analogues containing the TsDPEN ligand have also been studied, but the yield and enantioselectivity for the reduction of acetophenone (30° C, solvent and hydrogen source Isopropanol/*t*-BuOK), was shown to be lower than in the case of Ru(II).¹⁵⁷ Reduction of imines was also achieved successfully with Noyori's catalysts. The Rh(III) analogues were shown to be more active than Ru(II) analogues, but, in general, with lower enantioselectivities (20°C, hydrogen source triethylamine/formic acid).¹⁵⁸⁻¹⁶¹ The ruthenium catalysts have also been used for the reduction of double C=C bonds.^{158,162}

Xiao *et al.* reported in 2004 a significant increase in activity with [(*p*-cym)Ru(TsDPEN)Cl] in water using formate as a hydride source.¹⁶³

After the publication of Noyori's work with the TsDPEN ligand, many studies were performed to develop Noyori-type modified ligands to achieve better activities and enantioselectivities. Complexes containing the mono-tosylated diaminocyclohexane (TsCYDN) ligand, synthesized by Knochel *et al.* and co-workers, were found to be amongst the most successful (Figure 1.11).¹⁶⁴ High enantioselectivity and conversion was achieved in reduction of ketones, using either isopropanol/KOH or acid formic/triethylamine as the hydride source.¹⁶⁴ When performing the reactions in isopropanol, Ru(II)-TsCYDN complexes gave higher conversion and enantioselectivities than the Rh(III) or Ir(III) analogues.¹⁵⁷ However, when the reaction was performed in water using formate or formic acid/triethylamine, Rh(III) TsCYDN catalyst was more active than the Ru(II) and Ir(III) analogues. Furthermore, higher conversion and enantioselectivity was obtained using Rh(III) analogues.¹⁶⁵

Ikariya *et al.* have recently published Ru(II), Ir(III) and Rh(III) TsCYDN catalysts in combination with silver salts and H₂ for the reduction of imines. The reaction was performed at 30° C and isopropanol as a solvent. The Ir(III) catalyst gave the best results with a 99 % conversion and 70 % enantioselectivity.¹⁶⁶

Another interesting family of Noyori-type catalysts, which achieved great success in asymmetric transfer hydrogenation of ketones, are the tethered complexes synthesized by Wills *et al.*, especially (S,S)-teth-TsDPEN-RuCl and (R,R)-teth-TsDPEN-RuCl (Figure 1.11). In this type of complexes the TsDPEN is bound to the η^6 - or η^5 -arene group.¹⁶⁷⁻¹⁷¹ These catalysts have a rigid structure, which improves the enantioselectivity, both in ketone and imine reduction. A rigid structure blocks the rotation of the arenes, which allows the addition of bulky groups on the arene. This enhances the enantioselectivity of the complex as one site of the complex will be hindered. Furthermore, the tethered ligand provides the complex with extra stability towards metal-ligand dissociation.¹⁶⁷⁻¹⁷¹

Mechanism of Noyori-Ru(III) complexes

Studies on the mechanism of action of TsDPEN complexes, have been performed since the first publication of the Ru(II) complex in 1995 by Noyori *et al.* In their initial reports, Noyori described the isolation of the chlorido complex, the 16-electron species and the hydride species.¹⁷² The NH₂ protons, from the TsDPEN chelating ligand, are acidic. Under basic conditions (for example KOH, used for transfer hydrogenation reaction), the complex $[(\eta^6\text{-arene})\text{Ru}(\text{TsDPEN})\text{Cl}]$ is deprotonated and HCl is released to afford a 16-electron species (active catalyst). The 16-electron species, reacts with isopropanol (hydride source) to form a hydride adduct *via* a concerted process (β -elimination), with simultaneous transfer of a hydride and a proton.¹⁷² This process was confirmed by Casey *et al.* *via* a kinetic isotopic effect, investigating the variation of the reaction rate when using isopropanol or deuterated-isopropanol ((CH₃)₂CHOD, (CH₃)₂CDOH and (CH₃)₂CDOD).¹⁷³ The reduction of the

substrate, involves a second concerted process.^{172,174} The 6 member ring transition state is formed due to a hydrogen bond between the carbonyl of the substrate, and the NH₂ from the chelating ligand (TsDPEN). Figure 1.12. It was also reported that the hydrogen on the amino group of the ligand TsDPEN, is essential for the catalytic reaction.^{174, 175}

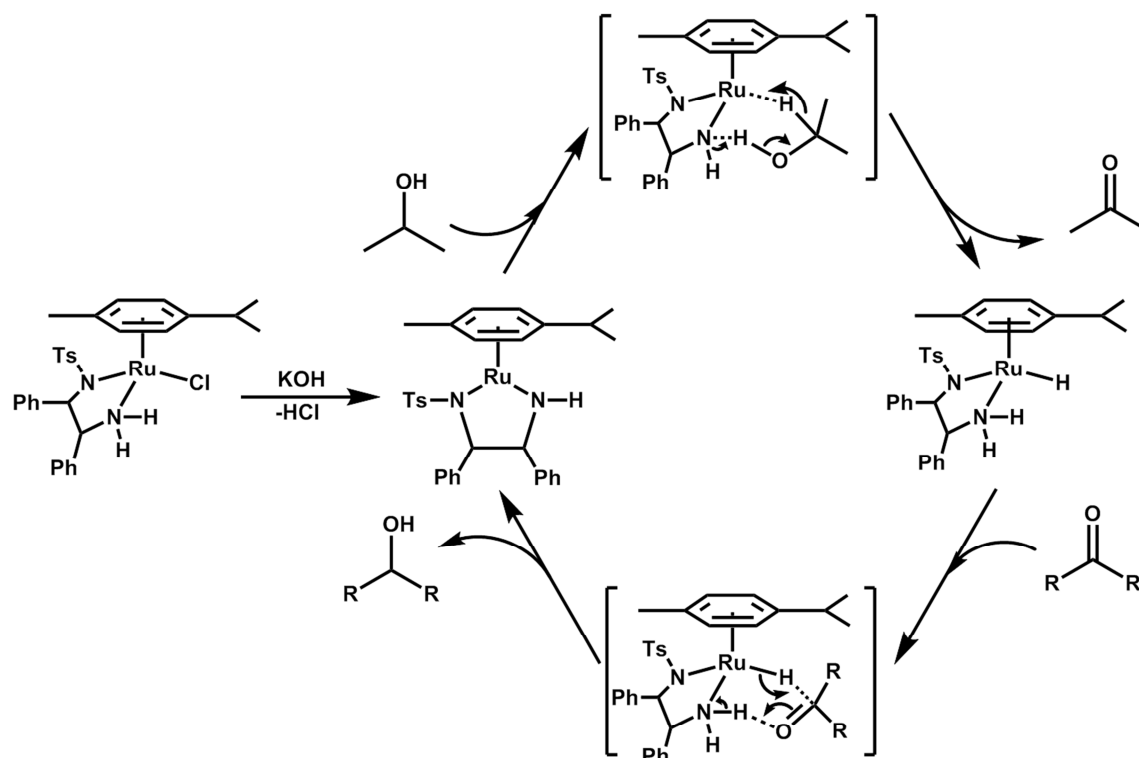


Figure 1.12. Proposed mechanism for the reduction of ketones and imines using $[(p\text{-cym})\text{Ru}(\text{TsDPEN})\text{Cl}]$ catalyst and isopropanol/KOH as a hydride source.¹⁷³

When using formic acid/triethylamine as a hydride source, a similar mechanism has been reported by Ikarya *et al.*¹⁷⁶

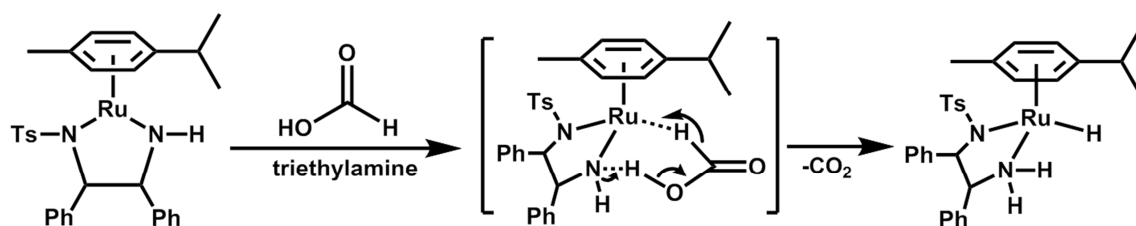


Figure 1.13. Formation of ruthenium hydride using formic acid/triethylamine.¹⁷⁶

Recently, Wills *et al.* have reported the formation of hydride complexes and the reduction of a cyclic imine (91 % conversion, 18 % enantiomeric excess in 5 days) when using a dimethylated version of TsDPEN (Figure 1.13). For the imine reduction, the use of *N*-methylated tethered complexes resulted in a decrease in activity compared to the reaction with non-methylated catalysts. However, the reaction achieved more than 95 % conversion within 20 h. The same reactions using the *N*-methylated TsDPEN complex to reduce acetophenone, gave conversions of 1.7 % after 6 days, and a 6 % conversion after 18 h when using the *N*-methylated tethered compound.^{177,178} (Figure 1.14)

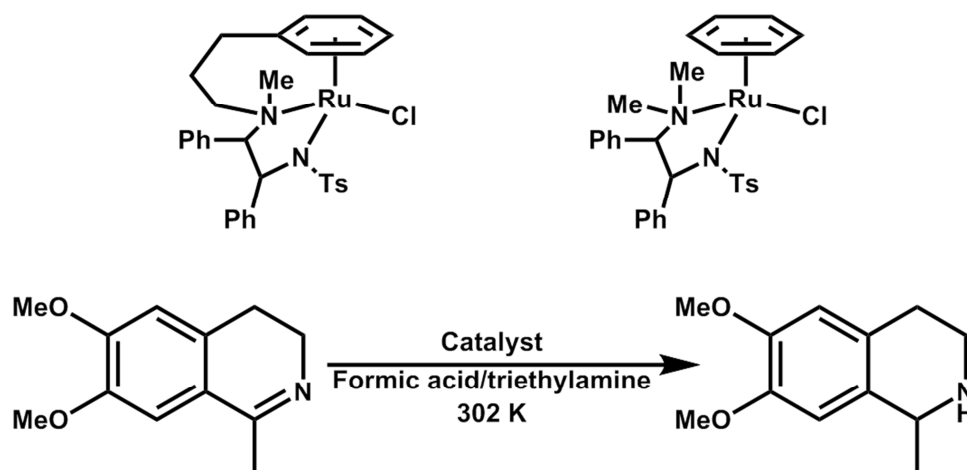


Figure 1.14. Reduction of cyclic imine.

Traditionally, transfer hydrogenation reactions have been carried out in isopropanol, organic solvents or in an azeotropic mixture of formic acid and triethylamine. Until 2004 very little attention was focused on transfer hydrogenation reactions in water. Xiao *et al.* reported a significant increase in the activity when using $[(p\text{-cym})\text{Ru}(\text{TsDPEN})\text{Cl}]$ complex in water, and using formate as a hydride source.¹⁶³ While the reduction of acetophenone in water achieved full conversion in 1 h, the same reaction in formic acid/triethylamine achieved full conversion after 12 h.¹⁶³ It has been hypothesised that the presence of water can stabilize the intermediates by hydrogen bond formation with the substrate.

Mechanistic studies of the reaction in water were also performed by Xiao and co-workers.¹⁷⁹ At basic pH, the catalytic cycle follows a similar mechanism than that

described in non-aqueous media. Interestingly, at low pH, the amide is protonated, and the catalytic activity of the complex decreases. This effect is due to a partial ligand-metal dissociation (Figure 1.15).

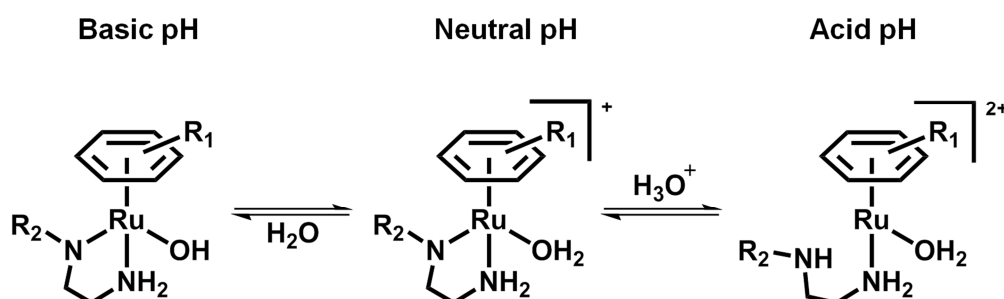


Figure 1.15. Effect of the pH on the diamine complexes. $\text{R}_1 = p\text{-cym, bn, hmb, bip}$ or other arenes. $\text{R}_2 = \text{sulfonate group}$

Water-soluble Noyori-type catalysts

Water-soluble compounds have received much attention since the presence of water has been shown to facilitate the transfer hydrogenation reactions. Furthermore, water is a more environmentally friendly and less toxic solvent.^{180,181,182}

A series of modified ligands containing water-soluble groups has been developed. The first examples by Bubert *et al.*, who added a hydrophilic sulfonate group in the *para*- and *ortho*- positions of the *N*-arylsulfonyl fragment of the TsDPEN and TsCYDN (Figure 1.16). The reaction was performed in isopropanol/water at 22°C. The transfer hydrogenation rate was low, but the enantioselectivity of the reaction was excellent. The Ir(III) complexes were the most successful catalysts, followed by the Rh(III) and, finally, the Ru(II) complexes. It was also shown that a higher percentage of water in the reaction mixture increased the reaction rate.¹⁸³ The addition of sulfonic acid or sulfonate groups to the complexes in order to increase the water solubility has also been used by Deng *et al.*¹⁸⁴ Two sulfonate groups were added to the *ortho*- positions of the Ph in the backbone of the ligand, Figure 1.16. The Ru(II) complex was shown to achieve 99 % conversion with high enantioselectivity (84-95 %) after

24 h in water at 40°C, using sodium formate as a hydride source and 0.04 mol equiv. of a surfactant. However, the use of Rh(III) or Ir(III) resulted in low conversions and enantioselectivities.¹⁸⁴ High conversion and enantioselectivity for the reduction of cyclic imines was also achieved with these complexes, in water at 28°C, using sodium formate as a hydride source and 0.5 mol equiv. of CTAB (cetyltrimethylammonium bromide, surfactant).¹⁸⁵ In 2011, Gebbink *et al.* synthesized a compound containing a TsDPEN chelating ligand and a sulfonate-containing η^6 -arene.¹⁸⁶ This complex is capable of reducing acetophenone, with a 99 % conversion and 97 % enantiomeric excess, in water at 40°C, and using sodium formate as a hydride donor. The catalyst was shown to be recyclable, but there is an important loss of activity after the third run.¹⁸⁶

Another way to increase water solubility was the addition of amino groups by Deng *et al.* (Figure 1.16) Although the catalytic activity of the Ru(II) catalyst was not remarkable using HCOONa, the Rh(III) analogue furnished high conversion with excellent enantioselectivities in a great variety of ketones.¹⁸⁷

Zhou *et al.* published the synthesis and catalytic activities of a series of water-soluble complexes containing imidazolium, triethylammonium and pyridinium attached to the TsDPEN moiety. Figure 1.16.^{188, 189} These complexes achieved 100 % conversion in 2-3 h with enantioselectivities of up to 93 % when the reaction was performed in water at 40°C and using sodium formate as a hydride source. Interestingly, the pyridinium complexes were recyclable, up to 6 times, with a minimum loss of conversion and enantioselectivity.¹⁸⁹

Süss-Fink *et al.* reported the catalytic activity of a series of ruthenium complexes containing TsCYDN ligand and different η^6 -arenes.¹⁹⁰ The *p*-cym analogue was shown to be the most active (TOF = 46.5 h⁻¹) with 92 % conversion and 81 % enantiomeric excess when reducing acetophenone in water/formate, pH 9 and 60° C. Water-soluble

2-S-(*p*-toluenesulfonylamino) methylpyrrolidine (Figure 1.16) complexes were found to catalyse the transfer hydrogenation of α -aryl ketones and α -aryl imines in aqueous solution using formate as the hydrogen source. However, Ru(II)-TsCYDN complexes gave higher reaction rates and enantioselectivities.¹⁹¹

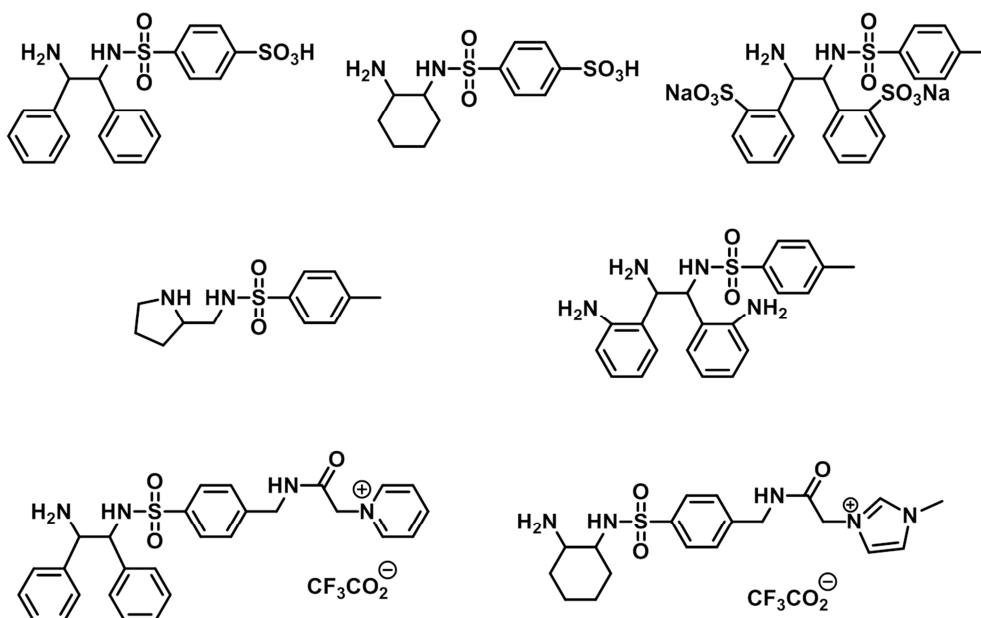


Figure 1.16. Some water-soluble modified Noyori-type ligands.

In his research on tethered complexes, Wills *et al.* reported the synthesis and catalytic activity of some water-soluble analogues. The Rh(III) complex containing 2-(2,3,4,5-tetramethylcyclopentadienyl)-benzyl (1*R*,2*R*)-toluenesulfonyl-cyclohexyldiamine was the most successful achieving full conversion and 96 % enantiomeric excess in the reduction of acetophenone after 3 h, in water at 28° C, and using sodium formate as a hydrogen source.¹⁷¹

In the search for recyclable immobilized catalyst, polyethyleneglycol(PEG)-TsDPEN Ru(II) complexes were synthesized. However, this was only recyclable when the catalytic reaction was performed in water. The complex was water-soluble and catalysed the reduction

of ketones with high yields and enantioselectivities at 22 or 40 °C and using sodium formate as a hydride donor.¹⁹²

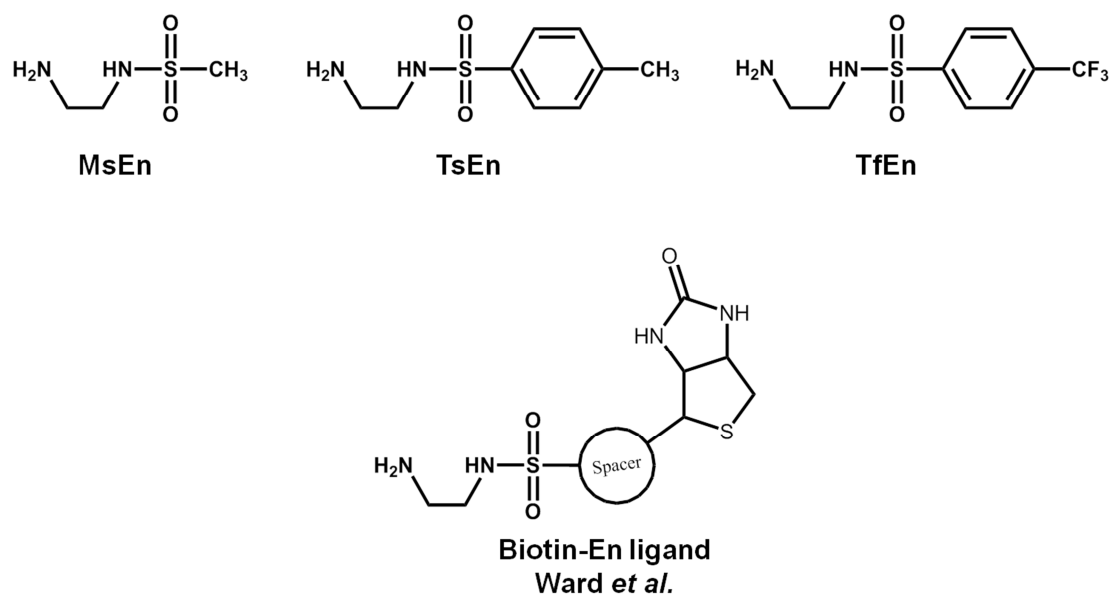


Figure 1.17. Structures of monosulfonamide ethyleneamine ligands.

Water-soluble monosulfonamide ethyleneamine complexes have also been synthesized. Figure 1.17. These kinds of complexes have been used for the catalytic reduction of aldehydes,¹⁹³ α,β -unsaturated ketones¹⁹⁴ or α,β -unsaturated esters.¹⁹⁵ The absence of phenyl groups in the diamine backbone, makes the complexes more soluble. However, the ligands also lose their chirality and cannot be used for asymmetric transfer hydrogenation. The Ir(III) analogues were shown to be the most active for the reduction of aldehydes, in water, at 65 °C using sodium formate (Table 1.2).

Some interesting work on the monosulfonamide ethyleneamine complexes has been performed by Ward *et al.* Biotin labelled ligands interact with streptavidin and avidin and act as metalloenzymes (Figure 1.17). This kind of complex has achieved good enantioselectivities (> 90 %) with ketone substrates.^{196, 197}

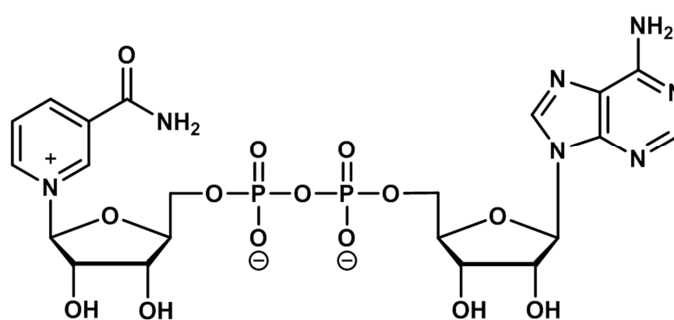
Table 1.2. Turnover frequencies and conversions of some Ru(II), Rh(III) and Ir(III) monosulfonamide ethyleneamine catalysts for the reduction of benzaldehyde. The reactions were performed in water at 65 °C using sodium formate as a hydride source.¹⁹³

Catalyst	Conversion (%)	TOF (h ⁻¹)
Ru(II)-MsEn	1.2	12
Rh(III)-MsEn	74	900
Ir(III)-MsEn	99	1800
Ru(II)-TsEn	99	1000
Rh(III)-TsEn	99	6000
Ir(III)-TsEn	99	12000
Ir(III)-TfEn	98	132000

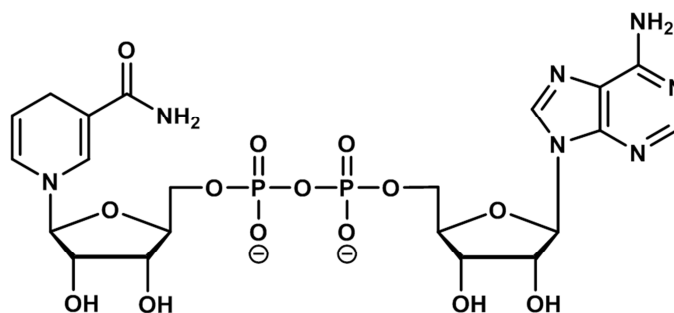
Many other modifications of Noyori-type catalysts have been studied, for example catalysts attached to solid supports, raisins and dendrimers.^{198, 199} However, they are beyond the scope of this thesis.

1.4. Nicotinamide adenine dinucleotide (NAD⁺/NADH)

Nicotinamide adenine dinucleotide (NAD(H)), is a coenzyme found in living cells. The compound consists of two nucleotides joined *via* diphosphate groups. One nucleotide contains an adenine base and the other nicotinamide. Nicotinamide adenine dinucleotide exists in two different forms, oxidized (NAD⁺) and reduced (NADH). The total concentration of NAD⁺ and NADH in most cells is in the range of 10⁻³ M to 10⁻⁶ M. The ratio between the two varies from 1 to 700. The coenzyme is predominantly found in the nucleus, mitochondria and cytosol.^{200, 201}



Nicotinamide adenine dinucleotide



Nicotinamide adenine dinucleotide reduced

Figure 1.18. Structures of nicotinamide adenine dinucleotide (NAD⁺) and nicotinamide adenine dinucleotide reduced (NADH).

1.4.1. Functions

One of the important functions of NAD^+ is to control the redox state of the cell, NAD^+ is also involved in energy production and modulation processes of the cell. Furthermore, NAD^+ and NADH are used as substrates in many enzymatic reactions (mono-ADP-ribosylation, poly-ADP-ribosylation, ADP-ribose cyclisation and formation of *O*-acetyl-ADP-ribose). NAD^+ and NADH have also been shown to function as signalling agents, both intra- and extracellular.

Modulating metabolic energy

Molecules like NADH , ATP or FADH store and transport electrons that are required in other metabolic pathways.

In the specific case of NADH :



NAD^+ and NADH are involved in many important energy metabolism-related reactions, such as glycolysis, Krebs cycle, the lactate dehydrogenase-catalyzed lactate-pyruvate conversions, mitochondrial oxidative phosphorylation, mitochondrial tricarboxylic acid (TCA) cycle, regulating Sir2 family proteins.^{201, 202}

Controlling redox state of the cell

The NAD^+/NADH couple has a major role in controlling the redox state of the cell:

- NAD^+/NADH has a reduction potential which allows the reduction or oxidation of species necessary in other metabolic processes.²⁰³
- The NAD^+/NADH couple contributes in the overall reducing potential of the cell. NADH can act as an antioxidant.

- NAD^+ can act as an inhibitor of some metabolic processes which generate ROS.
- Even though the antioxidant function of NAD^+/NADH by itself is minor, NAD^+ is necessary for the generation of NADP^+ . To a lesser extent NADH can also be converted into NADPH by enzymes.

NADP(H) is a substrate of various enzymes which reduce themselves of ROS, furthermore the main antioxidant action of $\text{NADP}^+/\text{NADPH}$ is the regulation and regeneration of GSH from GSSG.

GSH is one of the main antioxidants in cells and one of the most abundant. $[\text{GSH}]_{\text{cytosol}} = 1\text{-}11 \text{ mM}$, $[\text{GSH}]_{\text{mitochondria}} = 5\text{-}11 \text{ mM}$ and $[\text{GSH}]_{\text{nucleus}} = 1\text{-}11 \text{ mM}$.²⁰⁴ Small changes in the GSH/GSSG ratio will affect greatly the reduction potential of the cell.²⁰⁴

Excess of NADH , NADPH or GSH might trigger reductive stress. For example, excess of NADH will result in the generation of ROS by some enzymes which oxidise the excess NADH (xanthine oxidase) or the release of iron from ferritin. Excess of NADPH could also contribute to the generation of ROS by the activity of NADPH oxidases.^{200, 203, 205}

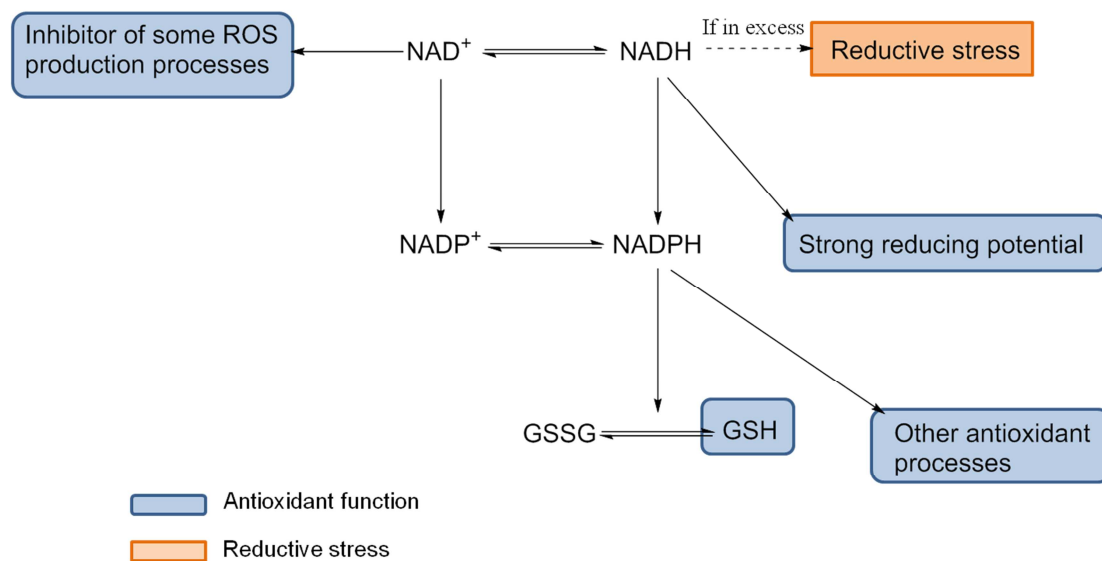


Figure 1.19. Summary of the processes for redox state regulation which involve NAD^+/NADH .

Substrate in enzymatic reactions

NAD^+ can act as a substrate for some enzymatic reactions, in which NAD^+ is hydrolysed to obtain an ADP-ribose group and later transferred to proteins, amino-acids or acetyl groups.

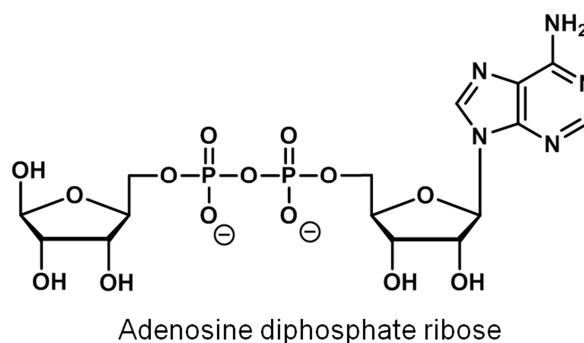


Figure 1.20. Structure of ADP-ribose.

- **Mono-ADP-ribosylation.** Mono-ADP-ribosylation is the process by which an ADP-ribose is transferred to specific proteins or amino-acids (usually arginine, cysteine, asparagine and glutamate). The metabolic functions of mono-ADP-ribosylation are believed to be related to DNA repair and transcription, extracellular signalling and to some immunological functions^{200, 203, 205-207}

- **Poly-ADP-ribosylation.** Poly-ADP-ribosylation is the process by which polymers of ADP-ribose are synthesized. The ADP-ribose polymers are found free or bound to proteins or amino acids. The metabolic function of poly-ADP-ribosylation is still under investigation, however it is closely related with DNA damage sensing and repair, genome integrity, telomere maintenance and synthesis, detoxification, anti-viral, and they have been shown to be closely involved with B and T cells²⁰⁶⁻²⁰⁸

- **Formation of *O*-acetyl-ADP-ribose.** *O*-acetyl-ADP-ribose and the enzymes involved and its synthesis are key compounds in many processes. For example, they are

involved controlling the metabolism homeostasis in situations of stress, prevention of oxidative damage in pancreas, induction of apoptosis, control of gene expression in mitochondria, regulation of glucose, lipid and fatty acids metabolism, synthesis of ketonic bodies and regulation of chromatin structure, maintenance of telomeres and DNA repair.²⁰⁶

209

- **ADP-ribose cyclation.** Cyclic ADP-ribose (cADP-ribose) is a second messenger involved in the Ca^{2+} homeostasis. cADP-ribose stimulates the uptake of Ca^{2+} by the endoplasmatic reticulum.

1.4.2. Metabolism of nicotinamide adenine dinucleotide in cancer cells

Cancer cells grow and divide uncontrollably, without being regulated by the organism and in many cases show an accelerated rate of cell division. Rapid ATP generation to maintain energy status, increased biosynthesis of macromolecules and a tight regulation and maintenance of the redox state of the cells are the three basic needs of dividing cells. In order to maintain cell growth and division, cancer cells acquire alterations in the metabolism.²¹⁰

For example, in many cases cancer cells display an accelerated glycolysis rate, consuming an abnormal concentration of glucose and generating high quantities of NADH, which is used in the anaerobic reduction of pyruvate to produce some aminoacids, lipids and nucleotide precursors (Warburg effect).²¹⁰⁻²¹²

As a result of the abnormal accelerated metabolism, together with the effect of the immune response from the body, cancer cells generate elevated levels of reactive oxygen and nitrogen species (ROS, RNS) and they are in a state of constant oxidative stress.²¹⁰

ROS are essential molecules since they perform some bactericidal activities and they are involved in signal transduction pathways, regulating cell growth and redox state of the

cell. A moderate increase of ROS production may stimulate cell division and proliferation. However, high levels of ROS can be toxic to cells. For example, elevated ROS levels are usually a cause of DNA damage.²¹⁰ In order to maintain optimum levels of ROS, a tight regulation of the oxidative stress in cancer cells is necessary. The concentrations of ROS in tumour cells must be compensated with that of antioxidants, ROS scavengers or enzymes that react with ROS.²¹⁰ Small changes in the redox state of the malignant cells might lead to cell death.

In general, cancer cells require high levels of NADH as a substrate for enzymatic reactions. However, the ratio of NAD^+/NADH must be tightly controlled to avoid cell death by oxidative stress.^{211, 212} An excess of NADH, might also lead to inhibition of some of the abnormal metabolic processes which generate NADH

Manipulating intracellular balance of NAD^+/NADH , reducing the levels of NAD^+ and destabilizing the redox balance of the cell, can be a suitable strategy for anticancer therapy.

Recently, regulation of the NAD^+ levels has been investigated for the treatment of cancer and some other diseases.^{200, 213-215} For example, FK866 is a small organic drug, currently in clinical trials, which can stop the biosynthesis of NAD^+ by inhibition of nicotinamide phosphoribosyl transferase.²¹⁶ Other drugs in clinical trials, such as 2-deoxyglucose, 3-bromopyruvate or TLN232, inhibit the glycolysis process by blocking the active side of hexokinase or pyruvate kinase.²¹²

1.5. Previous work on transfer hydrogenation reactions with NAD⁺

Chemical, electrochemical, photochemical and enzymatic methods for the regeneration of NADH or regeneration of NAD⁺ have been intensively studied for many years.²¹⁷ However, for the interest of this thesis, this section will be focussed on the chemical methods, and more specifically, hydrogenation and transfer hydrogenation reactions.

In the field of hydrogenation and transfer hydrogenation reactions, the regeneration of NADH has been studied mainly for applications in enzymatic reduction of ketones for organic synthesis.²¹⁷ The first series of complexes capable of reducing NAD⁺ to NADH via transfer hydrogenation was discovered by Steckhan *et al.* His group published the synthesis and catalytic properties of a series of Rh(III) bipyridine complexes.²¹⁸ The most successful compound was [(Cp*)Rh(bipy)Cl]⁺, and its mechanism of action and possible applications were very well studied by Fish *et al.*²¹⁹⁻²²⁴ Furthermore, the complex has been extensively studied by many groups.^{225, 226}

Süss-Fink *et al.* published in 2007 the catalytic reduction of NAD⁺ by using a series of Ru(II), Rh(III) and Ir(III) phenanthroline-containing catalysts.²²⁷ The complex [(Cp*)Rh(phen)Cl]⁺ was capable of conversions and turnover frequencies of up to twice that obtained previously with [(Cp*)Rh(bipy)Cl]⁺ in aqueous media, at 333 K and pH 7.²²⁷ Sadler *et al.* group the catalytic regeneration of 1,4-NADH with some Ru(II) complexes containing ethylenediamine or acetylacetonate was studied. However, the turnover frequencies were relatively low compared to the literature values.¹⁰⁸ In 2011, Salmain *et al.* published a series of Rh(III) and Ru(II) complexes using dipyriddy amine ligands functionalised by maleimide. The complexes were not as active as the bipyridine-containing complex [(Cp*)Rh(bipy)Cl]⁺. However, similar turnover frequencies and conversions were achieved with one of their

Rh(III) complexes.²²⁸ More recently the complex [(Cp*)Ir(4-(1*H*-pyrazol-1-yl- κ N²)benzoic acid κ C³)H₂O)]₂SO₄ synthesized by Fukuzumi *et al.* was reported to catalyze H₂ oxidation while generating NADH by using a neutral and slightly basic media.²²⁹ Hollmann *et al.* published in 2012 a tethered Rh(III) complex containing an analogue of Noyori ligand (TsDPEN) immobilised in a poly(ethylene) polimner.²³⁰ The catalytic activity of the heterogeneous catalyst was shown to be lower than that of other soluble Rh(II) complexes.

The regeneration of NAD⁺ has also been achieved by transfer hydrogenation. In 2011, a series of water-soluble iron(III) porphyrins was synthesised and used for oxidation on NADH, using O₂ as an electron catcher.²¹⁷ Fukuzumi *et al.* presented the regeneration of NADH using [(Cp*)Ir(4-(1*H*-pyrazol-1-yl- κ N²)benzoic acid κ C³)H₂O)]₂SO₄ and H₂ when at neutral pH. However, the same compound can also react with NADH to give NAD⁺ in acidic conditions (pH \approx 3). Mechanistic studies on this catalytic system are currently being carried out. Finally, a series of [(η^6 -arene)Ru(bpm)Cl]⁺ and [Cp^xIr(phen)H₂O]²⁺ were shown to be able to use NADH as a hydride donor for transfer hydrogenation reaction.¹⁰⁹ The Ir(III) compounds have recently been shown to perform transfer hydrogenation reactions *in vitro*.¹¹⁰

1.6. Aims

The overall aim of this thesis is concerned with the rational design of catalytic organometallic drugs which can reduce nicotinamide adenine dinucleotide (NAD⁺) under biologically relevant conditions. The aims of each individual chapters are as follows

- Study the catalytic properties and mechanism of a series of Ru(II) complexes containing monosulfonamide ethyleneamine ligands towards the reduction of NAD⁺ by transfer hydrogenation using sodium formate as a hydride source

- Investigate the possibility to perform the catalytic reaction in cells by administering the complex to A2780 ovarian cancer cells, in combination of sodium formate
- Explore the potential of Ru(II) complexes containing monosulfonamide ethyleneamine ligands, to interact with DNA
- Explore the potential of Ru(II) complexes containing monosulfonamide ethyleneamine ligands, to interact with GSH
- Explore the possibility to increase the catalytic activity of the complexes containing monosulfonamide ethyleneamine ligand towards reduction of NAD^+ by changing the $(\eta^6\text{-arene})\text{Ru(II)}$ system to $(\text{Cp}^{\text{X}})\text{Rh(III)}$

1.7. References

- (1) Patrick, G. L. *An introduction to medicinal chemistry*; 4th ed.; Oxford University Press: New York, **2009**.
- (2) Sekhon, B. S. *J. Pharm. Educ. Res.* **2011**, *2*, 1-20.
- (3) Thompson, K. H.; Orvig, C. *Dalton Trans.* **2006**, 761-764.
- (4) Rosenberg, B.; Van Camp, L.; Trosko, J. E.; Mansour, V. H. *Nature* **1969**, *222*, 385-386.
- (5) Rosenberg, B.; Van Camp, L.; Krigas, T. *Nature* **1965**, *205*, 698-699.
- (6) Todd, R. C.; Lippard, S. J. *Metallomics* **2009**, *1*, 280-291.
- (7) Kelland, L. *Nature Rev. Cancer* **2007**, *7*, 573-584.
- (8) Zhu, G.; Song, L.; Lippard, S. J. *Cancer Res.* **2013**, *73*, 4451-4460.
- (9) Sancho-Martínez, S. M.; Prieto-García, L.; Prieto, M.; López-Novoa, J. M.; López-Hernández, F. J. *Pharmacol. Ther.* **2012**, *136*, 35-55.
- (10) Boulikas, T. *Cancer Therapy* **2007**, *5*, 351-376.

- (11) Shen, D.-W.; Pouliot, L. M.; Hall, M. D.; Gottesman, M. M. *Pharmacol. Rev.* **2012**, *64*, 706-721.
- (12) Reedijk, J. *Eur. J. Inorg. Chem.* **2009**, *2009*, 1303-1312.
- (13) Abu-Surrah, A. S.; M., K. *Cur. Med. Chem.* **2006**, *13*, 1337-1357.
- (14) Wheate, N. J.; Walker, S.; Craig, G. E.; Oun, R. *Dalton Trans.* **2010**, *39*, 8113-8127.
- (15) Mackay, F. S.; Woods, J. A.; Heringová, P.; Kašpárková, J.; Pizarro, A. M.; Moggach, S. A.; Parsons, S.; Brabec, V.; Sadler, P. J. *Proc. Natl. Acad. Sci. U. S. A.* **2007**, *104*, 20743-20748.
- (16) Hall, M. D.; Hambley, T. W. *Coord. Chem. Rev.* **2002**, *232*, 49-67.
- (17) Harper, B. W.; Krause-Heuer, A. M.; Grant, M. P.; Manohar, M.; Garbutcheon-Singh, K. B.; Aldrich-Wright, J. R. *Chem. Eur. J.* **2010**, *16*, 7064-7077.
- (18) Bruijninx, P. C. A.; Sadler, P. J. In *Advances in inorganic chemistry*; 1st ed.; Academic Press: **2009**; Volume 61, 1-62.
- (19) Durig, J. R.; Danneman, J.; Behnke, W. D.; Mercer, E. E. *Chem.-Biol. Interact.* **1976**, *13*, 287-294.
- (20) Clarke, M. J. *J. Am. Chem. Soc.* **1978**, *100*, 5068-5075.
- (21) Clarke, M. J.; Taube, H. *J. Am. Chem. Soc.* **1974**, *96*, 5413-5419.
- (22) Clarke, M. J.; Bitler, S.; Rennert, D.; Buchbinder, M.; Kelman, A. D. *J. Inorg. Biochem.* **1980**, *12*, 79-87.
- (23) Clarke, M. J. *Coord. Chem. Rev.* **2003**, *236*, 209-233.
- (24) Kelman, A. D.; Clarke, M. J.; Edmonds, S. E.; Peresie, H. J. *J. Clin. Hematol. Oncol.* **1977**, *7*, 274-288.
- (25) Pieper, T.; Keppler, B., K. *Analisis* **1998**, *26*, 84-90.
- (26) Keppler, B. K.; Rupp, W.; Juhl, U. M.; Endres, H.; Niebl, R.; Balzer, W. *Inorg. Chem.* **1987**, *26*, 4366-4370.

- (27) Sava, G.; Pacor, S.; Zorzet, S.; Alessio, E.; Mestroni, G. *Pharmacol. Res.* **1989**, *21*, 617-628.
- (28) Bergamo, A.; Gaiddon, C.; Schellens, J. H. M.; Beijnen, J. H.; Sava, G. *J. Inorg. Biochem.* **2012**, *106*, 90-99.
- (29) Goswami, S.; Chakravarty, A. R.; Chakravorty, A. *Inorg. Chem.* **1983**, *22*, 602-609.
- (30) Hotze, A. C. G.; Velders, A. H.; Ugozzoli, F.; Biagini-Cingi, M.; Manotti-Lanfredi, A. M.; Haasnoot, J. G.; Reedijk, J. *Inorg. Chem.* **2000**, *39*, 3838-3844.
- (31) Velders, A. H.; Kooijman, H.; Spek, A. L.; Haasnoot, J. G.; de Vos, D.; Reedijk, J. *Inorg. Chem.* **2000**, *39*, 2966-2967.
- (32) Suss-Fink, G. *Dalton Trans.* **2010**, *39*, 1673-1688.
- (33) Jungwirth, U.; Kowol, C. R.; Keppler, B. K.; Hartinger, C. G.; Berger, W.; P., H. *Antioxid. Redox Signaling* **2011**, *15*, 1085-1127.
- (34) Farrell, N. In *Comprehensive Coordination Chemistry II*; 2nd ed.; Elsevier Science Ltd: **2003**; *9*, 809-840.
- (35) Lainé, A.-L.; Passirani, C. *Curr. Opin. Pharmacol.* **2012**, *12*, 420-426.
- (36) Barry, N. P. E.; Sadler, P. J. *Chem. Commun.* **2013**, *49*, 5106-5131.
- (37) Köpf-Maier, P.; Köpf, H.; Neuse, E. W. *Angew. Chem. Int. Ed.* **1984**, *23*, 456-457.
- (38) Osella, D.; Ferrali, M.; Zanello, P.; Laschi, F.; Fontani, M.; Nervi, C.; Cavigliolo, G. *Inorg. Chim. Acta.* **2000**, *306*, 42-48.
- (39) van Staveren, D. R.; Metzler-Nolte, N. *Chem. Rev.* **2004**, *104*, 5931-5986.
- (40) Hanzlik, R. P.; Soine, W. H. *J. Am. Chem. Soc.* **1978**, *100*, 1290-1291.
- (41) Gasser, G.; Ott, I.; Metzler-Nolte, N. *J. Med. Chem.* **2010**, *54*, 3-25.
- (42) Braga, S. S.; Silva, A. M. S. *Organometallics* **2013**, *32*, 5626-5639.
- (43) Vessières, A.; Corbet, C.; Heldt, J. M.; Lories, N.; Jouy, N.; Laïos, I.; Leclercq, G.; Jaouen, G.; Toillon, R.-A. *J. Inorg. Biochem.* **2010**, *104*, 503-511.

- (44) Hillard, E.; Vessières, A.; Thouin, L.; Jaouen, G.; Amatore, C. *Angew. Chem. Int. Ed.* **2006**, *45*, 285-290.
- (45) Köpf-Maier, P. *Eur. J. Clin. Pharmacol.* **1994**, *47*, 1-16.
- (46) Meléndez, E. *Crit. Rev. Oncol. Hematol.* **2002**, *42*, 309-315.
- (47) Allen, O. R.; Gott, A. L.; Hartley, J. A.; Hartley, J. M.; Knox, R. J.; McGowan, P. C. *Dalton Trans.* **2007**, 5082-5090.
- (48) Allen, O. R.; Croll, L.; Gott, A. L.; Knox, R. J.; McGowan, P. C. *Organometallics* **2003**, *23*, 288-292.
- (49) Strohfeldt, K.; Tacke, M. *Chem. Soc. Rev.* **2008**, *37*, 1174-1187.
- (50) Wang, F.; Chen, H.; Parsons, S.; Oswald, I. D. H.; Davidson, J. E.; Sadler, P. J. *Chem. Eur. J.* **2003**, *9*, 5810-5820.
- (51) Wang, F.; Habtemariam, A.; van der Geer, E. P. L.; Fernández, R.; Melchart, M.; Deeth, R. J.; Aird, R.; Guichard, S.; Fabbiani, F. P.; Lozano-Casal, P.; Oswald, I. D. H.; Jodrell, D. I.; Parsons, S.; Sadler, P. J. *Proc. Natl. Acad. Sci. U. S. A.* **2005**, *102*, 18269-18274.
- (52) Yan, Y. K.; Melchart, M.; Habtemariam, A.; Sadler, P. J. *Chem. Commun.* **2005**, 4764-76.
- (53) Liu, H.-K.; Wang, F.; Parkinson, J. A.; Bella, J.; Sadler, P. J. *Chem. Eur. J.* **2006**, *12*, 6151-6165.
- (54) Aird, R. E.; Cummings, J.; Ritchie, A. A.; Muir, M.; Morris, R. E.; Chen, H.; Sadler, P. J.; Jodrell, D. I. *Brit. J. Cancer* **2002**, *86*, 1652 - 1657.
- (55) Bugarcic, T.; Nováková, O.; Halámiková, A.; Zerzánková, L.; Vrána, O.; Kaspárková, J.; Habtemariam, A.; Parsons, S.; Sadler, P. J.; Brabec, V. *J. Med. Chem.* **2008**, *51*, 5310-9.
- (56) Chen, H.; Parkinson, J. A.; Morris, R. E.; Sadler, P. J. *J. Am. Chem. Soc.* **2003**, 173-186.
- (57) Allardyce, C. S.; Dyson, P. J.; Ellis, D. J.; Heath, S. L. *Chem. Commun.* **2001**, 1396-1397.

- (58) Liu, Z.; Habtemariam, A.; Pizarro, A. M.; Fletcher, S. A.; Kisova, A.; Vrana, O.; Salassa, L.; Bruijninx, P. C. A.; Clarkson, G. J.; Brabec, V.; Sadler, P. J. *J. Med. Chem.* **2011**, *54*, 3011-3026.
- (59) Peacock, A. F. A.; Habtemariam, A.; Fernández, R.; Walland, V.; Fabbiani, F. P. A.; Parsons, S.; Aird, R. E.; Duncan, I.; Sadler, P. J. *J. Am. Chem. Soc.* **2006**, *128*, 1739-1748.
- (60) Peacock, A. F. A.; Melchart, M.; Deeth, R. J.; Habtemariam, A.; Parsons, S.; Sadler, P. *J. Chem. Eur. J.* **2007**, *13*, 2601 - 2613.
- (61) van Rijt, S. H.; Peacock, A. F. A.; Johnstone, R. D. L.; Parsons, S.; Sadler, P. J. *Inorg. Chem.* **2009**, *48*, 1753-62.
- (62) Liu, H.-K.; Berners-Price, S. J.; Wang, F.; Parkinson, J. A.; Xu, J.; Bella, J.; Sadler, P. J. *Angew. Chem. Int. Ed.* **2006**, *45*, 8153-8156.
- (63) Hearn, J. M.; Romero-Canelón, I.; Qamar, B.; Liu, Z.; Hands-Portman, I.; Sadler, P. J. *ACS Chem. Biol.* **2013**, *8*, 1335-1343.
- (64) Yellol, G. S.; Donaire, A.; Yellol, J. G.; Vasylyeva, V.; Janiak, C.; Ruiz, J. *Chem. Commun.* **2013**, *49*, 11533-11535.
- (65) Raja, M. U.; Tauchman, J.; Therrien, B.; Süß-Fink, G.; Riedel, T.; Dyson, P. J. *Inorg. Chim. Acta.* **2014**, *409*, Part B, 479-483.
- (66) Almodares, Z.; Lucas, S. J.; Crossley, B. D.; Batri, A. M.; Pask, C. M.; Hebden, A. J.; Phillips, R. M.; McGowan, P. C. *Inorg. Chem.* **2014**, *53*, 727-736.
- (67) Chen, H.; Parkinson, J. A.; Nováková, O.; Bella, J.; Wang, F.; Dawson, A.; Gould, R.; Parsons, S.; Brabec, V.; Sadler, P. J. *Proc. Natl. Acad. Sci. U. S. A.* **2003**, *100*, 14623-14628.
- (68) Gossens, C.; Dorcier, A.; Dyson, P. J.; Rothlisberger, U. *Organometallics* **2007**, *26*, 3969-3975.
- (69) Schäfer, S.; Ott, I.; Gust, R.; Sheldrick, W. S. *Eur. J. Inorg. Chem.* **2007**, *2007*, 3034-3046.

- (70) Casini, A.; Gabbiani, C.; Michelucci, E.; Pieraccini, G.; Moneti, G.; Dyson, P.; Messori, L. *J. Biol. Inorg. Chem.* **2009**, *14*, 761-770.
- (71) Casini, A.; Hartinger, C. G.; Nazarov, A. A.; Dyson, P. In *Medicinal Organometallic Chemistry*; 1st ed.; Springer Berlin Heidelberg, **2010**; 57-80.
- (72) Casini, A.; Mastrobuoni, G.; Ang, W. H.; Gabbiani, C.; Pieraccini, G.; Moneti, G.; Dyson, P. J.; Messori, L. *ChemMedChem* **2007**, *2*, 631-635.
- (73) Melchart, M.; Sadler, P. J. *Bioorganometallics: biomolecules, labelling, medicine*; 1st ed.; Wiley VCH: Weinheim, **2006**.
- (74) Novakova, O.; Kasparikova, J.; Bursova, V.; Hofr, C.; Vojtiskova, M.; Chen, H.; Sadler, P. J.; Brabec, V. *Chem. Biol.* **2005**, *12*, 121-129.
- (75) Novakova, O.; Chen, H.; Vrana, O.; Rodger, A.; Sadler, P. J.; Brabec, V. *Biochemistry* **2003**, *42*, 11544-11554.
- (76) Wang, F.; Chen, H.; Parsons, S.; Oswald, I. D. H.; Davidson, J. E.; Sadler, P. J. *Chem. Eur. J.* **2003**, *9*.
- (77) Wang, F.; Xu, J.; Habtemariam, A.; Sadler, P. J. *J. Am. Chem. Soc.* **2005**, *127*, 17734-17743.
- (78) Wang, F.; Xu, J.; Wu, K.; Weidt, S. K.; Mackay, C. L.; Langridge-Smith, P. R. R.; Sadler, P. J. *Dalton Trans.* **2013**, *42*, 3188-3195.
- (79) Dyson, P. J.; Sava, G. *Dalton Trans.* **2006**, 1929-1933.
- (80) Ang, W. H.; Casini, A.; Sava, G.; Dyson, P. J. *J. Organomet. Chem.* **2011**, *696*, 989-998.
- (81) Chatterjee, S.; Kundu, S.; Bhattacharyya, A.; Hartinger, C.; Dyson, P. J. *J. Biol. Inorg. Chem.* **2008**, *13*, 1149-1155.
- (82) Nazarov, A. A.; Hartinger, C. G.; Dyson, P. J. *J. Organomet. Chem.* **2014**, *751*, 251-260.
- (83) Schmid, W. F.; John, R. O.; Mühlgassner, G.; Heffeter, P.; Jakupec, M. A.; Galanski, M.; Berger, W.; Arion, V. B.; Keppler, B. K. *J. Med. Chem.* **2007**, *50*, 6343-6355.

- (84) Schmid, W. F.; John, R. O.; Arion, V. B.; Jakupec, M. A.; Keppler, B. K. *Organometallics* **2007**, *26*, 6643-6652.
- (85) Ang, W. H.; Parker, L. J.; De Luca, A.; Juillerat-Jeanneret, L.; Morton, C. J.; Lo Bello, M.; Parker, M. W.; Dyson, P. J. *Angew. Chem. Int. Ed.* **2009**, *48*, 3854-3857.
- (86) Vock, C. A.; Ang, W. H.; Scolaro, C.; Phillips, A. D.; Lagopoulos, L.; Juillerat-Jeanneret, L.; Sava, G.; Scopelliti, R.; Dyson, P. J. *J. Med. Chem.* **2007**, *50*, 2166-2175.
- (87) Smalley, K. S. M.; Contractor, R.; Haass, N. K.; Kulp, A. N.; Atilla-Gokcumen, G. E.; Williams, D. S.; Bregman, H.; Flaherty, K. T.; Soengas, M. S.; Meggers, E.; Herlyn, M. *Cancer Res.* **2007**, *67*, 209-217.
- (88) Debreczeni, J. É.; Bullock, A. N.; Atilla, G. E.; Williams, D. S.; Bregman, H.; Knapp, S.; Meggers, E. *Angew. Chem. Int. Ed.* **2006**, *45*, 1580-1585.
- (89) Monnard, F. W.; Heinisch, T.; Nogueira, E. S.; Schirmer, T.; Ward, T. R. *Chem. Commun.* **2011**, *47*, 8238-8240.
- (90) Ali Nazif, M.; Bangert, J.-A.; Ott, I.; Gust, R.; Stoll, R.; Sheldrick, W. S. *J. Inorg. Biochem.* **2009**, *103*, 1405-1414.
- (91) Nazif, M. A.; Rubbiani, R.; Alborzina, H.; Kitanovic, I.; Wolf, S.; Ott, I.; Sheldrick, W. S. *Dalton Trans.* **2012**, *41*, 5587-5598.
- (92) Liu, Z.; Habtemariam, A.; Pizarro, A. M.; Clarkson, G. J.; Sadler, P. J. *Organometallics* **2011**, *30*, 4702-4710.
- (93) Liu, Z.; Salassa, L.; Habtemariam, A.; Pizarro, A. M.; Clarkson, G. J.; Sadler, P. J. *Inorg. Chem.* **2011**, *50*, 5777-5783.
- (94) Lucas, S. J.; Lord, R. M.; Wilson, R. L.; Phillips, R. M.; Sridharan, V.; McGowan, P. C. *Dalton Trans.* **2012**, *41*, 13800-13802.
- (95) Romero-Canelón, I.; Sadler, P. J. *Inorg. Chem.* **2013**, *52*, 12276-12291.
- (96) Romero-Canelón, I.; Salassa, L.; Sadler, P. J. *J. Med. Chem.* **2013**, *56*, 1291-1300.

- (97) Amouri, H.; Moussa, J.; Renfrew, A. K.; Dyson, P. J.; Rager, M. N.; Chamoreau, L.-M. *Angew. Chem. Int. Ed.* **2010**, *49*, 7530-7533.
- (98) Hocharoen, L.; Cowan, J. A. *Chem. Eur. J.* **2009**, *15*, 8670-8676.
- (99) Li, J.; Chen, P. R. *ChemBioChem* **2012**, *13*, 1728-1731.
- (100) Noffke, A. L.; Habtemariam, A.; Pizarro, A. M.; Sadler, P. J. *Chem. Commun.* **2012**, *48*, 5219-5246.
- (101) Sasmal, P. K.; Streu, C. N.; Meggers, E. *Chem. Commun.* **2013**, *49*, 1581-1587.
- (102) Josefsen, L. B.; Boyle, R. W. *Metal-Based Drugs* **2008**, 2008.
- (103) Holder, A. A.; Taylor, P.; Magnusen, A. R.; Moffett, E. T.; Meyer, K.; Hong, Y.; Ramsdale, S. E.; Gordon, M.; Stubbs, J.; Seymour, L. A.; Acharya, D.; Weber, R. T.; Smith, P. F.; Dismukes, G. C.; Ji, P.; Menocal, L.; Bai, F.; Williams, J. L.; Cropek, D. M.; Jarrett, W. L. *Dalton Trans.* **2013**, *42*, 11881-11899.
- (104) Liochev, S. I. *Chem. Res. Toxicol.* **2013**, *26*, 1312-1319.
- (105) Salvemini, D.; Wang, Z.-Q.; Zweier, J. L.; Samouilov, A.; Macarthur, H.; Misko, T. P.; Currie, M. G.; Cuzzocrea, S.; Sikorski, J. A.; Riley, D. P. *Science* **1999**, *286*, 304-306.
- (106) Filipović, M. R.; Koh, A. C. W.; Arbault, S.; Niketić, V.; Debus, A.; Schleicher, U.; Bogdan, C.; Guille, M.; Lemaître, F.; Amatore, C.; Ivanović-Burmazović, I. *Angew. Chem. Int. Ed.* **2010**, *49*, 4228-4232.
- (107) Dougan, S. J.; Habtemariam, A.; McHale, S. E.; Parsons, S.; Sadler, P. J. *Proc. Natl. Acad. Sci. U. S. A.* **2008**, *105*, 11628-33.
- (108) Yan, Y. K.; Melchart, M.; Habtemariam, A.; Peacock, A. F.; Sadler, P. J. *J. Biol. Inorg. Chem.* **2006**, *11*, 483-488.
- (109) Betanzos-Lara, S.; Liu, Z.; Habtemariam, A.; Pizarro, A. M.; Qamar, B.; Sadler, P. J. *Angew. Chem. Int. Ed.* **2012**, *51*, 3897-3900.

- (110) Liu, Z.; Romero-Canelón, I.; Qamar, B.; Hearn, J. M.; Habtemariam, A.; Barry, N. P. E.; Pizarro, A. M.; Clarkson, G. J.; Sadler, P. J. *Angew. Chem. Int. Ed.* **2014**, *53*, 3941-3946.
- (111) Chae, P. S.; Kim, M.-s.; Jeung, C.-S.; Lee, S. D.; Park, H.; Lee, S.; Suh, J. *J. Am. Chem. Soc.* **2005**, *127*, 2396-2397.
- (112) Jeon, J. W.; Son, S. J.; Yoo, C. E.; Hong, I. S.; Suh, J. *Bioorg. Med. Chem.* **2003**, *11*, 2901-2910.
- (113) Jeon, J. W.; Son, S. J.; Yoo, C. E.; Hong, I. S.; Song, J. B.; Suh, J. *Org. Lett.* **2002**, *4*, 4155-4158.
- (114) Lee, J.; Yoo, S. H.; Jeong, K.; Lee, T. Y.; Ahn, J. Y.; Suh, J. *Bull. Korean Chem. Soc.* **2008**, *29*.
- (115) Suh, J.; Chei, W.; Lee, T.; Kim, M.; Yoo, S.; Jeong, K.; Ahn, J. *J. Biol. Inorg. Chem.* **2008**, *13*, 693-701.
- (116) Suh, J.; Yoo, S. H.; Kim, M. G.; Jeong, K.; Ahn, J. Y.; Kim, M.-s.; Chae, P. S.; Lee, T. Y.; Lee, J.; Lee, J.; Jang, Y. A.; Ko, E. H. *Angew. Chem. Int. Ed.* **2007**, *46*, 7064-7067.
- (117) Lee, T. Y.; Suh, J. *Chem. Soc. Rev.* **2009**, *38*, 1949-1957.
- (118) Kayed, R.; Head, E.; Thompson, J. L.; McIntire, T. M.; Milton, S. C.; Cotman, C. W.; Glabe, C. G. *Science* **2003**, *300*, 486-489.
- (119) Bradford, S.; Cowan, J. A. *Chem. Commun.* **2012**, *48*, 3118-3120.
- (120) Streu, C.; Meggers, E. *Angew. Chem. Int. Ed.* **2006**, *45*, 5645-5648.
- (121) Sasmal, P. K.; Carregal-Romero, S.; Parak, W. J.; Meggers, E. *Organometallics* **2012**, *31*, 5968-5970.
- (122) Lippert, A. R.; New, E. J.; Chang, C. J. *J. Am. Chem. Soc.* **2011**, *133*, 10078-10080.
- (123) Sasmal, P. K.; Carregal-Romero, S.; Han, A. A.; Streu, C. N.; Lin, Z.; Namikawa, K.; Elliott, S. L.; Köster, R. W.; Parak, W. J.; Meggers, E. *ChemBioChem* **2012**, *13*, 1116-1120.

- (124) Wang, Q.; Chan, T. R.; Hilgraf, R.; Fokin, V. V.; Sharpless, K. B.; Finn, M. G. *J. Am. Chem. Soc.* **2003**, *125*, 3192-3193.
- (125) Yusop, R. M.; Unciti-Broceta, A.; Johansson, E. M. V.; Sánchez-Martín, R. M.; Bradley, M. *Nature Chem.* **2011**, *3*, 239-243.
- (126) Chalker, J. M.; Wood, C. S. C.; Davis, B. G. *J. Am. Chem. Soc.* **2009**, *131*, 16346-16347.
- (127) Spicer, C. D.; Triemer, T.; Davis, B. G. *J. Am. Chem. Soc.* **2011**, *134*, 800-803.
- (128) Davis, L.; Chin, J. W. *Nature Rev. Mol. Cell Biol.* **2012**, *13*, 168-182.
- (129) Li, N.; Lim, R. K. V.; Edwardraja, S.; Lin, Q. *J. Am. Chem. Soc.* **2011**, *133*, 15316-15319.
- (130) Hanzlik, R. P.; Fowler, S. C.; Eells, J. T. *Drug Metab. Dispos.* **2005**, *33*, 282-286.
- (131) Sodium formate. (24/12/2013),
<http://www.accessdata.fda.gov/scripts/cfn/fcnDetailNavigation.cfm?rpt=scogsListing&id=297>
- (132) Chelucci, G.; Orrù, G.; Pinna, G. A. *Tetrahedron* **2003**, *59*, 9471-9515.
- (133) Noyori, R.; Ohkuma, T. *Pure Appl. Chem.* **1999**, *71*, 1493-1501.
- (134) Noyori, R.; Ohkuma, T. *Angew. Chem. Int. Ed.* **2001**, *40*, 40-73.
- (135) Türkmen, H. *Appl. Organomet. Chem.* **2012**, *26*, 731-735.
- (136) Maeda, T.; Makino, K.; Iwasaki, M.; Hamada, Y. *Chem. Eur. J.* **2010**, *16*, 11954-62.
- (137) Dykeman, R. R.; Luska, K. L.; Thibault, M. E.; Jones, M. D.; Schlaf, M.; Khanfar, M.; Taylor, N. J.; Britten, J. F.; Harrington, L. *J. Mol. Catal. A: Chemical* **2007**, *277*, 233-251.
- (138) Chelucci, G.; Thummel, R. P. *Chem. Rev.* **2002**, *102*, 3129-3170.
- (139) Ghosh, A. K.; Mathivanan, P.; Cappiello, J. *Tetrahedron: Asymmetry* **1998**, *9*, 1-45.
- (140) Helmchen, G.; Pfaltz, A. *Acc. Chem. Res.* **2000**, *33*, 336-345.
- (141) Gamez, P.; Fache, F.; Lemaire, M. *Tetrahedron: Asymmetry* **1995**, *6*, 705-718.

- (142) Vázquez-Villa, H.; Reber, S.; Ariger, M. A.; Carreira, E. M. *Angew. Chem. Int. Ed.* **2011**, *50*, 8979-8981.
- (143) Krasik, P.; Alper, H. *Tetrahedron* **1994**, *50*, 4347-4354.
- (144) Warner, M.; Casey, C.; Bäckvall, J.-E. In *Bifunctional Molecular Catalysis*; 1st ed.; Springer Berlin Heidelberg: **2011**; *37*, 85-125.
- (145) Noyori, R.; Hashiguchi, S. *Acc. Chem. Res.* **1997**, *30*, 97-102.
- (146) Cross, D. J.; Houson, I.; Kawamoto, A. M.; Wills, M. *Tetrahedron Lett.* **2004**, *45*, 843-846.
- (147) Nordin, S. J. M.; Roth, P.; Tarnai, T.; Alonso, D. A.; Brandt, P.; Andersson, P. G. *Chem. Eur. J.* **2001**, *7*, 1431-1436.
- (148) Pablo, Ó.; Guijarro, D.; Yus, M. *Appl. Sci.* **2012**, *2*, 1-12.
- (149) Palmer, M. J.; Kenny, J. A.; Walsgrove, T.; Kawamoto, A. M.; Wills, M. *J. Chem. Soc., Perkin Trans. 1* **2002**, 416-427.
- (150) Wills, M.; Palmera, M.; Smitha, A.; Kennya, J.; Walsgroveb, T. *Molecules* **2000**, *5*, 4-18.
- (151) Takehara, J.; Hashiguchi, S.; Fujii, A.; Inoue, S.-i.; Ikariya, T.; Noyori, R. *Chem. Commun.* **1996**, 233-234.
- (152) Zhou, Z.; Wu, L. *Catal. Commun.* **2008**, *9*, 2539-2542.
- (153) Rhyoo, H. Y.; Yoon, Y.-A.; Park, H.-J.; Chung, Y. K. *Tetrahedron Lett.* **2001**, *42*, 5045-5048.
- (154) Rhyoo, H. Y.; Park, H.-J.; Suh, W. H.; Chung, Y. K. *Tetrahedron Lett.* **2002**, *43*, 269-272.
- (155) Mao, J.; Guo, J. *Chirality* **2010**, *22*, 173-181.
- (156) Shohei Hashiguchi, A. F., Jun Takehara, Takao Ikariya, and Ryoji Noyon *J. Am. Chem. Soc.* **1995**, *117*, 7562-7563.

- (157) Murata, K.; Ikariya, T.; Noyori, R. *J. Org. Chem.* **1999**, *64*, 2186-2187.
- (158) Gladiali, S.; Alberico, E. *Chem. Soc. Rev.* **2006**, *35*, 226-236.
- (159) Gladiali, S.; Alberico, E. In *Transition Metals for Organic Synthesis*; 2nd ed.; Wiley-VCH: **2004**; *2*, 145-166.
- (160) Baker, D. C.; Mao, J. *Org. Lett.* **1999**, *1*, 841-843.
- (161) Uematsu, N.; Fujii, A.; Hashiguchi, S. *J. Am. Chem. Soc.* **1996**, *118*, 4916-4917.
- (162) Xue, D.; Chen, Y.-C.; Cui, X.; Wang, Q.-W.; Zhu, J.; Deng, J.-G. *J. Org. Chem.* **2005**, *70*, 3584-91.
- (163) Wu, X.; Li, X.; Hems, W.; King, F.; Xiao, J. *Org. Biomol. Chem.* **2004**, *2*, 1818-1821.
- (164) Püntener, K.; Schwink, L.; Knochel, P. *Tetrahedron Lett.* **1996**, *37*, 8165-8168.
- (165) Wu, X.; Vinci, D.; Ikariya, T.; Xiao, J. *Chem. Commun.* **2005**, 4447-4449.
- (166) Shirai, S.; Nara, H.; Kayaki, Y.; Ikariya, T. *Organometallics* **2009**, *28*, 802-809.
- (167) Soni, R.; Jolley, K. E.; Clarkson, G. J.; Wills, M. *Org. Lett.* **2013**, *15*, 5110-5113.
- (168) Hannedouche, J.; Clarkson, G. J.; Wills, M. *J. Am. Chem. Soc.* **2004**, *126*, 986-987.
- (169) Hayes, A. M.; Morris, D. J.; Clarkson, G. J.; Wills, M. *J. Am. Chem. Soc.* **2005**, *127*, 7318-7319.
- (170) Morris, D. J.; Hayes, A. M.; Wills, M. *J. Org. Chem.* **2006**, *71*, 7035-7044.
- (171) Matharu, D. S.; Morris, D. J.; Clarkson, G. J.; Wills, M. *Chem. Commun.* **2006**, 3232-3234.
- (172) Haack, K. J.; Hashiguchi, S.; Fujii, A.; Ikariya, T.; Noyori, R. *Angew. Chem. Int. Ed.* **1997**, *36*, 285-288.
- (173) Casey, C. P.; Johnson, J. B. *J. Org. Chem.* **2003**, *68*, 1998-2001.
- (174) Yamakawa, M.; Ito, H.; Noyori, R. *J. Am. Chem. Soc.* **2000**, *122*, 1466-1478.
- (175) Gao, J.-X.; Ikariya, T.; Noyori, R. *Organometallics* **1996**, *15*, 1087-1089.
- (176) Koike, T.; Ikariya, T. *Adv. Synth. Catal.* **2004**, *346*, 37-41.

- (177) Soni, R.; Cheung, F. K.; Clarkson, G. C.; Martins, J. E. D.; Grahamb, M. A.; Wills, M. *Org. Biomol. Chem.* **2011**, *9*, 3290-3294.
- (178) Martins, J. E. D.; Clarkson, G. J.; Wills, M. *Org. Lett.* **2009**, *11*, 847-850.
- (179) Wu, X.; Li, X.; King, F.; Xiao, J. *Angew. Chem. Int. Ed.* **2005**, *44*, 3407-3411.
- (180) Robertson, A.; Matsumoto, T.; Ogo, S. *Dalton Trans.* **2011**, *40*, 10304-10310.
- (181) Wu, X.; Wang, C.; Xiao, J. *Plat. Met. Rev.* **2010**, *54*, 3-19.
- (182) Chanda, A.; Fokin, V. V. *Chem. Rev.* **2009**, *109*, 725-48.
- (183) Bubert, C.; Blacker, J.; Brown, S. M.; Crosby, J.; Fitzjohn, S.; Muxworthy, J. P.; Thorpe, T.; Williams, J. M. J. *Tetrahedron Lett.* **2001**, *42*, 4037-4039.
- (184) Tang, Y.; Li, X.; Lian, C.; Zhu, J.; Deng, J. *Tetrahedron: Asymmetry* **2011**, *22*, 1530-1535.
- (185) Wu, J.; Wang, F.; Ma, Y.; Cui, X.; Cun, L.; Zhu, J.; Deng, J.; Yu, B. *Chem. Commun.* **2006**, 1766-1768.
- (186) Virboul, M. A. N.; Klein Gebbink, R. J. M. *Organometallics* **2011**, *31*, 85-91.
- (187) Li, L.; Wu, J.; Wang, F.; Liao, J.; Zhang, H.; Lian, C.; Zhu, J.; Deng, J. *Green Chem.* **2007**, *9*, 23-25.
- (188) Zhou, Z.; Ma, Q.; Sun, Y.; Zhang, A. *Heteroat. Chem.* **2010**, *21*, 505-514.
- (189) Zhou, Z.; Ma, Q.; Zhang, A.; Wu, L. *Appl. Organomet. Chem.* **2011**, 556-561.
- (190) Canivet, J.; Labat, G.; Stoeckli-Evans, H.; Süss-Fink, G. *Eur. J. Inorg. Chem.* **2005**, *2005*, 4493-4500.
- (191) Canivet, J.; Suss-Fink, G. *Green chem.* **2007**, *9*, 391-397.
- (192) Li, X.; Wu, X.; Chen, W.; Hancock, F. E.; King, F.; Xiao, J. *Org. Lett.* **2004**, *6*, 3321-3324.
- (193) Zhou, Z.; Ma, Q.; Zhang, A.; Wu, L. *Appl. Organomet. Chem.* **2011**, n/a-n/a.

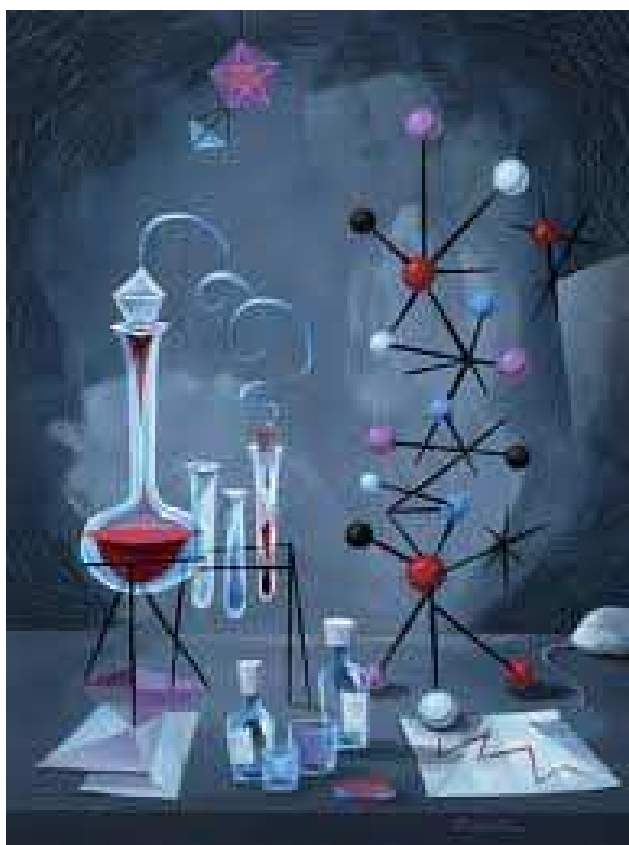
- (194) Li, X.; Li, L.; Tang, Y.; Zhong, L.; Cun, L.; Zhu, J.; Liao, J.; Deng, J. *J. Org. Chem.* **2010**, *75*, 2981-2988.
- (195) Wu, X.; Liu, J.; Li, X.; Zanotti-Gerosa, A.; Hancock, F.; Vinci, D.; Ruan, J.; Xiao, J. *Angew. Chem. Int. Ed.* **2006**, *45*, 6718-22.
- (196) Ward, T. R. *Acc. Chem. Res.* **2011**, *44*, 47-57.
- (197) Letondor, C.; Pordea, A.; Humbert, N.; Ivanova, A.; Mazurek, S.; Novic, M.; Ward, T. *R. J. Am. Chem. Soc.* **2006**, *128*, 8320-8328.
- (198) Václavík, J.; Kačer, P.; Kuzma, M.; Červený, L. *Molecules* **2011**, *16*, 5460-5495.
- (199) Wang, C.; Villa-Marcos, B.; Xiao, J. *Chem. Commun.* **2011**, *47*, 9773-9785.
- (200) Lin, S.-J.; Guarente, L. *Curr. Opin. Cell Biol.* **2003**, *15*, 241-246.
- (201) Ying, W. *Front. Biosci.* **2006**, *1*, 3129-3148.
- (202) Matthew, C. K.; Ahern, K. G.; Van Holde, K. E. *Biochemistry*; 3rd ed.; Pearson Educacion: Madrid, **2002**.
- (203) Ying, W. *Antioxid. Redox Signaling* **2008**, *10*, 179-206.
- (204) Schafer, F. Q.; Buettner, G. *Free Radic. Biol. Med.* **2001**, *30*, 1191-1212.
- (205) Houtkooper, R. H.; Canto, C.; Wanders, R. J.; Auwerx, J. *Endocr. Rev.* **2010**, *31*, 194-223.
- (206) Hassa, P. O.; Haenni, S. S.; Elsser, M.; Hottiger, M. O. *Microbiol. Mol. Biol. Rev.* **2006**, *70*, 789-826.
- (207) Schreiber, V.; Dantzer, F.; Ame, J. C.; de Murcia, G. *Nature rev.* **2006**, *7*, 517-528.
- (208) Gibson, B. A.; Kraus, W. L. *Nature rev.* **2012**, *13*, 411-424.
- (209) Houtkooper, R. H.; Pirinen, E.; Auwerx, J. *Nature Rev.* **2012**, *13*, 225-238.
- (210) Cairns, R. A.; Harris, I. S.; Mak, T. W. *Nature Rev.* **2011**, *11*, 85-95.
- (211) Chiarugi, A.; Dölle, C.; Felici, R.; Ziegler, M. *Nature Rev.* **2012**, *12*, 741-752.
- (212) Tennant, D. A.; Durán, R. V.; Gottlieb, E. *Nature Rev.* **2010**, *10*, 267-277.

- (213) Massudi, H.; Grant, R.; Braidy, N.; Guest, J.; Farnsworth, B.; Guillemin, G. J. *PloS one* **2012**, *7*, e42357.
- (214) Belenky, P.; Bogan, K. L.; Brenner, C. *Trends Biochem. Sci.* **2007**, *32*, 12-19.
- (215) Houtkooper, R. H.; Auwerx, J. J. *Cell Biol.* **2012**, *199*, 205-209.
- (216) Hasmann, M.; Schemainda, I. *Cancer Res.* **2003**, *63*, 7436-7442.
- (217) Wu, H.; Tian, C.; Song, X.; Liu, C.; Yang, D.; Jiang, Z. *Green Chem.* **2013**, *15*, 1773-1789.
- (218) Ruppert, R.; Herrmann, S.; Steckhan, E. *Chem. Commun.* **1988**, 1150-1151.
- (219) Lo, H. C.; Leiva, C.; Buriez, O.; Kerr, J. B.; Olmstead, M. M.; Fish, R. H. *Inorg. Chem.* **2001**, *40*, 6705-6716.
- (220) Leiva, C.; Lo, H. C.; Fish, R. H. *J. Organomet. Chem.* **2010**, *695*, 145-150.
- (221) Fish, R. H. *Aust. J. Chem.* **2010**, *63*, 1505-1513.
- (222) Lutz, J.; Hollmann, F.; Ho, T. V.; Schnyder, A.; Fish, R. H.; Schmid, A. *J. Organomet. Chem.* **2004**, *689*, 4783-4790.
- (223) Lo, H. C.; Fish, R. H. *Angew. Chem. Int. Ed.* **2002**, *41*, 478-481.
- (224) Buriez, O.; Kerr, J.; Fish, R. *Angew. Chem. Int. Ed.* **1999**, *38*, 1997-2000.
- (225) Hollmann, F.; Witholt, B.; Schmid, A. *J. Mol. Catal. B: Enzymatic* **2002**, *19-20*, 167-176.
- (226) Grau, M. M.; Poizat, M.; Arends, I. W. C. E.; Hollmann, F. *Appl. Organomet. Chem.* **2010**, *24*, 380-385.
- (227) Canivet, J.; Süß-Fink, G.; Štěpnička, P. *Eur. J. Inorg. Chem.* **2007**, 4736-4742.
- (228) Haquette, P.; Talbi, B.; Barilleau, L.; Madern, N.; Fosse, C.; Salmain, M. *Org. Biomol. Chem.* **2011**, *9*, 5720-5727.
- (229) Maenaka, Y.; Suenobu, T.; Fukuzumi, S. *J. Am. Chem. Soc.* **2012**, *134*, 367-374.

(230) de Torres, M.; Dimroth, J.; Arends, I. W. C. E.; Keilitz, J.; Hollmann, F. *Molecules* **2012**, *17*, 9835-9841.

Chapter 2

Materials, methods and instrumentation



2. Materials, methods and instrumentation

This chapter describes the experimental techniques and instrumentation used in this thesis. Detailed description of the synthesis of ruthenium and rhodium dimers, as well as the ligands used in the following chapters is also covered here. More detailed procedures for specific experiments are described in the appropriate chapters.

2.1. Materials

Ruthenium(III) trichloride ($\text{RuCl}_3 \cdot X \text{H}_2\text{O}$) and rhodium(III) trichloride ($\text{RhCl}_3 \cdot X \text{H}_2\text{O}$) was purchased from Precious Metals Online (PMO Pty Ltd.) and used as received. 4-(Trifluoromethyl)benzenesulfonyl chloride, 4-nitrobenzenesulfonyl chloride, di-*tert*-butyl dicarbonate anhydride, 4-bromo-biphenyl, *n*-butyllithium in hexane 1.6 M, phenyllithium, 2,4-pentamethylcyclopentadiene, 2,3,4,5-tetramethyl-2-cyclopentanone, hexamethylbenzene (hmb), were obtained from Sigma-Aldrich. 3-phenyl-1,4-cyclohexadiene was synthesised by Dr Abraha Habtemariam following the procedure in the literature.¹⁻³ Magnesium sulphate, sodium carbonate and hydrochloric acid were obtained from Fisher Scientific. α -phellandrene was purchased from Sigma-Aldrich. Methylsulfonyl chloride, toluenesulfonyl chloride and triflic acid were obtained from Fluka. $\text{DMSO-}d_6$, $\text{MeOD-}d_4$, D_2O , acetone- d_6 and CDCl_3 for NMR spectroscopy were purchased from Sigma-Aldrich and Cambridge Isotope Labs Inc. Dried solvents were purchased from Sigma-Aldrich. Non-dried solvents used in syntheses were obtained from Fisher Scientific and Prolabo. Solvents were used as received, except in the case of ethanol which was freshly distilled in the presence of magnesium/iodine.

2.1.1. Preparation of Cp^X ligands⁴

3-Phenyl-1,2,4,5-tetramethyl-1,3-cyclopentadiene (Cp^XPh). A solution of phenyllithium (50 mL) was treated with 2,3,4,5-tetramethyl-2-cyclopentenone (12 mL) at 273 K. The reaction was allowed to warm slowly to 298 K with stirring overnight. The yellow solution was cooled down by addition of ice and then acidified with HCl (36 % v/v). The aqueous solution was extracted with diethyl ether (3 x 50 mL). The combined organic portions were dried over anhydrous magnesium sulphate, filtered, and the solvents evaporated to dryness on a rotary evaporator to obtain a yellowish oil. The product was purified by distillation under vacuum (fraction at 410 K, 0.5 mbar). Yield: 12.7 g (81.7 %). ¹H NMR (400 MHz, CDCl₃): The spectrum was very difficult to analyse due to the presence of 3 isomers.

3-Biphenyl-1,2,4,5-tetramethyl-1,3-cyclopentadiene (Cp^XPhPh). A solution of 4-bromo-biphenyl (16 g) in dried tetrahydrofuran (400 mL) was treated with a solution of n-butyllithium in hexane 1.6 M (50 mL) at 195 K. After reacting for 3 h, 2,3,4,5-tetramethyl-2-cyclopentenone (12 mL) was added. The solution was allowed to warm slowly to 298 K with stirring overnight. The orange solution was acidified with HCl (36 %) and the organic phase removed. The aqueous layer was extracted with diethyl ether (3 x 50 mL). The combined organic portions were dried over anhydrous magnesium sulphate, filtered, and the solvents evaporated to dryness on a rotary evaporator to obtain a dark yellow powder. The product was washed in methanol (3 x 20 mL) to give a yellow powder. Yield: 14.1 g (94.38 %). ¹H NMR (400 MHz, CDCl₃): $\delta_{\text{H}} = 7.63$ (d, 2H, J = 7.4 Hz), 7.60 (d, 2H, J = 8.3 Hz), 7.45 (t, 2H, J = 7.5 Hz), 7.34 (m, 3H), 3.25 (q, 1H, J = 7.7 Hz), 2.09 (d, 3H, J = 1.4 Hz), 1.96 (s, 3H), 1.89 (s, 3H), 1.01 (d, 3H, J = 7.7 Hz).

2.1.2. Preparations of Rh(III) dimers⁵

[(Cp*)RhCl₂]₂. Hydrated rhodium(III) trichloride (500 mg, 2.12 mmol) was reacted with 2,4-pentamethylcyclopentadiene (302 mg, 2.22 mmol) dissolved in dry methanol (50 mL) and heated to reflux (343 K) under a nitrogen atmosphere for 48 h. The dark red precipitate obtained was filtered and washed with ether (3 x 20 mL) to give a dark red powder. The crude product product was then recrystallized from methanol. Yield: 410.6 mg (62.7 %). ¹H NMR (400 MHz, DMSO-*d*₆): δ_H 1.627 (s, 10H).

[(Cp^xPh)RhCl₂]₂. [(Cp^xPh)RhCl₂]₂ was synthesised following the same procedure described for [(Cp^{*})RhCl₂]₂ using 500 mg of hydrated rhodium(III) trichloride and 532 mg of Cp^xPhPh. The red precipitated obtained was recrystallized in methanol. Yield: 592.7 mg (75.47 %). ¹H NMR (400 MHz, DMSO-*d*₆): δ_H 7.67 (m, 4H), 7.43 (m, 6H), 1.71 (s, 4H), 1.67 (m, 4H).

[(Cp^xPhPh)RhCl₂]₂. [(Cp^xPhPh)RhCl₂]₂ was synthesised following the same procedure described for [(Cp^{*})RhCl₂]₂ using 1 g of hydrated rhodium(III) trichloride and 962 mg of Cp^xPhPh. The red-orange precipitate obtained was recrystallized from methanol. Yield: 613.4 mg (33.2 %). ¹H NMR (400 MHz, DMSO-*d*₆): δ_H 7.75 (m, 12H), 7.49 (t, 4H, J = 7.4 Hz), 7.40 (t, 2H, J = 7.4 Hz), 1.73 (s, 24H).

2.1.3. Preparation of Ru(II) dimers¹⁻³

[(*p*-cymene)RuCl₂]₂. RuCl₃ · X H₂O (1.05 g, 0.57 mol) and α-phellandrene (9.3 mL, 5.73 mol) were dissolved in freshly distilled ethanol (75 mL) and the reaction mixture heated to reflux (353 K) under a nitrogen atmosphere for 18 h. The red precipitate formed was

filtered and washed with ice cold ethanol (3 x 20 mL) and ether (3 x 20 mL) and dried under vacuum. Yield: 1.174 g (66.7 %). ^1H NMR (250 MHz, $\text{DMSO-}d_6$): δ_{H} 5.82 (d, 2H, $J = 6.4$ Hz), 5.76 (d, 2H, $J = 6.4$ Hz), 2.84 (septet, 1H, $J = 7.1$ Hz), 2.09 (s, 3H), 1.20 (d, 6H, $J = 6.9$ Hz)

[(hmb)RuCl₂]₂. [(*p*-cymene)RuCl₂]₂ (0.8 g, 1.3 mmol) and a large excess of hexamethylbenzene (9 g) were placed in a 50 mL round-bottom flask fitted with an air condenser and heated at 463 K for 4 hours. Sublimed hexamethylbenzene was scraped off the condenser every 10 minutes. The red precipitate formed was washed with hexane (6 x 30 mL) to remove excess hexamethylbenzene. The crude product product was redissolved in chloroform and filtered to give a red solution. The solvent was then removed on the rotavaporator to give a red powder which was recrystallized from chloroform/hexane (9:1). Yield: 237 mg (87.4 %). ^1H NMR (300 MHz, $\text{DMSO-}d_6$): δ_{H} 2.27 (s, 18H).

[(bip)RuCl₂]₂. 3-phenyl-1,4-cyclohexadiene (2.94 g, 18.9 mmol) was added to a solution of RuCl₃ · X H₂O (1.64 g, 6.29 mmol) in freshly distilled ethanol (100 mL). The reaction mixture was heated to reflux (363 K) under nitrogen atmosphere for 18 h. The brown precipitate formed was filtered and washed with ice cold ethanol (3 x 20 mL) and ether (3 x 20 mL) dried under vacuum. Yield: 2.00 g (81.9 %). ^1H NMR (250 MHz, $\text{DMSO-}d_6$): δ_{H} 6.07 (m, 3H), 6.42 (d, 2H, $J = 6.1$ Hz), 7.50 (m, 3H), 7.82 (m, 2H).

2.1.4. Preparation of the ligands⁶⁻⁸

***N*-(2-Aminoethyl)-4-toluensulfonamide (TsEnH)**. A solution of ethylenediamine (14 mL, 0.21 mol) in dichloromethane (50 mL) was placed in a round-bottom flask. A solution of toluenesulfonyl chloride (4.0 g, 21 mmol) in dichloromethane (25 mL) was added slowly *via* a dropping funnel, and the mixture stirred vigorously for one hour. The solution was then washed with water (3 x 25 mL), and dried over MgSO₄. The solvent was

removed on a rotary evaporator to give a white solid which was recrystallized from hot water. Yield: 2.63 g (52.3 %). ^1H NMR (400 MHz, CDCl_3): δ_{H} 2.43 (s, 3H), 2.78 (t, 2H, $J = 5.6$ Hz), 2.95 (t, 2H, $J = 5.6$ Hz), 7.30 (d, 2H, $J = 8.0$ Hz), 7.75 (d, 2H, $J = 8.0$ Hz).

N-(2-Aminoethyl)-4-(trifluoromethyl)benzenesulfonamide (TfEnH). This was obtained following the method described above using 2 g of trifluoromethylbenzenesulfonyl chloride. The compound was purified by recrystallisation from hot water. Yield: 1.59 g (72.5 %). ^1H NMR (300 MHz, CDCl_3): δ_{H} 2.82 (m, 2H), 3.00 (m, 2H), 7.79 (d, 2H, $J = 8.3$ Hz), 8.00 (d, 2H, $J = 8.3$ Hz).

N-(2-Aminoethyl)-4-nitrobenzenesulfonamide (NbEnH). This was obtained following the method described above for TsEnH using 3 g of 4-nitrobenzenesulfonyl chloride. The crude product was washed with methanol (3 x 20 mL) to give a yellow compound. Yield: 1.78 g (53.6 %). ^1H NMR (250 MHz, CDCl_3): δ_{H} 2.55 (t, 2H, $J = 6.5$ Hz), 2.80 (t, 2H, $J = 6.5$ Hz), 8.05 (d, 2H, $J = 9.0$ Hz), 8.42 (d, 2H, $J = 9.0$ Hz).

N-(*t*-Boc)-ethylenediamine. A solution of *t*Boc-anhydride (6.1 g, 28 mmol) in dichloromethane (250 mL) was added drop-wise over 2 h to a solution of ethylenediamine (11.2 mL, 166.7 mmol) in dichloromethane (50 mL) during which the mixture slowly turned cloudy. The mixture was stirred overnight at ambient temperature. The solvent was removed on a rotary evaporator to obtain a yellow oil which was redissolved in aqueous sodium carbonate (500 mL) and extracted with dichloromethane. The organic layer was dried over Na_2SO_4 , filtered and concentrated in *vacuo* to afford a yellow oil. Yield: 3.64 g (81.3 %). ^1H NMR (300 MHz, CDCl_3): δ_{H} 4.85 (s, 1H), 3.17 (m, 2H), 2.80 (t, 2H, $J = 5.9$ Hz), 1.44 (s, 9H).

N-(*t*-Boc)-*N'*-(2-aminoethyl)methylsulfonamide. A solution of methanesulfonyl chloride (1.85 mL, 25.77 mmol) in dichloromethane (25 mL) was added drop-wise over 45 min to a

solution of *t*-Boc-protected ethylenediamine prepared above (3.64 g, 22.72 mmol) and triethylamine (5 mL). The reaction mixture was stirred overnight at ambient temperature. The solution was washed with water, dried over MgSO₄ and filtered. After removal of the solvent on a rotary evaporator, a yellow oil was obtained. A white powder precipitated after washing with diethyl ether. Yield: 2.83 g (52.3 %). ¹H NMR (300 MHz, CDCl₃): δ_H 4.89 (s, 1H), 3.29 (m, 4H), 2.97 (s, 3H), 1.44 (s, 9H).

***N*-(2-Aminoethyl)methylsulfonamide (MsEnH).** To a cooled solution (273 K) of *t*-Boc protected *N*-(2-aminoethyl)methylsulfonamide (2.83 g, 11.87 mmol) in dry dichloromethane (50 mL) was added 3.11 mL of triflic acid (5 mol equiv.) under a N₂ atmosphere. The reaction mixture was stirred for 5 h at room temperature during which a white precipitate gradually formed. The solvent was removed on a rotary evaporator to give an orange oil which was washed with diethyl ether to precipitate an orange powder. After filtration, the orange product was washed with ether to remove the triflic acid and a white powder was collected by filtration. Yield: 3.25 g (95.3 %). ¹H NMR (400 MHz, D₂O/dioxane): δ_H = 3.42 (t, 2H, J = 5.7 Hz), 3.16 (t, 2H, J = 5.7 Hz), 3.10 (s, 3H).

2.2. Methods and instrumentation

2.2.1. pH measurements

A minilab IQ125 pH meter equipped with a ISFET silicon chip pH sensor and referenced in KCl gel was used to measure the pH. The electrode was calibrated with Aldrich buffer solutions of pH 4, 7 and 10. pH* values (pH meter reading without correction for the effect of deuterium on glass electrode) of NMR samples in D₂O were measured at 298 K. pH* values were adjusted with KOD or DCIO₄ solutions in D₂O. pH values of the reaction

mixtures and UV-Vis samples H₂O were also measured at 298 K. pH values were adjusted with KOH or HClO₄ solutions in H₂O.

2.2.2. Nuclear magnetic resonance spectroscopy (NMR)

¹H NMR spectra were acquired in 5 mm NMR tubes at 298 K or 310 K on either a Bruker DPX-300, AV-400, DRX-500 or Bruker AV III 600 spectrometers. Data processing was carried out using XWIN-NMR version 3.6 (Bruker U.K. Ltd). ¹H NMR chemical shifts were internally referenced to TMS *via* 1,4-dioxane in D₂O ($\delta = 3.75$) or residual DMSO ($\delta = 2.52$ ppm), acetone ($\delta = 2.05$ ppm), MeOH ($\delta = 3.31$ ppm) or CHCl₃ ($\delta = 7.26$ ppm). 1D spectra were recorded using standard pulse sequences. Typically, data were acquired with 16-128 transients into 32 k data points over a spectral width of 14 ppm, and for the kinetic experiment 32 transient into 32 k data points over a spectral width of 30 ppm with the centre at 0 ppm, relaxation time of T₁ = 2 s.

Water suppression was performed by irradiation at the frequency of water in between pulse sequences.

2.2.2.1. pK_a determination⁹

Changes in the chemical shifts of the peaks corresponding aqua-adducts of the complexes analyzed with the pH* over a range from 2 to 12 were followed by ¹H NMR spectroscopy. The pH* (pH meter reading without correction for the effect of deuterium on glass electrode) were adjusted with KOD or DCLO₄ solutions in D₂O. The data were fitted to the Henderson–Hasselbalch equation using Origin 7.5.

Henderson–Hasselbalch equation:



$$K_a = \frac{[A^-][H^+]}{[AH]}$$

$$-\log H = -\log K_a + \log_{10} \left(\frac{[A^-]}{[AH]} \right)$$

Considering that the chemical shift observed (δ_{obs}) corresponds to the weighted average of the chemical shifts according to the populations of the protonated and deprotonated species.

$$\delta_{obs}[A]_{total} = \delta_{[AH]}[AH] + \delta_{[A^-]}[A^-]$$

$$\text{Henderson-Hasselbalch: } \delta_{obs} = \left[\frac{\delta_{AH} + \delta_{A^-} \times 10^{(pK_a^* - pH^*)}}{1 + 10^{(pK_a^* - pH^*)}} \right]$$

Where δ_{AH} and δ_{A^-} are the chemical shifts from the protonated and deprotonated forms respectively.

2.2.2.2. Kinetics of reaction^{10,11}

A solution of the complex in D₂O or MeOD-*d*₄/D₂O (5:1) was prepared in a glass vial. Solutions of sodium formate and β -nicotinamide adenine dinucleotide hydrate (NAD⁺) in D₂O were also prepared and incubated at 310 K. In a typical experiment the corresponding volume of each solution (to reach the required concentrations) was added to a 5 mm NMR tube and pH* adjusted to 7.2 ± 0.1 . The ¹H NMR spectrum was recorded every 162 s at 310 K until completion of the reaction.

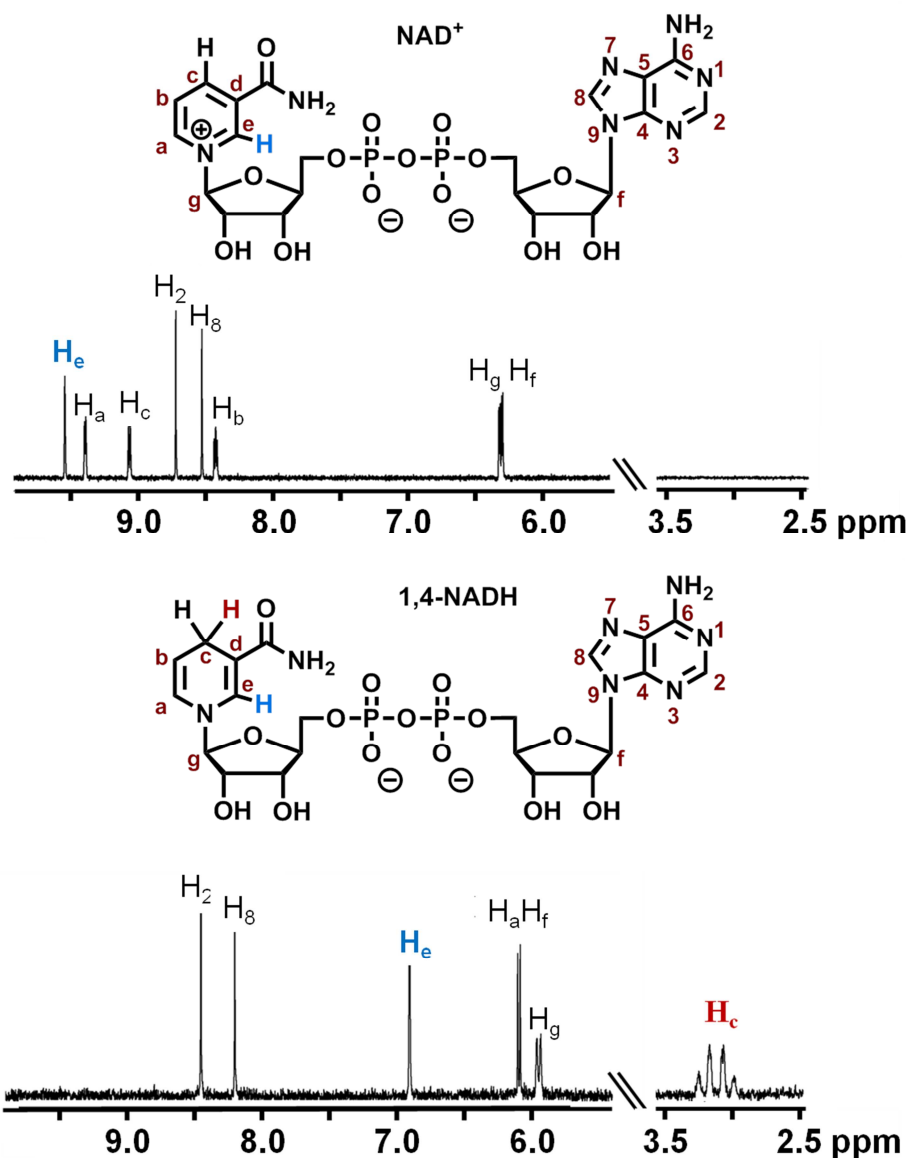


Figure 2.1. ¹H NMR spectra of NAD⁺ and 1,4-NADH in D₂O.

Molar ratios of NAD⁺ and NADH were determined by integrating the peaks corresponding to H_e of NAD⁺ (9.33 ppm) and H_e of 1,4-NADH (6.96 ppm). (Figure 2.1) Turnover number (TON, defined as the maximum number of molecules of substrate that a catalyst can convert to product) was calculated:

$$\text{TON}_t = \frac{I_{6.96} [\text{NAD}^+]_0}{I_{6.96} + I_{9.93} [\text{Catalyst}]}$$

Where TON_t is the turnover number at a specific time, I_n is the integral of the signal at n ppm and $[\text{NAD}^+]_0$ is the concentration of NAD^+ at the start of the reaction.

Turnover frequency (TOF, defined as the turnover number per unit of time) calculated using the equation obtained from the graphical plot of TON vs time (h)

$$\text{TOF} = K_{\text{cat}} = \frac{V_{\text{reaction}}}{[\text{catalyst}]} = \frac{\delta[\text{NADH}]}{\delta t} \frac{1}{[\text{catalyst}]}$$

$$\text{TOF} \cdot t = \frac{I_{6.96}}{I_{6.96} + I_{9.93}} \frac{[\text{NAD}^+]_0}{[\text{Catalyst}]}$$

Michaelis-Menten model¹²

The Michaelis-Menten model is a simple approach to enzyme kinetics. It correlates reaction rate to substrate concentration for a system where a substrate (S) binds reversibly to an enzyme (E) (or catalyst in our case) to form an enzyme-substrate complex (ES), which then reacts irreversibly to generate a product (P) and to regenerate the free enzyme.



- 1) Velocity defined as the rate of formation of the product: $V = \frac{\delta P}{\delta t} = K_2[\text{ES}]$
- 2) The rate of formation of the intermediate: $\frac{\delta[\text{ES}]}{\delta t} = K_1[\text{S}][\text{E}] - (K_{-1} + K_2)[\text{ES}] = 0$

$$K_M = \frac{K_{-1} + K_2}{K_1} = \frac{[\text{S}][\text{E}]}{[\text{ES}]}$$

- 3) If $[\text{E}] = [\text{E}]_t - [\text{ES}]$

$$K_M = \frac{[\text{S}]([\text{E}]_t - [\text{ES}])}{[\text{ES}]}$$

$$[\text{ES}] = [\text{E}]_t \frac{[\text{S}]}{[\text{S}] + K_M}$$

4) Replacing [ES] in $V = \frac{\delta P}{\delta t} = K_2[ES]$

$$V = K_2[ES] = K_2[E]_t \frac{[S]}{[S] + K_M}$$

5) Maximum velocity is obtained when [ES] is equal to [E]_t, $V_{max} = K_2[E]_t$:

$$V = V_{max} \frac{[S]}{[S] + K_M}$$

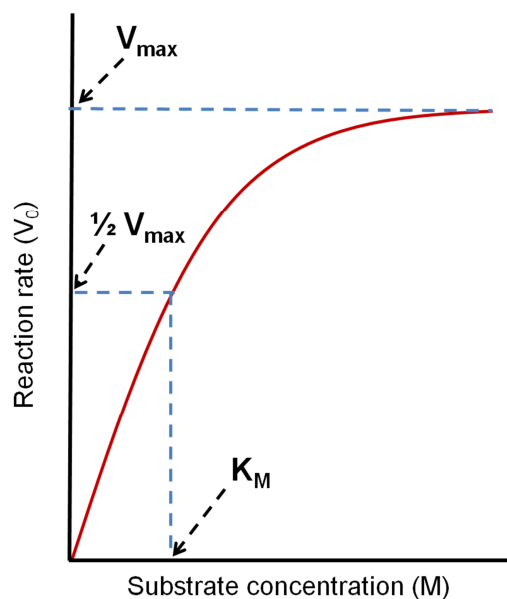


Figure 2.2. Michaelis-Menten plot.

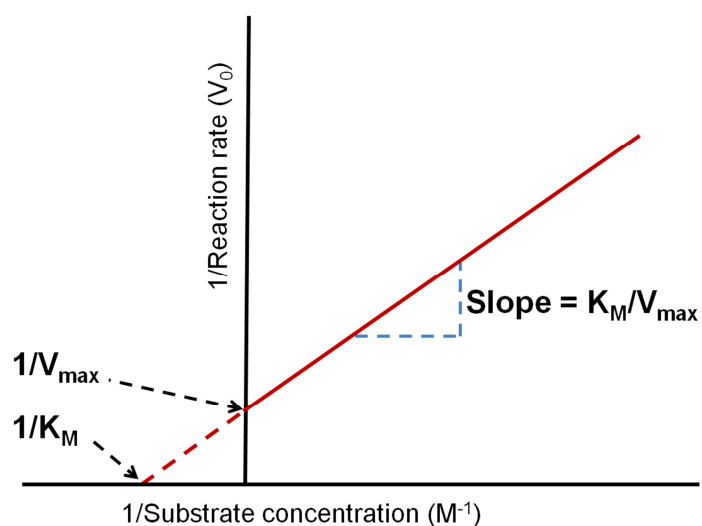


Figure 2.3. Double reciprocal plot of the reaction rate *versus* concentration of substrate (Michaelis-Menten).

2.2.3. Elemental analysis

Elemental analyses were performed by Warwick Analytical Service using an Exeter Analytical elemental analyzer (CE440).

2.2.4. Electrospray ionization mass spectrometry (ESI-MS)

Positive-ion mass spectra were obtained on a Bruker Daltonics Esquire 2000 ion trap mass spectrometer. All samples were prepared in double deionised water (ddw), methanol (95 %)/water (5 %), or methanol (100 %). Injection 2 mL min^{-1} , nebuliser gas (N_2) 25 psi, dry gas (N_2) 9 L min^{-1} , dry temp 300°C , capillary -4000V (positive mode) end plate offset -500V . Capillary exit 70-170 V, and Octapole RF 50-400Vpp. Mass spectra were recorded with a scan range of 500 to 1000 m/z. Data were processed using Data-Analysis version 3.3 (Bruker Daltonics).

2.2.5. High resolution mass spectrometry (HR-MS)

Positive-ion mass spectra were obtained on a Bruker MaXis UHR-TOF. All the samples were analysed by positive electrospray ionization mass spectra. All samples were prepared in double deionised water (ddw), methanol (95 %)/water, or methanol (100 %). Injection $2 \mu\text{L min}^{-1}$, nebuliser gas (N_2) 0.4 bar, dry gas (N_2) 4 L min^{-1} , dry temp 180°C , capillary -3000V (positive mode) end plate offset -500V . Capillary exit 166 V, funnel RF 300 Vpp, Multipole RF 300 vpp, quadrupole ion energy 4 eV, Collision cell 1200 eV, ion cooler RF settings, ramp from 50 to 250 V. Mass spectra were recorded with a scan range of 50 to 3000 m/z. Data were processed using Data-Analysis version 3.3 (Bruker Daltonics).

The HR-MS spectra were recorded by Dr Lijiang Song or Mr Philip Aston. Data were processed using Data-Analysis version 3.3 (Bruker Daltonics).

2.2.6. Electronic absorption spectroscopy (UV-Vis)

UV-Vis absorption spectra were recorded on a Cary 300 spectrometer using quartz cuvettes of 1 cm pathlength (600 μ L). The sample temperature was adjusted to 298 K or 310 K by a PTP1 Peltier temperature controller. Spectra were recorded from 200 to 800 nm. Data were processed with UV Winlab software and Origin Lab 8.5.

2.2.6.1. Thermal denaturalization of DNA

Stability of DNA was monitored by measuring the absorbance at 260 nm (1 nm bandwidth) as a function of temperature (every 0.5 K between 293 and 371 K, ramp rate 1 $^{\circ}$ C/min. The experiment was run on 1 cm pathlength cuvettes of 0.6 ml volume. The data were fitted to the Boltzmann equation using Origin 7.5. The melting temperature value (T_m , temperature where 50% of the CT-DNA denaturalize) was determined as the inflection point.

2.2.7. X-ray crystallography

X-ray diffraction data were collected and the structures solved by Dr Guy Clarkson at the University of Warwick.

Diffraction data were collected on an Oxford Diffraction Gemini four-circle system with a Ruby CCD area detector. All structures were refined by full-matrix least squares against F^2 using SHELXL 97¹³ and were solved by direct methods using SHELXS¹⁴ (TREF) with additional light atoms found by Fourier methods. Hydrogen atoms were added at calculated positions and refined using a riding model, except the hydrogens on the NH nitrogens which were located in a difference map. Anisotropic displacement parameters were used for all non-H atoms; H-atoms were given an isotropic displacement parameter equal to 1.2 (or 1.5 for methyl and NH H-atoms) times the equivalent isotropic displacement

parameter of the atom to which they are attached. The data were processed by the modelling program Mercury 1.4.1.

The distances were considered statistically different when the difference between them was greater than 3σ . Where $\sigma = \sqrt{(\sigma_1^2 + \sigma_2^2)}$. Being σ_1 and σ_2 the standard deviations of the values 1 and 2.

2.2.8. Circular dichroism (CD)

CD spectra were recorded on a Jasco-815 spectrometer from Prof. Alison Rodger group, using quartz cuvettes of 0.1 cm pathlength (200 μL). Spectra were recorded from 190 to 500 nm, bandwidth 1 nm, scan speed 100 nm min^{-1} . Six scans over the wavelength range gave sufficient signal-to-noise ratio for each spectrum. Data were processed with Jasco 815 spectra manager and Origin Lab 8.5.

2.2.9. Flow linear dichroism (LD)

LD spectra were recorded on a Jasco J-815 circular dichroism spectropolarimeter from Prof. Alison Rodger group, adapted for LD measurements using a microvolume couette flow cell manufactured by Crystal Precision Optics couette (70 μL). The flow cell consists of a fixed outer cylinder and a rotating solid quartz inner cylinder, separated by a gap of 0.5 mm, giving a total pathlength of 1 mm. The rotation motor potential of the cell was 3.0 V (~3000 rpm). Spectra were recorded from 190 to 500 nm, bandwidth 1 nm, scan speed 100 nm min^{-1} . Two scans over the wavelength range gave sufficient signal-to-noise ratio for each spectrum. Data were processed with Jasco 815 spectra manager and Origin Lab 8.5.

For each sample, spectra were taken with cell rotation on and off. The spectra with cell rotation off were used as a baseline, and were subtracted from the spectra with cell rotation to give the LD spectra.

2.2.10. High performance liquid chromatography (HPLC)

HPLC studies were performed in collaboration with Prof. P. Socorro Murdoch.

HPLC was performed on a HP 1200 Series HPLC System (Agilent) with a 100 μL loop. The column used was an Agilent ZORBAX Eclipse Plus C-18 (250 x 4.6 mm, 5 μm pore size) column. The mobile phases were A: water (HPLC grade, Aldrich) containing 0.1 % trifluoroacetic acid, and B: acetonitrile (HPLC grade, Aldrich) containing 0.1 % trifluoroacetic acid. Gradients of $t = 0 - 10\%$ B, $t = 30 - 80\%$ B, $t = 40 - 80\%$ B, $t = 41 - 10\%$ B and $t = 55 - 10\%$ B over a 55 min period. Flow rate was 1 mL min^{-1} . A wavelength of detection of 254 nm with the reference wavelength at either 360 or 510 nm was used unless otherwise stated. Samples were prepared in ddw or a mixture methanol (5 %, HPLC grade)/ddw. Sample injections were half the loop volume (50 μL). All complexes described in other chapters were analyzed by HPLC and contain less than 5 % impurities detectable by HPLC.

2.2.11. Liquid chromatography – mass spectrometry (LC-MS)

LC-MS was performed on a HP 1200 Series HPLC System (Agilent) coupled to a Bruker HCT-Ultra ETD II PTR PTM mass spectrometer. The column used was an Agilent ZORBAX Eclipse Plus C-18 (4.6 x 250 mm, 5 μm pore size). The mobile phases were A: water (HPLC grade, Aldrich) containing 0.1% trifluoroacetic acid, and B: acetonitrile (HPLC grade, Aldrich) containing 0.1% trifluoroacetic acid. Specific gradients are described on the corresponding chapter. Samples were prepared in ddw. Sample injections were 50 μL . The mass spectrometer was operated in electrospray positive mode with scan range 50-2000 m/Z, Nebuliser gas (N_2) 40 psi, dry gas (N_2) 10 L min^{-1} , dry temp 300°C , HV capillary -4000 V (positive mode) end plate offset -500 V. Capillary exit 166 V, and Octapole RF 200 Vpp.

2.2.12. Liquid chromatography – MAXIS (LC-HRMS)

Liquid chromatography-MAXIS was carried out by Phil Aston at the University of Warwick

LC-MS was performed on a Dionex Ultimate 3000 with a VWD detector coupled to a Bruker MaXis UHR-ESI-TOF mass spectrometer. The column used was an Agilent Eclipse Plus C-18 (2.1 x 100 mm, 1.8 μm pore size). The mobile phases were A: water (HPLC grade, Aldrich) containing 0.1 % trifluoroacetic acid, and B: acetonitrile (HPLC grade, Aldrich) containing 0.1 % trifluoroacetic acid. Specific gradients are described on the corresponding chapter. Samples were prepared in ddw. Sample injections were 50 μL . The mass spectrometer was operated in electrospray positive mode with scan range 50-3000 m/Z, Nebuliser gas (N_2) 1.4 Bar, dry gas (N_2) 8 L min^{-1} , dry temp 180° C, capillary -4500 V (positive mode) end plate offset -500 V. Capillary exit 166 V, funnel RF 200 Vpp, Multipole RF 200 vpp, quadrupole ion energy 4 eV, Collision cell 1200 eV, ion cooler RF settings, ramp from 50 to 250 V. Data were processed using Data-Analysis version 3.3 (Bruker Daltonics).

2.2.13. Inductively coupled plasma mass spectrometry (ICP-MS)

Ruthenium (^{101}Ru) and rhodium (^{103}Rh) content was determined using ICP-MS Agilent technologies 7500 series. Data acquisition was carried out on ICP-MS Top (B.03.05) and analysed on Offline Data Analysis (B.03.05). Standards for Ru (ruthenium chloride 1000 ppm in 10 % v/v hydrochloric acid) and Rh (rhodium nitrate 10 ppm in nitric acid 0.5 M) were purchased from Inorganic Ventures and Fluka, respectively. Calibration curves were prepared in double deionised water (ddw) with 3% nitric acid, range between 500 and 1 ppb (9 points). Standards and samples were freshly prepared in ddw with 3% metal free nitric acid. Readings were made in no-gas mode with a detection limit of 0.8 ppt for ^{101}Ru and 7 ppt for ^{103}Rh .

2.2.14. Computational Details

All calculations were carried out by Prof. Rob Deeth at the University of Warwick

All calculations used the ORCA program version 2.8.¹⁵ Minimum-energy structures and transition states were located using the OPBE functional, spin restricted, in conjunction with the def2-TZVP basis sets^{16,17} and the resolution of identity approximation. Solvation effects were included *via* the conductor-like screening model implemented in ORCA with water as the solvent. Stationary points were confirmed as local minima or transition states *via* numerical frequency calculations. Final free energies were computed using the statistical mechanics corrections computed from the OPBE optimizations with B3LYP energies using the def2-TZVP basis sets plus the COSMO solvation corrections¹⁸ and Grimme's empirical correction for dispersion.¹⁹

2.2.15. Biological studies

All the biological studies were performed by Dr. Isolda Romero-Caneón at the University of Warwick. The following sections outline the general cell experiments used in this thesis. More specific experiments will be described in the appropriate chapter.

2.2.15.1. Cell maintenance^{20, 21}

A2780 human ovarian carcinoma cells were obtained from the European Collection of Cell Cultures (ECACC, Salisbury, UK). All cells were grown in Roswell Park Memorial Institute medium (RPMI-1640) supplemented with 10% of fetal calf serum, 1 % of 2 mM glutamine and 1 % penicillin/streptomycin and used between passages 5-15. The cells were grown as adherent monolayers at 310 K in a 5 % CO₂ humidified atmosphere and passaged at approximately 70-80 % confluence, using 0.25 % trypsin/EDTA.

2.2.15.2. *In vitro* growth inhibition assay

Stock solutions of the Ru(II) or Rh(III) complexes were freshly prepared in 5 % DMSO and a mixture 0.9 % saline (v/v): medium (1:1 v/v) following serial dilutions in RPMI-1640 to achieve working concentrations. Metal concentrations were determined by ICP-MS.

The antiproliferative activities of the complexes in A2780 ovarian cancer cells were determined. 96-well plates were used to seed 5000 cells per well. The plates were pre-incubated in drug-free media at 310 K for 48 h before addition of various concentrations of the compounds. The drug exposure period was 24 h, after which, the supernatant was removed by suction and each well washed with PBS. A further 48 h was allowed for the cells to recover in drug-free medium at 310 K. The sulforhodamine B (SRB) colorimetric assay was used to determine cell viability. IC₅₀ values, as the concentration which caused 50 % of cell death, were determined as duplicates of triplicates in two independent sets of experiments and their standard deviations were calculated.

The data were analysed using Origin 8.5. IC₅₀ values were obtained from plots of the survival percentage of cells versus the logarithm of the concentration expressed in millimolar units and fitted to a sigmoidal curve. IC₅₀ values of cisplatin were determined in each well-plate as a validation.

Sulforhodamine B assay (SRB)²²

SRB is a pink dye which binds quantitatively to aminoacid residues in acid conditions, however under basic conditions the dye is liberated and can be extracted and analyzed by optical absorption spectroscopy ($\lambda = 568$ nm).

To each well, 50 μ L of trichloroacetic acid (TCA) (10 % v/v) was added and incubated for an hour at 277 K. The well plates were washed with water 10 times and then dried in air.

Aliquots of 50 μL of SRB (0.4 %, prepared in 1 % acetic acid) were added and the wells left standing for 30 min at ambient temperature. Excess dye was removed by washed with 1 % acetic acid 5 times and the plate left to dry.

A 10 mM of Tris base solution (200 μL , pH 10.5) were added to each well plate and left to stand for 1 h to solubilise the dye. Absorbance was measured with a multi reader at 570 nm.

2.2.15.3. Cell viability modulation experiments

Cell viability assays were carried out in A2780 ovarian cancer cells. These experiments were performed as described above for IC_{50} determination with the following experimental modifications:

- 1) Fixed concentration of complexes was $1/3 \times \text{IC}_{50}$
- 2) Co-administration of the complex with three different concentrations of sodium formate (0.5, 1 and 2 mM). Both solutions (complex and sodium formate) were added to each well independently, but within 5 min of each other

Stock solutions of the Ru(II) or Rh(III) complexes were freshly prepared in 5 % DMSO and a mixture 0.9 % saline : medium (1:1 v/v). The stock solution was further diluted using RPMI-1640 to achieve working concentrations. Metal concentrations were determined by ICP-MS.

Cell viability percentages were determined as duplicates of triplicates in two independent sets of experiments and their standard deviations were calculated.

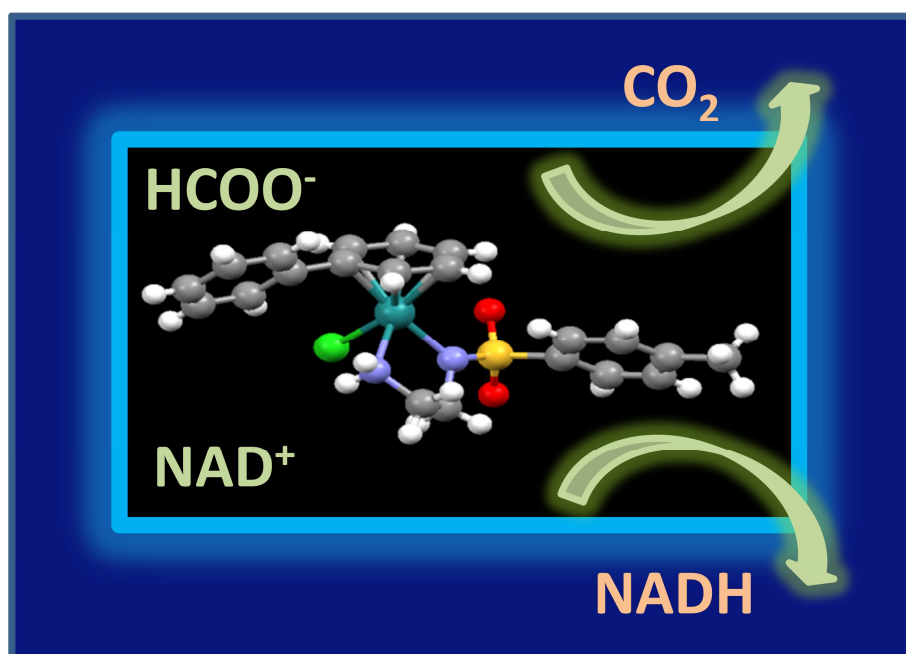
2.3. References

- (1) Harvey, R. G.; Lindow, D. F.; Rabideau, P. W. *J. Am. Chem. Soc.* **1972**, *94*, 5412-5420.
- (2) Zelonka, R. A.; Baird, M. C. *Can. J. Chem.* **1972**, *50*, 3063-3072.
- (3) Habtemariam, A.; Melchart, M.; Fernandez, R.; Parsons, S.; Oswald, I. D. H.; Parkin, A.; Fabbiani, F. P.; Davidson, J. E.; Dawson, A.; Aird, R. E.; Jodrell, D. I.; Sadler, P. J. *J. Med. Chem.* **2006**, *49*, 6858-6868.
- (4) Betanzos-Lara, S.; Liu, Z.; Habtemariam, A.; Pizarro, A. M.; Qamar, B.; Sadler, P. J. *Angew. Chem. Int. Ed.* **2012**, *51*, 3897-3900.
- (5) White, C.; Yates, A.; Maitlis, P. M.; Heinekey, D. M. In *Inorganic Syntheses*; ed.; John Wiley & Sons, Inc.: **2007**; 228-234.
- (6) Wu, X.; Liu, J.; Li, X.; Zanotti-Gerosa, A.; Hancock, F.; Vinci, D.; Ruan, J.; Xiao, J. *Angew. Chem. Int. Ed.* **2006**, *45*, 6718-6722.
- (7) Li, X.; Li, L.; Tang, Y.; Zhong, L.; Cun, L.; Zhu, J.; Liao, J.; Deng, J. *J. Org. Chem.* **2010**, *75*, 2981-2988.
- (8) Tan, J.; Tang, W.; Sun, Y.; Jiang, Z.; Chen, F.; Xu, L.; Fan, Q.; Xiao, J. *Tetrahedron* **2011**, *67*, 6206-6213.
- (9) Tribolet, R.; Sigel, H. *Eur. J. Biochem.* **1987**, *163*, 353-363.
- (10) Boudart, M. *Chem. Rev.* **1995**, *95*, 661-666.
- (11) Yan, Y. K.; Melchart, M.; Habtemariam, A.; Peacock, A. F.; Sadler, P. J. *J. Biol. Inorg. Chem.* **2006**, *11*, 483-488.
- (12) Matthew, C. K.; Ahern, K. G.; Van Holde, K. E. *Biochemistry*; 3rd ed.; Pearson Educacion: Madrid, **2002**.
- (13) Sheldrick, G. M., In *SHELXL97*: University of Gottingen, Gottingen, Germany, 1997.
- (14) Sheldrick, G. M. *Acta Crystallogr A* **2007**, *64*, 112-122.
- (15) Neese, F. *WIREs Comput. Mol. Sci.* **2012**, *2*, 73-78.

- (16) Schäfer, A.; Horn, H.; Ahlrichs, R. *J. Chem. Phys.* **1992**, *97*, 2571-2577.
- (17) Weigend, F.; Ahlrichs, R. *Phys. Chem. Chem. Phys.* **2005**, *7*, 3297-3305.
- (18) Sinnecker, S.; Rajendran, A.; Klamt, A.; Diedenhofen, M.; Neese, F. *J. Phys. Chem A* **2006**, *110*, 2235-2245.
- (19) Grimme, S.; Antony, J.; Ehrlich, S.; Krieg, H.; Grimme, S.; Antony, J.; Ehrlich, S.; Krieg, H. *J. Chem. Phys.* **2010**, *132*, 154104-154117.
- (20) Davis, J. *Basic cell culture: a practical approach*; Oxford University Press.: New York, **2002**.
- (21) Maramorosch, K.; Himrumi, H. *Practical tissue culture applications*; New York Academic Press: New York, **1979**.
- (22) Skehan, P.; Storeng, R.; Scudiero, D.; Monks, A.; Vistica, D.; Warren, J. T.; Bokesch, H.; Boyd, M. R. *J. Natl. Cancer inst.* **1990**, *82*, 1107-1112.

Chapter 3

Ruthenium(II) arene complexes for the catalytic reduction of NAD^+



3. Ruthenium(II) arene complexes for the catalytic reduction of NAD⁺

3.1. Introduction

The coenzyme nicotinamide adenine dinucleotide (NAD⁺) and its reduced form 1,4-NADH have crucial roles in many cellular processes such as regulation of energy metabolism, antioxidative function, DNA repair and transcription, immunological functions and cell death.¹ These coenzymes are involved in many other processes acting as substrates and cofactors for enzymes.^{2,3}

NAD⁺/NADH coenzymes have been studied intensively due to their important role in different areas such as medicine, industry and organic synthesis.^{4, 5} From the medical perspective, it has been demonstrated that changes in metabolism result in fluctuations in the ratio NAD⁺/NADH or, conversely, changes in this ratio can produce metabolic changes.³ In some cases, alterations in the cellular redox status have been shown to play an important role in cell death and therefore these coenzymes have become possible drug targets for chronic or autoimmune diseases such as Parkinson's, hepatitis C, diabetic vascular dysfunction, hyperglycemia and cancer.⁶

The concentration NAD⁺ as well as the ratio NAD⁺/NADH has been shown to be very important for cancer cells to maintain their redox balance.⁷ Furthermore, due to their increased metabolism, cancer cells generate high levels of oxidizing species and, therefore, they are under constant oxidative stress.⁷ This makes cancer cells more dependent on redox regulatory systems, and more sensitive to variations in the NAD⁺/NADH ratio. Furthermore, NAD⁺ is required as substrate for many enzymatic reactions such as ADP-ribosylation which

is crucial for genome stability and DNA repair.⁶ Due to the up-regulation of some enzymes required for the biosynthesis of NAD⁺ in cancer cells, a decrease in the NAD⁺ concentration can cause apoptosis of cancer cells while having little effect in normal cells.⁷

From an industrial perspective, NADH regeneration is an important process due to its high applicability in chiral organic synthesis and biocatalysis.^{8,9} The coenzyme 1,4-NADH, for instance, is required as substrate for many enzymatic reactions used for stereo-selective synthesis, such as the formation of D-lactate from pyruvate or chiral alcohols by alcohol dehydrogenases.^{8,9}

Due to the high cost of the NAD⁺ and NADH, their stoichiometric use in organic synthesis, biocatalysis or enzymatic reactions is not sustainable, and hence nicotinamide adenine dinucleotide models have been developed.¹⁰ The capability of regenerating 1,4-NADH has been the subject of intense studies by enzymatic, chemical, photochemical or electrochemical reactions.^{11,12}

Recently, the regeneration of NADH or NAD⁺ under mild conditions in aqueous media has been studied.^{13,14} Significant attention has been focused on transition metal complexes as catalysts for the regeneration of 1,4-NADH via hydrogenation¹³ (H₂) or transfer hydrogenation using 2-propanol,¹⁵ glycerol,¹⁶ phosphate,¹⁷ formic acid together with a base,¹⁸ or formate¹⁴ as hydride sources in water. Some Ru(II),¹⁹ Rh(III)^{20,21} and Ir(III)²² half-sandwich complexes can catalyze the hydrogenation or transfer hydrogenation of ketones,²³ aldehydes,²⁴ imines²⁵ or carbon dioxide,²⁶ although the optimum conditions for the reactions are usually not biologically relevant. In some cases, hydride adducts can be isolated showing that the mechanism involves a hydride formation.^{27, 28} Of particular interest in this field are ruthenium complexes that employ Noyori's chelating ligand Ts-DPEN (*N*-[(1*R*,2*R*)-2-amino-1,2-diphenylethyl]-4-toluenesulfonamide) and its derivatives (Figure 3.1) which allow high

enantioselectivity in transfer hydrogenation of ketones,²⁹ imines³⁰ and C=C double bonds,³¹ affording up to 100 % conversions. However, the use of similar complexes under biologically relevant conditions requires high aqueous solubility and thermodynamic stability. The coordination of Noyori's ligand renders the complexes highly insoluble in water, due to the presence of lipophilic phenyl groups. However, recently some water-soluble complexes have been synthesised.^{24,32,33} Given that enantioselectivity is not a requirement in NAD⁺/NADH catalysis, avoiding chiral centres offers an plausible strategy.

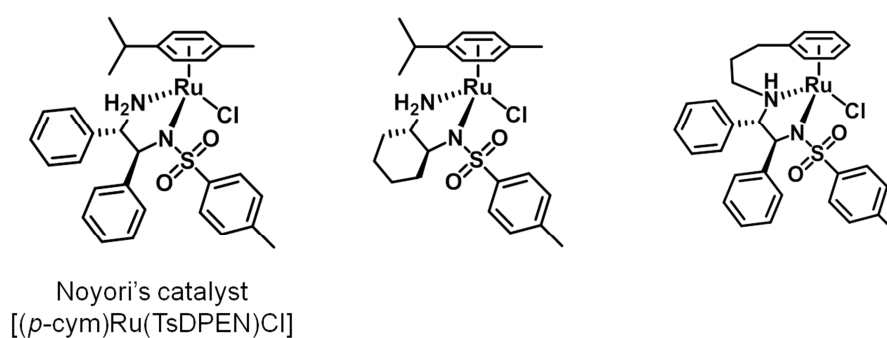
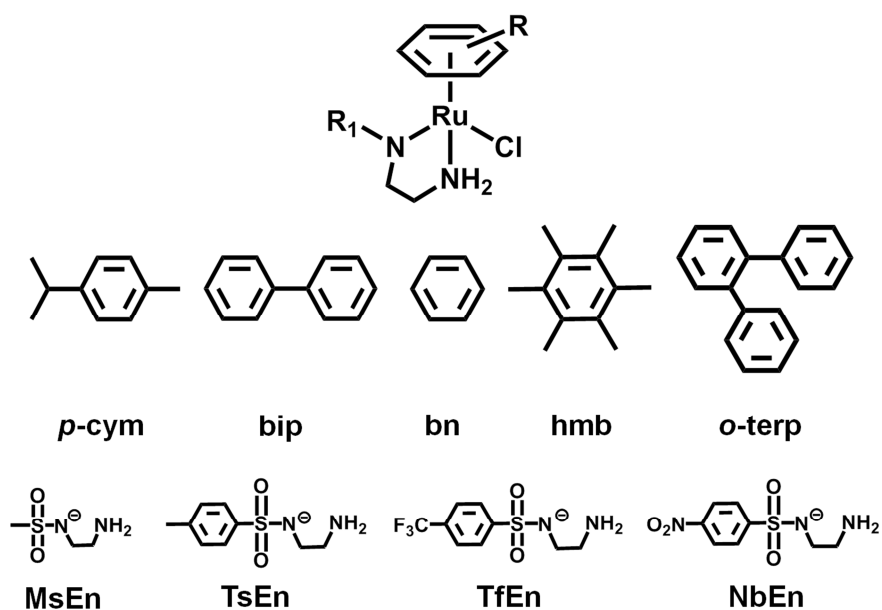


Figure 3.1. Noyori's catalyst [(*p*-cym)Ru(TsDPEN)Cl] and some well known derivatives

It has been previously reported that the Ru(II) complexes of general formula [(η^6 -arene)Ru(en)Cl]⁺ (η^6 -arene = hexamethylbenzene, *p*-cymene, indane, and en = ethylenediamine) can reduce NAD⁺ to NADH using formate as the hydride source, and that such reactions might be feasible in cells since millimolar levels of formate can be tolerated by cells.³⁴ However, due to the low catalytic activity of the complexes no effect attributed to the combination with formate was detected on A2780 human ovarian cancer cells *in vitro*.³⁴ In this chapter, the ethylenediamine chelating ligand has been modified by the addition of a sulfonamide group so that it resembles Noyori's ligand with the main goal of improving the catalytic activity of the complexes. The synthesised series of Ru(II) complexes of the type [(η^6 -arene)Ru(*N,N'*)Cl], where *N,N'* are water-soluble mono-sulphonate ethylenediamine ligands (Figure 3.2), *N*-(2-aminoethyl)-4-nitrobenzenesulfonamide (NbEn), *N*-(2-aminoethyl)-4-(trifluoromethyl)benzenesulfonamide (TfEn), *N*-(2-aminoethyl)-4-

toluenesulfonamide (TsEn), or *N*-(2-aminoethyl)methylenesulfonamide (MsEn), derived from Noyori's ligand Ts-DPEN (*N*-[(1*R*,2*R*)-2-amino-1,2-diphenylethyl]-4-toluenesulfonamide), were envisaged to give rise to good catalytic properties while maintaining their water solubility and facilitating the synthesis and purification by avoiding enantiomeric resolution.

The catalytic activity of the complexes towards the reduction of NAD^+ through transfer hydrogenation has been investigated and compared with reported ethylenediamine Ru(II) arene complexes. The mechanism of the catalysis has also been studied both experimentally and computationally in order to compare it to similar known compounds such as those reported by Steckhan and Fish.^{35, 36} The optimum conditions for the reaction have also been studied in relation to the potential of these complexes to act as catalytic anticancer drugs which modulate NAD^+/NADH levels in cells.



Complex	η^6 -arene (R)	R ₁
1	<i>p</i> -cym	methyl (MsEn)
2	<i>p</i> -cym	<i>p</i> -toluene (TsEn)
3	<i>p</i> -cym	<i>p</i> -trifluoromethylbenzene (TfEn)
4	hmb	methyl (MsEn)
5	hmb	<i>p</i> -toluene (TsEn)
6	hmb	<i>p</i> -trifluoromethylbenzene (TfEn)
7	bip	methyl (MsEn)
8	bip	<i>p</i> -toluene (TsEn)
9	bip	<i>p</i> -trifluoromethylbenzene (TfEn)
10	bn	methyl (MsEn)
11	bn	<i>p</i> -toluene (TsEn)
12	bn	<i>p</i> -trifluoromethylbenzene (TfEn)
13	<i>o</i> -terp	methyl (MsEn)
14	<i>o</i> -terp	<i>p</i> -toluene (TsEn)
15	<i>o</i> -terp	<i>p</i> -trifluoromethylbenzene (TfEn)
16	<i>p</i> -cym	<i>p</i> -nitrobenzene (NbEn)

Figure 3.2. Structures of the complexes studied in this chapter

3.2. Experimental

3.2.1. Materials

The Ru(II) arene precursor dimers $[(\eta^6\text{-arene})\text{RuCl}_2]_2$ where the $\eta^6\text{-arene}$ is *p*-cymene (*p*-cym), hexamethylbenzene (hmb), biphenyl (bip) or benzene (bn) were prepared following literature methods,³⁷ as were the ligands *N*-(2-aminoethyl)-4-(trifluoromethyl)benzenesulfonamide (TfEnH),²² *N*-(2-aminoethyl)-4-nitrobenzenesulfonamide (NbEnH),³¹ *N*-(2-aminoethyl)methylsulfonamide (MsEnH),³¹ *N*-(2-aminoethyl)-toluenesulfonamide (TsEnH).³¹ Ru(II) arene precursor dimer $[(\eta^6\text{-arene})\text{RuCl}_2]_2$ where the arene is *o*-terphenyl (*o*-terp) was kindly provided by Dr. Abraha Habtemariam from the Department of Chemistry at the University of Warwick and synthesised according to a published method.^{38,39} Magnesium sulphate, silver nitrate, potassium hydroxide, sodium chloride, perchloric acid and hydrochloric acid were obtained from Fisher Scientific. β -nicotinamide adenine dinucleotide hydrate, β -nicotinamide adenine dinucleotide, reduced dipotassium sal and sodium formate were purchased from Sigma-Aldrich. Non-dried solvents used in syntheses were obtained from Fisher Scientific and Prolabo. Solvents were used as received, except in the case of 2-propanol and methanol, which were degassed prior to use by bubbling with nitrogen.

3.2.2. Synthesis and characterisation of the complexes

$[(p\text{-cym})\text{Ru}(\text{MsEn})\text{Cl}]$ (1). $[(p\text{-cym})\text{RuCl}_2]_2$ (84.2 mg, 0.138 mmol) and MsEnH (101.6 mg, 0.35 mmol) were placed in a round-bottom flask to which 2-propanol (50 mL) and triethylamine (146 μL , 1.047 mmol) were added. The solution was heated under reflux in a nitrogen atmosphere overnight, after which the solvent was removed on a rotary evaporator to

obtain a light brown powder. The crude product was redissolved in dichloromethane and washed with brine, after which the organic layer was dried over MgSO_4 and filtered. A brown-reddish powder was obtained after removal of the solvent *in vacuo*. Brown crystals were obtained after recrystallisation from methanol/ether (1:10 v/v) by standing in a freezer for two months at 253 K. Yield: 45.3 mg (40.4 %). ^1H NMR (400 MHz, methanol- d_4): δ_{H} 5.59 (s, 2H), 5.42 (d, 2H, $J = 5.7$ Hz), 2.85 (sept, 1H, $J = 7.1$ Hz), 2.74 (s, 3H), 2.134 (s, 3H), 1.265 (d, 6H, $J = 7.1$ Hz). Anal: Calc for $\text{C}_{13}\text{H}_{23}\text{ClN}_2\text{O}_2\text{RuS}$ C: 38.28, H: 5.68, N: 6.87; Found C: 38.27, H: 5.65, N: 6.82. ESI-MS: Calc for $\text{C}_{13}\text{H}_{23}\text{ClN}_2\text{O}_2\text{RuS} (\text{M-Cl})^+$ 373.1 m/z found 373.0 m/z.

[(*p*-cym)Ru(TsEn)Cl] (2). Complex **2** was obtained following the method described above for complex **1** using the ligand TsEnH (100.6 mg, 0.42 mmol). Recrystallisation from methanol resulted in dark red crystals. Yield: 58.8 mg (36.7 %). ^1H NMR (400 MHz, acetone- d_6): δ_{H} 7.73 (d, 2H, $J = 8.3$ Hz), 7.11 (d, 2H, $J = 8.3$ Hz), 5.85 (s, 1H), 5.71 (d, 1H, $J = 5.6$ Hz), 5.64 (d, 1H, $J = 5.6$ Hz), 5.52 (d, 1H, $J = 5.6$ Hz), 5.45 (d, 1H, $J = 5.6$ Hz), 3.24 (s, 1H), 2.94 (sept, 1H, $J = 7.1$ Hz), 2.84 (m, 1H), 2.68 (m, 1H), 2.31 (s, 3H), 2.18 (m, 1H), 2.15 (s, 3H), 1.27 (d, 3H, $J = 7.0$ Hz), 1.24 (d, 3H, $J = 7.0$ Hz). Anal: Calc for $\text{C}_{19}\text{H}_{27}\text{ClN}_2\text{O}_2\text{RuS}$ C: 47.15, H: 5.62, N: 5.79; Found C: 46.70, H: 5.62, N: 5.79. ESI-MS: Calc for $\text{C}_{19}\text{H}_{27}\text{ClN}_2\text{O}_2\text{RuS} (\text{M-Cl})^+$ 449.1 m/z found 449.0 m/z.

[(*p*-cym)Ru(TfEn)Cl] (3). Complex **3** was obtained following the method described above for complex **1** using ligand TfEnH (125.0 mg, 0.47 mmol). Purification by recrystallisation was not successful and the product was used as such. Yield: 171.1 mg (85.3 %) ^1H NMR (400 MHz, acetone- d_6): δ_{H} 8.00 (d, 2H, $J = 8.1$ Hz), 7.62 (d, 2H, $J = 8.1$ Hz), 5.74 (m, 1H), 5.51 (m, 2H), 5.41 (d, 1H), 4.23 (s, 1H), 3.27 (s, 1H), 3.10 (s, 1H), 2.76 (sept, 1H, $J = 6.9$),

2.75 (m, 1H), 2.29 (m, 2H), 2.17 (s, 3H), 1.27 (m, 6H). Anal: Calc for $C_{19}H_{24}ClF_3N_2O_2RuS$ C: 42.42, H: 4.50, N: 5.21; Found C: 41.94, H: 4.45, N: 5.03. ESI-MS: Calc for $C_{19}H_{24}ClF_3N_2O_2RuS (M-Cl)^+$ 503.1 m/z, found 503.0 m/z.

[(hmb)Ru(MsEn)Cl] (4). [(hmb)RuCl₂]₂ (81.2 mg, 0.12 mmol) and *N*-(2-aminoethyl)methylsulfonamide (MsEnH) (105 mg, 0.37 mmol) were dissolved in 2-propanol (25 mL). Triethylamine (155 μ L, 1.11 mmol) was added and the solution heated to reflux (363 K) under nitrogen atmosphere for 3 h. Solvent was removed on a rotary evaporator to give a dark orange product. The crude product was redissolved in dichloromethane and washed with brine, after which the organic layer was dried over MgSO₄ and filtered. The solution was concentrated *in vacuo* and the product recrystallised from methanol to afford an orange powder. Yield: 44.1 mg (41.6 %). ¹H NMR (400 MHz, acetone-*d*₆): δ_H 2.11 (s, 18H), 2.32 (m, 2H), 2.72 (s, 3H), 2.67 (m, 2H), 4.58 (s, 2H). Anal: Calc for $C_{15}H_{27}ClN_2O_2RuS$ C: 41.32, H: 6.24, N: 6.43; Found C: 41.92, H: 6.31, N: 6.32. ESI-MS: Calc. for $C_{15}H_{27}ClN_2O_2RuS (M-Cl)^+$ 401.1 m/z, found 401.0 m/z.

[(hmb)Ru(TsEn)Cl] (5). Complex **5** was obtained following the method described above for complex **4** using ligand TsEnH (64.1 mg, 0.267 mmol). The product was recrystallised from methanol giving yellow crystals. Crystals suitable for X-ray diffraction were obtained from a methanol solution stored at 255 K. Yield: 20.5 mg (13.4%). ¹H NMR (400 MHz, acetone-*d*₆): δ_H 7.83 (d, 2H, J = 8.3 Hz), 7.07 (d, 2H, J = 8.3 Hz), 4.56 (s, 1H), 2.54 (m, 1H), 2.29 (s, 3H), 2.17 (s, 18H). Anal: Calc for $C_{21}H_{31}ClN_2O_2RuS$ C: 49.35, H: 5.92, N: 5.48; Found C: 49.17, H: 6.04, N: 5.29. ESI-MS: Calc for $C_{21}H_{31}ClN_2O_2RuS (M-Cl)^+$ 477.1 m/z, found 477.0 m/z.

[(hmb)Ru(TfEn)Cl] (6). Complex **6** was obtained following the method described above for complex **4** using ligand TfEnH (87.5 mg, 0.33 mmol). The product was recrystallised from methanol giving red crystals. Yield: 82.2 mg (58.9 %). ^1H NMR (400 MHz, CDCl_3): δ_{H} 8.05 (d, 2H, $J = 8.2$ Hz), 7.56 (d, 2H, $J = 8.2$ Hz), 3.38 (s, 1H), 3.21 (s, 1H), 3.12 (m, 1H), 2.74 (m, 1H), 2.34 (m, 1H), 2.18 (s, 18H). Anal: Calc for $\text{C}_{21}\text{H}_{28}\text{ClF}_3\text{N}_2\text{O}_2\text{RuS}$ C: 44.56, H: 4.99, N: 4.95; Found C: 44.38, H: 5.04, N: 4.87. ESI-MS: Calc for $\text{C}_{21}\text{H}_{28}\text{ClF}_3\text{N}_2\text{O}_2\text{RuS}$ (M-Cl) $^+$ 531.1 m/z, found 531.0 m/z. Crystals suitable for X-ray diffraction of **6** · **1/3 MeOH** were obtained from a methanol solution stored at 277 K.

[(bip)Ru(MsEn)Cl] (7). [(bip)RuCl₂]₂ (64 mg, 0.098 mmol) and MsEnH (70 mg, 0.243 mmol) were placed in a round-bottom flask and dissolved in methanol (25 mL). Triethylamine (109 μL , 0.783 mmol) was added and the solution was stirred at ambient temperature under nitrogen overnight, after which solvent was removed on the rotary evaporator to give a dark brown product. The crude product was redissolved in dichloromethane and washed with brine, the organic layer was dried over MgSO_4 and filtered. The solution was concentrated *in vacuo* and the product recrystallised from methanol to afford red crystals. Yield: 45.2 mg (54.3 %). Crystals suitable for X-ray diffraction were obtained from solution in methanol/ether (10:1 v/v) stored at 255 K. ^1H NMR (400 MHz, CDCl_3): δ_{H} 7.69 (m, 2H), 7.54 (m, 3H), 6.22 (t, 1H, $J = 5.6$ Hz), 6.01 (t, 1H, $J = 5.6$ Hz), 5.82 (m, 3H), 3.78 (s, 1H), 3.23 (s, 1H), 3.09 (m, 1H), 2.81 (s, 3H), 2.64 (m, 1H), 2.45 (m, 1H), 2.15 (m, 1H). Anal: Calc for $\text{C}_{15}\text{H}_{19}\text{ClN}_2\text{O}_2\text{RuS}$ C: 42.10, H: 4.48, N: 6.55; Found C: 41.88, H: 4.49, N: 6.46. ESI-MS: Calc for $\text{C}_{15}\text{H}_{19}\text{ClN}_2\text{O}_2\text{RuS}$ (M-Cl) $^+$ 393.0 m/z, found 393.0 m/z.

[(bip)Ru(TsEn)Cl] (8). Complex **8** was obtained following the method described above for complex **7** using ligand TsEnH (69.9 mg, 0.29 mmol). The product was recrystallised from methanol to give a dark orange powder. Yield: 39.9 mg (33.9 %). Crystals suitable for X-ray diffraction were obtained from a methanol solution stored at 277 K. ^1H NMR (400 MHz, CDCl_3): δ_{H} 2.35 (s, 3H), 2.51 (m, 1H), 3.08 (m, 1H), 3.22 (m, 1H), 3.68 (m, 1H), 5.77 (m, 1H), 5.96 (m, 1H), 6.03 (m, 1H), 6.39 (m, 1H), 7.17 (d, 2H, $J = 7.7$ Hz), 7.53 (m, 3H), 7.71 (m, 2H), 7.77 (d, 2H, $J = 7.7$ Hz), Anal: Calc for $\text{C}_{21}\text{H}_{23}\text{ClN}_2\text{O}_2\text{RuS}$ C: 50.04, H: 4.60, N: 5.56; Found C: 49.57, H: 4.60, N: 5.44. ESI-MS: Calc for $\text{C}_{21}\text{H}_{23}\text{ClN}_2\text{O}_2\text{RuS} (\text{M}-\text{Cl})^+$ 469.1 m/z, found 469.0 m/z.

[(bip)Ru(TfEn)Cl] (9). Complex **9** was obtained following the method described above for complex **7** using ligand TfEnH (40 mg, 0.15 mmol). The product was recrystallised from methanol to give an orange solid. Yield: 45.6 mg (54.3%). ^1H NMR (400 MHz, CDCl_3): δ_{H} 2.17 (m, 1H), 2.31 (m, 1H), 2.55 (m, 1H), 3.11 (m, 1H), 3.21 (s, 1H), 3.74 (s, 1H), 5.80 (m, 2H), 5.95 (d, 1H, $J = 5.5$ Hz), 6.04 (t, 1H, $J = 5.3$ Hz), 6.34 (t, 1H, $J = 5.8$ Hz), 7.54 (m, 3H), 7.62 (d, 2H, $J = 8.3$ Hz), 7.70 (m, 2H), 8.00 (d, 2H, $J = 8.3$ Hz). Anal: Calc for $\text{C}_{21}\text{H}_{20}\text{ClF}_3\text{N}_2\text{O}_2\text{RuS}\cdot 0.5 \text{H}_2\text{O}$ C: 44.49, H: 3.73, N: 4.94; Found C: 44.22, H: 3.59, N: 4.81. ESI-MS: Calc for $\text{C}_{21}\text{H}_{20}\text{ClF}_3\text{N}_2\text{O}_2\text{RuS} (\text{M}-\text{Cl})^+$ 523.0 m/z, found 522.9 m/z.

[(bn)Ru(MsEn)Cl] (10). $[(\text{bn})\text{RuCl}_2]_2$ (64 mg, 0.098 mmol) and MsEnH (70 mg, 0.243 mmol) were placed in a round-bottom flask and were dissolved in methanol (25 mL). Triethylamine (109 μL , 0.783 mmol) was added and the solution was stirred at ambient temperature under nitrogen overnight, after which solvent was removed on the rotary evaporator to give a dark brown oil that was dissolved in dichloromethane, washed with brine, dried over MgSO_4 and filtered. After removal of solvent on a rotary evaporator, a dark

brown oil was obtained, which was washed with ether to give a brown solid. The product was recrystallised from methanol to give a brown solid. Yield: 30 mg (49.2 %). ^1H NMR (400 MHz, CDCl_3): δ_{H} 5.67 (s, 6H), 2.80 (s, 3H). Anal: Calc for $\text{C}_9\text{H}_{15}\text{ClN}_2\text{O}_2\text{RuS}$ C: 30.73, H: 4.30, N: 7.96; Found C: 30.29, H: 4.14, N: 7.76 ESI-MS: Calc. for $\text{C}_9\text{H}_{15}\text{ClN}_2\text{O}_2\text{RuS}$ (M-Cl) $^+$ 316.4 m/z found 317.0 m/z.

[(bn)Ru(TsEn)Cl] (11). Complex **11** was obtained following the method described above for complex **10** using ligand TsEnH (100 mg, 0.417 mmol). The crude product was recrystallised from methanol to give an orange powder. Yield: 47 mg (52.4 %). ^1H NMR (400 MHz, CDCl_3): δ_{H} 7.75 (d, 2H, $J = 7.8$ Hz), 7.28 (d, 2H, $J = 7.8$ Hz), 5.71 (s, 6H), 4.89 (s, 1H), 3.14 (s, 1H), 3.05 (s, 1H), 2.75 (s, 1H), 2.35 (m, 1H), 2.35 (s, 3H). Anal: Calc for $\text{C}_{15}\text{H}_{19}\text{ClN}_2\text{O}_2\text{RuS}$ C: 42.1, H: 4.48, N: 6.55; Found C: 41.83, H: 4.48, N: 6.74. ESI-MS: calc. for $\text{C}_{15}\text{H}_{19}\text{ClN}_2\text{O}_2\text{RuS}$ (M-Cl) $^+$ 393.0 m/z, found 393.0 m/z.

[(bn)Ru(TfEn)Cl] (12). Complex **12** was obtained following the method described above for complex **10** using ligand TfEnH (100 mg, 0.380 mmol). The crude product was recrystallised from methanol to give a red powder. Yield: 53.6 mg (59.0 %). ^1H NMR (400 MHz, CDCl_3): δ_{H} 7.99 (d, 2H, $J = 8.2$ Hz), 7.62 (d, 2H, $J = 8.2$ Hz), 5.73 (s, 6H), 4.71 (s, 1H), 3.12 (m, 2H), 2.79 (m, 1H), 2.25 (m, 2H). Anal: Calc for $\text{C}_{15}\text{H}_{16}\text{ClF}_3\text{N}_2\text{O}_2\text{RuS}$ C: 37.39, H: 3.35, N: 5.81; Found C: 37.00, H: 3.39, N: 5.81 ESI-MS: Calc. for $\text{C}_{15}\text{H}_{16}\text{ClF}_3\text{N}_2\text{O}_2\text{RuS}$ (M-Cl) $^+$ 447.0 m/z, found 446.9 m/z.

[(*o*-terp)Ru(MsEn)Cl] (13). [(*o*-terp)RuCl $_2$] $_2$ (110.0 mg, 0.137 mmol) and MsEnH (79.3 mg, 0.275 mmol) were placed in a round-bottom flask and dissolved 2-propanol (50 mL). Triethylamine (42 μL , 0.299 mmol) was added and the solution was heated overnight at

reflux temperature under nitrogen atmosphere, after which solvent was removed on the rotary evaporator to give a dark brown product. The crude product was redissolved in dichloromethane and washed with brine, the organic layer was dried over MgSO_4 and filtered. The solution was concentrated *in vacuo* and the product recrystallised from methanol to afford a clear brown product. Yield: 33.3 mg (24.2 %). ^1H NMR (250 MHz, acetone- d_6): δH 7.57 (m, 4H), 7.39 (m, 6H), 6.23 (t, 1H, $J = 5.6$ Hz), 6.05 (t, 1H, $J = 5.6$ Hz), 6.02 (t, 1H, $J = 5.6$ Hz), 5.80 (t, 1H, $J = 5.6$ Hz), 5.10 (s, 1H), 3.36 (s, 1H), 2.94 (m, 1H), 2.78 (s, 3H), 2.75 (m, 1H), 2.31 (m, 1H), 2.14 (m, 3H). Anal: Calc for $\text{C}_{21}\text{H}_{23}\text{ClN}_2\text{O}_2\text{RuS}$ C: 50.04, H: 4.60, N: 5.56; Found C: 49.15, H: 4.48, N: 5.56. ESI-MS: Calc for $\text{C}_{21}\text{H}_{23}\text{ClN}_2\text{O}_2\text{RuS}$ (M-Cl) $^+$ 469.0 m/z, found 469.0 m/z.

[(*o*-terp)Ru(TsEn)Cl] (14). Complex **14** was obtained following the method described above for complex **13** using ligand TsEnH (106.3 mg, 0.497 mmol). The crude product was recrystallised from methanol to give a brown powder. Yield: 51.2 mg (23.8 %). ^1H NMR (250 MHz, acetone- d_6): δH 7.76 (d, 2H, $J = 7.6$ Hz), 7.22-7.60 (m, 12H), 6.33 (t, 1H, $J = 5.6$ Hz), 6.08 (d, 1H, $J = 5.9$ Hz), 6.05 (t, 1H, $J = 5.9$ Hz), 5.85 (t, 1H, $J = 5.5$ Hz), 5.15 (s, 1H), 3.31 (s, 1H), 2.98 (m, 1H), 2.70 (s, 3H), 2.47 (s, 3H). Anal: Calc for $\text{C}_{27}\text{H}_{27}\text{ClN}_2\text{O}_2\text{RuS}$ C: 55.90, H: 4.69, N: 4.83; Found C: 55.41, H: 4.77, N: 4.52. ESI-MS: calc. for $\text{C}_{27}\text{H}_{27}\text{ClN}_2\text{O}_2\text{RuS}$ (M-Cl) $^+$ 545.0 m/z, found 545.0 m/z.

[(*o*-terp)Ru(TfEn)Cl] (15). Complex **15** was obtained following the method described above for complex **13** using ligand TfEnH (100.2 mg, 0.374 mmol). The crude product was recrystallised from methanol to give a reddish-brown crystalline powder. Yield: 58.8 mg (24.9 %). ^1H NMR (250 MHz, acetone- d_6): δH 7.97 (d, 2H, $J = 8.4$ Hz), 7.70 (d, 2H,

$J = 8.4$ Hz), 7.27-7.57 (m, 10H), 6.32 (t, 1H, $J = 5.7$ Hz), 6.14 (t, 1H, $J = 5.7$ Hz), 6.04 (t, 1H, $J = 5.7$ Hz), 5.88 (t, 1H, $J = 5.7$ Hz), 5.22 (s, 1H), 3.28 (s, 1H), 3.08 (m, 1H), 2.75 (m, 1H), 2.33 (m, 1H), 2.14 (m, 1H), Anal: Calc for $C_{27}H_{24}ClF_3N_2O_2RuS$ C: 51.14, H: 3.82, N: 4.42; Found C: 50.85, H: 3.77, N: 4.38. ESI-MS: calc. for $C_{27}H_{24}ClF_3N_2O_2RuS$ (M-Cl)⁺ 599.0 m/z, found 599.0 m/z.

[(*p*-cym)Ru(NbEn)Cl] (16). Complex **16** was obtained following the method described above for complex **1** using ligand NbEnH (89.0 mg, 0.363 mmol). The crude product was recrystallised from methanol to give an orange crystalline powder. Yield: 117.3 mg (58.59 %). ¹H NMR (400 MHz, acetone-*d*₆): δH 8.25 (d, 2H, $J = 8.8$ Hz), 8.02 (d, 2H, $J = 8.8$ Hz), 5.81 (d, 1H, $J = 6.0$ Hz), 5.65 (d, 1H, $J = 6.0$ Hz), 5.56 (d, 1H, $J = 6.0$ Hz), 5.51 (d, 1H, $J = 6.0$ Hz), 5.34 (s, 1H), 3.03 (m, 2H), 2.94 (septet, 1H, $J = 7.0$ Hz), 2.76 (m, 1H), 1.35 (m, 6H, $J_1 = 7.0$ Hz, $J_2 = 4.6$ Hz). Anal: Calc for $C_{18}H_{24}ClN_3O_4RuS$ C: 41.98, H: 4.70, N: 8.16; Found C: 41.94, H: 4.64, N: 8.22. ESI-MS: Calc for $C_{18}H_{24}ClN_3O_4RuS$ (M-Cl)⁺ 480.0 m/z, found 480.0 m/z.

3.2.3. X-ray crystallography

Crystals of complexes **5** and **8** were obtained by Dr. Pieter Bruijninx.

X-ray crystallographic data for complexes **1**, **2**, **5**, **6** • 1/3 MeOH, **7** and **8** were collected by Dr. Guy Clarkson from the Department of Chemistry at the University of Warwick. The structures were solved by direct methods using SHELXS⁴⁰ (TREF) with additional light atoms found by Fourier transform methods. Hydrogen atoms were added at calculated positions and refined using a riding model, except the hydrogens on the NH nitrogens which were located in a difference map. Anisotropic displacement parameters were used for all non-H atoms; H-atoms were given an isotropic displacement parameter equal to

1.2 (or 1.5 for methyl and NH H-atoms) times the equivalent isotropic displacement parameter of the atom to which they are attached. The data were processed by the modeling program Mercury 1.4.1. Details of the instrumentation are described in Chapter 2.

3.2.4. Aqueous solution chemistry

Hydrolysis of the Ru-Cl bond

Solutions of complexes **1-3**, **5**, **8**, **11**, **13**, **14** and **16** (1.4 mM, 10 % MeOD-*d*₄/90 % D₂O) were prepared and monitored by ¹H NMR spectroscopy. ¹H NMR spectra were recorded at 310 K over a period of 24 h on a Bruker AV III 600 spectrometer (¹H = 600 MHz) using 5 mm diameter NMR tubes. All data processing was carried out using Topspin 2.1.

Aqua adducts of complexes **1-3**, **5**, **8**, **11**, **13**, **14** and **16** were prepared by treatment of a solution of the corresponding chlorido complex (10 % MeOD-*d*₄/90 % D₂O) with silver nitrate (1 mol equiv.) overnight and followed by filtration through Celite to remove the AgCl salt formed.

pK_a^{*} of Ruthenium aqua complexes

Changes in the chemical shifts of the arene protons of the aqua adducts for complexes **1-3**, **5**, **8**, **11**, **13**, and **16** with the pH^{*} over a range from 2 to 12 were followed by ¹H NMR spectroscopy. pH^{*} values were measured at ambient temperature using a minilab IQ125 pH meter, pH sensor and referenced in KCl gel. The pH^{*} were adjusted with KOD or DCIO₄ solutions in D₂O. ¹H-NMR spectra were recorded at 298 K on a Bruker AV III 600 spectrometer (¹H = 600 MHz) using 5mm diameter tubes. The data were fitted to the Henderson–Hasselbalch equation using Origin 7.5.

3.2.5. Reduction of NAD⁺ by [(η^6 -arene)Ru(XEn)Cl] and sodium formate

Complexes **1-12** and **16** were dissolved in D₂O or MeOD-*d*₄/D₂O (5:1) (1.4 mM, 4 mL) in a glass vial. Solutions of sodium formate (35 mM, 4 mL) and NAD⁺ in D₂O (2.8 mM, 2 mL) were also prepared and incubated at 310 K. In a typical experiment, an aliquot of 200 μ L from each solution was added to a 5 mm NMR tube and the pH* adjusted to 7.2 \pm 0.1 bringing the total volume to approximately 0.635 mL (final concentrations were: Ru complex 0.44 mM; NAD⁺ 0.88 mM; sodium formate 11.02 mM; molar ratio 1:2:25). ¹H NMR spectra were recorded at 310 K every 162 s until the completion of the reaction.

Experiments with complexes **13-15** were performed as described above, however the reduction of NAD⁺ was too fast to be able to follow by NMR and so the reactions were performed with 5 mol equiv. of NAD⁺ (final concentrations: Ru complex 0.44 mM; NAD⁺ 2.20 mM; sodium formate 11.02 mM; molar ratio 1:5:25).

3.2.6. Mechanistic studies

Hydride formation using sodium formate

Solutions of complexes **1-3** and **13-15** (1.4 mM) in MeOD-*d*₄/D₂O (5:1) were reacted with sodium formate (11.02 mM, 25 mol equiv.) at pH* 7.2 \pm 0.1. ¹H NMR spectra were recorded at 310 K every 162 s for a period of 4 h.

High resolution mass spectrometry (HR-MS) was performed on the freshly prepared samples obtained from reacting sodium formate (1000 mol equiv.) with complex **13** in order to verify the formation of the hydride adduct.

Rate-limiting step

A kinetic isotopic effect (KIE) experiment was performed by reacting complex **3** with sodium deuterio-formate (25 mol equiv.) as a deuteride source. The procedure for the kinetic experiment is described in section 3.2.5

Dependence on NAD⁺ and formate concentrations

A series of experiments were performed on complex **2** (1.4 mM) which was selected as a model catalyst. Following the same procedure described in section 3.2.5, the kinetics of the reaction was studied using different concentrations of NAD⁺ (1, 2, 3, 4 and 6 mol equiv.).

A second series of experiments using different concentrations of sodium formate (2, 5, 10, 25, 50, 100, 200 and 1000 mol equiv.) was also performed. ¹H NMR spectra were recorded at 310 K every 162 s until completion of the reaction in each case

Transfer hydrogenation reaction with 1,4-NADH

An aqueous solution of complex **2** (200 μL, 1.4 mM) was added to a NMR tube containing 1,4-NADH (400 μL, 1.4 mM) in D₂O and the pH* adjusted to 7.2 ± 0.1. ¹H NMR of the reaction mixture was recorded every 162 s for 12 hours at 310 K.

pH dependence

The optimum pH range for the catalytic process was studied in a series of experiments following the same procedure described in section 3.2.5. Each experiment was performed at a different pH* over a range from 6 to 10. The pH* of the reactions was adjusted using deuterated aqueous solutions of KOD and DCIO₄.

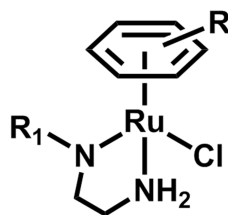
Methanol effect

A series of six experiments with complex **2** and different methanol- d_4 /D₂O ratios (0, 5, 10, 23.3, 50, 66.6 % v/v of MeOD- d_4 in D₂O) was performed in order to elucidate the effect of the mixed solvent on the turnover frequency (TOF) of the complexes.

3.3. Results

3.3.1. Synthesis and characterization

Ru(II) complexes **1-16** were synthesised (Figure 3.2) using a similar procedure. Typically, triethylamine (4 - 6 mol equiv.) and the ligand (2 - 2.5 mol equiv.), were added to an alcoholic solution of the ruthenium dimer $[(\eta^6\text{-arene})\text{RuCl}_2]_2$ and the reaction mixture stirred under an N₂ atmosphere, heating reflux or at ambient temperature. The details for individual reactions are described in the experimental section. All of the synthesised complexes were characterized by elemental analysis (CHN), mass spectrometry (ESI-MS) and ¹H NMR spectroscopy. X-ray crystal structures for complexes **1**, **2**, **5**, **6** • 1/3 MeOH, **7** and **8** were obtained. ¹H-NMR spectra were fully assigned although peaks corresponding to the CH₂ of the chelating ethylenediamine backbone, expected between 2 and 3 ppm, were broad.

Table 3.1. Complexes studied in this chapter

Complex	η^6 -arene (R)	R ₁
1	<i>p</i> -cym	methyl (MsEn)
2	<i>p</i> -cym	<i>p</i> -toluene (TsEn)
3	<i>p</i> -cym	<i>p</i> -trifluoromethylbenzene (TfEn)
4	hmb	methyl (MsEn)
5	hmb	<i>p</i> -toluene (TsEn)
6	hmb	<i>p</i> -trifluoromethylbenzene (TfEn)
7	bip	methyl (MsEn)
8	bip	<i>p</i> -toluene (TsEn)
9	bip	<i>p</i> -trifluoromethylbenzene (TfEn)
10	bn	methyl (MsEn)
11	bn	<i>p</i> -toluene (TsEn)
12	bn	<i>p</i> -trifluoromethylbenzene (TfEn)
13	<i>o</i> -terp	methyl (MsEn)
14	<i>o</i> -terp	<i>p</i> -toluene (TsEn)
15	<i>o</i> -terp	<i>p</i> -trifluoromethylbenzene (TfEn)
16	<i>p</i> -cym	<i>p</i> -nitrobenzene (NbEn)

3.3.2. X-ray crystal structures

Crystallographic data for complexes **1**, **2**, **5**, **6** • 1/3 MeOH, **7** and **8** are listed in Table 3.2 and selected bond lengths and angles in Table 3.3 and Table 3.4 Their molecular structures are depicted in Figure 3.3. These complexes adopt the familiar pseudo-octahedral ‘piano-stool’ geometry with the η^6 -bonded arene occupying one face of the complex. The chelating ligand appeared to be deprotonated and coordinated as a mono-anionic bidentate *N,N'*-ligand (amine and amide coordination). A chloride anion completes the coordination sphere around ruthenium. Especially interesting for further discussion are the distances Ru-Cl 2.4444(11) Å for [(bip)Ru(TsEn)Cl] (**8**), 2.4331(6) Å for [(bip)Ru(MsEn)Cl] (**7**), 2.4425(4) Å for [(*p*-cym)Ru(MsEn)Cl] (**1**), 2.4576 (5) Å for [(*p*-cym)Ru(TsEn)Cl] (**2**), 2.4146(8) Å for [(hmb)Ru(TsEn)Cl] (**5**) and 2.4344(6), 2.4229(6), 2.4240(6) Å for [(hmb)Ru(TfEn)Cl] (**6** • 1/3 MeOH).

Table 3.2. Crystallographic data for complexes **1**, **2**, **5**, **6** · 1/3 MeOH, **7** and **8**.

	1	2
Crystal character	orange plate	orange block
Formula	C ₁₃ H ₂₃ ClN ₂ O ₂ RuS	C ₁₉ H ₂₇ ClN ₂ O ₂ RuS
FW	407.91	484
Temp (K)	100(2)	150(2)
Crystal system	Monoclinic	triclinic
Space group	P2(1)/c	P-1
<i>a</i> (Å)	12.9751(2)	6.2342(4)
<i>b</i> (Å)	11.28045(16)	10.7643(7)
<i>c</i> (Å)	11.08448(19)	15.3024(9)
α (°)	90	89.632(5)
β (°)	105.2614(17)	85.868(5)
γ (°)	90	74.757(5)
U(A ³)	1565.17(4)	988.11(11)
λ (Å)	0.71073	0.71073
Z	4	2
D _{calc} (mg/cm ³)	1.731	1.627
μ (mm ⁻¹)	1.308	1.05
F (000)	832	496
Crystal size (mm ³)	0.30 x 0.30 x 0.02	0.23 x 0.20 x 0.14
Reflections measured	8294	16141
Indep reflection	3210	5329
R1 [I>2 σ (I)] ^a	0.0198	0.0283
wR ₂ (all data) ^b	0.0506	0.0709
CCDC n ^o .	885977	N/a

	5	6 • 1/3 MeOH
Crystal character	orange needle	orange block
Formula	$C_{22}H_{37}ClN_2O_2RuS$	$C_{21.33}H_{29.33}ClF_3N_2O_{2.33}RuS$
FW	560.12	576.71
Temp (K)	273(2)	100(2)
Crystal system	Monoclinic	Triclinic
Space group	C2/c	P-1
a (Å)	19.0923(5)	13.5906(3)
b (Å)	20.2170(5)	15.0052(4)
c (Å)	13.6455(3)	20.2331(5)
α (°)	90	94.602(2)
β (°)	111.5680(10)	105.333(2)
γ (°)	90	116.927(2)
U(A ³)	4898.2(2)	3450.54(14)
λ (Å)	0.71073	0.71073
Z	8	6
D _{calc} (mg/cm ³)	1.519	1.665
μ (mm ⁻¹)	0.863	0.936
F (000)	2328	1764
Crystal size (mm ³)	0.34 x 0.04 x 0.02	0.60 x 0.10 x 0.08
Reflections measured	30276	35851
Indep reflection	5608	16507
R1 [$I > 2\sigma(I)$] ^a	0.0412	0.0313
wR ₂ (all data) ^b	0.0922	0.0562
CCDC n ^o .	885979	885978

	7	8
Crystal character	orange rod	orange needle
Formula	$C_{15}H_{19}ClN_2O_2RuS$	$C_{25}H_{23}ClN_2O_2RuS$
FW	427.9	503.99
Temp (K)	296(2)	120(2)
Crystal system	trigonal	Monoclinic
Space group	R3c	P2(1)/c
a (Å)	25.556(5)	13.6614(4)
b (Å)	25.556(5)	6.16380(10)
c (Å)	12.7090(2)	23.7143(7)
α (°)	90	90
β (°)	90	120.2320(10)
γ (°)	120	90
U(A ³)	7188.1(3)	1951.59(9)
λ (Å)	0.71073	0.71073
Z	18	4
D _{calc} (mg/cm ³)	1.779	1.715
μ (mm ⁻¹)	1.287	1.068
F (000)	3888	1024
Crystal size (mm ³)	0.4 x 0.1 x 0.5	0.15 x 0.03 x 0.01
Reflections measured	14136	26659
Indep reflection	3939	4453
R1 [$I > 2\sigma(I)$] ^a	0.0194	0.0485
wR ₂ (all data) ^b	0.0352	0.0973
CCDC n ^o .	885976	885980

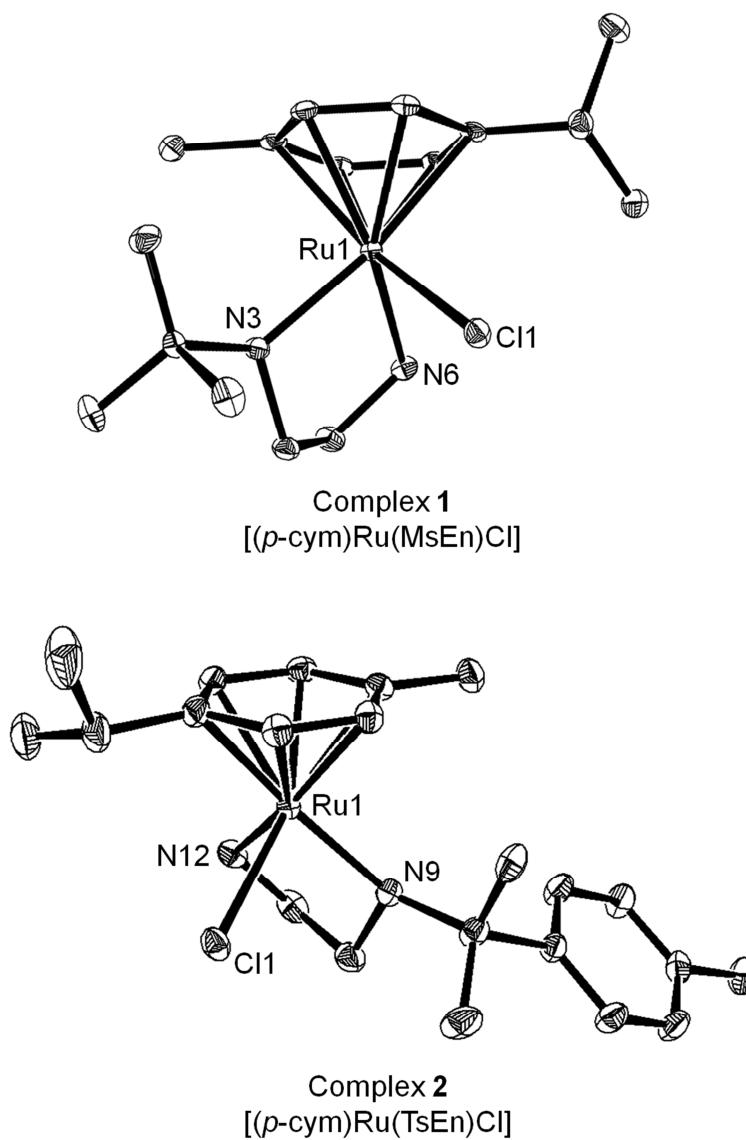


Figure 3.3. ORTEP diagrams for complexes 1, 2, 8, 7, 6 and 5. Ellipsoids are shown at the 50 % probability level. All hydrogen atoms and solvent molecules have been omitted for clarity.

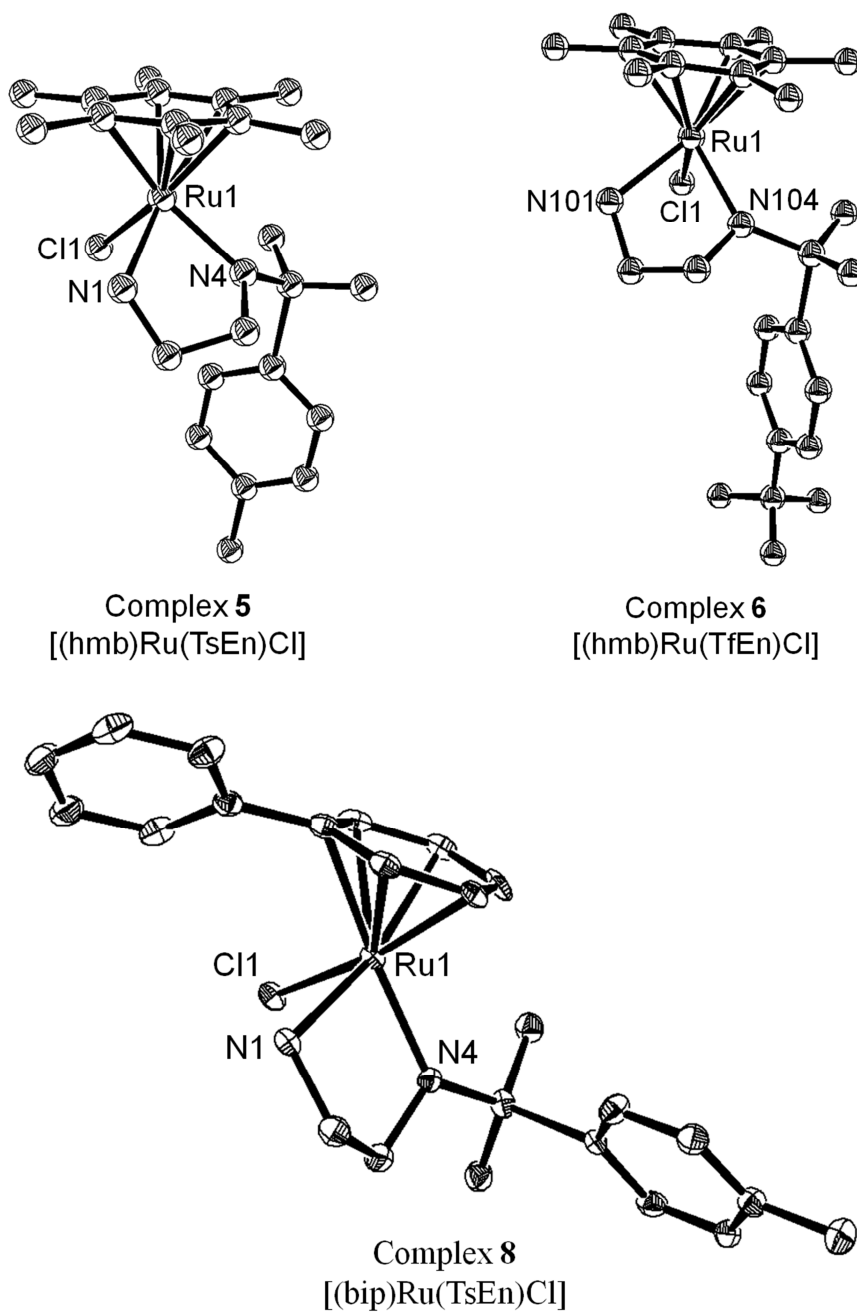


Figure 3.3. ORTEP diagrams for complexes 1, 2, 8, 7, 6 and 5. Ellipsoids are shown at the 50 % probability level. All hydrogen atoms and solvent molecules have been omitted for clarity.

Table 3.3. Selected bond length (Å) angles (°) for complexes **1**, **2**, **5**, **7** and **8**.

	1 ^a	2 ^b	5 ^c	7 ^a	8 ^c
Ru1-Na	2.1331(15)	2.1201 (18)	2.141(3)	2.1276(19)	2.122(3)
Ru1-N ⁻	2.1339(13)	2.1055 (18)	2.129(3)	2.1073(16)	2.096(4)
Ru1-Cl1	2.4425(4)	2.4576 (5)	2.4146(8)	2.4331(6)	2.4444(11)
Ru1- arene(centroid)	1.672	1.658	1.6742	1.672	1.6742
N ⁻ -Ru1-Na	78.74(6)	78.13 (7)	78.00(11)	77.80(7)	78.54(14)
Na-Ru1-Cl1	87.91(4)	86.66 (5)	89.44(8)	82.57(6)	85.44(11)
N ⁻ -Ru1-Cl1	84.53(5)	84.61 (5)	85.63(8)	88.61(5)	82.97(11)

^a N⁻ = N3, Na = N6, ^b N⁻ = N9, Na = N12, ^c N⁻ = N4, Na = N1 (see Figure 3.3 for labels)

Single crystal X-ray diffraction studies for complex **6** • 1/3 MeOH showed three crystallographic independent structures in the asymmetric unit (Figure 3.4), **6a** and **6a'** correspond to one enantiomer, **6a'** forms a H-bond to MeOH and **6b** corresponding to the other enantiomer.

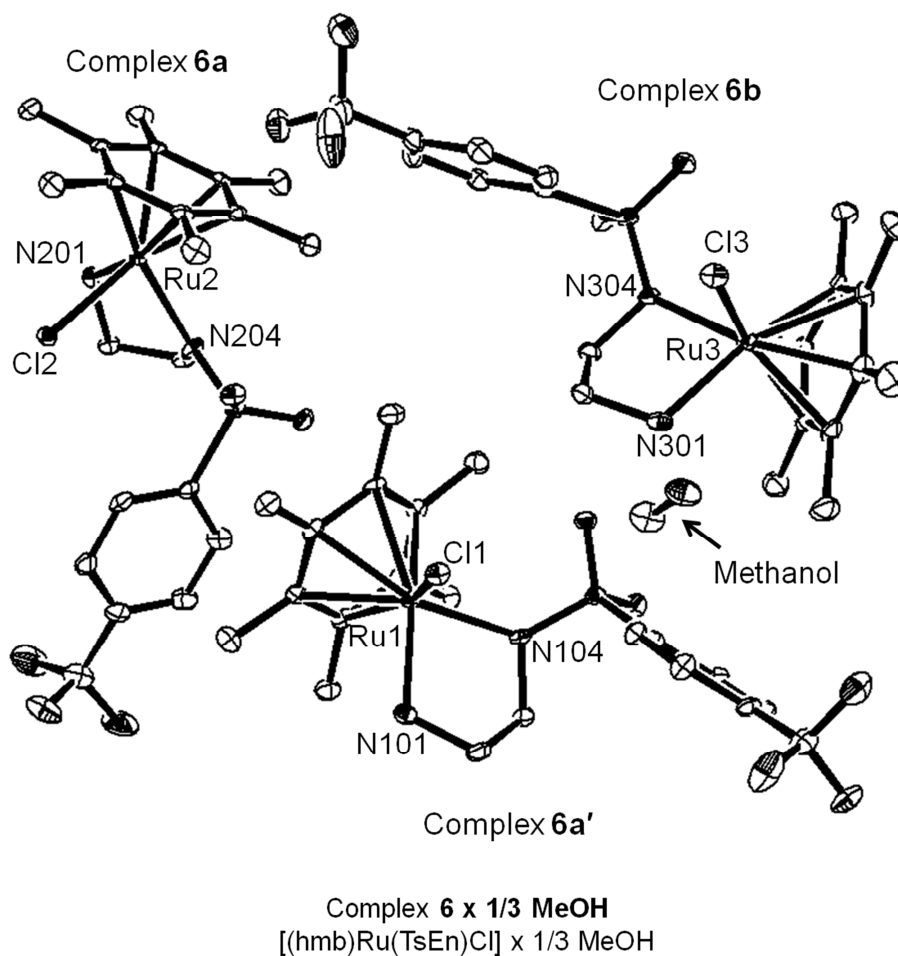


Figure 3.4. Molecular structures of the three crystallographically-independent molecules present in the unit cell of $[(\eta^6\text{-hmb})\text{Ru}(\text{TfEn})\text{Cl}] \times 1/3 \text{ MeOH}$ (**6** • 1/3 MeOH). All C-H hydrogen atoms and a methanol solvent molecule have been omitted for clarity. Displacement ellipsoids are drawn at the 50 % probability level. Structure **6a** and **6a'** are the same enantiomer but have a different bond length due to the hydrogen bond to the methanol molecule. Structure **6b** correspond to the second enantiomer.

Table 3.4. Selected bond lengths (Å) angles (°) for the three crystallographically independent molecules of complex **6** • 1/3 MeOH.

Bond length	6a	6a'	6b
Ru1-N104	2.1234(18)	2.116(2)	2.133(2)
Ru1-N101	2.134(2)	2.151(2)	2.142(2)
Ru1-Cl1	2.4229(6)	2.4344(6)	2.4240(6)
Ru1-arene(centroid)	1.675	1.679	1.674
Angle	6a	6a'	6b
N4-Ru1-N1	77.69(8)	77.58(8)	77.54(8)
N3-Ru1-Cl1	87.49(5)	90.39(6)	89.43(5)
N6-Ru1-Cl1	84.81(6)	84.74(6)	84.64(6)

3.3.3. Aqueous solution chemistry

Hydrolysis of complexes of the type $[(\eta^6\text{-arene})\text{M}(\text{N},\text{N}')\text{Cl}]$ and $[(\eta^5\text{-Cp}^x)\text{M}(\text{N},\text{N}')\text{Cl}]$ has been previously described and it is believed to precede further reactions in aqueous media.^{21,41} In order to study the hydrolysis process, aquation of complexes **1-3**, **5**, **8**, **11**, **13**, **14** and **16** was followed by ^1H NMR over a period of 24 h and no apparent changes on the spectra were observed. The peaks in the ^1H NMR spectra were assigned to the aqua adducts of the complexes since the chemical shifts of the resonances correlate to those obtained when silver nitrate (1 mol equiv.) was reacted with the corresponding chlorido complex (to remove the Cl^- ligand by formation of AgCl insoluble salt), leading to formation of the aqua complex. The rate of aquation was too fast to be determined by ^1H NMR.

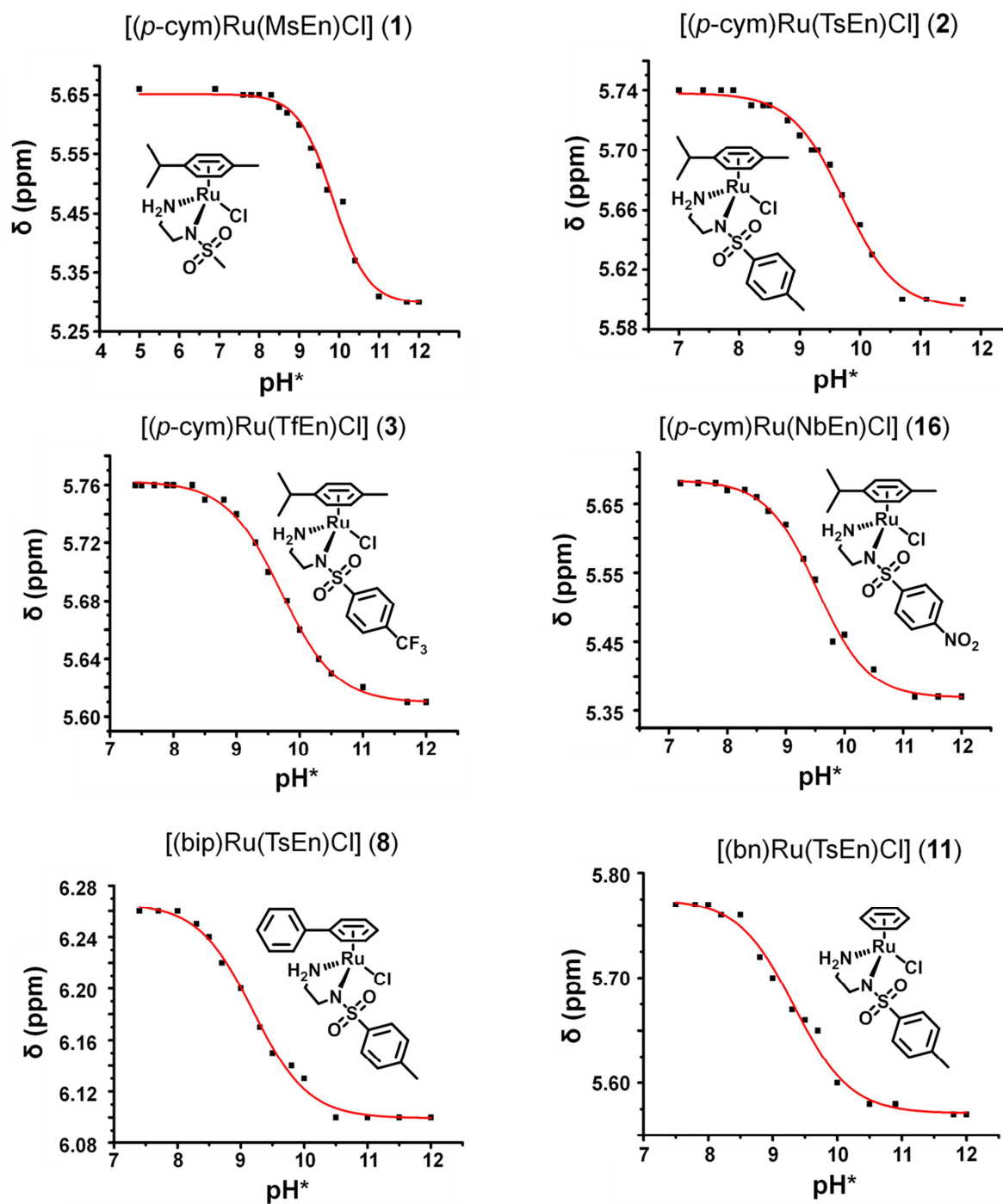


Figure 3.5. Dependence of the chemical shift of the protons in the arene rings of complexes **1**, **2**, **3**, **16**, **8** and **11** on the pH^* . The red line represent computer fits corresponding to the pK_a^* values in Table 3.5 (Henderson-Hasselbalch equation).

Changes in the ^1H NMR chemical shifts of the arene protons from the aqua adduct of complexes **1-3**, **5**, **8**, **11** and **16** were followed by changing the pH^* over the range from 2 to 12. The data were fitted to the Henderson–Hasselbalch equation. pK_a^* values for complexes **1-3**, **5**, **8**, **11** and **16** are shown in Table 3.5 (Figure 3.5).

Table 3.5. pK_a^* values for the aqua adducts of complexes **1-3**, **5**, **8**, **11** and **16** at 298 K.

Compound	pK_a^*
[(<i>p</i> -cym)Ru(MsEn)Cl] (1)	9.86 ± 0.01
[(<i>p</i> -cym)Ru(TsEn)Cl] (2)	9.78 ± 0.06
[(<i>p</i> -cym)Ru(TfEn)Cl] (3)	9.71 ± 0.01
[(hmb)Ru(TsEn)Cl] (5)	NC ^a
[(bip)Ru(TsEn)Cl] (8)	9.22 ± 0.04
[(bn)Ru(TsEn)Cl] (11)	9.33 ± 0.05
[(<i>p</i> -cym)Ru(NbEn)Cl] (16)	9.56 ± 0.04

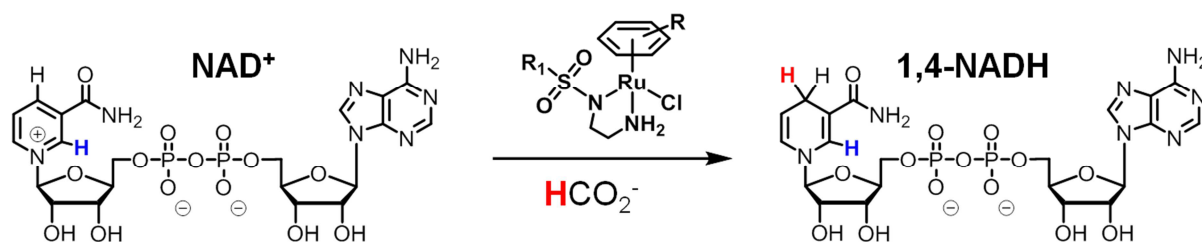
^a pK_a^* could not be determined.

3.3.4. Kinetics of transfer hydrogenation reactions

Catalytic transfer hydrogenation of nicotinamide adenine dinucleotide (NAD^+) in aqueous media using complexes **1-12** and **16** as catalyst and formate as hydride source (25 mol equiv.) was studied by ^1H NMR at 310 K and $\text{pH}^* 7.2 \pm 0.1$. In order to compare the catalytic activity of the complexes and due to the poor solubility of complexes **6-9**, the experiments were also performed in the mixed solvent $\text{MeOD-}d_4/\text{D}_2\text{O}$ (2:9 v/v).

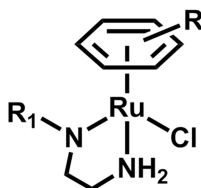
Molar ratios of NAD^+ and NADH were determined by integrating the signals corresponding to H of NAD^+ (9.33 ppm) and H of 1, 4- NADH (6.96 ppm) (Scheme 3.1). The turnover numbers (TON) for the reactions were determined as described in the experimental

section. An important increase on the catalytic activity due to the effect of methanol on the TON was discovered (*vide infra*).



Scheme 3.1. Scheme of the reduction of NAD^+ to 1,4-NADH in the presence of formate as an hydride source.

The turnover frequencies (TOF, the increment of turnover number over time), showed a marked dependence of the catalytic activity on the arene (Table 3.6). Complexes of the type $[(\eta^6\text{-arene})\text{Ru}(\text{XEn})\text{Cl}]$, where X is Nb, Tf, Ts or Ms, are more active when the arene is benzene and activity decreases in the order $\text{bn} > \text{bip} > p\text{-cym} > \text{hmb}$. It was also evident from the turnover frequencies that catalytic activity depends on the XEn ligand. The complex with the chelated ligand containing the more electron-withdrawing sulfonamide substituent (NbEn) exhibited the highest activity while the complex with the least electron-withdrawing sulfonamide substituent (MsEn) was the least active (Table 3.6). $[(\text{bn})\text{Ru}(\text{TfEn})\text{Cl}]$ (**12**) with a TOF of $10.4 \pm 0.5 \text{ h}^{-1}$ was the most active.

Table 3.6. Turnover frequencies for transfer hydrogenation reactions using catalysts **1-12** and **16**.

Complex	η^6 -arene (R)	XEn ligand (R ₁)	TOF (h ⁻¹)	
			D ₂ O/MeOD- <i>d</i> ₄ ^a	D ₂ O
Complex 1	<i>p</i> -cym	MsEn	1.25 ± 0.03	1.11 ± 0.02
Complex 2	<i>p</i> -cym	TsEn	2.88 ± 0.06	1.58 ± 0.04
Complex 3	<i>p</i> -cym	TfEn	5.77 ± 0.27	3.06 ± 0.05
Complex 4	hmb	MsEn	0.15 ± 0.01	0.14 ± 0.01
Complex 5	hmb	TsEn	0.38 ± 0.01	0.34 ± 0.02
Complex 6	hmb	TfEn	1.47 ± 0.04	— ^b
Complex 7	bip	MsEn	3.04 ± 0.19	— ^b
Complex 8	bip	TsEn	4.28 ± 0.14	— ^b
Complex 9	bip	TfEn	7.45 ± 0.38	— ^b
Complex 10	bn	MsEn	4.09 ± 0.16	2.94 ± 0.16
Complex 11	bn	TsEn	6.76 ± 0.45	4.50 ± 0.12
Complex 12	bn	TfEn	10.39 ± 0.51	6.62 ± 0.16
Complex 16	<i>p</i> -cym	NbEn	9.63 ± 0.31	4.05 ± 0.11

^a 23 % MeOD-*d*₄/ 77 % D₂O, ^b not soluble in D₂O

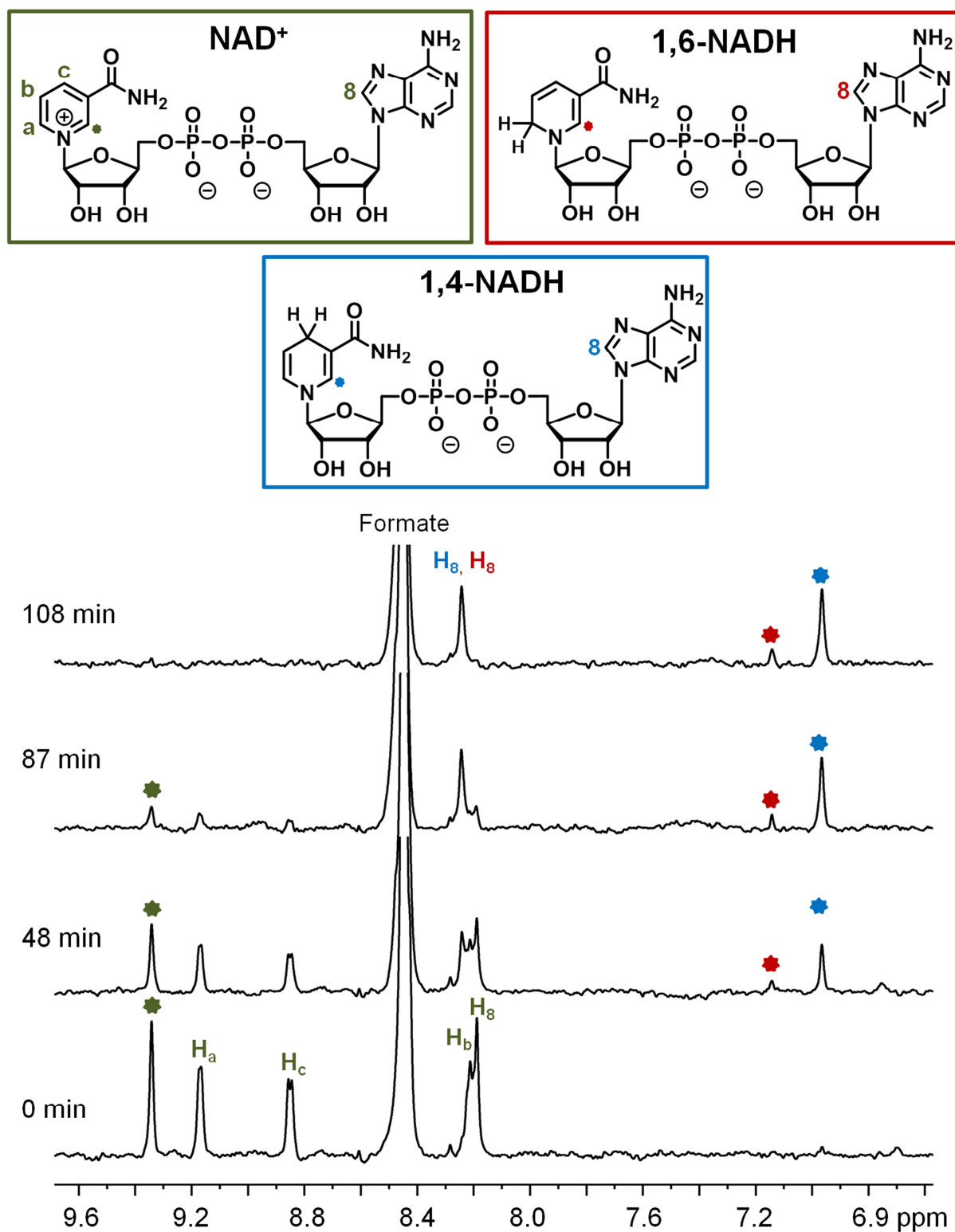


Figure 3.6. ^1H NMR spectra recorded during NAD^+ reduction using complex **1** [$p\text{-cym}$] $\text{Ru}(\text{MsEn})\text{Cl}$] as a catalyst, (ratio 1:2:25, Complex: NAD^+ :formate). The experiment was performed in D_2O at $\text{pH}^* 7.2 \pm 0.1$ and temperature 310 K. **Green** = NAD^+ , **Blue** = 1,4-NADH and **Red** = 1,6-NADH.

The reaction was regioselective giving 1,4-NADH in 93% yield when complex **4** was used. A similar regioselectivity was achieved with complexes containing hexamethylbenzene (**5** and **6**). Use of the *p*-cymene complexes **1**, **2**, **3** and **16** as catalysts also produced 1,6-NADH (up to 18 %) with complex [(*p*-cym)Ru(NbEn)Cl] (**16**) giving the lower regioselectivity from the three *p*-cymene complexes (17.5 % of 1,6-NADH formed). Finally complexes **10**, **11** and **12** containing benzene as arene, gave 23 to 25 % of 1,6-NADH.

Transfer hydrogenation reactions with complexes containing ortho-terphenyl

Catalytic transfer hydrogenation to nicotinamide adenine dinucleotide (NAD⁺) in MeOD-*d*₄/D₂O (2:9 v/v) using complexes **13-15** as catalyst and formate as a hydride source (ratio 5:1:25 mol equiv, NAD⁺:complex:formate) was studied by ¹H NMR at 310 K and pH* 7.2 ± 0.1. During the reaction, formation of a brown precipitate was observed. As a consequence, the TON of these complexes could not be determined since the concentration of the ruthenium catalyst in solution was unknown.

Completion of the catalytic reaction was achieved within the first 10 min of using any of the complexes (**13-15**). When comparing the reaction times of the complexes **13-15** with complex **12** [(bn)Ru(TfEn)Cl], which shows higher catalytic activity amongst those previously described (19 min for completion), a significant improvement can be observed. Furthermore the reaction using complexes **13-15** were performed with 2.5 x times higher concentration of NAD⁺ compared to the experiments using complex **12**.

In order to determine whether the precipitation of the complex could lead to quenching of the catalytic process, experiments with 100 mol equiv. of NAD⁺ (46.6 mM) were performed. ¹H NMR recorded every 162 s at 310 K for 5 h 48 min showed a 88.5 % conversion from NAD⁺ to NADH of which 20 % was 1,6-NADH.

3.3.5. Mechanistic studies

The rate-limiting step of the catalytic cycle in the NAD^+ reduction was investigated by studying the reaction of complex **3** ($[(p\text{-cym})\text{Ru}(\text{TfEn})\text{Cl}]$) with deuterio-formate (25 mol equiv.) as a deuteride source. The turnover frequency ($\text{TOF} = 1.26 \pm 0.02 \text{ h}^{-1}$) was 2.4 times slower than that obtained using formate as the hydride source ($\text{TOF} = 3.06 \text{ h}^{-1}$).

The dependence of the rate of catalytic activity on the concentrations of NAD^+ and formate was determined using complex **2** ($[(p\text{-cym})\text{Ru}(\text{TsEn})\text{Cl}]$) as a model system. Accordingly, five experiments were performed with complex **2**, sodium formate and NAD^+ with ratio of 1:25:x, respectively, where $x = 1, 2, 3, 4$ or 6 mol equiv., and ^1H NMR spectra were recorded every 2 min until 100 % conversion was achieved. The analysis of the experiments gave an unchanged turnover frequency (1.58 h^{-1}).

A second series of experiments was performed in order to investigate the dependence of the reaction rate on the formate concentration. Experiments with complex **2**, sodium formate and NAD^+ in the ratio 1:x:2, respectively, where $x = 2, 5, 10, 25, 50, 100$ or 200 mol equiv. of formate were performed. The plot of the data obtained shows a strong dependence of the turnover frequency on formate concentration (Figure 3.7).

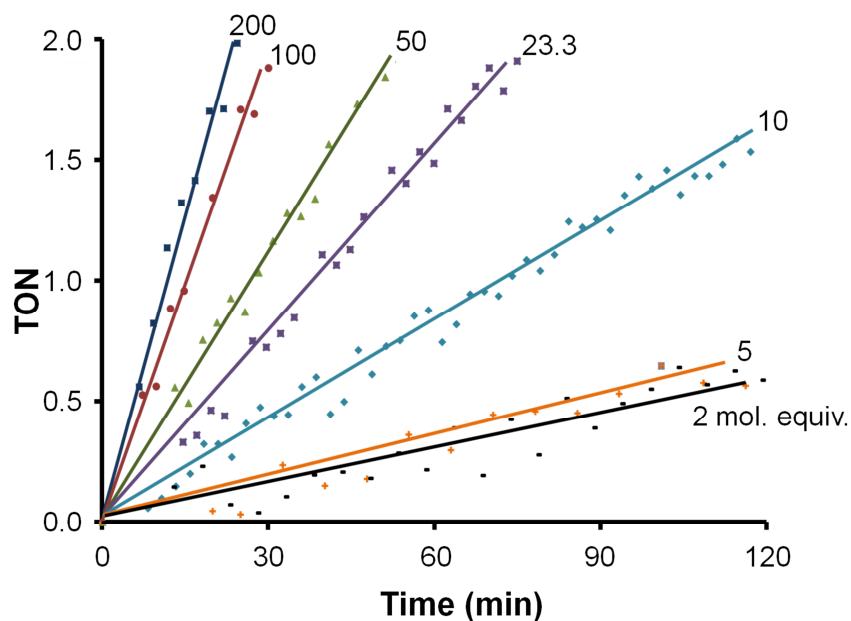


Figure 3.7. Plot of the turnover number against time for the reduction of NAD^+ by complex **2** using formate as a hydride source (ratio 2:1:x, $x=2, 5, 10, 25, 50, 100$ or 200 mol equiv., respectively. $\text{pH}^* 7.4$, temperature 310 K , solvent D_2O). Time is referenced to the mixing time.

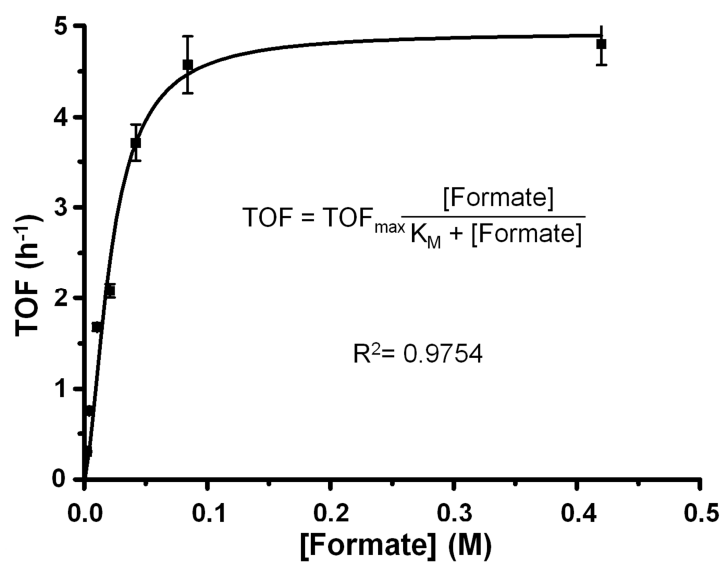


Figure 3.8. Plot of the TOF against the formate concentration, for the reduction of NAD^+ in the presence of different formate concentrations, catalysed by complex **2**.

A typical Michaelis-Menten kinetic behaviour is apparent from a plot of turnover frequency versus formate concentration (Figure 3.8).³⁴ Thus, from the double-reciprocal plot (Figure 3.9), the Michaelis constant ($K_M = 42.1$ mM) and the maximum turnover frequency ($\text{TOF}_{\text{max}} = 6.9$ h⁻¹) were calculated.

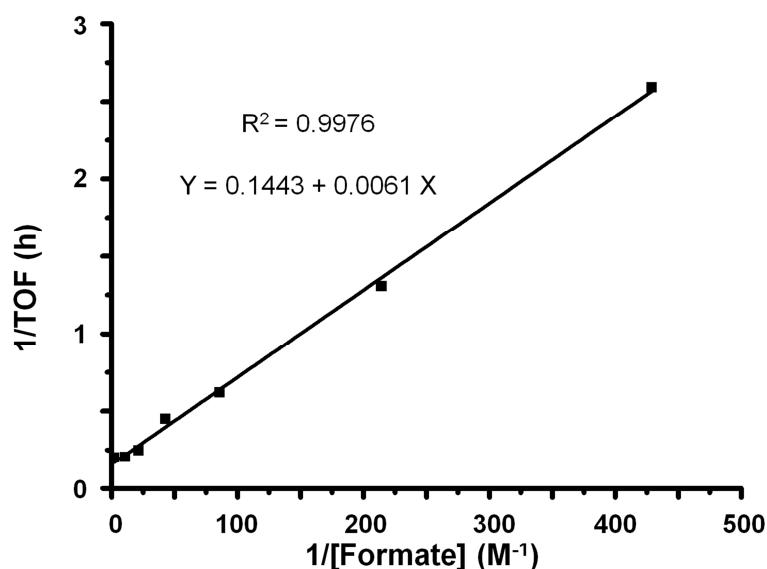


Figure 3.9. A plot of the reciprocal of the TOF against formate concentration, for the reduction of NAD^+ in the presence of different mol equiv. of formate, catalysed by complex **2**. For a reaction following Michaelis-type kinetics, $\text{TOF} = \text{TOF}_{\text{max}} [\text{S}]/(K_M + [\text{S}])$, where TOF_{max} is the turnover frequency at infinite substrate (formate) concentration, $[\text{S}]$ is the substrate concentration, and K_M is the Michaelis constant. Hence, $\text{TOF}^{-1} = (K_M/\text{TOF}_{\text{max}})(1/[\text{S}]) + (1/\text{TOF}_{\text{max}})$ and K_M (42.14 mM) and TOF_{max} (6.93 h⁻¹) can be obtained from the gradient and y intercept, respectively, of the double-reciprocal plot.

In order to explore the possibility of hydride transfer from 1,4-NADH to ruthenium(II) arene complexes containing XEn chelating ligands (X = Ts, Tf, Ms, Nb) an experiment with complex **2** and 1,4-NADH (ratio 1:2) in D_2O and $\text{pH}^* 7.2 \pm 0.1$ was performed. ¹H NMR spectra of the reaction mixture were recorded every 162 s for 12 hours at 310 K. Neither the formation of hydride adducts nor NAD^+ was observed.

The pH^* dependence of the catalytic reaction (from pH^* 6 to 10) was also investigated *via* a series of experiments using complex **2**, sodium formate and NAD^+ (ratio 1:25:2, respectively) in D_2O . A strong dependence on pH^* was observed. The highest TOF (1.58 h^{-1}) was achieved at pH^* 7.2, followed by a decrease in the activity when the pH^* increased (Figure 3.10).

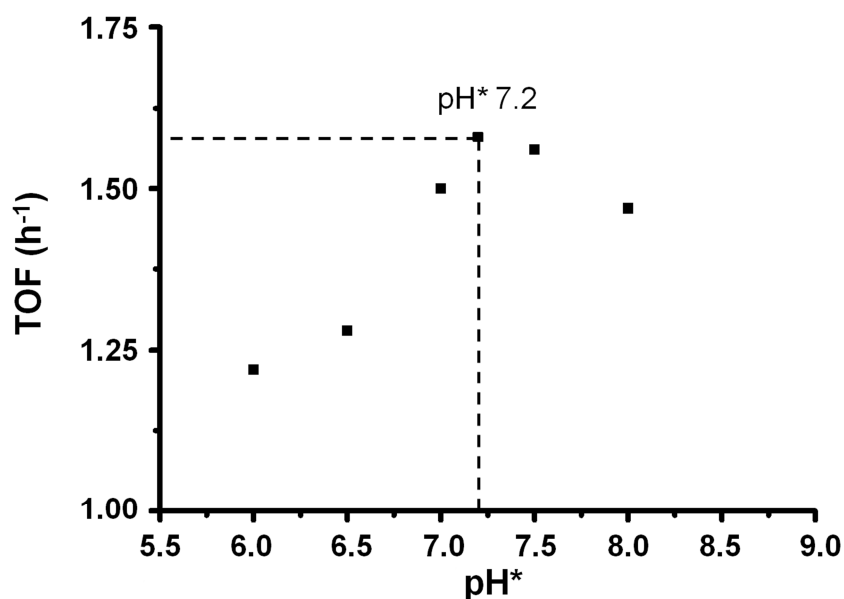


Figure 3.10. Dependence of turnover frequency on the pH^* for the reduction of NAD^+ by complex **2** using formate as a hydride source (mol ratio 2:1:25, respectively, 310 K in D_2O). Maximum turnover frequency is achieved at $\text{pH} 7.2 \pm 0.1$.

The catalytic activity of all the complexes was initially studied in D_2O , but complexes **6-9** and **13-15** could not be dissolved at the same concentration (1.4 mM). For this reason, experiments were also performed in a D_2O /methanol (9:2 v/v) mixture in order to increase the solubility. The addition of methanol in the reaction mixture resulted in higher turnover frequencies (Table 3.6) for catalysts **1-5** and **10-12** compared to the reaction in pure D_2O . In order to study the effect of methanol on the reaction, five experiments with catalyst **2**, sodium formate and NAD^+ (ratio 1:25:2, pH^* 7.2 ± 0.1 , 310 K) were performed in $\text{D}_2\text{O}/\text{MeOD-}d_4$

(5, 10, 23.3, 50 or 66% v/v in MeOD- d_4). Increased percentage of methanol resulted in faster reaction rate and therefore higher turnover frequency (Figure 3.11).

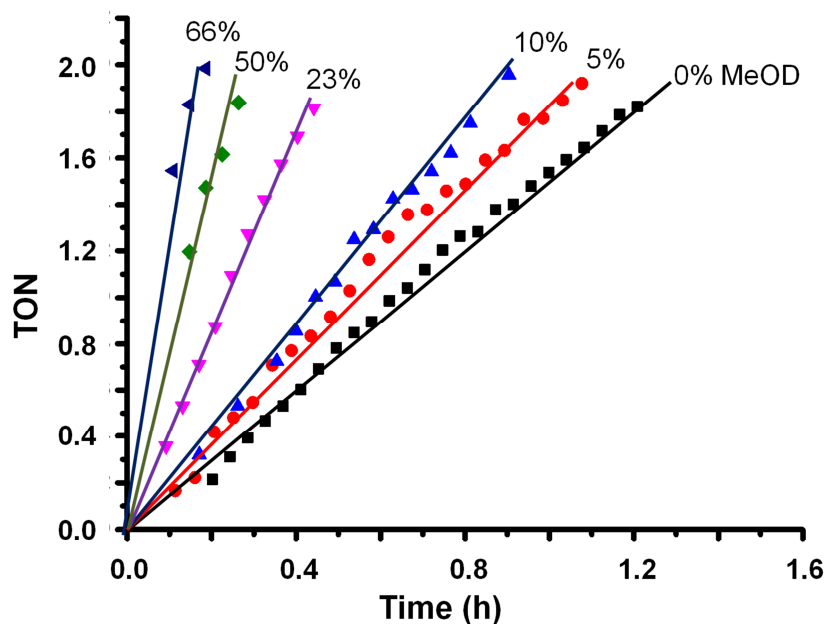


Figure 3.11. Dependence of the turnover number on time for the reduction of NAD^+ by complex **2** in various $\text{D}_2\text{O}/\text{MeOD-}d_4$ mixtures (5, 10, 23, 50 or 66 % v/v of MeOD- d_4).

Hydride formation using sodium formate

Solutions of complexes **1-3** and **12** (0.4 mM in D_2O) and **13-15** (0.44 mM in MeOD- $d_4/\text{D}_2\text{O}$ 2:9 v/v) were added to an aqueous solution of sodium formate (4.4 mM) and pH* adjusted to 7.4 ± 0.1 . ^1H NMR experiments were recorded every 162 s at 310 K for a period of 4 h. No signals corresponding to hydride adducts were detected for complex **1-3** and **15** in the high field region (0 to -20 ppm). However peaks assigned to the hydride adduct for complexes **12-14** were identified at -7.0 ppm, -5.5 ppm and -5.6 ppm, respectively. (Figure 3.12). Interestingly, complex **12** decomposes releasing benzene (Figure 3.13).

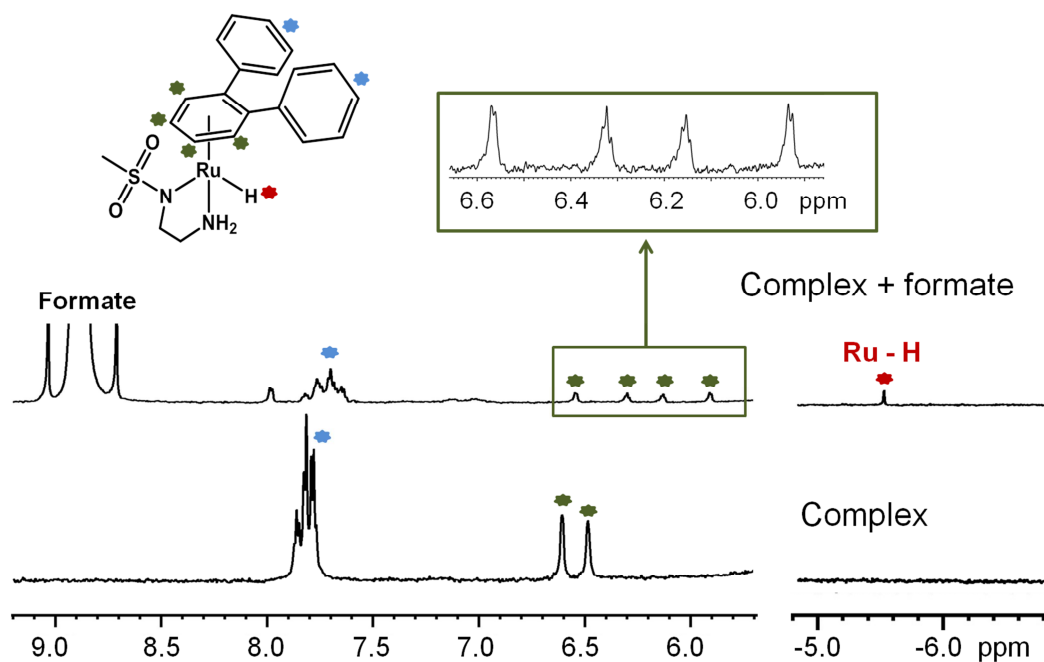


Figure 3.12. ^1H NMR spectra of the reaction between complex **13** and sodium formate (ratio 1:1000). The experiment was performed in D_2O , pH^* 7.2 and temperature 310 K.

Green arene, **blue** phenyl groups of the arene and **red** hydride.

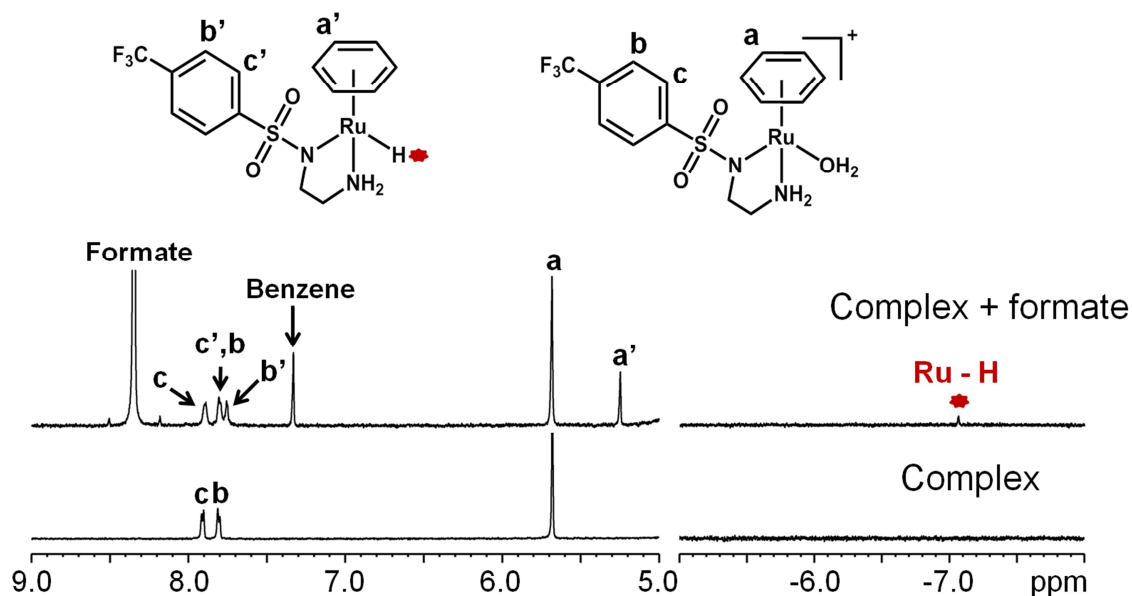


Figure 3.13. ^1H NMR spectra of the reaction between complex **12** and sodium formate (ratio 1:1000). The experiment was performed in D_2O , pH^* 7.2 and temperature 310 K. **red** hydride.

In order to confirm the formation of the ruthenium hydride species HR-mass spectrum was recorded (Table 3.7). A peak with a mass-to-charge ratio of 493.0499 was detected and assigned as hydride adduct. Interestingly, a peak identified as a formate adduct of complex **13** with a mass-to-charge ratio of 537.0392 was also detected (Figure 3.14, Figure 3.15).

Table 3.7. All relevant mass-to-charge ratios from the high resolution-mass spectrum of the reaction between sodium formate and complex [(*o*-terp)Ru(MsEn)Cl] (**13**) at pH 7.3 ± 0.1 .

Proposed chemical formula		Calculated (m/z)	Found (m/z)
$C_{21}H_{23}N_2O_2RuS^+$	$[M-Cl]^+$	469.0518	469.0533
$C_{21}H_{22}N_2NaO_2RuS^+$	$[M-HCl+Na]^+$	491.0343	491.0377
$C_{21}H_{24}N_2NaO_2RuS^+$	$[M(H)+Na]^+$	493.0499	493.0456
$C_{22}H_{24}N_2NaO_4RuS^+$	$[M(HCOO)+Na]^+$	537.0392	537.0396

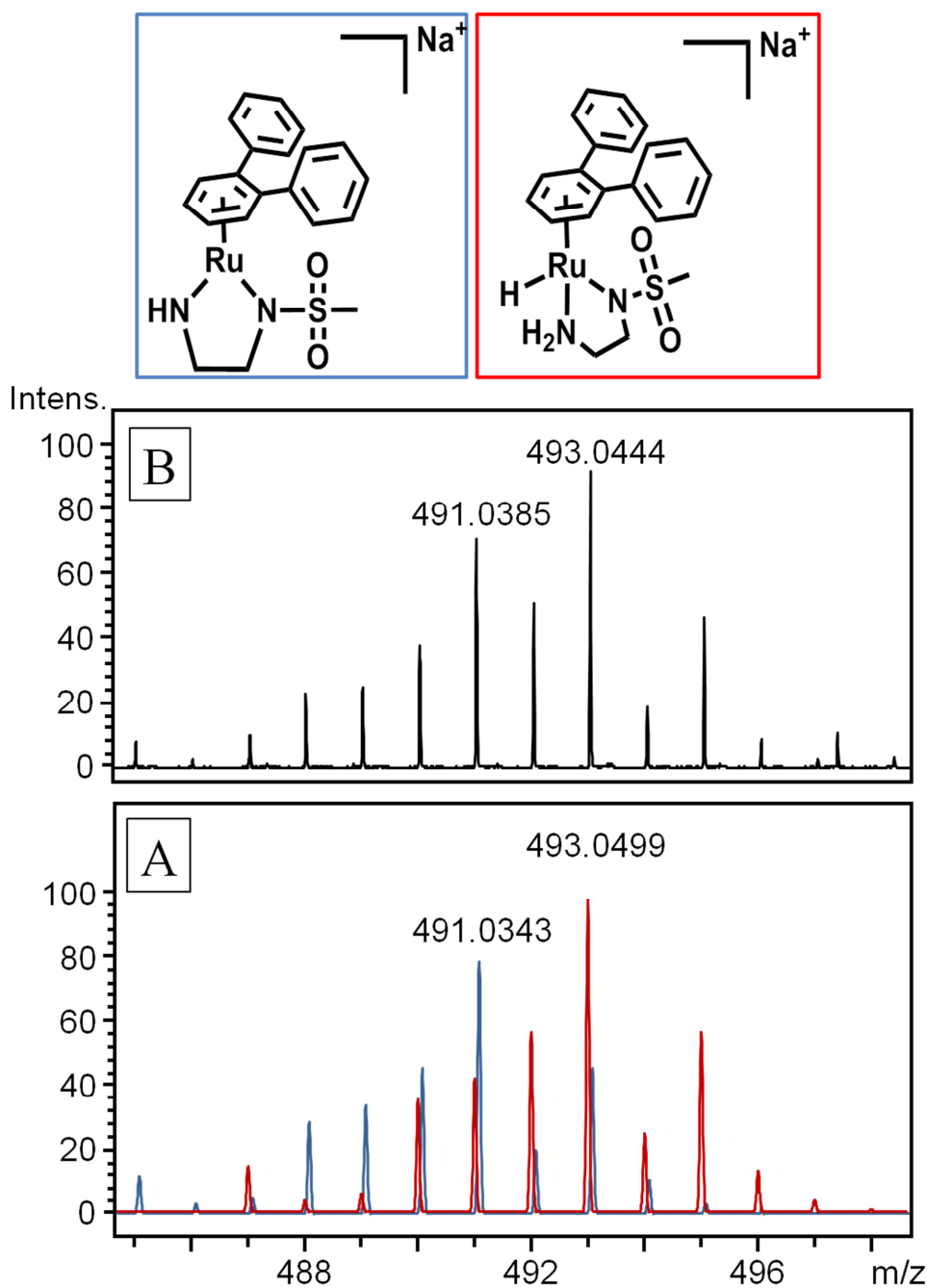


Figure 3.14. High resolution mass spectrum of the reaction mixture between complex **13** and formate. (A) Calculated spectra (red) hydride adduct of complex **13**, (blue) complex **13** - HCl, (B) experimental spectrum.

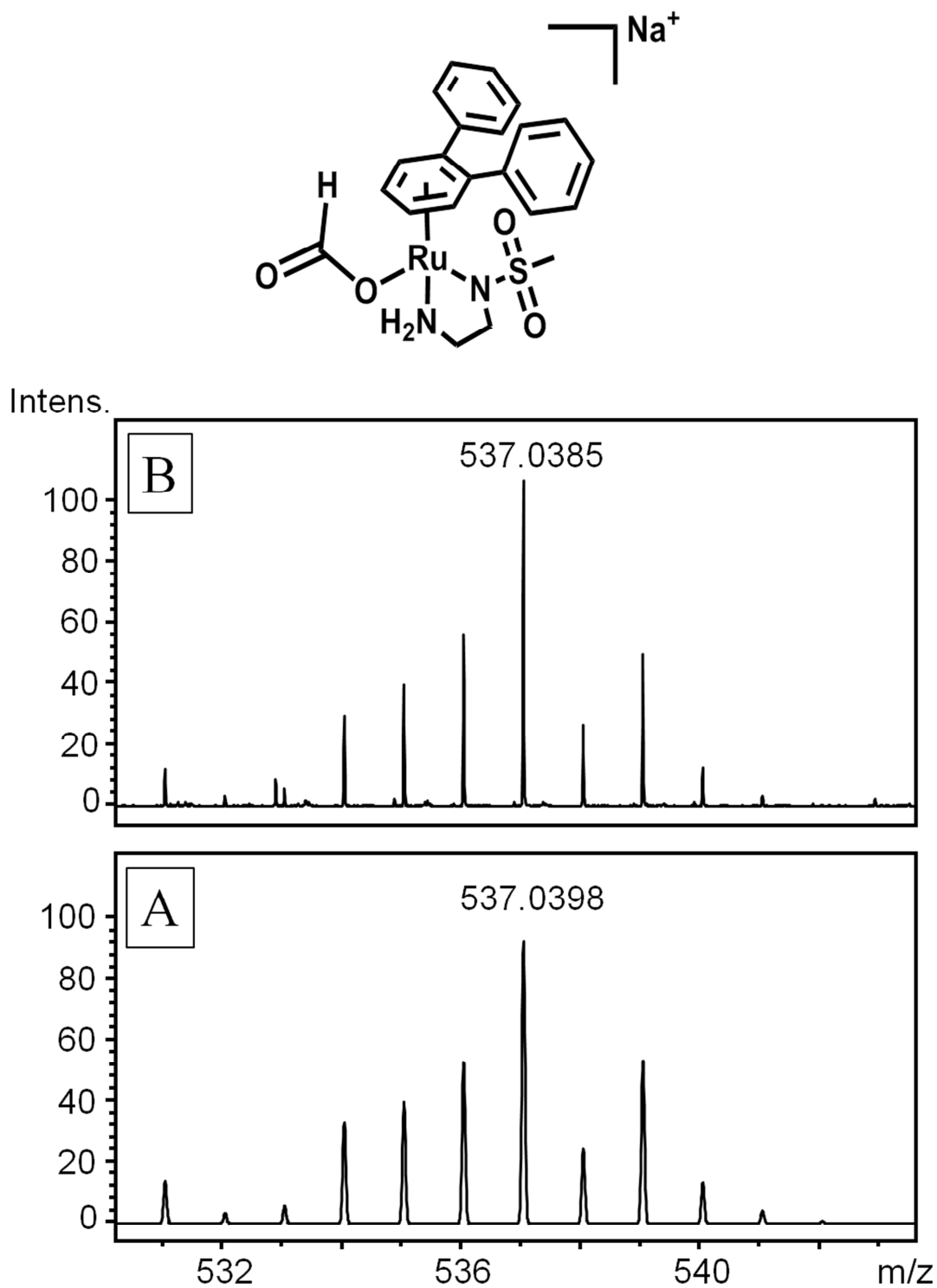


Figure 3.15. High resolution mass spectrum of the reaction mixture between complex **13** and formate. (A) Calculated spectrum for the formate adduct of complex **13**, (B) experimental spectrum.

DFT Calculations

Computational experiments were carried out by Prof. Rob Deeth at university of Warwick.

A DFT mechanistic study was performed with the aqua complex $[(bn)Ru(MsEn)(H_2O)]^+$ (**10**) in the presence of formate. The energy of the formate complex plus water was found to be lower than the energy of the aqua complex plus formate, so the formate complex was taken as the reference point for determining barriers to CO_2 elimination.

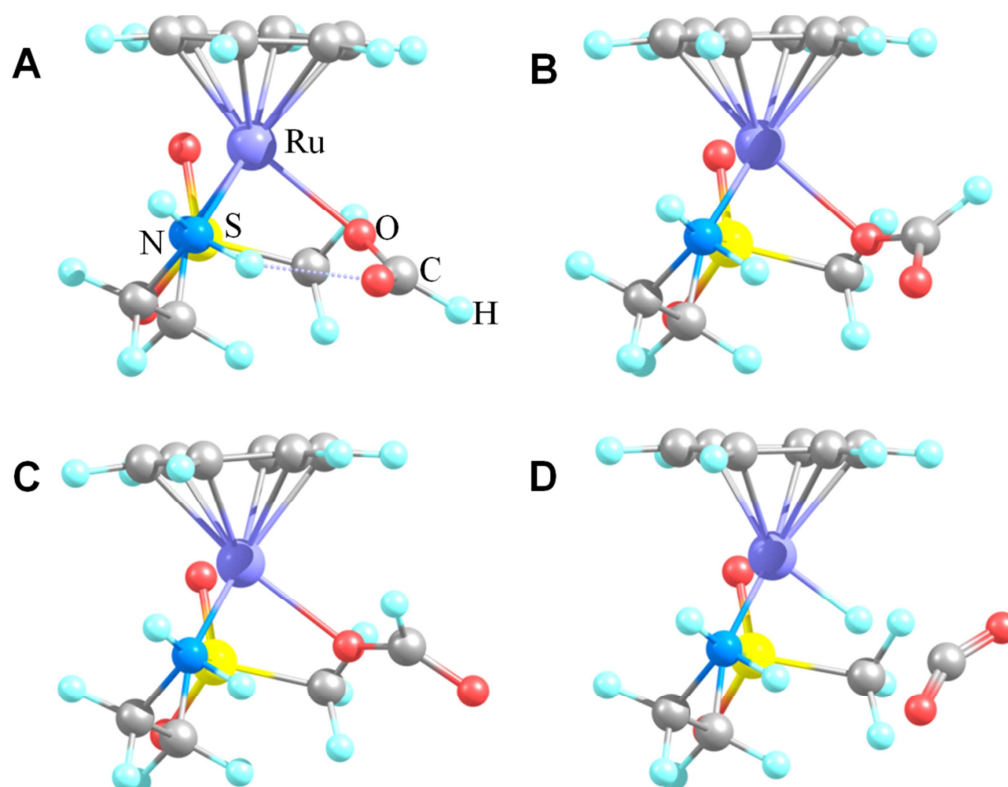


Figure 3.16. Calculated DFT structures for the formate adduct of $\{(bn)Ru(MsEn)\}^+$ (from **10**). (A) Intermediate complex with formate bound *via* a single oxygen with an H-bond between the second formate oxygen and NH from the chelating ligand. (B) Transition state for the rotation of formate which orients the hydrogen towards the metal centre. (C) Intermediate showing the hydrogen now oriented towards the Ru centre, and finally (D) the transition state for the formation of the ruthenium-hydride bond and CO_2 elimination.

The formate coordinates *via* a single oxygen with the carbonyl moiety making an H-bond with an NH proton (Figure 3.16). It then rotates *via* a low-energy transition state to an intermediate with the formate H now oriented towards the Ru centre. From here, the Ru-H bond is formed *via* a higher energy transition state (TS).

The energies of this process and for CO₂ elimination for the formate adducts of the complexes {(bn)Ru(MsEn)}⁺ (**10**), {(bn)Ru(TsEn)}⁺ (**11**) and {(bn)Ru(TfEn)}⁺ (**12**) and for the formate adduct of the hmb complex {(hmb)Ru(MsEn)}⁺ (**4**) are shown in Table 3.8

Table 3.8. Computed DFT(B3LYP) free energy barriers ΔG^\ddagger (kcal mol⁻¹) leading to CO₂ elimination.

Complex	ΔG^\ddagger Twist	ΔG^\ddagger CO ₂ elim
10	5.9	13.7
11	4.2	12.9
12	4.2	12.6
4	-	18.1

3.4. Discussion

3.4.1. Structures of the complexes

The ligands NbEnH, TsEnH, TfEnH and MsEnH (Figure 3.17) were selected in order to compare the catalytic activity properties of the complexes of the type [(η^6 -arene)Ru(XEn)Cl], where X = Ms, Ts, Tf or Nb, with an increasing electron-withdrawing power of the sulfonamide.

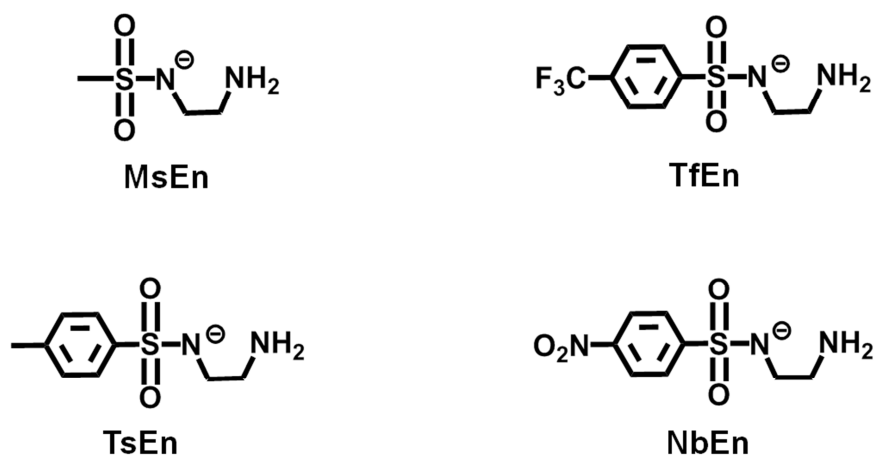


Figure 3.17. Structures of the N,N' ligands used for this chapter

Single crystals of complexes $[(p\text{-cym})\text{Ru}(\text{MsEn})\text{Cl}]$ (**1**), $[(p\text{-cym})\text{Ru}(\text{TsEn})\text{Cl}]$ (**2**), $[(\text{hmb})\text{Ru}(\text{TsEn})\text{Cl}]$ (**5**), $[(\text{bip})\text{Ru}(\text{MsEn})\text{Cl}]$ (**7**) and $[(\text{bip})\text{Ru}(\text{TsEn})\text{Cl}]$ (**8**) were obtained and analyzed by X-ray diffraction. The crystal structure of complex $[(\text{hmb})\text{Ru}(\text{TfEn})\text{Cl}] \times 1/3 \text{ MeOH}$ (**6** • **1/3 MeOH**) shows an asymmetric unit containing three crystallographically-independent molecules. One of the ruthenium molecules (**6a'**) establishes an intramolecular hydrogen bond with a methanol molecule. The other two molecules (**6a** and **6b**) are enantiomers with similar bond lengths and angles (Table 3.4) which are slightly different than those of complex **6a**.

Comparison with the analogous ethylenediamine complex,^{42,43} shows no significant difference between the Ru-NH₂ distance and the distance Ru-N⁻ despite the higher electron density on the imino nitrogen (2.130 (3) Å for $[(p\text{-cym})\text{Ru}(\text{en})\text{Cl}]$), 2.1331 (15) Å for $[(p\text{-cym})\text{Ru}(\text{MsEn})\text{Cl}]$ **1**), 2.11 Å for $[(\text{bip})\text{Ru}(\text{en})\text{Cl}]$, 2.096 (4) Å and 2.1073 (16) Å for complexes **8** and **7**, respectively). However, comparing with the complexes containing hmb, the distance Ru-N⁻ is slightly shorter (*ca.* 0.02 - 0.03 Å). The Ru-N⁻ distance of $[(p\text{-cym})\text{Ru}(\text{en})\text{Cl}]$ (2.130 (3) Å) compared with that from complex **2** $[(p\text{-cym})\text{Ru}(\text{TsEn})\text{Cl}]$ (2.1055 (18) Å) is also slightly shorter. The respective Ru-Cl bond lengths in complexes **1**, **2**,

5, 6, 7 and **8** (2.4146 (8) - 2.4576 (5) Å) are within the range displayed by other compounds of the type $[(\eta^6\text{-arene})\text{Ru}(\text{en})\text{Cl}]^+$ (2.41 – 2.44 Å).⁴²

When comparing the complexes with different η^6 -arene but the same *N,N'* chelating ligand (**1** and **7**/ **2**, **5** and **8**), the Ru-N⁻ and the Ru-Cl distances both differ by ca. 0.01-0.03 and 0.01-0.04 Å, respectively. Similarly, comparing the influence of the chelating ligand when the same arene is used, an increase in the electron-withdrawing effect of the R₁ group (Tf > Ts > Ms) appears to increase the Ru-Cl bond length, whereas the Ru-N⁻ bond length decreases (Table 3.3).

3.4.2. Hydrolysis of the chlorido complexes and acidity of the aqua complexes

Aquation of the complexes **1-3**, **5**, **8**, **11**, **13** and **16** in D₂O was confirmed by comparing the ¹H NMR spectra of the D₂O solution of the complexes and the solution obtained after removal of the chloride by reaction with silver ions (AgNO₃). Hydrolysis of the complexes appeared to be rapid under biologically relevant conditions (310 K, pH* 7.2), since equilibrium was reached by the time the first ¹H-NMR spectrum was recorded (< 6 min). Consequently the turnover frequency for the transfer hydrogenation to form NAD⁺ does not depend on whether the chlorido or aqua adduct are used.

A ¹H-NMR pH* titration of complexes **1-3**, **5**, **8**, **11** and **16** gave a pK_a* values between 9.22 and 11 for the deprotonation of the water from the aqua adducts (Table 3.5). These results suggest that those complexes would exist mainly as aqua adducts over the pH* range used during the experiment (pH* 7.2 ± 0.1).

Complexes with higher electron density on the metal centre display higher pK_a*. Therefore the more electron donating arenes will produce an increase in the basicity of the aqua adducts, hence an increase in the pK_a* value compared to the more electron

withdrawing arenes (pK_a^* *p*-cym > bip > bn). Similarly more electron withdrawing *N,N'* chelating ligands will result in a lower pK_a^* value (pK_a^* NbEn < TfEn < TsEn < MsEn).

3.4.3. Mechanism of the catalytic reduction of NAD^+

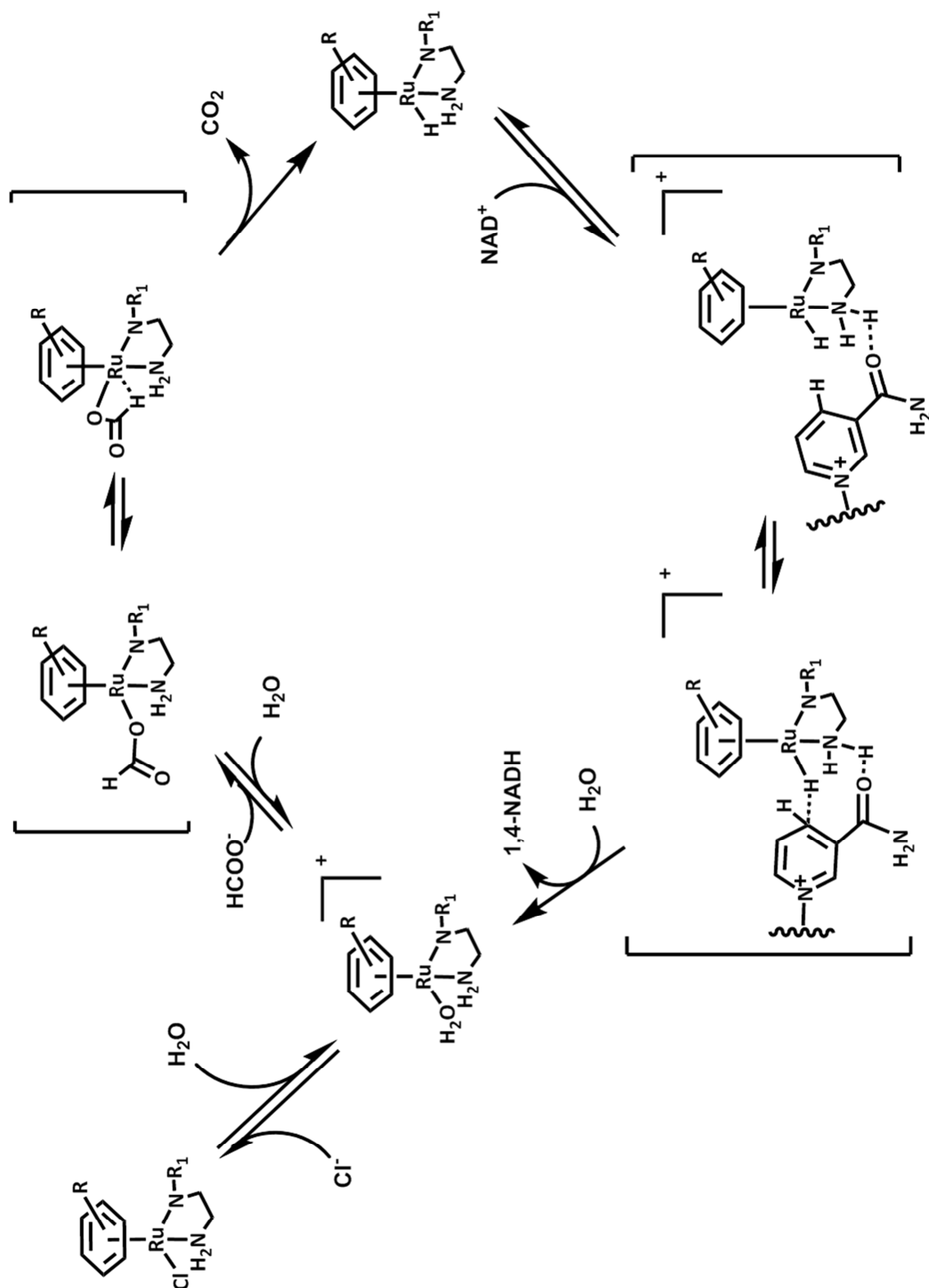
Use of deuterated-formate and complex **3** gave a turnover frequency 2.4 times smaller than that with protonated formate. Since the formation rate of the hydride (β -elimination) with the heavier atom is lower, the difference in the turnover frequency between the two reactions suggests that the rate-limiting step of the reaction is the hydride transfer. However whether the limiting step is the transfer from formate to the ruthenium complex or from the ruthenium hydride to the NAD^+ is not clear. Previously reported studies with similar complexes suggest that hydride formation will be the rate-limiting step.⁴⁴ Furthermore, the high reactivity of the hydride ruthenium species suggests the transfer from the ruthenium to the NAD^+ will be fast.

To determine the factors that influence the reaction rate, a series of experiments using complex **2** were performed varying the concentration of the different reactants. When the NAD^+ concentration was changed, no significant alterations in the rate were observed, implying that the reaction rate does not depend on the NAD^+ concentration. However the reaction rate decreased with lower concentrations of the hydride source (sodium formate) suggesting that formate is involved in the reaction rate (Figure 3.7).

The plot of turnover frequency against formate concentration showed Michaelis-Menten behaviour (Figure 3.8). The maximum turnover frequency for complex **2** ($\text{TOF}_{\text{max}} = 6.9 \text{ h}^{-1}$) is about 4 x times higher than that previously determined for the ethylenediamine complex $[(\text{hmb})\text{Ru}(\text{en})\text{Cl}]^+$ ($\text{TOF}_{\text{max}}=1.46 \text{ h}^{-1}$),³⁴ so achieving the desired increased efficiency in the reaction.

The possibility of employing 1,4-NADH as the hydride source as reported previously, was also attempted.⁴⁵ However experiments with complex **2** and 1,4-NADH did not show formation of the hydride adduct or NAD⁺. The results obtained imply that hydride transfer between NAD⁺ and the complexes is not a reversible process.

Based on the data obtained, it can be proposed a plausible catalytic cycle for the reduction of NAD⁺ *via* transfer hydrogenation with formate as a hydride source (Scheme 3.2). This cycle is comparable with that proposed by Fish *et al.*³⁶ for the reduction of NAD⁺ *via* transfer hydrogenation using [(Cp*)Rh(bipy)H₂O]²⁺ as the catalyst and formate as hydride source. In the first step, the pre-catalyst chlorido complex is converted to the aqua adduct. The reaction of the aqua complex with HCOO⁻ generates the formate adduct [(η⁶-arene)Ru(*N,N'*)(OHCO)]. The formate coordinates *via* a single oxygen with the carbonyl moiety making an H-bond with an NH proton. It then rotates to form an intermediate with the formate H now oriented towards the Ru centre. From here, the formate adduct undergoes β-elimination to give the hydride adduct, [(η⁶-arene)Ru(*N,N'*)(H)], and CO₂.³⁶ Transfer of hydride to produce 1,4-NADH regenerates the aqua adduct.



Scheme 3.2. Proposed mechanism for the reduction of NAD^+ to 1,4-NADH via transfer hydrogenation using formate as the hydride source. $\text{R}_1 = \text{Ms}$ (CH_3), Ts ($-(\text{C}_6\text{H}_4)\text{CH}_3$) or Tf ($-(\text{C}_6\text{H}_4)\text{CF}_3$), $\text{R} = p\text{-cym}$, hmb , bip or bn .

The low Michaelis constant for complex **2** ($K_M = 42.1$ mM) indicates a stronger affinity for formate compared to complexes $[(hmb)Ru(en)Cl]^+$ ($K_M = 58$ mM)³⁴ and $[(Cp^*)Rh(bipy)H_2O]^{2+}$ ($K_M = 140$ mM)⁴³, while the maximum turnover frequency ($TOF_{max} = 6.9$ h⁻¹) of the reaction indicated an increase in the catalytic activity compared to $[(hmb)Ru(en)Cl]^+$ ($TOF_{max} = 1.46$ h⁻¹)³⁴ but lower catalytic activity compared with the complex $[(Cp^*)Rh(bipy)H_2O]^{2+}$ ($TOF = 77.5$ h⁻¹ concentration of formate 0.5 M).⁴³

The reaction rate is dependent on the pH (Figure 3.10). The optimum pH* for the reaction is 7.2 ± 0.1 . At higher pH*, OH⁻ inhibits the reaction, and also at pH* 10 or higher, the complex decomposes. At lower pH* the protonation of the amido ligand and of the formate decreases the reaction rate (see section 1.3.1.).⁴⁶

Catalytic experiments with complexes **1-12** and **16** were performed in both D₂O and in D₂O/methanol (9:2). The addition of methanol resulted in an increase in the turnover frequency (Figure 3.11). Such an increase cannot be attributed to a simple solvent effect, but indicates the participation of methanol in the rate-limiting step of the reaction. The role of methanol in the transfer hydrogenation reactions has not been determined. However it has been shown that polar solvents, acting as hydrogen donors, form hydrogen bonds and interact with the substrate or formate, stabilizing the transition intermediates.^{46,47}

The energies of the intermediates calculated by DFT correlate well with other experimental data, and predict increasing barriers (and hence slower reactions) for bn complexes in the order TfEn (**12**) < TsEn (**11**) < MsEn (**10**), although it should be noted that the difference between barriers is small (*ca* 1.1 kcal mol⁻¹). For MsEn, the barrier for $\{(hmb)Ru(MsEn)\}^+$ (**4**) is substantially larger than for $\{(bn)Ru(MsEn)\}^+$ (**10**), which also agrees with experiment. Overall, the computational protocol appears to provide a very good

description of these systems. DFT thus could provide, in the future, a useful tool to help the *a priori* design of new complexes with desired properties.

3.4.4. Hydride adduct formation

^1H NMR experiments of the reaction between formate and complex **13** and **14** show a new set of signals that was assigned to the hydride adduct. The hydride resonance for complex **13-14** were identified at -5.5 ppm and -5.6 ppm respectively. (Figure 3.12) Similar values have been reported for other Ru-H complexes (from -5 to -20 ppm).^{45,48-50}

The hydride adduct for the complexes **1-3** and **15** could not be detected by ^1H NMR probably due to the high reactivity of the species. However high steric hindrance of the *o*-terphenyl complexes (**13-15**) complexes stabilized the hydride adduct. The increase on the hydride stability does not translate to a decrease in the reaction rate since the rate-limiting step has been determined to be the hydride formation and not hydride transfer to NAD^+ .⁵¹

HR-MS spectrum of the reaction mixture containing complex **13** and sodium formate in a ratio 1:1000 shows a peak at 493.04 m/z which was identified as the hydride adduct of the complex plus sodium ($\text{C}_{21}\text{H}_{24}\text{N}_2\text{NaO}_2\text{RuS}^+$). Interestingly, a peak at 537.04 m/z was also identified suggesting the existence of a stable formate adduct (Table 3.7). However, the lifetime for both species is very short and none of the adducts could be isolated.

The formate adduct was generated by the direct binding of the reactive Ru(II) centre in the aqua species to the negatively-charged oxygen from the formate. Formation of stable formate adducts and other carboxylate adducts has been previously reported for similar complexes.⁴⁵

3.4.5. Kinetics of transfer hydrogenation reactions

The catalytic reduction of NAD^+ under biologically relevant conditions (310 K, pH^* 7.2) using complexes **1-16** as catalysts and formate as a hydride source showed a general trend in which the more electron-withdrawing sulfonamides on the chelating ligand give higher catalytic activity (table 3.6). Accordingly, complexes containing NbEn (N-(2-aminoethyl)-4-nitrobenzensulfonamide) as the chelating ligand show the highest activity followed by complexes using TfEn, which are more active than those with TsEn ligand, and, in turn, all of them are more active than the complexes containing the MsEn ligand. Such a trend has been previously reported for the catalytic transfer hydrogenation to aldehydes⁵² and quinoxalines.²²

The nature of the arene had a dramatic effect on the reaction rate. The more electron withdrawing arene ligands such as benzene or biphenyl accept electron density from the central Ru(II) through back π -bonding. Consequently the lower electron density on the Ru(II) centre for complexes $[(\text{bn})\text{Ru}(\text{N},\text{N}')\text{Cl}]$ (**10**, **11** and **12**) compared with complexes $[(\text{hmb})\text{Ru}(\text{N},\text{N}')\text{Cl}]$ (**4**, **5** and **6**) stabilizes the coordination of the negatively-charged formate to Ru making hydride transfer from formate difficult.^{53,54} However, the experimental data show higher catalytic activity when the arene is more electron deficient (Table 3.6), $[(\text{bn})\text{Ru}(\text{N},\text{N}')\text{Cl}]$ being the more active complexes while $[(\text{hmb})\text{Ru}(\text{N},\text{N}')\text{Cl}]$ are the less active. This unexpected trend may be due to steric hindrance since the more sterically hindered arene (hmb) shows the lower activity while the less sterically hindered arene (bn) shows higher activity.

Several other Ru(II), Rh(III) and Ir(III) complexes have previously been reported to catalyze the regioselective reduction of NAD^+ to 1,4-NADH using formate as a hydride source.^{55,56} The complexes studied in the present work show comparable TOFs

(*ca.* 0.2 - 7 h⁻¹) to reported [(η⁶-arene)Ru(*N,N'*)Cl] complexes (*ca.* 0.0056-10 h⁻¹), although the turnover frequencies are much lower than those obtained using Rh(III) or Ir(III) complexes.^{55,56}

3.5. Conclusions

In this chapter a series of water-soluble Ru(II) half-sandwich complexes of the type [(η⁶-arene)Ru(*N,N'*)(Cl)] where *N,N'* are mono-sulfonamide chelating ligands derived from ethylenediamine have been studied. The X-ray crystal structures of complexes **1**, **2** and **5-9** showed the familiar piano stool geometry common to all [(η⁶-arene)Ru(X,Y)(L)] compounds.

¹H NMR studies show fast hydrolysis of the complexes in water to form the aqua adducts. The pK_a^{*} values of the aqua adducts of the complexes were higher than 9 for all the complexes, which suggests that the aqua adduct predominates over the hydroxido adduct at physiological pH. pK_a^{*} studies of the complexes show the expected trend where complexes with lower electron density on the metal centre show lower pK_a^{*} values.

The ability of the complexes to act as catalysts for the regioselective transfer hydrogenation of NAD⁺ to form 1,4-NADH was studied. The catalytic activity decreases in the order NbEn > TfEn > TsEn > MsEn showing that more electron-withdrawing sulfonamides increase the activity. The nature of the arene significantly influences the catalytic activity. Benzene complexes are the most active compounds while the activity decreases in the order biphenyl > *p*-cymene > hexamethylbenzene. Complex [(bn)Ru(TfEn)Cl] (**12**) was the most active with a TOF of 10.4 h⁻¹ when in MeOD-*d*₄/D₂O 5:1 v/v.

The formation of a hydride adduct by complexes **(13)** [(*o*-terp)Ru(MsEn)(Cl)] and **(14)** [(*o*-terp)Ru(TsEn)(Cl)] was demonstrated by ¹H NMR spectroscopy and HR-MS, as well as formation of a stable formate adduct. Mechanistic studies on complex **(2)** [(*p*-cym)Ru(TsEn)(Cl)] showed a dependence of the reaction rate on the formate concentration but not on NAD⁺ concentration. The formation of the hydride complex was shown to be the rate-limiting step through deuterium isotope experiments. The optimum pH* for the reaction was found to be (7.2 ± 0.1) which is close to physiological pH.

DFT calculations were performed for the coordination of formate, and subsequent CO₂ elimination to generate the hydride. The elimination of CO₂ occurs *via* a two-step process with the coordinated formate first twisting to present its hydrogen towards the metal centre followed by β-elimination and Ru-H formation. The computed barriers for complexes using η⁶-benzene follow the order MsEn > TsEn > TfEn and, for the MsEn chelating system the barrier follows the order bn < hmb, both consistent with the observed rates.

The series of compounds studied here showed improved catalytic activity by an order of magnitude higher compared to the ethylenediamine analogues, which could be significant if such catalytic reactions are to be used to modulate NADH levels in cells.

3.6. References

- (1) Matthew, C. K.; Ahern, K. G.; Van Holde, K. E. *Biochemistry*; 3rd ed.; Pearson Education: Madrid, **2002**.
- (2) Belenky, P.; Bogan, K. L.; Brenner, C. *Trends Biochem. Sci.* **2007**, *32*, 12-19.
- (3) Chiarugi, A.; Dölle, C.; Felici, R.; Ziegler, M. *Nature Rev.* **2012**, *12*, 741-752.
- (4) Chenault, H. K.; Whitesides, G. M. *Appl. Biochem. Biotechnol.* **1987**, *14*, 147-197.
- (5) Ying, W. *Antioxid. Redox Signaling* **2008**, *10*, 179-206.

- (6) Khan, J. A.; Forouhar, F.; Tao, X.; Tong, L. *Expert Opin. Ther. Targets* **2007**, *11*, 695-705.
- (7) Hileman, E. O.; Liu, J.; Albitar, M.; Keating, M. J.; Huang, P. *Cancer Chemoth. Pharm.* **2004**, *53*, 209-219.
- (8) Weckbecker, A.; Gro, H.; Hummel, W. *Adv. Biochem. Engin/Biotechnol.* **2010**, *120*, 195-242.
- (9) Held, M.; Schmid, A.; B., V. B. J.; Witholt, B. *Pure Appl. Chem.* **2000**, *72*, 1337-1343.
- (10) Chen, Q.; Gao, K.; Duan, Y.; Ye, Z.; Shi, L.; Yang, Y.; Zhou, Y. *J. Am. Chem. Soc.* **2012**, *134*, 2442-2448.
- (11) Dibenedetto, A.; Stufano, P.; Macyk, W.; Baran, T.; Fragale, C.; Costa, M.; Aresta, M. *ChemSusChem* **2012**, *5*, 373-378.
- (12) Kim, Y. H.; Yoo, Y. J. *Enzyme Microb.Tech.* **2009**, *44*, 129-134.
- (13) Maenaka, Y.; Suenobu, T.; Fukuzumi, S. *J. Am. Chem. Soc.* **2012**, *134*, 367-374.
- (14) Romain, C.; Gaillard, S.; Elmkaddem, M. K.; Toupet, L.; Fischmeister, C.; Thomas, C. M.; Renaud, J. L. *Organometallics* **2010**, *29*, 1992-1995.
- (15) Carrión, M. C.; Sepúlveda, F.; Jalón, F. A.; Manzano, B. R.; Rodríguez, A. M. *Organometallics* **2009**, *28*, 3822-3833.
- (16) Wolfson, A.; Dlugy, C.; Shotland, Y.; Tavor, D. *Tetrahedron Lett.* **2009**, *50*, 5951-5953.
- (17) Grau, M. M.; Poizat, M.; Arends, I. W. C. E.; Hollmann, F. *Appl. Organomet. Chem.* **2010**, *24*, 380-385.
- (18) Matharu, D. S.; Morris, D. J.; Clarkson, G. J.; Wills, M. *Chem. Commun.* **2006**, 3232-3234.
- (19) Noyori, R. *Angew. Chem. Int. Ed* **2002**, *41*, 2008-2022.
- (20) Fish, R. H. *Aust. J. Chem.* **2010**, *63*, 1505-1513.
- (21) Leiva, C.; Lo, H. C.; Fish, R. H. *J. Organomet. Chem.* **2010**, *695*, 145-150.

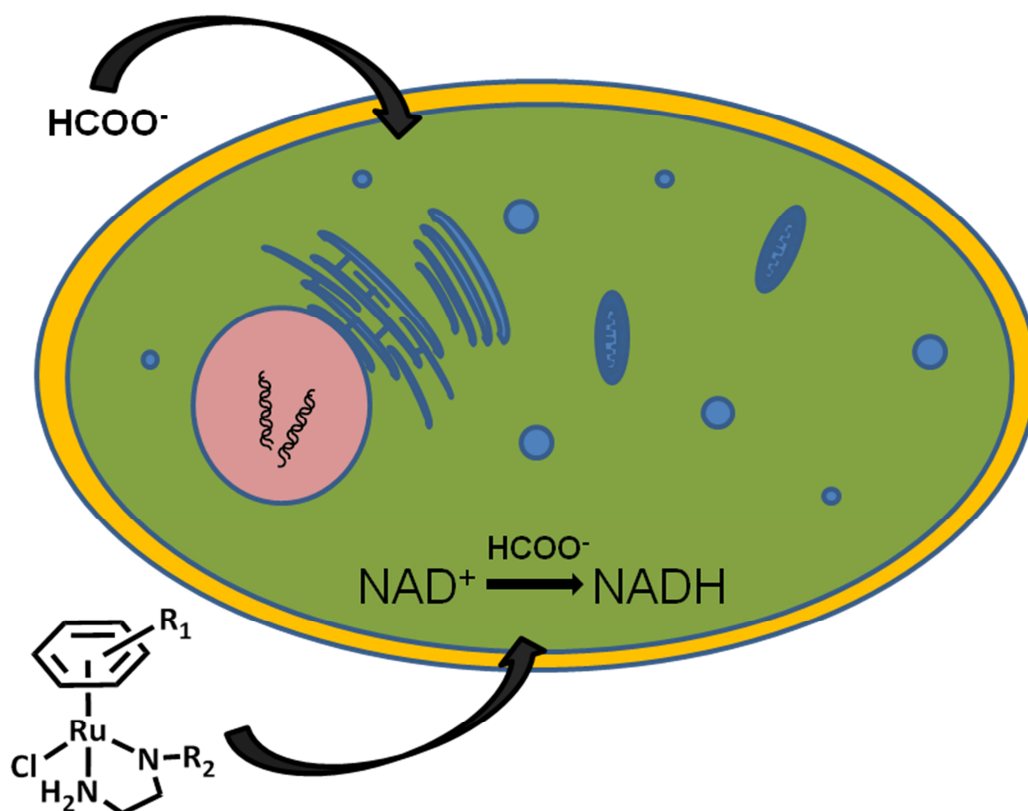
- (22) Tan, J.; Tang, W.; Sun, Y.; Jiang, Z.; Chen, F.; Xu, L.; Fan, Q.; Xiao, J. *Tetrahedron* **2011**, *67*, 6206-6213.
- (23) Watanabe, M.; Kashiwame, Y.; Kuwata, S.; Ikariya, T. *Eur. J. Inorg. Chem.* **2012**, 504-511.
- (24) Zhou, Z.; Ma, Q.; Zhang, A.; Wu, L. *Appl. Organomet. Chem.* **2011**, 556-561.
- (25) Wang, C.; Villa-Marcos, B.; Xiao, J. *Chem. Commun.* **2011**, *47*, 9773-9785.
- (26) Thai, T.; Therrien, B.; Süß-fink, G. *J. Organomet. Chem.* **2009**, *694*, 3973-3981.
- (27) Sandoval, C. A.; Bie, F.; Matsuoka, A.; Yamaguchi, Y.; Naka, H.; Li, Y.; Kato, K.; Utsumi, N.; Tsutsumi, K.; Ohkuma, T.; Murata, K.; Noyori, R. *Chem. Asian J.* **2010**, *5*, 806-816.
- (28) Creutz, C.; Chou, M. H. *J. Am. Chem. Soc.* **2009**, *131*, 2794-2795.
- (29) Robertson, A.; Matsumoto, T.; Ogo, S. *Dalton Trans.* **2011**, *40*, 10304-10310.
- (30) Martins, J. E. D.; Clarkson, G. J.; Wills, M. *Org. Lett.* **2009**, *11*, 847-850.
- (31) Li, X.; Li, L.; Tang, Y.; Zhong, L.; Cun, L.; Zhu, J.; Liao, J.; Deng, J. *J. Org. Chem.* **2010**, *75*, 2981-2988.
- (32) Wu, J.; Wang, F.; Ma, Y.; Cui, X.; Cun, L.; Zhu, J. *Chem. Commun.* **2006**, 1766-1768.
- (33) Zhou, Z.; Ma, Q.; Sun, Y.; Zhang, A. *Heteroat. Chem.* **2010**, *21*, 505-514.
- (34) Yan, Y. K.; Melchart, M.; Habtemariam, A.; Peacock, A. F.; Sadler, P. J. *J. Biol. Inorg. Chem.* **2006**, *11*, 483-488.
- (35) Ruppert, R.; Herrmann, S.; Steckhan, E. *J. Chem. Soc., Chem. Commun.* **1988**, 1150-1151.
- (36) Lo, H. C.; Leiva, C.; Buriez, O.; Kerr, J. B.; Olmstead, M. M.; Fish, R. H. *Inorg. Chem.* **2001**, *40*, 6705-6716.

- (37) Habtemariam, A.; Melchart, M.; Fernandez, R.; Parsons, S.; Oswald, I. D. H.; Parkin, A.; Fabbiani, F. P.; Davidson, J. E.; Dawson, A.; Aird, R. E.; Jodrell, D. I.; Sadler, P. J. *J. Med. Chem.* **2006**, *49*, 6858-6868.
- (38) Zelonka, R. A.; Baird, M. C. *Can. J. Chem.* **1972**, *50*, 3063-3072.
- (39) Harvey, R. G.; Lindow, D. F.; Rabideau, P. W. *J. Am. Chem. Soc.* **1972**, *94*, 5412-5420.
- (40) Sheldrick, G. M. *Acta Crystallogr A* **2007**, *64*, 112-122.
- (41) Wang, F.; Chen, H.; Parsons, S.; Oswald, I. D. H.; Davidson, J. E.; Sadler, P. J. *Chem. Eur. J.* **2003**, *9*, 5810-5820.
- (42) Morris, R. E.; Aird, R. E.; Murdoch, S.; Chen, H.; Cummings, J.; Hughes, N. D.; Parsons, S.; Parkin, A.; Boyd, G.; Jodrell, D. I.; Sadler, P. J. *J. Med. Chem.* **2001**, *6*, 3616-3621.
- (43) Peacock, A. F. A.; Habtemariam, A.; Fernández, R.; Walland, V.; Fabbiani, F. P. A.; Parsons, S.; Aird, R. E.; Duncan, I.; Sadler, P. J. *J. Am. Chem. Soc.* **2006**, *128*, 1739-1748.
- (44) Casey, C. P.; Johnson, J. B. *J. Org. Chem.* **2003**, *68*, 1998-2001.
- (45) Betanzos-Lara, S.; Liu, Z.; Habtemariam, A.; Pizarro, A. M.; Qamar, B.; Sadler, P. J. *Angew. Chem. Int. Ed.* **2012**, *51*, 3897-3900.
- (46) Wu, X.; Liu, J.; Di Tommaso, D.; Iggo, J. A.; Catlow, C. R. A.; Bacsa, J.; Xiao, J. *Chem. Eur. J.* **2008**, *14*, 7699-7715.
- (47) Almerindo, G. I.; Pliego, J. R. *Chem. Phys. Lett* **2006**, *423*, 459-462.
- (48) Haack, K. J.; Hashiguchi, S.; Fujii, A.; Ikariya, T.; Noyori, R. *Angew. Chem. Int. Ed* **1997**, *36*, 285-288.
- (49) Casey, C. P.; Singer, S. W.; Powell, D. R.; Hayashi, R. K.; Kavana, M. *J. Am. Chem. Soc.* **2001**, *123*, 1090-1100.
- (50) Jahncke, M.; Meister, G.; Rheinwald, G.; Stoeckli-Evans, H.; Süss-Fink, G. *Organometallics* **1997**, *16*, 1137-1143.

- (51) Soldevila-Barreda, J. J.; Bruijninx, P. C. A.; Habtemariam, A.; Clarkson, G. J.; Deeth, R. J.; Sadler, P. J. *Organometallics* **2012**, *31*, 5958-5967.
- (52) Wu, X.; Liu, J.; Li, X.; Zanotti-Gerosa, A.; Hancock, F.; Vinci, D.; Ruan, J.; Xiao, J. *Angew. Chem. Int. Ed* **2006**, *45*, 6718-6722.
- (53) Wang, F.; Habtemariam, A.; van der Geer, E. P. L.; Fernández, R.; Melchart, M.; Deeth, R. J.; Aird, R.; Guichard, S.; Fabbiani, F. P.; Lozano-Casal, P.; Oswald, I. D. H.; Jodrell, D. I.; Parsons, S.; Sadler, P. J. *Proc. Natl. Acad. Sci. U. S. A.* **2005**, *102*, 18269-18274.
- (54) Clayden, J.; Greeves, N.; Warren, S.; Wothers, P. *Organic Chemistry*; 1 ed.; Oxford University Press: New York, **2001**.
- (55) Canivet, J.; Süß-Fink, G.; Štěpnička, P. *Eur. J. Inorg. Chem.* **2007**, 4736-4742.
- (56) Haquette, P.; Talbi, B.; Barilleau, L.; Madern, N.; Fosse, C.; Salmain, M. *Org. Biomol. Chem.* **2011**, *9*, 5720-5727.

Chapter 4

Performing transfer hydrogenation reactions in cancer cells



4. Performing transfer hydrogenation reactions in cancer cells

4.1. Introduction

During the last few years, an increasing number of publications have been focused on the use of metal-based drugs with catalytic activity.^{1, 2, 3} So far the applications of those catalytic drugs have been mainly focused on the regulation of ROS levels in cells, depletion or transformation of specific biomolecules, functional group transformations and *in situ* synthesis of active compounds. However, catalytic drugs are still a recent research area and many other applications are likely to be found with time. Some examples on this area are as follows.

- SOD mimics like the manganese(II) Mn40403, can dismutate superoxide into O₂ and H₂O₂ with similar efficiency to the enzyme.⁴ This compound is currently undergoing clinical trials in co-administration with opioid Agent for treatment of pain in cancer patients (NCT00101621).

- Complexes of the type of [(bip)Ru(2(p-N,N-dimethylaminophenylazo)pyridine)] catalytically oxidise GSH to GSSG.⁵

- Meggers *et al.* synthesised a series of Ru(II) complexes which are capable of catalysing the cleavage of allylcarbamates from protected imine molecules in biological systems. This provides a strategy for the *in-cell* activation of fluorophores.⁶

- Complex [Fe(5,10,15,20-tetraphenylporphyrin)Cl] has been shown to catalyse the reduction of azides to imines in cells.⁷ This method could be useful for the synthesis of amine chromophores using biologically inherited organic azides as a substrate.

- Numerous Pd-catalyzed C-C bond formations reaction have also been shown to work in cells.^{8,9,10}

In the field of transfer hydrogenation reactions with biological applications, the regeneration of NADH has been intensively studied. The aim of this process is to regenerate NADH as a substrate for enzymes which can be used for the reduction of ketones in organic synthesis.¹¹ Currently, the most successful compound in this area is [(Cp*)Rh(bipy)Cl]⁺ synthesised by Stekhan *et al.* and intensively studied by Fish *et al.*¹²⁻¹⁶

More recently, other complexes capable of regenerating NADH have been reported. In 2007 Süß-Fink *et al.* published the catalytic reduction of NAD⁺ using a series of Ru(II), Rh(III) and Ir(III) phenantroline-containing catalysts. The complex [(Cp*)Rh(phen)Cl]⁺ was capable of good conversions and turnover frequencies of up to twice that obtained previously with [(Cp*)Rh(bipy)Cl]⁺¹⁷ In 2011, Salmain *et al.* published a series of Rh(III) and Ru(II) complexes using dipyridyl amine ligands functionalised by maleimide. The complexes were not as active as the bipyridine containing analogue [(Cp*)Rh(bipy)Cl]⁺.¹⁸ The complex [(Cp*)Ir(4-(1H-pyrazol-1-yl)-κN²)benzoic acid κC³)H₂O)]₂ SO₄ synthesised by Fukuzumi *et al.* was also reported to be able to catalyse H₂ oxidation while generating NADH in a neutral and slightly basic media.¹⁹

Interestingly, the application of transfer hydrogenation reactions was not attempted *in cellulo* until 2005, when Sadler *et al.* published the regeneration of 1,4-NADH with Ru(II) complexes containing *ethylenediamine* or acetylacetonate as chelating ligands. However, the turnover frequencies were relatively low compared to the literature values.²⁰ When treating

A549 lung cancer cells with the complex and sodium formate as a hydride source, no significant effect was observed.²⁰

Sodium formate was selected as a hydride source for these type of experiments. Despite the fact that high doses of formate (10-20 mM in human blood plasma) have been shown to be toxic in humans and primates, clinical reports suggest that irreversible damage occurs only when concentration of formate in plasma is 7 mM or higher for at least 24 continuous hours. Therefore the tolerance of the body to large amounts of formate appears to be relatively high and it can be used as a co-drug.^{21, 22}

In Chapter 3, the synthesis of a series of Ru(II) complexes containing Noyori type ligands which can effectively reduce NAD^+ to NADH at pH 7.2, 310 K and aqueous media, was described.²³

In this Chapter, the possibility to perform transfer hydrogenation reactions *in cellulo*, using the Ru(II) complexes described in Chapter 3 ($[(\eta^6\text{-arene})\text{Ru}(\text{XEn})\text{Cl}]$) is investigated. The use of these complexes as anticancer agents, and the potentiation of the antiproliferative activity achieved due to the catalytic transfer hydrogenation using sodium formate as a hydride donor is also studied.

4.2. Experimental

The experiments in biology were carried out in collaboration with Isolda Romero-Canelón (Warwick university)

4.2.1. Materials

Ruthenium(II) complexes are shown in Figure 4.1, [(*p*-cym)Ru(MsEn)Cl] (**1**), [(*p*-cym)Ru(TsEn)Cl] (**2**), [(*p*-cym)Ru(TfEn)Cl] (**3**), [(*p*-cym)Ru(NbEn)Cl] (**16**), [(hmb)Ru(MsEn)Cl] (**4**), [(hmb)Ru(TsEn)Cl] (**5**), [(hmb)Ru(TfEn)Cl] (**6**), [(bip)Ru(MsEn)Cl] (**7**), [(bip)Ru(TsEn)Cl] (**8**), [(bip)Ru(TfEn)Cl] (**9**), [(bn)Ru(MsEn)Cl] (**10**), [(bn)Ru(TsEn)Cl] (**11**), [(bn)Ru(TfEn)Cl] (**12**) [(*o*-terp)Ru(MsEn)Cl] (**13**), [(*o*-terp)Ru(TsEn)Cl] (**14**) and [(*o*-terp)Ru(TfEn)Cl] (**15**) were synthesised in Chapter 3. Ruthenium complex RM175 used for comparison was obtained following published procedures by Dr. Abraha Habtemarian.²⁴ Ruthenium ICP-MS standard was obtained from Inorganic Ventures. RPMI-1640 medium, foetal bovine serum, L-glutamine, penicillin/streptomycin mixture, trypsin, trypsin/EDTA, phosphate buffered saline (PBS) were purchased from PAA Laboratories GmbH. Cisplatin ($\geq 99.9\%$), trichloroacetic acid ($\geq 99\%$), sulforhodamine B (75%), sodium phosphate monobasic monohydrate ($\geq 99\%$), sodium phosphate dibasic heptahydrate ($\geq 99\%$), acetic acid ($\geq 99\%$) and pyocyanine were obtained from Sigma Aldrich.

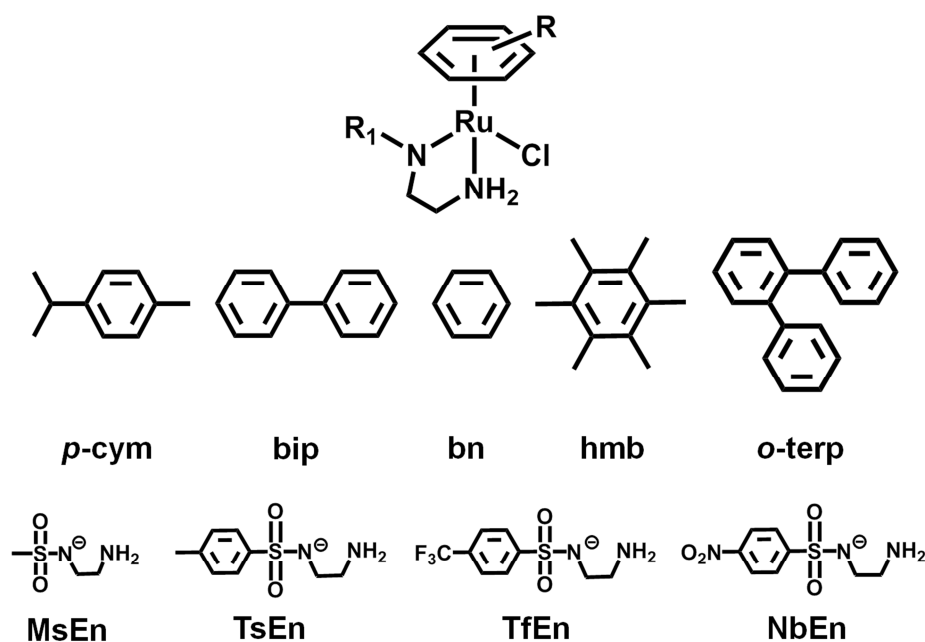


Figure 4.1. Structures of the complexes studied in this chapter

4.2.2. Cell maintenance

A2780 human ovarian carcinoma cells were obtained from the European Collection of Cell Cultures (ECACC) and their maintenance procedure has been described in Chapter 2.

4.2.3. *In vitro* growth inhibition assay

The antiproliferative activity of the complexes **1-16** and **RM175** was determined in A2780 ovarian cancer cells. The experimental details are described in Chapter 2. The SRB assay was used to determine cell viability. IC₅₀ values were determined as duplicates of triplicates in two independent set of experiments and their standard deviations were calculated.

4.2.4. Cell viability modulation experiments

Cell viability assays with complexes **1-3**, **13-16** and **RM175** in combination with sodium formate and sodium acetate, were carried out in A2780 ovarian cancer cells. These experiments were carried out as described in Chapter 2 with the following modifications: a fixed concentration of each ruthenium complex equal to $1/3 \times \text{IC}_{50}$ was used with co-administration of three different concentrations of sodium formate (0.5, 1 and 2 mM). In order to prepare the stock solution of the drug, the solid complex was dissolved first in 5 % DMSO to be then diluted in a 1:1 mixture of 0.9 % saline:cell culture medium. This stock was further diluted using RPMI-1640 until working concentrations were achieved. Separately, stock solutions of sodium formate were prepared in saline. Both solutions were added to each well independently, but within 5 min of each other.

Cell viability assays with Complex **2** in combination with sodium acetate were carried out as described above. The concentrations of sodium acetate were 0.5, 1 and 2 mM.

4.2.5. IC₅₀ modulation experiments of complex 2 by co-administration with sodium formate

Antiproliferative activity of complex **2** co-administered with 2 mM of sodium formate was carried out using A2780 ovarian cancer cells. This experiment was performed as described in Chapter 2, using a fixed concentration of formate and variable concentrations of the metal complex. The SRB assay was used to determine cell viability. IC₅₀ values were determined as duplicates of triplicates in two independent set of experiments and their standard deviations were calculated.

4.2.6. Metal accumulation in cancer cells

On a 6-well plate, 1.5×10^6 cells per well were seeded. After 24 h of pre-incubation time in drug free medium, the cells were treated with a fixed concentration of complexes **1-3** and **12-16** (final concentrations equal to $1/3 \times \text{IC}_{50}$) for 24 h. After this time, cells were washed with trypsin-EDTA, counted, and the cell pellets collected. Each pellet was digested overnight in concentrated nitric acid (73%) at 353 K; the resulting solutions were diluted using double-distilled water to a final concentration of 5 % HNO₃, and the amount of Ru accumulated by the cells was determined by ICP-MS. These experiments did not include any cell recovery time in drug-free media. The experiments were carried out in duplicates of triplicates.

This experiment was also carried out using complex **2**, co-administered with 2 mM of sodium formate.

4.2.7. Hydrophobicity

The relative hydrophobicity of the Ru(II) compound was measured by HPLC. The retention times were obtained using a HP 1200 Series HPLC System (Agilent). The column used was an Agilent ZORBAX Eclipse Plus C-18 (250 x 4.6 mm, 5 μm pore size). or

t = 0 – 10 % B, t = 25 – 70 % B, t = 30 – 70 % B, t = 31 – 10 % B and t = 36 – 10 % B over a 36 min. Flow rate was 1 mL min⁻¹. A wavelength of detection of 254 nm with the reference wavelength at either 360 nm was used. Samples were prepared in ddw or a mixture methanol (5 %, HPLC grade)/ddw. Sample injection 50 µL.

4.2.8. NAD/NADH determination

Experiments to determine the ratio of NAD⁺/NADH of A2780 ovarian cancer cells exposed to complex **2** were carried out using the NAD⁺/NADH assay kit from Abcam (ab65348) according to the manufacturer's instructions. A2780 cells were seeded in 6 well plates at a density of 1.0 x 10⁶ cells/well. After 24 h of pre-incubation time, cells were treated with a fixed concentration of complex **2**, equal to its IC₅₀, and in combination with four different concentrations of sodium formate (0, 0.5, 1 and 2 mM). These concentrations of sodium formate were also used on their own as a second set of negative controls. Drug exposure was allowed for 24 h, after which the supernatants were removed by suction and the wells washed with PBS. The cells were treated with trypsin, detached and counted before being pelleted by centrifugation. Cell pellets were extracted using the NAD/NADH extraction buffer and filtered using a 10 KDa molecular weight filter. Samples were split into two, the first half was used to determine total NADt (NAD⁺ + NADH), and the second half was used to determine NADH after heating the samples at 333 K for 30 min. Values obtained measuring the absorbance at 450 nm were normalised against the protein content in each sample which was determined using a Bradford assay.²⁵

4.2.9. Time-dependence of the NAD⁺/NADH ratio

Experiments to determine the variation of NAD/NADH ratio over time in A2780 ovarian cancer cells exposed to complex **2** (concentration equal to its IC₅₀) co-administered

with sodium formate (2 mM) were carried out using the NAD/NADH assay kit as described above. The NAD⁺/NADH were determined after 0, 2, 4, 12, 18 and 24 h drug exposure.

$$\text{TOF} = K_{\text{cat}} = \frac{V_{\text{reaction}}}{[\text{catalyst}]} = \frac{\delta[\text{NADH}]}{\delta t} \frac{1}{[\text{catalyst}]}$$

Where $\frac{\delta[\text{NADH}]}{\delta t} = \frac{([\text{NADH}] - [\text{NADH}]_0)}{([\text{NAD}^+] + [\text{NADH}])} [\text{NADH}]$ and $[\text{NADH}]_0$ is the initial concentration of

NADH

4.2.10. ROS determination

Flow cytometry analysis of total induction of ROS in A2780 cells caused by exposure to complex **2** and sodium formate was carried out using the Total ROS detection kit (Enzo Life Sciences) according to the supplier's instructions. 6-well plate were seeded with 1.0×10^6 A2780 cells per well. Cells were pre-incubated in drug-free media at 310 K for 24 h in a 5% CO₂ humidified atmosphere, after which they were exposed to either sodium formate (2 mM), complex **2** (concentration equal IC₅₀) or a combination of both. After 1 or 24 h of drug exposure, supernatants were removed by suction and the cells washed and harvested. Staining was achieved by re-suspending the cell pellets in buffer containing a green fluorescent reagent. Cells were analysed in a Becton Dickinson FACScan Flow Cytometer using Ex/Em: 490/525nm for the oxidative stress. Data were processed using Flowjo software. The experiment included cells treated with pyocyanin for 30 min as positive control.

4.3. Results

4.3.1. *In vitro* growth inhibition

The antiproliferative activity of complexes **1-16** and **RM175** was evaluated in A2780 ovarian cancer cells. Complexes **1-3**, **7-9** and **13-16** were found to be moderately active with IC_{50} values ranging from 11.92 and 14.7 μM , which is an order of magnitude higher than complex **RM175** (2.17 μM) and the clinically approved cisplatin (1.2 μM). Complexes $[(\text{hmb})\text{Ru}(\text{TsEn})\text{Cl}]$ (**5**), $[(\text{bn})\text{Ru}(\text{TsEn})\text{Cl}]$ (**10**), $[(\text{bn})\text{Ru}(\text{TsEn})\text{Cl}]$ (**11**) and $[(\text{bn})\text{Ru}(\text{TfEn})\text{Cl}]$ (**12**), containing hexamethylbenzene (hmb) or benzene (bn) as the η^6 -arene, displayed IC_{50} value higher than 100 μM (ie. were inactive). Interestingly, in the active series the most active complexes are the MsEn derivatives and their potency follows the order MsEn>TsEn>TfEn. IC_{50} values are depicted in Table 4.1.

Cellular accumulation in the A2780 ovarian cell line for complexes **1-3** and **13-15** was determined. Ru accumulation in A2780 for *p*-cymene complexes **1-3** (0.16-0.31 ng x 10^6 cells) was *ca.* 13 x times lower than for the more hydrophobic *o*-terphenyl complexes **13-15** (2.1-2.8 ng x 10^6 cells) (Table 4.1). There was no direct correlation between the amount of metal determined in cells, and the anticancer activity of the complexes.

Table 4.1. Antiproliferative activity of complexes **1-3**, **13-16** and **RM175** in A2780 ovarian cancer cells and their cellular accumulation expressed as ng of ruthenium per million cells.

The latter experiments were carried out using equipotent concentrations of the complexes ($1/3 \times IC_{50}$) and 24 h of drug exposure, without recovery time.

Complex	IC₅₀ (μM)	Ru in cells (ng x 10⁶ cells)
[(<i>p</i> -cym)Ru(MsEn)Cl] (1)	11.92 ± 0.8	0.16 ± 0.02
[(<i>p</i> -cym)Ru(TsEn)Cl] (2)	13.6 ± 0.6	0.15 ± 0.04
[(<i>p</i> -cym)Ru(TfEn)Cl] (3)	14.2 ± 0.8	0.31 ± 0.04
[(<i>p</i> -cym)Ru(NO ₂ En)Cl] (16)	14.7 ± 0.6	n/d
[(hmb)Ru(TsEn)Cl] (5)	>100	n/d
[(bip)Ru(MsEn)Cl] (7)	11.4 ± 1.0	n/d
[(bip)Ru(TsEn)Cl] (8)	11.5 ± 0.7	n/d
[(bip)Ru(TfEn)Cl] (9)	13.0 ± 0.9	n/d
[(bn)Ru(TfEn)Cl] (10)	>80	n/d
[(bn)Ru(TfEn)Cl] (11)	>80	n/d
[(bn)Ru(TfEn)Cl] (12)	>80	n/d
[(<i>o</i> -terp)Ru(MsEn)Cl] (13)	12.4 ± 0.9	2.8 ± 0.3
[(<i>o</i> -terp)Ru(TsEn)Cl] (14)	15.8 ± 0.8	2.1 ± 0.4
[(<i>o</i> -terp)Ru(TfEn)Cl] (15)	21.2 ± 0.1	2.4 ± 0.3
[(bip)Ru(en)Cl] ⁺ (RM175)	2.17 ± 0.08	n/d

n/d = not determined.

Relative hydrophobicity of the complexes was measured by plotting the HPLC retention times (Figure 4.2). The more hydrophilic complexes will move faster, while the more hydrophobic will interact better with the column (*ie.* longer retention times). The hydrophobicity is dependent on the η^6 -arene following the order *o*-terp > bip > *p*-cym > hmb > bn. The chelating ligand also affects greatly the hydrophobicity of the complexes, the more hydrophilic compound being those containing MsEn and following the order MsEn < TsEn < NbEn < TfEn.

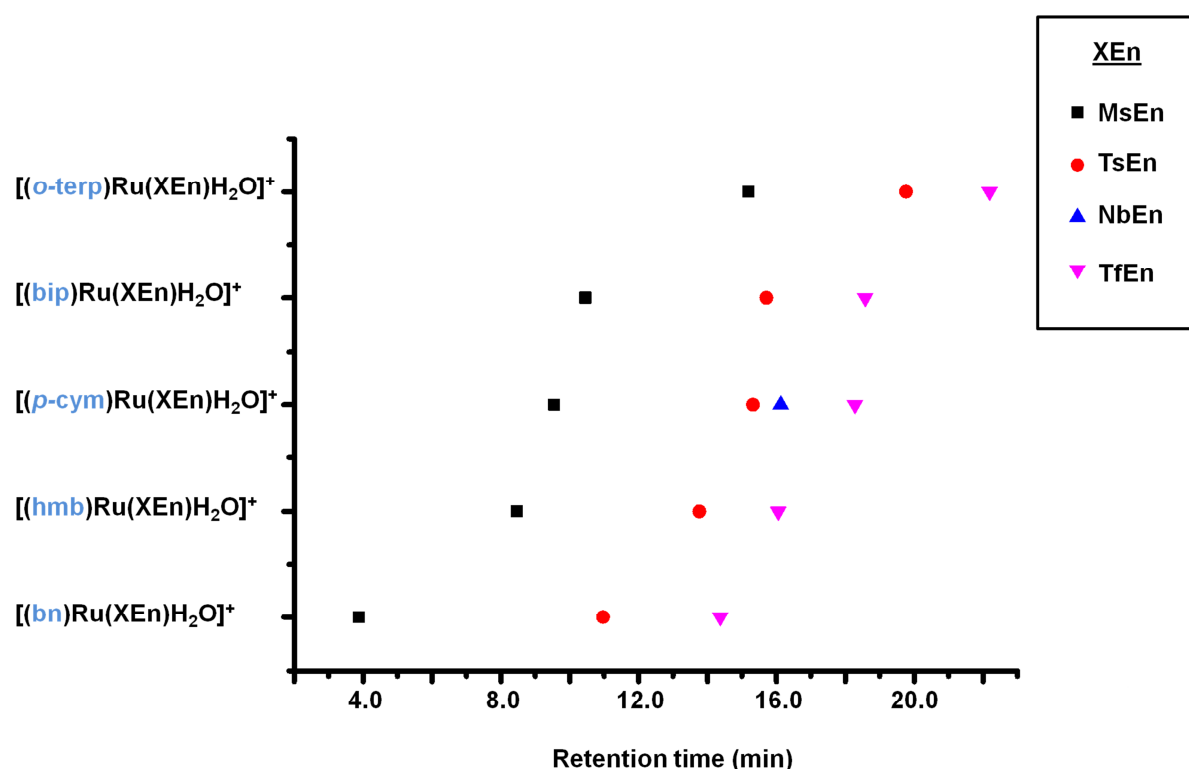


Figure 4.2. Relative hydrophobicity of complexes **1-16**, measured as retention time in HPLC. XEn = NbEn, TfEn, TsEn or MsEn.

4.3.2. *In vitro* experiments with co-administration of a hydride source

In order to investigate the possibility of *in cellulo* catalysis, as a potentiation strategy for metal-based anticancer agents, A2780 cells were co-incubated with equipotent concentrations of ruthenium complexes **1-3**, **13-16** and **RM175** ($1/3 \times IC_{50}$) and three different concentrations of sodium formate (0.5, 1 and 2 mM). The potency of all complexes

increases upon co-administration of the hydride source (formate), with decrease of the cell survival of *ca.* 69.5 to 97.9 % was achieved using 2 mM formate, Figure 4.3. A linear relation between cell viability and the formate concentration can be observed (Figure 4.4). The largest increment in potency is observed for complexes [(*p*-cym)Ru(MsEn)Cl] (**1**) and [(*p*-cym)Ru(TsEn)Cl] (**2**) respectively, with a cell viability decrease from *ca.* 69.9 to 1.5 % and 68.4 to 1.5 %, when using 2 mM sodium formate, keeping Ru concentration constant. Within the *o*-terp derivatives, the greatest improvement is observed for complex [(*o*-terp)Ru(TfEn)Cl] (**15**), with a decrease from *ca.* 40.0 to 2.5 %. In contrast, results for complex **RM175**, show a decrease of cell survival from 71.3 to 38.9 %. These experiments included two different sets of negative controls. In the first, cells were kept untreated, in the second set, cells were exposed to the different concentrations of sodium formate. In all cases there was no difference in cell viability between the two sets of controls; excluding the hypothesis that formate is responsible for the decrease in the population.

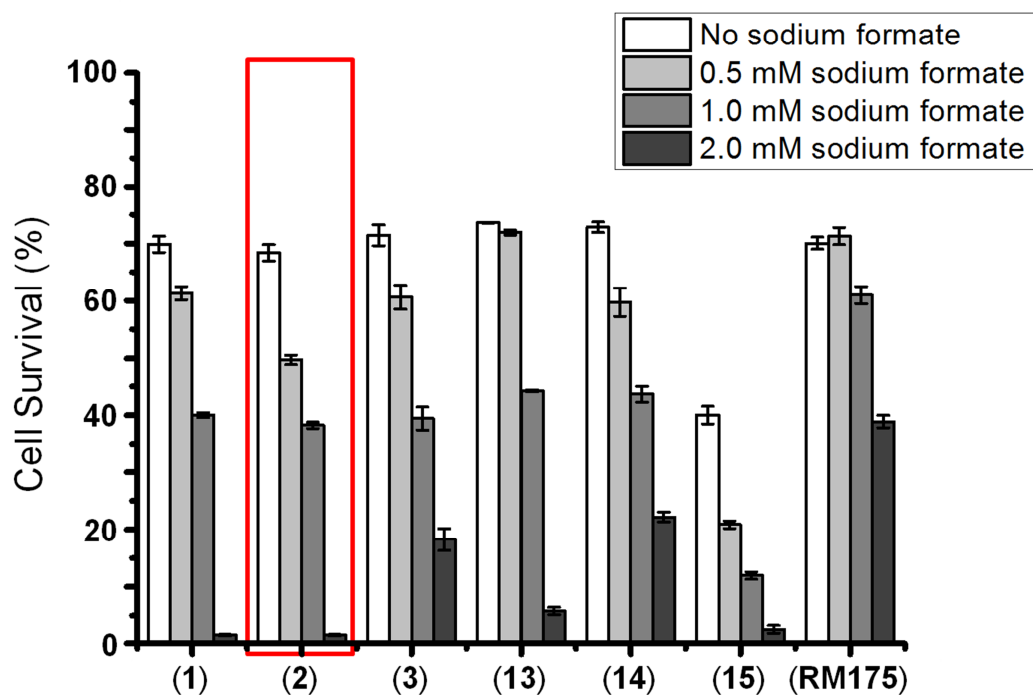
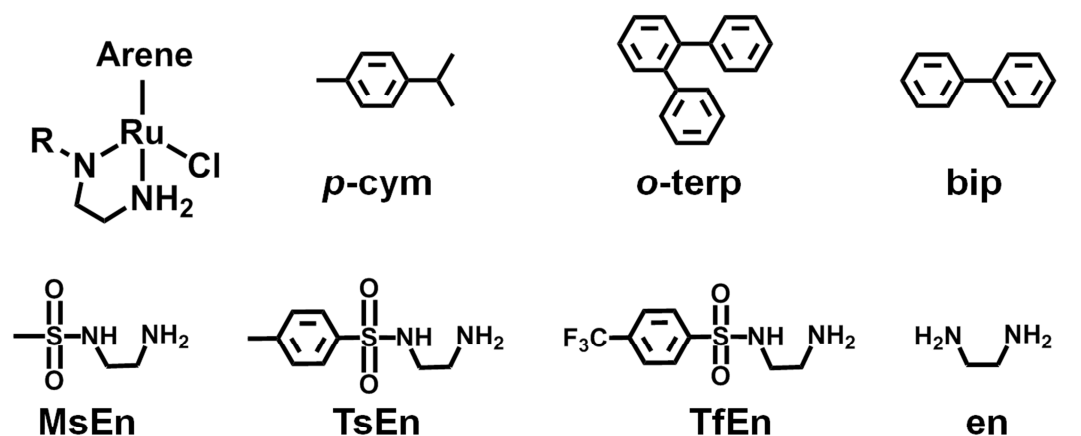


Figure 4.3. Plot of cell survival of A2780 ovarian cancer cells, in the presence of complex 1-3, 13-15 and RM175 (concentration equal to $1/3$ IC_{50}) co-administered with sodium formate at 0, 0.5, 1 and 2 mM. Complex 2 was selected for further experiments.

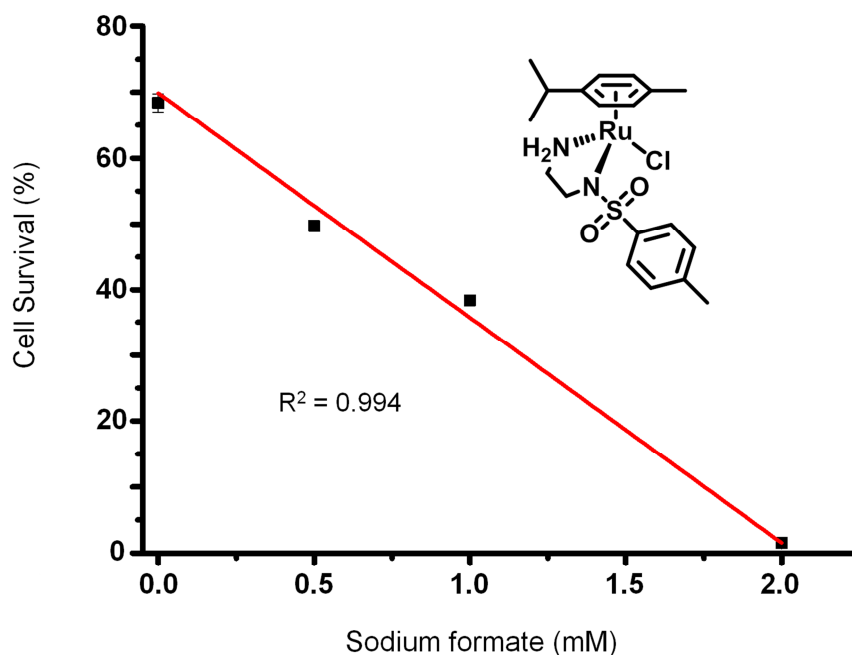


Figure 4.4. Plot of cell survival *versus* concentration of sodium formate. The experiment was performed with complex **2** at a concentration equal to $1/3$ IC_{50} . A linear relationship is observed.

Complex **2** was selected for further experiments. Results for the cellular accumulation studies on A2780 cells exposed to complex **2** and different concentrations of sodium formate showed no statistically significant differences in intracellular ruthenium concentration, regardless the amount of sodium formate used, Table 4.2. The IC_{50} values determined when complex **2** was co-administered with sodium formate were determined (Table 4.2). An improvement of *ca.* 13-fold is observed (from $13.57 \pm 0.62 \mu\text{M}$ to $1.02 \pm 0.15 \mu\text{M}$) upon addition of 2 mM formate, which places this ruthenium complex at the same potency level as cisplatin.

Table 4.2. Antiproliferative activity and cellular uptake of complex **2** in A2780 ovarian cancer cells when co-administered with different concentrations of sodium formate (0, 0.5, 1 and 2 mM).

	Sodium formate concentration (mM)			
	0	0.5	1	2
IC₅₀ (μM)	13.6 ± 0.6	10.8 ± 0.6	5.4 ± 0.8	1.0 ± 0.2
Accumul. (ng Ru x 10⁶ cells)	0.15 ± 0.03	0.145 ± 0.009	0.129 ± 0.005	0.13 ± 0.02

Complexes **2** and **RM175** were also co-administered with sodium acetate on A2780 cells, maintaining the same conditions as in previous experiments (complex concentration at $1/3 \times IC_{50}$, sodium acetate concentration at 0.5, 1 and 2 mM). No statistically significant changes in potency upon addition of increasing concentrations of acetate were observed (Table 4.3). For complex **2**, the cell viability varies from $70.78 \pm 0.56 \%$ to $67.1 \pm 0.6 \%$, and for complex **RM178**, the variation is between $75.4 \pm 2 \%$ and $71.8 \pm 1.4 \%$.

Table 4.3. Cell viability percentages of A2780 ovarian cancer cells exposed for 24 h to equipotent concentrations of complexes **2** and **RM175** ($1/3 \times IC_{50}$) co-administered with different concentrations of sodium acetate (0, 0.5, 1 and 2 mM).

Complex	Sodium acetate concentration (mM)			
	0	0.5	1	2
[(<i>p</i> -cym)Ru(TsEn)Cl] (2)	70.8 ± 0.6	69.4 ± 0.9	68.9 ± 0.3	67.1 ± 0.6
[(bip)Ru(en)Cl] ⁺ (RM175)	75.4 ± 2	73.1 ± 0.8	72 ± 1	71 ± 1

4.3.3. Modulation of NAD⁺/NADH in cells

In order to investigate whether complex **2** in combination with formate can be used for transfer hydrogenation reactions, and to catalytically regenerate NADH *in cellulo*, the concentrations of NAD⁺ and NADH in A2780 cancer cells were determined.

In a first experiment, A2780 cells were exposed for 24 h to complex **2**, in combination with different concentration of sodium formate (0, 0.5, 1, 2 mM). Negative controls with untreated cells, and cells exposed only to sodium formate were included. There is no significant difference between the NAD⁺/NADH ratio for both sets of controls and those from cells exposed only to IC₅₀ concentrations of complex **2**. The experiment demonstrates that there is a decrease in the NAD⁺/NADH ratio (Figure 4.5), which directly correlates with the concentration of sodium formate added.

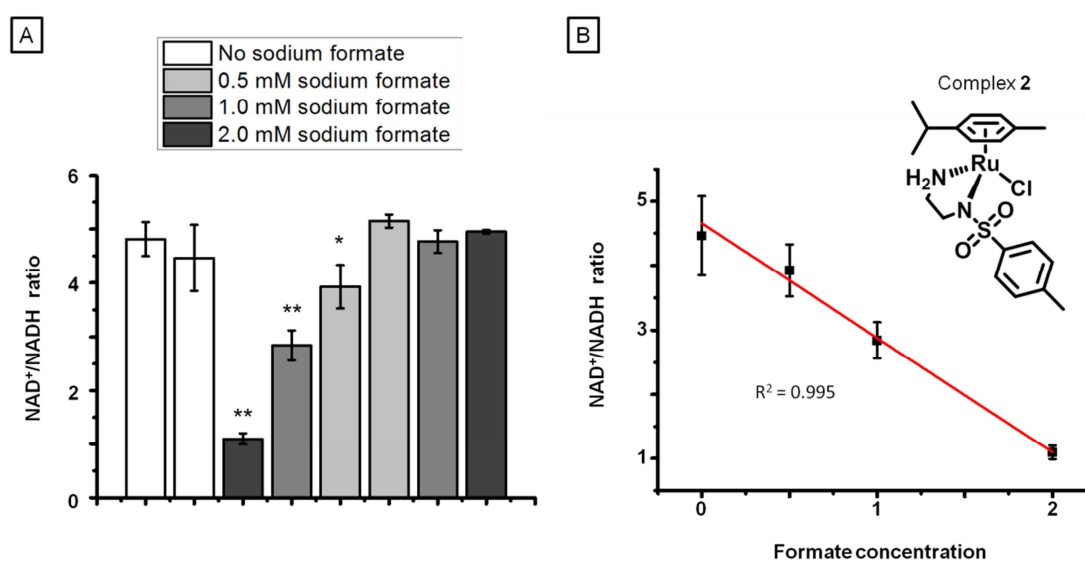


Figure 4.5. Perturbation of the NAD⁺/NADH ratio in A2780 cells exposed to complex **2** (concentration equal to IC₅₀) and sodium formate (0, 0.5, 1 or 2 mM). A) NAD⁺/NADH ratios determined after 24 h of drug exposure. B) Inverse linear correlation between the concentration of sodium formate and the NAD⁺/NADH ratio.

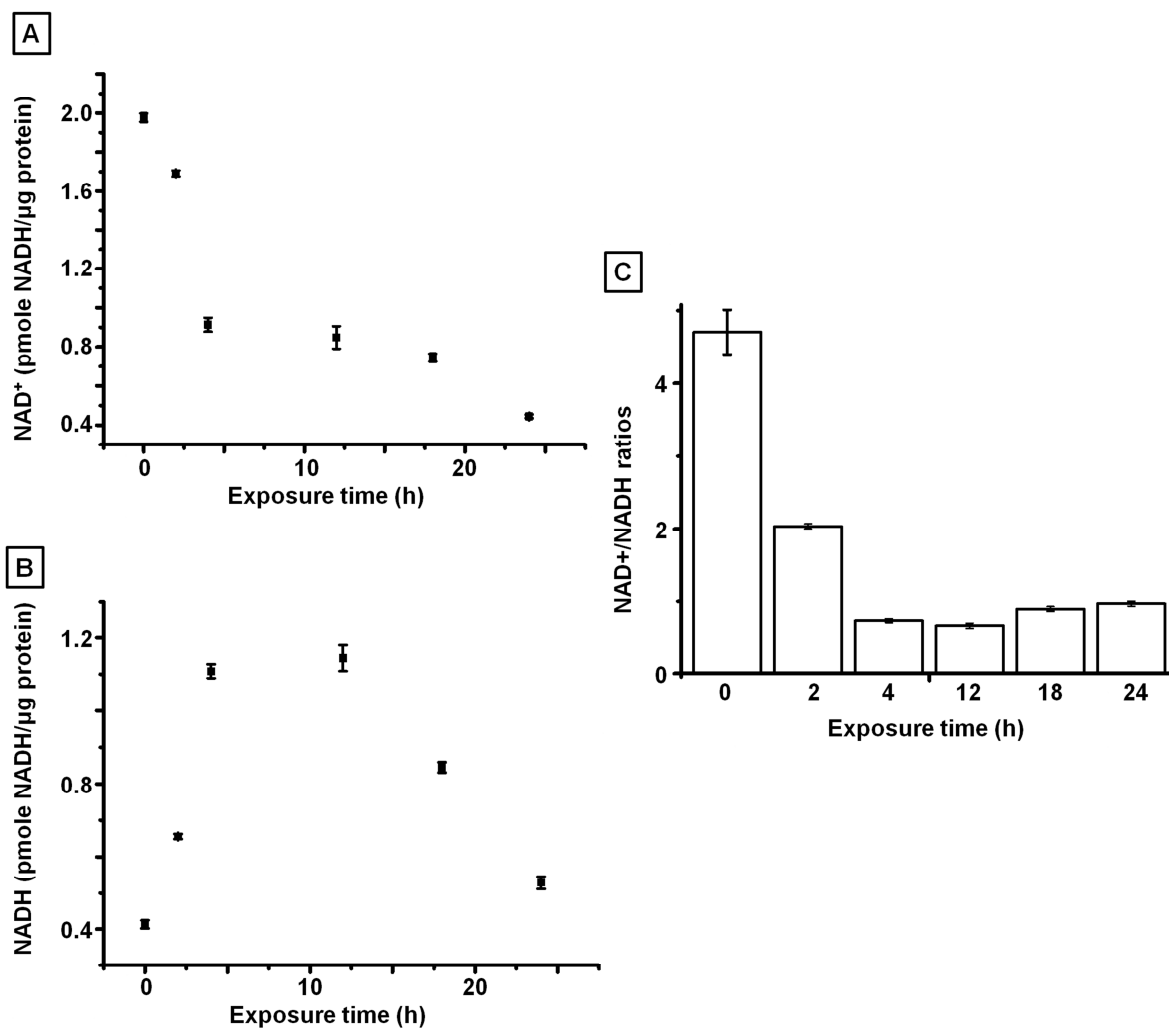


Figure 4.6. Perturbation of A) NAD⁺ concentration, B) NADH concentration and C) NAD⁺/NADH ratios in A2780 cells exposed to complex 2 (concentration equal to IC₅₀) and sodium formate (2 mM). NAD⁺ and NADH concentrations were determined at variable drug exposure times (0, 2, 4, 12, 18 and 24 h).

A second experiment was carried out, at variable drug exposure times (2, 4, 12, 18 and 24 h). The experiment was performed using fixed concentrations of complex 2 (IC₅₀) and sodium formate (2 mM). The NAD⁺/NADH ratio decreases with exposure time, changing from 4.70 (t = 0 h, untreated cells) to 0.65 (t = 12 h), (Figure 4.6). After 12 h the NAD⁺/NADH ratio starts to increase slightly, going up to 0.98 (t = 24 h). NAD⁺ concentration decreases with exposure time changing from 1.97 (t = 0 h, untreated cells) to

0.91 ($t = 4$ h). After 4 h the concentration of NAD^+ is constant, and after 12 hours the concentration of NAD^+ continues to drop. The NADH concentration increases over the initial period of 4 h. After that it follows a similar pattern as the NAD^+ concentration.

An apparent TOF of $0.19 \pm 0.01 \text{ h}^{-1}$ was calculated with the concentrations of NAD^+ and NADH determined in pmol per 10^5 cells. However, the linear regression was performed with only 3 points.

4.3.4. ROS detection

Flow cytometry analysis of A2780 cells exposed to complex 2 (concentration equal to IC_{50}) and 2 mM of sodium formate was performed to detect the ROS levels in cells. The levels of ROS in treated cells are comparable to those treated with NAC, an important reductant (Figure 4.7).²⁶

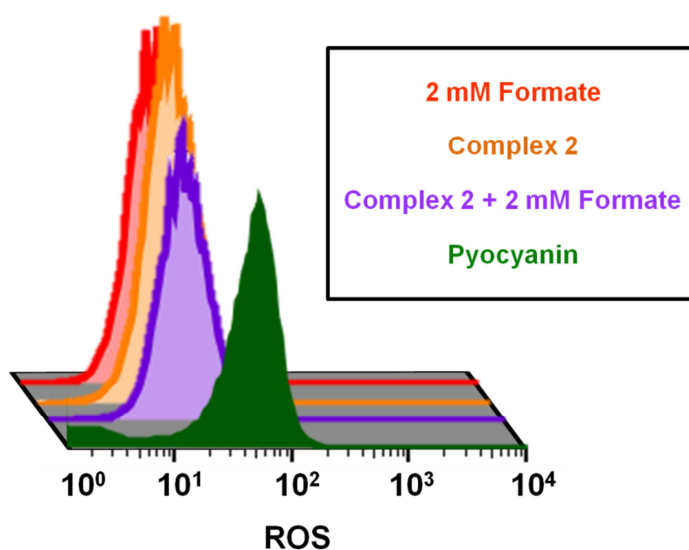


Figure 4.7. Induction of ROS in A2780 cancer cells. In green, (positive control) cells treated with pyocyanin, which generates ROS.

4.4. Discussion

4.4.1. *In vitro* growth inhibition

The antiproliferative activity of complexes **1-16** and **RM175** was evaluated in A2780 ovarian cancer cells. Complexes containing biphenyl, *p*-cymene or *o*-terphenyl as a η^6 -arene (**1-3**, **7-9** and **13-16**) were shown to be active towards A2780 ovarian cancer cells. However, complexes containing hexamethylbenzene or benzene as the η^6 -arene (**5**, **10-12**) were shown to have IC₅₀ values higher than 100 μ M, and are considered inactive. IC₅₀ values are depicted in Table 4.1.

Cell accumulation experiments were carried out with complexes **1-3** and **13-15**. It can be observed that the more hydrophobic complexes (*o*-terphenyl complexes **13-15**) have higher accumulation in cells than the *p*-cymene containing complexes **1-3**. However, the correlation between hydrophobicity and cellular accumulation does not occur within the complexes containing the same arene (Figure 4.2). Cellular accumulation decreases in the order [(*p*-cym)Ru(TfEn)Cl] (**3**) > [(*p*-cym)Ru(MsEn)Cl] (**1**) > [(*p*-cym)Ru(TsEn)Cl] (**2**) and in the case of *o*-terphenyl complexes, [(*o*-terp)Ru(MsEn)Cl] (**13**) > [(*o*-terp)Ru(TfEn)Cl] (**15**) > [(*o*-terp)Ru(TsEn)Cl] (**14**).

4.4.2. *In vitro* experiments with co-administration of an hydride source

In order to investigate the possibility of *in cellulo* catalysis, a series of experiments in A2780 cancer cells, using the complexes **1-3**, **13-16** and **RM175** co-administered with sodium formate, were performed.

Complexes of the type $[(\eta^6\text{-arene})\text{Ru}(\text{en})\text{Cl}]^+$ have been intensively studied during the last few years due to their antiproliferative activity. In particular, complex **RM175** was shown to be active, with an IC₅₀ in the range of cisplatin, in a variety of cancer cell lines.

Studies with Ru(II)-ethylenediamine compounds, in order to elucidate the mechanism of action, have been carried out. It has been reported that the ethylenediamine-Ru(II) complexes react with GSH. The GSH is then oxidized to its sulphenato form, the complex then undergoes ligand substitution, releasing the GSH(O) and binding to DNA.^{27, 28} Some of these en complexes were tested in 2005 for their catalytic activity towards reduction of NAD⁺ *via* transfer hydrogenation. The complexes were catalysts, however, the catalytic activity was low compared with other Ru(II) complexes reported. Furthermore, the compounds were tested in A549 lung cancer cells, in combination with formate, but no significant effect was observed.²⁰ For these reason, **RM175** was used here for comparison purposes.

Complexes containing *p*-cym (**1-3** and **16**) were selected for these studies since they display good catalytic activity towards transfer hydrogenation, good water solubility and good stability (Table 4.4). Furthermore, complex [(*p*-cym)Ru(TsEn)Cl] (**2**) has been used as a model in Chapter 3 to understand the catalytic cycle of this type of complexes, and therefore, the knowledge on this compound is more extensive.

Table 4.4. Summary of the properties of the complexes [(η^6 -arene)Ru(XEn)Cl] where η^6 -arene is bip, bn, *p*-cym or hmb.

Property	[(η^6 -arene)Ru(XEn)Cl]			
	bn	hmb	bip	<i>p</i> -cym
Solubility in water	Very high	High	Low	High
Stability in water + formate	Poor ^a	Stable	Stable	Stable
Catalytic activity	High ^b	Low ^b	High ^b	High ^b

^a The complex decomposes in the presence of formate when there is no hydride acceptor (Figure 3.13.). ^b TOFs values in Table 3.6., Chapter 3.

Complexes containing *o*-terp (**13-15**) were also selected for these studies due to the high catalytic activity. Per contra, the solubility of those complexes is a major drawback. It has been previously described in Chapter 3, that these type of complexes need to be dissolved in a mixture 23.3 % methanol/water v/v in order to achieve working concentrations. Furthermore, although the transfer hydrogenation reaction proceeds, a brown precipitate can be observed.

Cell viability experiments were performed with equipotent concentrations of the ruthenium complexes **1-3**, **13-16** and **RM175** ($1/3 \times IC_{50}$) and three different concentrations of sodium formate (0.5, 1 and 2 mM). The potency of all complexes is enhanced upon co-administration with increasing concentrations of formate, Figure 4.3. However, no antiproliferative activity can be observed when cells are treated only with sodium formate. Those results suggest that the enhancement of the potency is due to the combination of Ru(II) complex and sodium formate. In contrast, results for complex **RM175**, show the lower decrease of cell survival from 71.3 to 38.9 %. Interestingly, despite the higher catalytic activity of the *o*-terp complexes **10-13** compared to the *p*-cym analogues, lower potentiation of the antiproliferative activity in the presence of formate was observed. This behaviour could be due to the fact that upon reaction with formate the complexes partially precipitate, either due to decomposition products or poor water solubility of a neutral formate adduct. This effect has previously been discussed in Chapter 3, section 3.3.4.1.

The largest increment in potency is observed for complexes [(*p*-cym)Ru(MsEn)Cl] (**1**) and [(*p*-cym)Ru(TsEn)Cl] (**2**) respectively, with a cell viability decrease from *ca.* 69.87 to 1.5 % and 68.4 to 1.5 %, when using 2 mM sodium formate, keeping metal the Ru constant. This results were unexpected, since the catalytic activity of the *p*-cym complexes follows the order NbEn (**16**) > TfEn (**3**) > TsEn (**2**) > MsEn (**1**) (Table 4.5).

Table 4.5. Turnover frequencies for transfer hydrogenation using catalysts **1-3** and **16**.

Complex	TOF (h ⁻¹) D ₂ O/MeOD- <i>d</i> ₄ ^a	TOF (h ⁻¹) D ₂ O
[(<i>p</i> -cym)Ru(MsEn)Cl] (1)	1.25 ± 0.03	1.11 ± 0.02
[(<i>p</i> -cym)Ru(TsEn)Cl] (2)	2.88 ± 0.06	1.58 ± 0.04
[(<i>p</i> -cym)Ru(TfEn)Cl] (3)	5.7 ± 0.3	3.06 ± 0.05
[(<i>p</i> -cym)Ru(NbEn)Cl] (16)	9.6 ± 0.3	4.1 ± 0.1

^a 23% MeOD-*d*₄/ 77% D₂O

These results can readily be explained if it is considered that the reaction occurs in a cellular environment. Cells are complex systems which contain a large amount of molecules capable of coordinating with metals, and can poison metal anticancer drugs, or in this case, poison the catalyst. Examples of side reactions between biomolecules and metal drugs can easily be found in the literature. In particular glutathione (GSH), a tripeptide containing cysteine (nucleophilic S), has been shown to have an important role as a detoxifier in cells.^{29, 30} The clinically approved drug cisplatin, for instance, reacts with glutathione (GSH) to form a GS-Pt adduct that can be excreted from the cells.³¹

Complexes [(*p*-cym)Ru(NbEn)Cl] (**16**) and [(*p*-cym)Ru(TfEn)Cl] (**3**) could be more reactive and therefore easier to poison by reaction with other biomolecules such as GSH (reactions with GSH explained in Chapter 5).

A linear relationship between cell viability and the formate concentration is observed (Figure 4.4). Furthermore, cellular accumulation studies on A2780 cells exposed to complex **2** and different concentrations of sodium formate exclude the possibility that the co-incubation with both agents resulted in an enhanced uptake that could translate in to a decrease of cell survival (Table 4.2). Taking into account that the concentration of sodium

formate (0.5, 1 or 2 mM) is in high excess compared to the concentration of the complexes, it suggests that the reaction between the complex and formate is catalytic.

IC₅₀ values for complex **2** co-administered with sodium formate were determined (Table 4.2). A linear decrease on the IC₅₀ *versus* formate can be observed. Upon addition of 2 mM sodium formate the antiproliferative activity of complex **2** decreases from 13.6 ± 0.6 to 1.0 ± 0.2 μM , which is comparable to that of cisplatin (1.2 ± 0.1 μM).

Platinum-based anticancer drugs are the most common in a course of treatment for a wide variety of cancers. The mechanism of action of cisplatin, carboplatin and oxaliplatin is believed to involve DNA binding and distort replication. However, these drugs display major side effects due to unespecificity towards cancer cells and binding to undesired targets. Furthermore, cancer cells develop resistance to the drugs. Some of the mechanisms of resistance towards platinum drugs are detoxification by GSH conjugates, metallothioneins and other antioxidants, increase of the DNA damage repair levels or alterations of membrane protein trafficking. These drawbacks expose the need to develop drugs with new mechanisms of action.³²

The Ru(II) complexes here described are capable of achieving similar IC₅₀ values as cisplatin. However, the mechanism of action does not involve DNA coordination (see Chapter 5) but disruption of the NAD⁺ and NADH. The modulation of NAD⁺/NADH levels is closely related to the redox balance of the cells, and therefore, the full signalling system of the cells is compromised.^{33, 34}

Recently, Sadler *et al.* reported a series of Ir(III) anticancer catalytic compounds designed to target the redox system. In contrast with the drugs here described, the mechanism of the Ir(III) compounds involves the catalytic oxidation of NADH to generate a hydride Ir

adduct and NAD^+ .²⁶ The catalytic process was also shown to occur *in cellulose*. During this process, increasing ROS levels are observed which results in cell death.²⁶

In order to demonstrate that the catalytic process is due to transfer hydrogenation, an experiment using sodium acetate, instead of sodium formate, was performed. Acetate is a carboxylate which differs from formate in a methyl group, however, acetate does not have the ability to act as a hydride donor.

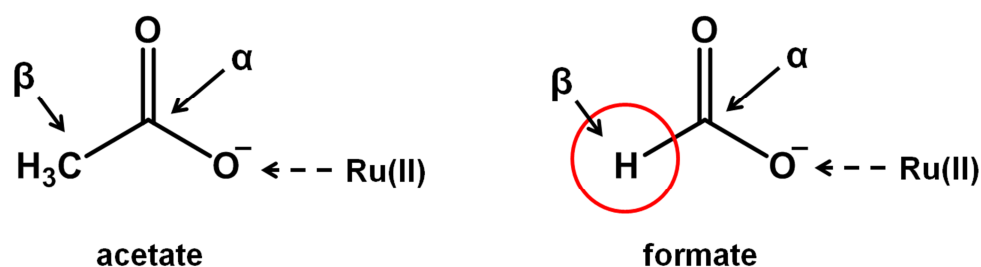


Figure 4.8. Structures of acetate and formate. Transfer hydrogenation reactions with carboxylates as a hydride source require hydrogen in the β position (β elimination). Ru(II) coordinates via the negatively charged oxygen.

In experiments in which A2780 ovarian cancer cells were treated with complexes **2** or **RM175** (concentration equal to $1/3 \text{ IC}_{50}$) in combination with sodium acetate (0.5, 1 or 2 mM), no statistically significant changes in potency upon addition of increasing concentrations of acetate were observed (Table 4.3). Therefore, it is probable that the hydride donation ability of formate is essential for the observed increase in potency.

4.4.3. Modulation of NAD^+/NADH in cells

In a first experiment, A2780 cells were exposed for 24 h to complex **2** (IC_{50} concentrations), in combination with different concentration of sodium formate (0, 0.5, 1, 2 mM). Control experiments, untreated cells, cells treated with only complex **2**

(IC₅₀ concentrations) or only formate at different concentrations (0, 0.5, 1, 2 mM), were also performed.

The NAD⁺/NADH ratio of untreated cells (4.8 ± 0.3) is the same as that obtained for cells treated only with complex **2** or formate at different concentrations (Figure 4.5). However, a decrease on the NAD⁺/NADH ratio is observed upon treatment of A2780 cells with complex **2** and increasing concentrations of formate (Figure 4.5). These experiments show that the decrease in NAD⁺/NADH ratios directly correlates with the concentration of sodium formate added (Figure 4.5). This experiment demonstrates that the co-administration of complex **2** and sodium formate can reduce the NAD⁺/NADH ratio in A2780 ovarian cancer cells.

In a second experiment, A2780 cancer cells were treated with complex **2** (IC₅₀ concentration) and sodium formate (2 mM). The NAD⁺/NADH ratio was determined at time 0 (untreated cells) and at time 2, 4, 12, 18 and 24 h. The experiments were performed with the aim to observe the kinetic decrease of the ratio and the behaviour of NAD⁺ and NADH and calculate a turnover frequency. The TOF that would be obtained from this experiment will be an apparent TOF, since many processes occur in cells and NAD⁺/NADH could be involved in more than one process.

A decrease on the NAD⁺/NADH ratio in A2780 cells can be observed during a period of 12 h. The apparent TOF ($0.19 \pm 0.01 \text{ h}^{-1}$) was calculated. However, the number of points is insufficient to obtain an accurate value.

After 12 h, the catalyst is probably poisoned, and there is an apparent slight recovery of the NAD⁺/NADH ratio. However, observing the individual concentrations of NAD⁺ and NADH, a decrease of the total concentration of NAD⁺ and NADH was detected after 12 h (Figure 4.6). It is probable that the cell is undergoing a process of destruction of the

coenzymes. Whether this reduction of NADH and NAD^+ concentrations is due to a side effect of the poisoned catalyst or due to cellular processes, either in an attempt to restore the redox balance or as a shut-down process when the cell dies, has not yet been investigated.

4.4.4. ROS detection

As mentioned previously, NAD^+ and NADH are closely involved in the redox system of the cells. The coenzymes are involved in the synthesis of NADP^+ and NADPH, which at the same time is involved in the regeneration of GSH from GSSG. Furthermore NADH itself is a reductant.^{34, 35} Increasing concentrations of NADH should translate into a reducing environment, and lower levels of ROS.

In a final experiment, ROS levels in A2780 cancer cells were measured after cells were treated with complex **2** (concentration equal to IC_{50}) and 2 mM of sodium formate. Interestingly, low levels of ROS were detected (Figure 4.7). This result is in agreement with the hypothesis of *in cellulo* transfer hydrogenation. Reduction of reactive oxygen species could occur by direct transfer hydrogenation or be due to an increase in the level of reducing agents in the cell, such as NADH.

These results are also in agreement with the literature. The Ir(III) complex $[(\text{Cp}^x\text{PhPh})\text{Ir}(\text{PhPy})\text{py}]^+$ has been shown to catalyze hydride transfer from the NADH to O_2 to form H_2O_2 .²⁶ This process generates ROS, and simultaneously, reduces the levels of NADH. In their report, Sadler *et al.* demonstrate that the ROS levels in cells increase significantly, and relates this increase of reactive oxygen species with a redox imbalance which translates in cell death.²⁶

4.5. Conclusions

This Chapter aimed to demonstrate that ruthenium complexes containing Noyori-type ligands, originally designed for catalytic reduction of ketones and imines, can be modified for the purpose of exerting biological applications. In Chapter 3 it was shown that complexes **1-16** can be catalysts for transfer hydrogenation reactions, and allowed the conversion of NAD^+ into NADH in the presence of sodium formate as a hydride source. This chapter highlights the possibility of potentiating the antiproliferative activity of these ruthenium complexes in A2780 cells by co-administration with non-toxic doses of sodium formate.

Cell viability experiments in A2780 cells, using the Ru(II) complex $[(p\text{-cym})\text{Ru}(\text{TsEn})\text{Cl}]$ and different concentrations of formate, demonstrate that the antiproliferative activity of this kind of complexes can be greatly potentiated by the addition of formate. Furthermore, a linear relationship between formate concentration and decreasing cell survival was obtained, suggesting that the formate is directly correlated with such an increase of the anticancer activity.

Cellular accumulation experiments exclude the possibility of disruption of Ru(II) accumulation in cells. Together with the cell viability experiments, this suggests that a catalytic reaction between the complex and formate might be the cause of the reduction in the IC_{50} values and, therefore, increasing the potency.

Experiments with sodium acetate, instead of sodium formate, were performed. However, no potentiation of the anticancer activity could be observed with acetate. These results can readily be explained, since acetate cannot act as a hydride donor. The lack of effect of acetate in A2780 cells, suggests that hydride is required for the potentiation, and therefore, transfer hydrogenation might occur.

The possibility of *in cellulo* NAD^+ reduction, by transfer hydrogenation was studied in two series of experiments. The NAD^+/NADH ratio in cells was first determined using different concentrations of formate. The NAD^+/NADH ratio decreases as a function of the concentration of formate, when in the presence of complex **2**, indicating that the presence of formate directly affects the NAD^+/NADH ratio.

A second experiment, where the NAD^+ and NADH concentrations were determined at different time points, was also performed. This decrease in the NAD^+/NADH ratio, continued over time during the initial 12 hours. After which, the catalyst is poisoned and no more transfer hydrogenation occurs. However, both, NAD^+ and NADH concentration decrease.

The co-administration of the Ru(II) complex and the hydride source (formate) caused the inhibition of ROS species, comparable to the effect of NAC, a powerful reductant. This is consistent with the transfer hydrogenation process (reduction) and the generation of high levels of reducing agents like NADH and NADPH .

This Chapter provides evidence that transfer hydrogenation reactions can be carried out in cells.

4.6. References

- (1) Noffke, A. L.; Habtemariam, A.; Pizarro, A. M.; Sadler, P. J. *Chem. Commun.* **2012**, *48*, 5219-5246.
- (2) Sasmal, P. K.; Streu, C. N.; Meggers, E. *Chem. Commun.* **2013**, *49*, 1581-1587.
- (3) Hocharoen, L.; Cowan, J. A. *Chem. Eur. J.* **2009**, *15*, 8670-8676.
- (4) Filipović, M. R.; Koh, A. C. W.; Arbault, S.; Niketić, V.; Debus, A.; Schleicher, U.; Bogdan, C.; Guille, M.; Lemaître, F.; Amatore, C.; Ivanović-Burmazović, I. *Angew. Chem. Int. Ed.* **2010**, *49*, 4228-4232.

- (5) Dougan, S. J.; Habtemariam, A.; McHale, S. E.; Parsons, S.; Sadler, P. J. *Proc. Natl. Acad. Sci. U. S. A.* **2008**, *105*, 11628-33.
- (6) Streu, C.; Meggers, E. *Angew. Chem. Int. Ed.* **2006**, *45*, 5645-5648.
- (7) Sasmal, P. K.; Carregal-Romero, S.; Han, A. A.; Streu, C. N.; Lin, Z.; Namikawa, K.; Elliott, S. L.; Köster, R. W.; Parak, W. J.; Meggers, E. *ChemBioChem* **2012**, *13*, 1116-1120.
- (8) Li, J.; Chen, P. R. *ChemBioChem* **2012**, *13*, 1728-1731.
- (9) Unciti-Broceta, A.; Johansson, E. M. V.; Yusop, R. M.; Sanchez-Martin, R. M.; Bradley, M. *Nat. Protocols* **2012**, *7*, 1207-1218.
- (10) Gao, Z.; Gouverneur, V.; Davis, B. G. *J. Am. Chem. Soc.* **2013**, *135*, 13612-13615.
- (11) Wu, H.; Tian, C.; Song, X.; Liu, C.; Yang, D.; Jiang, Z. *Green Chem.* **2013**, *15*, 1773-1789.
- (12) Ruppert, R.; Herrmann, S.; Steckhan, E. *Chem. Commun.* **1988**, 1150-1151.
- (13) Steckhan, E.; Herrmann, S.; Ruppert, R.; Dietz, E.; Frede, M. *Organometallics* **1991**, *10*, 1568-1577.
- (14) Leiva, C.; Lo, H. C.; Fish, R. H. *J. Organomet. Chem.* **2010**, *695*, 145-150.
- (15) Lo, H. C.; Leiva, C.; Buriez, O.; Kerr, J. B.; Olmstead, M. M.; Fish, R. H. *Inorg. Chem.* **2001**, *40*, 6705-6716.
- (16) Lutz, J.; Hollmann, F.; Ho, T. V.; Schnyder, A.; Fish, R. H.; Schmid, A. *J. Organomet. Chem.* **2004**, *689*, 4783-4790.
- (17) Canivet, J.; Süß-Fink, G.; Štěpnička, P. *Eur. J. Inorg. Chem.* **2007**, 4736-4742.
- (18) Haquette, P.; Talbi, B.; Barilleau, L.; Madern, N.; Fosse, C.; Salmain, M. *Org. Biomol. Chem.* **2011**, *9*, 5720-5727.
- (19) Maenaka, Y.; Suenobu, T.; Fukuzumi, S. *J. Am. Chem. Soc.* **2012**, *134*, 367-374.
- (20) Yan, Y. K.; Melchart, M.; Habtemariam, A.; Peacock, A. F.; Sadler, P. J. *J. Biol. Inorg. Chem.* **2006**, *11*, 483-488.

- (21) Hanzlik, R. P.; Fowler, S. C.; Eells, J. T. *Drug Metab. Dispos.* **2005**, *33*, 282-286.
- (22) Sodium formate. (24/12/2013),
<http://www.accessdata.fda.gov/scripts/fcn/fcnDetailNavigation.cfm?rpt=scogsListing&id=297>
- (23) Soldevila-Barreda, J. J.; Bruijnincx, P. C. A.; Habtemariam, A.; Clarkson, G. J.; Deeth, R. J.; Sadler, P. J. *Organometallics* **2012**, *31*, 5958-5967.
- (24) Morris, R. E.; Aird, R. E.; Murdoch, S.; Chen, H.; Cummings, J.; Hughes, N. D.; Parsons, S.; Parkin, A.; Boyd, G.; Jodrell, D. I.; Sadler, P. J. *J. Med. Chem.* **2001**, *6*, 3616-3621.
- (25) Bradford, M. M. *Anal. Biochem.* **1976**, *72*.
- (26) Liu, Z.; Romero-Canelón, I.; Qamar, B.; Hearn, J. M.; Habtemariam, A.; Barry, N. P. E.; Pizarro, A. M.; Clarkson, G. J.; Sadler, P. J. *Angew. Chem. Int. Ed.* **2014**, *53*, 3941-3946.
- (27) Wang, F.; Xu, J.; Habtemariam, A.; Sadler, P. J. *J. Am. Chem. Soc.* **2005**, *127*, 17734-17743.
- (28) Wang, F.; Xu, J.; Wu, K.; Weidt, S. K.; Mackay, C. L.; Langridge-Smith, P. R. R.; Sadler, P. J. *Dalton Trans.* **2013**, *42*, 3188-3195.
- (29) Franco, R.; Cidlowski, J. A. *Cell Death Differ.* **2009**, *16*, 1303-1314.
- (30) Lushchak, V. I. *J. amino acids* **2012**, *2012*, 1-26.
- (31) Chen, H. H. W.; Kuo, M. T. *Met. Based. Drugs* **2010**, 1-7.
- (32) Shen, D.-W.; Pouliot, L. M.; Hall, M. D.; Gottesman, M. M. *Pharmacol. Rev.* **2012**, *64*, 706-721.
- (33) Romero-Canelón, I.; Sadler, P. J. *Inorg. Chem.* **2013**, *52*, 12276-12291.
- (34) Ying, W. *Antioxid. Redox Signaling* **2008**, *10*, 179-206.
- (35) Schafer, F. Q.; Buettner, G. *Free Radic. Biol. Med.* **2001**, *30*, 1191-1212.

Chapter 5

Interactions of half sandwich Ru(II) mono-sulfonamide complexes with DNA and GSH



5. Interactions of half sandwich Ru(II) mono-sulfonate complexes with DNA and GSH

In the previous chapters, a series of $[(\eta^6\text{-arene})\text{Ru}(\text{XEn})\text{Cl}]$ compounds, (XEn = *N*-(2-aminoethyl)-4-nitrobenzenesulfonamide (NbEn), *N*-(2-aminoethyl)-4-(trifluoromethyl)benzenesulfonamide (TfEn), *N*-(2-aminoethyl)-4-toluenesulfonamide (TsEn) or *N*-(2-aminoethyl)methylenesulfonamide (MsEn)), were synthesized with the aim of obtaining a catalytic anticancer drug. In an ideal situation the complexes will not show antiproliferative activity towards cancer cells unless activated upon reaction with sodium formate. However, *in vitro* experiments performed in Chapter 4 showed that the complexes **1-3** and **7-16** exhibit moderate antiproliferative activity against A2780 ovarian cancer cells in the absence of sodium formate. Therefore, it is important to understand the chemical and biological behaviour of those complexes in the absence of sodium formate. Nevertheless, the activity of the complexes can be significantly increased by the addition of sodium formate.

This chapter is focused on the reactivity of the complexes towards DNA and GSH.

5.1. DNA

The history of metal based cancer drugs starts in 1965 with B. Rosenberg and cisplatin.^{1,2} Soon cisplatin demonstrated limitations like acquired resistance in some tumours or severe side effects.³⁻⁵ Since then, there has been research aiming to understand the mechanism of cisplatin, and to develop alternative drugs which complement or replace cisplatin. Currently, DNA is commonly accepted as the primary target for the platinum drug.⁶⁻⁸ The activated form of cisplatin (after hydrolysis) binds to N7-guanine (Less common binding sites are N7-adenine and N3-cytosine). Binding to a second N7-guanine gives a

bisfunctional crosslink.⁶⁻⁸ The most common DNA-platinum adducts are 1,2-intrastrand cross links, where a $[\text{Pt}(\text{NH}_3)_2]^{2+}$ unit is bound to two guanines from the same DNA strand, causing the bending of the DNA and inhibiting replication.⁶⁻⁸

Ruthenium, osmium, rhodium and iridium complexes have also been designed with the aim of targeting DNA.⁹⁻¹¹ For instance, the family of organometallic ruthenium(II) arene compounds $[(\eta^6\text{-arene})\text{Ru}(\text{en})\text{Cl}]^+$, has shown similar affinity for DNA as some platinum drugs.¹²⁻¹⁶ Furthermore, direct correlation between cytotoxicity of those complexes and DNA binding has been reported.¹²⁻¹⁷ Specifically, $[(\text{bip})\text{Ru}(\text{en})\text{Cl}]^+$ (**RM175**), displayed good *in vitro* and *in vivo* activity due to its dual mode of interaction with DNA; direct metal coordination to DNA and intercalation between DNA bases through the aromatic ligand.¹⁸ DNA intercalation is the process where extended planar aromatic molecules are inserted in between base pairs. These interactions are stabilized by π -interaction of the intercalator and the nearby nucleobases. Intercalation increases the separation between base pairs and unwinding of the DNA. DNA becomes more rigid and stiff.¹⁹

Another common type of interaction with DNA is groove binding. These molecules bind through van-der-Waals interactions, hydrogen bonds and hydrophobic interactions with nucleobases.¹¹ The presence of DNA groove binders inhibits the action of transcription proteins. Furthermore, steric hindrance can play a role in DNA bending in cases where there is groove binding.

Complexes of the type $[(\eta^6\text{-arene})\text{Ru}(\text{XEn})\text{Cl}]$ (X= Nb, Tf, Ts or Ms), derived from the ethylenediamine analogues, have shown reasonably high *in vitro* anticancer activity (11-20 μM). However, the possible targets for those compounds are still unknown. Due to the resemblance of those complexes with their ethylenediamine analogues, and **RM175**, their

interactions of those complexes with DNA and the possibility of DNA being the primary target will be studied in this chapter.

5.1.1. Experimental

5.1.1.1. Materials

Ruthenium(II) complexes [(*p*-cym)Ru(MsEn)Cl] (**1**), [(*p*-cym)Ru(TsEn)Cl] (**2**), [(*p*-cym)Ru(TfEn)Cl] (**3**), [(hmb)Ru(TsEn)Cl] (**5**), [(bip)Ru(TsEn)Cl] (**8**), [(bn)Ru(TsEn)Cl] (**11**) and [(*p*-cym)Ru(NbEn)Cl] (**16**) were synthesised as described in Chapter 3. Complex [(bip)Ru(en)Cl]PF₆ was synthesized by Dr Pieter Bruijninx following the method described in the literature. 9-ethylguanine (9-EtG) and 9-methyladenine (9-MeA) were obtained from Sigma-Aldrich. silver nitrate, potassium hydroxide, sodium chloride and perchloric acid were obtained from Fisher Scientific. Calf thymus DNA was obtained in water solution from Invitrogen and as a solid from Sigma-Aldrich. Concentration of calf thymus DNA was measured by UV-Vis as described in Chapter 2. Sodium cacodylate was obtained from Fluka. Absolute ethanol was purchased in AnalaR NORMAPUR. The solvents used for UV-Vis absorption, linear dichroism, fluorimetry and circular dichroism were double distilled water (18 MΩ·cm) (ddw) and acetonitrile (HPLC grade). Double distilled water (18 MΩ·cm) (ddw) was collected from Purelab UHQ system model UHQ-PS-MK3. Acetonitrile (HPLC grade) was obtained from Fisher Scientific. MeOD-*d*₄ and 99.9 % D₂O for NMR spectroscopy were purchased from Sigma-Aldrich and Cambridge Isotope Labs Inc.

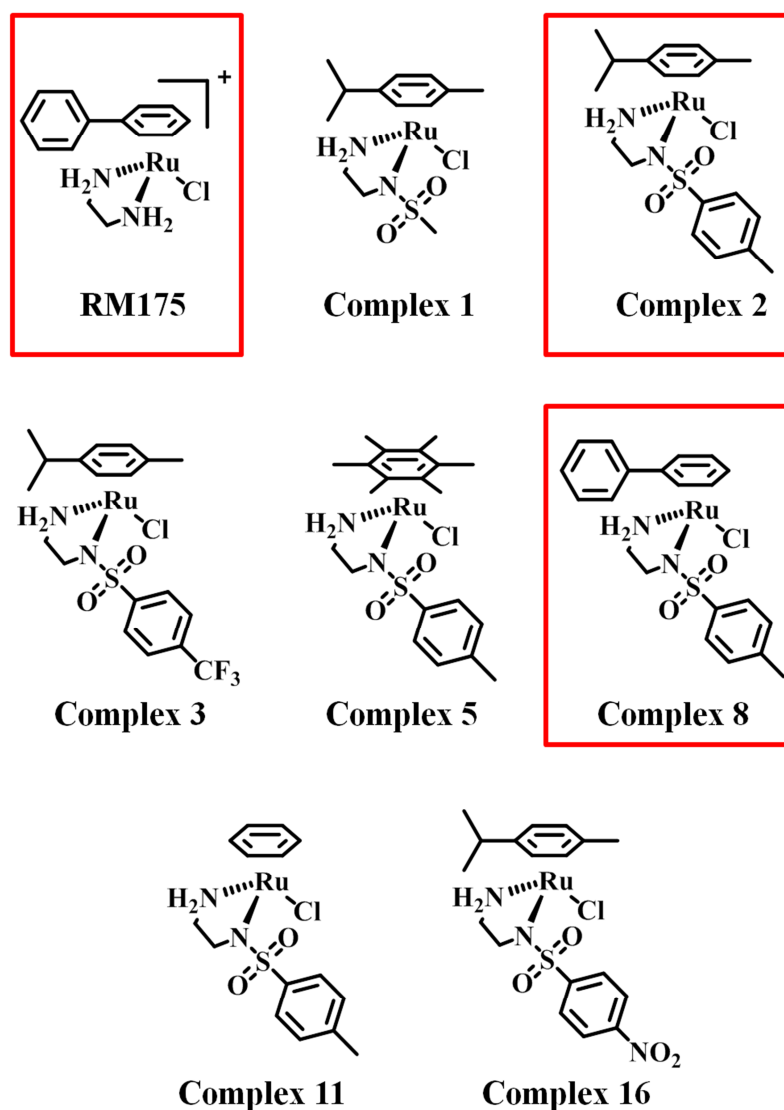


Figure 5.1. Complexes used for the studies with nucleobases and DNA.

5.1.1.2. Interaction with nucleobases

Solutions of the complexes **1-3**, **5**, **8**, **11** and **16** in D₂O (1.4 mM) were prepared and added to 5 mm diameter NMR tubes containing 9-ethylguanine or 9-methyladenine (final ratio 1:1 complex to 9-EtG, 1:2 complex to 9-MeA). The pH* of the reaction mixture was adjusted to 7.2 ± 0.1 and the reaction monitored by ¹H NMR spectroscopy. ¹H NMR spectra at 310 K were recorded at time < 10 min and 24 h (5 h for reactions with 9-MeA) on a Bruker AV III 600 spectrometer (¹H = 600 MHz). All data processing was carried out using Topspin 2.0. ¹H NMR chemical shifts were internally referenced to TMS *via* 1,4-dioxane in D₂O (δ = 3.75).

Exact concentrations of the Ru were determined by ICP-MS. Concentration of the substrate was verified by integration of the ^1H NMR peaks and compared to those from the complex. Binding constants were calculated using the equation:^{20, 21}

$$K_a = \frac{[\text{MS}]}{[\text{S}][\text{M}]}$$

$$[\text{M}]_{\text{total}} = [\text{MS}] + [\text{M}] = \frac{I_{\delta[\text{MS}]}}{I_{\delta[\text{MS}]} + I_{\delta[\text{M}]}} [\text{M}]_{\text{total}} + \frac{I_{\delta[\text{M}]}}{I_{\delta[\text{MS}]} + I_{\delta[\text{M}]}} [\text{M}]_{\text{total}}$$

where I_x is the integral of the peak at x ppm.

$$\text{When } [\text{S}] = [\text{M}] = \frac{I_{\delta[\text{M}]}}{I_{\delta[\text{MS}]} + I_{\delta[\text{M}]}} [\text{M}]_{\text{total}}$$

$$K_a = \frac{I_{\delta[\text{MS}]}}{I_{\delta[\text{M}]}} \times \frac{I_{\delta[\text{MS}]} + I_{\delta[\text{M}]}}{I_{\delta[\text{M}]}} \frac{1}{[\text{M}]_{\text{total}}}$$

High resolution mass spectra of the reaction mixture obtained from reacting complexes **1-3**, **5**, **8**, **11** and **16** with 9-EtG were recorded on freshly prepared samples.

Changes in the chemical shifts of protons from the complex $[(p\text{-cym})\text{Ru}(\text{TsEn})(9\text{-EtG})]^+$ (**2-9EtG**) with the pH^* over a range from 2 to 12 were followed by ^1H NMR spectroscopy. ^1H -NMR spectra were recorded at 278 K on a Bruker AV III 600 spectrometer ($^1\text{H} = 600$ MHz).

5.1.1.3. CT-DNA binding kinetics

Solutions of CT-DNA (200 μM) in cacodylate buffer (2 mM, pH 7.4) and NaCl (20 mM or 2 mM) were incubated at 310 K with complexes $[(p\text{-cym})\text{Ru}(\text{TsEn})\text{Cl}]$ (**2**) and $[(\text{bip})\text{Ru}(\text{TsEn})\text{Cl}]$ (**8**) (66 μM , final ratio 1:3) for 27 h. Aliquots of 300 μL were withdrawn from the incubator, cooled down on an ice bath and treated with absolute ethanol to

precipitate the DNA (700 μ L, final concentration 70 % ethanol). Samples were centrifuged for 10 minutes and the ruthenium content of the supernatant was determined by ICP-MS.

The experiment was also performed with complex [(bip)Ru(en)Cl]⁺ (**RM175**) in 2 mM cacodylate and 2 mM NaCl. This experiment was used as a control since it is well known that **RM175** can coordinate to DNA.²²

5.1.1.4. CT-DNA melting temperature

CT-DNA (100 μ M) was incubated at 310 K for 2 h in the presence and absence of complex **2** or **8** (33.3 μ M in 5 % acetonitrile/95 % ddw, ratio 1:3 complex:DNA) in cacodylate buffer (2 mM, pH 7.4) and NaCl (20 mM) or cacodylate buffer solution (2 mM, pH 7.4) containing NaCl (2 mM).

Thermal denaturation of CT-DNA in the presence and absence of complex **2** or **8** was recorded by following the changes of absorbance at 260 nm while increasing the temperature from 283 to 371 K. The melting curve for unruthenated DNA was determined under the same conditions as for complex **2** and **8**. The data were fitted to the Boltzmann equation using Origin 7.5. The melting temperature value (T_m , temperature where 50 % of the CT-DNA was denatured) was determined as the inflection point.

Experiments with complex **RM175** under the same conditions as described for complex **2** and **8** were performed for comparison purposes.

5.1.1.5. Conformational changes of CT-DNA

CT-DNA (1 mM) was incubated at 310 K for 24 h in the presence and absence of complex **2** and **8** (0.3 mM in 5 % acetonitrile/95 % ddw, final ratio 1:3 complex:DNA) in cacodylate buffer (2 mM, pH 7.4) and NaCl (20 mM). Circular dichroism spectra of the reaction mixture were recorded at 0 h and after incubation 24 h at 310 K. Titration of CT-DNA (1 mM) in cacodylate buffer (2 mM, pH 7.4) and NaCl (20 mM) with different

concentrations of complex **8** (ratios 1:3, 1:5, 1:10, 1:20 and 1:4 complex:DNA) was followed by circular dichroism

Titration of CT-DNA (300 μM) in cacodylate buffer (2 mM, pH 7.4) and NaCl (20 mM) using complex $[(\text{bip})\text{Ru}(\text{TsEn})\text{Cl}]$ (**8**) and $[(p\text{-cym})\text{Ru}(\text{TsEn})\text{Cl}]$ (**2**) (5 % acetonitrile/95 % ddw, ratios 1:3, 1:5, 1:10, 1:20 and 1:40 complex:DNA) was followed by linear dichroism. A final experiment with CT-DNA (150 μM) in cacodylate buffer (2 mM, pH 7.4) and NaCl (20 mM) using 150 μM complex **8** or **2** (5 % acetonitrile/95 % ddw, ratios 1:1) was monitored by linear dichroism

5.1.2. Results

A series of complexes of the type $[(\eta^6\text{-arene})\text{Ru}(\text{XEn})\text{Cl}]$ (arene = *p*-cym, hmb, bn or bip, X= Nb, Tf, Ts or Ms) was selected to investigate the potential of DNA interactions. Nucleobases binding studies were performed with all the complexes depicted in Figure 5.1. However, reactions with CT-DNA were explored using complex $[(p\text{-cym})\text{Ru}(\text{TsEn})\text{Cl}]$ (**2**) and $[(\text{bip})\text{Ru}(\text{TsEn})\text{Cl}]$ (**8**). Some DNA-binding experiments were also carried out with complex **RM175** for comparison purposes.

5.1.2.1. Interaction with nucleobases

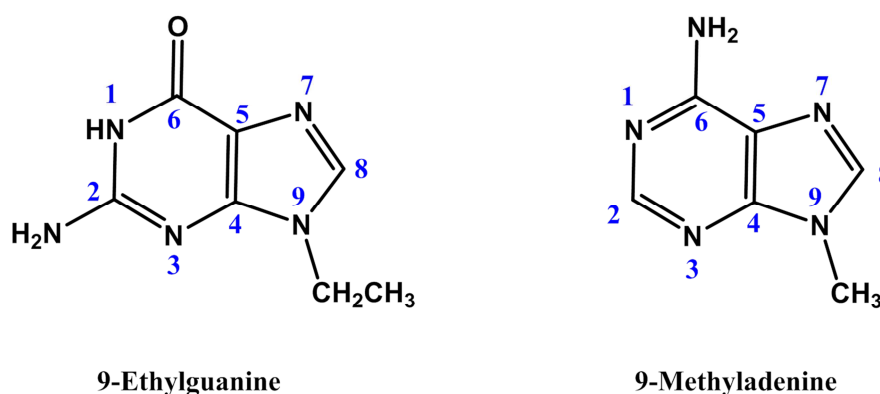


Figure 5.2. Atom numbering scheme for 9-EtG and 9-MeA.

Solutions of 9-ethylguanine (9-EtG) and 9-methyladenine (9-MeA) were reacted with complexes **1-3**, **5**, **8**, **11** and **16**.

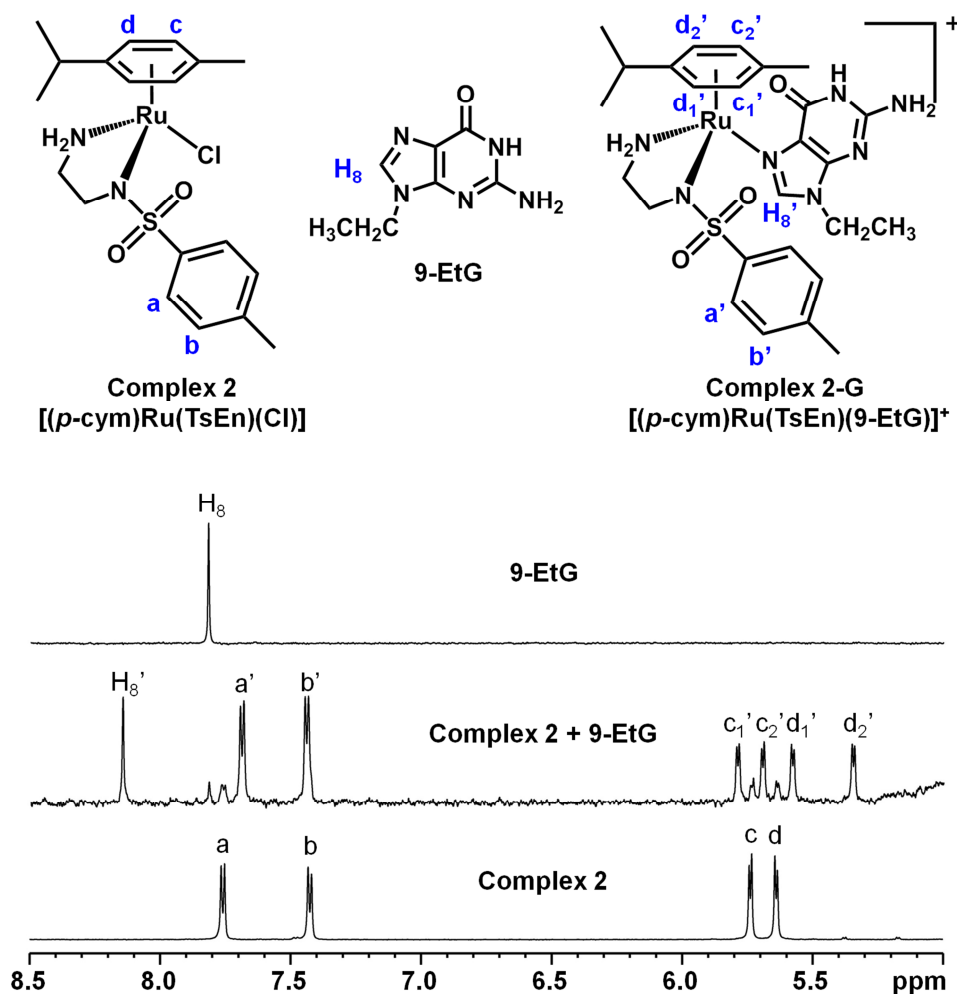
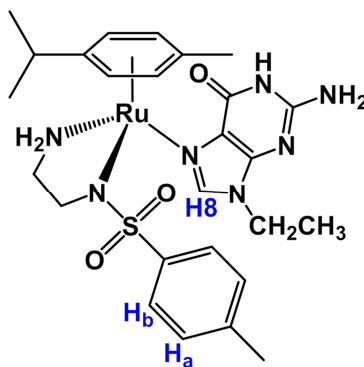


Figure 5.3. ^1H NMR spectra of 9-EtG, complex **2** and the reaction mixture of complex **2** + 9-EtG (ratios 1:1). All the samples were prepared in D_2O and $\text{pH}^* 7.2 \pm 0.1$, the spectra were recorded within 10 min after preparation at 310 K.

^1H NMR spectra of the reaction of complexes **1-3**, **5**, **8**, **11** and **16** with 9-EtG recorded at time 0 h (<10 min) show two sets of peaks corresponding to 9-EtG (Figure 5.3). One set was assigned to unbound 9-ethylguanine and the other set assigned to the complex-(9-EtG) adduct. The chemical shift of H_8 from (9-EtG)-adducts of complexes **1-3**, **5**, **11** and **16** was displaced downfield by approximately *ca.* 0.33-0.72 ppm. In the case of

$[(\text{bip})\text{Ru}(\text{TsEn})(9\text{-EtG})]^+$ (**8-G**), the chemical shift for H₈ was displaced downfield only by 0.04 ppm. The ¹H NMR spectra exhibits no further change over a period of 24 h at 310 K.

Table 5.1. Chemical shift of H₈ (9-ethylguanine)-adducts. The reaction was carried out in D₂O, pH* 7.2 ± 0.1 and 310 K.



R₁ = *p*-cym, bn, hmb or bip. R₂ = Ms, Ts, Tf or Nb.

Complex		δ_{H8} (ppm)	$\Delta\delta_{\text{H8}}^{\text{a}}$ (ppm)
$[(\text{p-cym})\text{Ru}(\text{TsEn})(9\text{-EtG})]^+$	(1-G)	8.15	0.33
$[(\text{p-cym})\text{Ru}(\text{MsEn})(9\text{-EtG})]^+$	(2-G)	8.18	0.36
$[(\text{p-cym})\text{Ru}(\text{TfEn})(9\text{-EtG})]^+$	(3-G)	8.24	0.42
$[(\text{hmb})\text{Ru}(\text{TsEn})(9\text{-EtG})]^+$	(5-G)	8.54	0.72
$[(\text{bip})\text{Ru}(\text{TsEn})(9\text{-EtG})]^+$	(8-G)	7.85	0.04
$[(\text{bn})\text{Ru}(\text{TsEn})(9\text{-EtG})]^+$	(11-G)	8.17	0.35
$[(\text{p-cym})\text{Ru}(\text{NbEn})(9\text{-EtG})]^+$	(16-G)	8.30	0.48

^a $\Delta\delta_{\text{H8}} = \delta_{\text{H8}} - \delta_{\text{H8}}(9\text{-EtG})$, $\delta_{\text{H8}}(9\text{-EtG}) = 7.82$ ppm.

Table 5.2. Binding constant of complexes **1-3**, **5**, **8**, **11**, **13**, and **16** with 9-EtG determined by ^1H NMR. The experiments were performed in D_2O , $\text{pH}^* 7.2 \pm 0.1$ and 310 K. Equilibrium was reached by the time the first ^1H NMR spectrum was recorded (< 10 min).

Complex	Binding constant (mM^{-1})
$[(p\text{-cym})\text{Ru}(\text{MsEn})\text{Cl}]$ (1)	105.4 ± 2.3
$[(p\text{-cym})\text{Ru}(\text{TsEn})\text{Cl}]$ (2)	104.9 ± 3.9
$[(p\text{-cym})\text{Ru}(\text{TfEn})\text{Cl}]$ (3)	60.5 ± 6.0
$[(\text{hmb})\text{Ru}(\text{TsEn})\text{Cl}]$ (5)	97.8 ± 0.5
$[(\text{bip})\text{Ru}(\text{TsEn})\text{Cl}]$ (8)	39.3 ± 3.6
$[(\text{bn})\text{Ru}(\text{TsEn})\text{Cl}]$ (11)	478.3 ± 44.8
$[(p\text{-cym})\text{Ru}(\text{NbEn})\text{Cl}]$ (16)	92.8 ± 1.0

No reaction between complexes **1-3**, **5**, **8**, **11** and **16** and 9-MeA was detected by ^1H NMR during a period of 5 h.

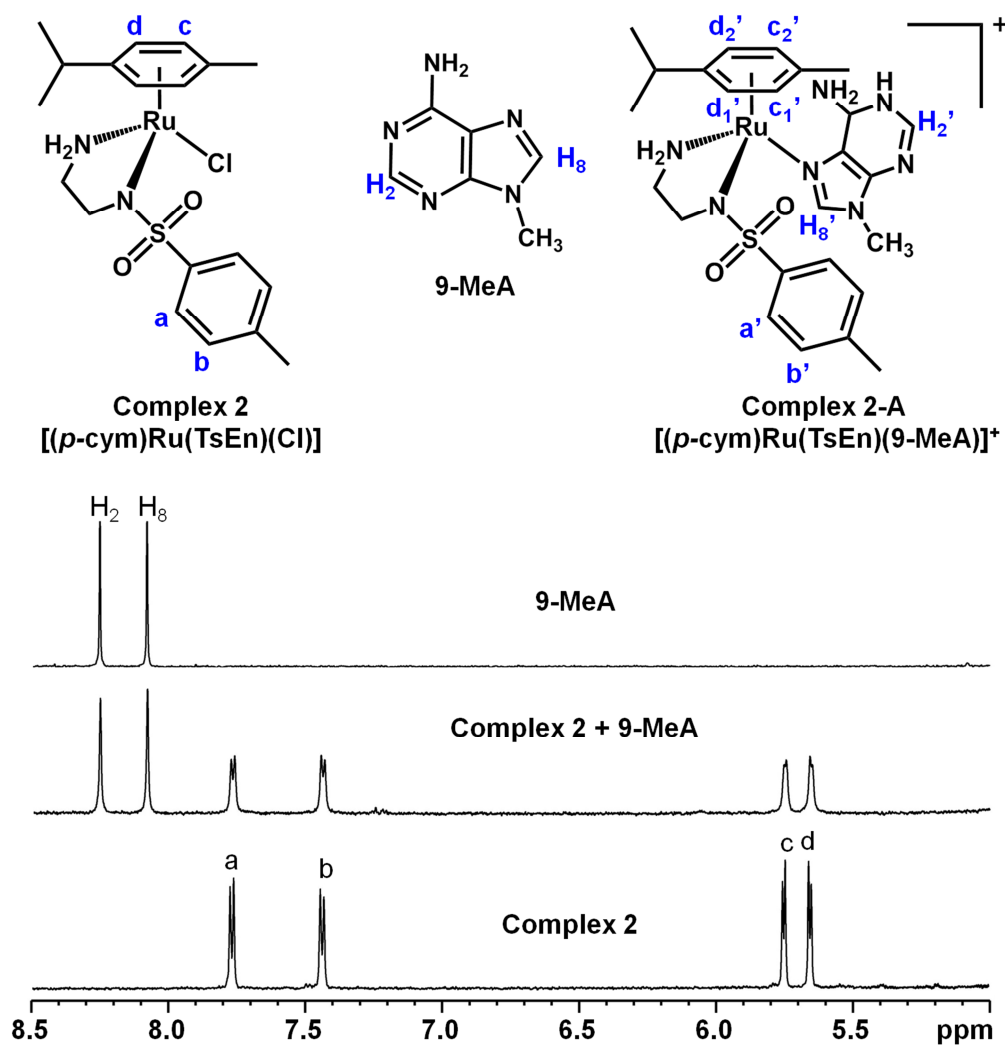


Figure 5.4. ^1H NMR spectra of 9-MeA, complex **2** and the reaction mixture of complex **2** + 9-MeA (ratios 1:2). All the samples were prepared in D_2O and $\text{pH}^* 7.2 \pm 0.1$, the spectra were recorded within 10 min after preparation at 310 K.

High resolution mass spectrometry was performed on freshly prepared samples obtained from reacting 9-EtG with the complexes **1-3**, **5**, **8**, **11** and **16** in order to verify the formation of the corresponding adduct. Calculated and found mass-to-charge ratios for the 9-EtG adducts are shown in Table 5.3.

Table 5.3. Mass-to-charge ratios for the 9-EtG adducts of complexes **1-3**, **5**, **8**, **11**, **13**, and **16**.

Complex		Chemical Formula	Calc. mass m/z	Found mass m/z
$[(p\text{-cym})\text{Ru}(\text{MsEn})(9\text{-EtG})]^+$	(1-G)	$\text{C}_{20}\text{H}_{32}\text{N}_7\text{O}_3\text{RuS}^+$	552.1330	552.1337
$[(p\text{-cym})\text{Ru}(\text{TsEn})(9\text{-EtG})]^+$	(2-G)	$\text{C}_{26}\text{H}_{36}\text{N}_7\text{O}_3\text{RuS}^+$	628.1644	628.1647
$[(p\text{-cym})\text{Ru}(\text{TfEn})(9\text{-EtG})]^+$	(3-G)	$\text{C}_{26}\text{H}_{33}\text{F}_3\text{N}_7\text{O}_3\text{RuS}^+$	682.1362	682.1362
$[(\text{hmb})\text{Ru}(\text{TsEn})(9\text{-EtG})]^+$	(5-G)	$\text{C}_{28}\text{H}_{40}\text{N}_7\text{O}_3\text{RuS}^+$	656.1958	656.1971
$[(\text{bip})\text{Ru}(\text{TsEn})(9\text{-EtG})]^+$	(8-G)	$\text{C}_{28}\text{H}_{32}\text{N}_7\text{O}_3\text{RuS}^+$	648.1332	648.1333
$[(\text{bn})\text{Ru}(\text{TsEn})(9\text{-EtG})]^+$	(11-G)	$\text{C}_{22}\text{H}_{28}\text{N}_7\text{O}_3\text{RuS}^+$	572.1017	572.1020
$[(p\text{-cym})\text{Ru}(\text{NbEn})(9\text{-EtG})]^+$	(16-G)	$\text{C}_{25}\text{H}_{33}\text{N}_8\text{O}_5\text{RuS}^+$	659.1339	659.1338

Coordination to position N7 of 9-EtG as preferred binding site for the Ru(II) complexes was confirmed *via* pH* titration. Changes on the chemical shifts of H₈ of $[(p\text{-cym})\text{Ru}(\text{TsEn})(9\text{-EtG})]^+$ (**2-G**), with increasing pH* were plotted and fitted to a Henderson–Hasselbalch equation to obtain a pK_a* value of 8.78 ± 0.04.

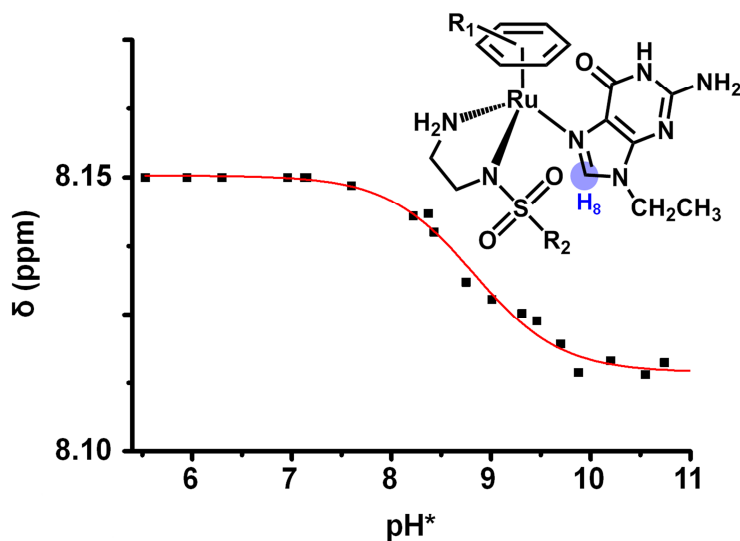


Figure 5.5. Dependence of the ^1H NMR chemical shifts of H_8 in $[(p\text{-cym})\text{Ru}(\text{TsEn})(9\text{-EtG})]^+$ on the pH^* . $\text{pK}_a^* 8.78 \pm 0.04$ determined using the Henderson-Hasselbalch equation.

5.1.2.2. Interactions with calf thymus DNA

Solutions of CT-DNA (200 μM) in cacodylate buffer (2 mM, pH 7.4) and NaCl (2 mM) were incubated at 310 K with either complexes $[(p\text{-cym})\text{Ru}(\text{TsEn})\text{Cl}]$ (**2**), $[(\text{bip})\text{Ru}(\text{TsEn})\text{Cl}]$ (**8**) or $[(\text{bip})\text{Ru}(\text{en})\text{Cl}]^+$ (**RM175**) (60 μM , final ratio 1:3 complex:DNA) for 27 h. Aliquots of 300 μL were withdrawn every hour, cooled down in a ice bath and the DNA precipitated by addition of absolute ethanol (700 μL , final concentration 70 % v/v). The concentration of Ru in the supernatant was measured by ICP-MS. No change in the ruthenium concentration of the supernatant, compared with the initial concentration, was observed for complexes **2** and **8**. However, a decrease of $\approx 14\%$ in ruthenium was observed for complex **RM175**, indicating binding to CT-DNA.

The experiment with complex **2** and **8** was repeated using a 2 mM cacodylate buffer and 20 mM NaCl. Similarly to the above experiment, no change on the ruthenium concentration of the supernatant, compared with the initial concentration was observed for complexes **2** and **8**.

Table 5.4. Concentrations of Ru measured by ICP-MS in the supernatant from the reaction between complex **2**, **8** or **RM175** and CT-DNA. The reaction was carried out in 2 mM NaCl and 2 mM cacodylate buffer, pH 7.4 ± 0.1 , temperature 310 K

Ru in supernatant (μM)			
Time (h)	[(bip)Ru(TsEn)Cl] (8)	[(<i>p</i> -cym)Ru(TsEn)Cl] (2)	[(bip)Ru(en)Cl] ⁺ (RM175)
Initial (No DNA)	53.4 ± 1.2	64.2 ± 0.7	58.3 ± 0.3
0.5	- ^a	66.7 ± 0.6	50.3 ± 0.3
1	52.8 ± 1.1	59.2 ± 1.0	49.3 ± 0.4
2	53.9 ± 1.1	63.6 ± 1.1	- ^a
3	53.7 ± 0.9	67.4 ± 0.7	- ^a
4	50.6 ± 0.6	65.0 ± 0.1	- ^a
5	53.2 ± 0.2	63.3 ± 1.0	50.3 ± 0.8
12	51.4 ± 1.2	64.2 ± 1.1	51.2 ± 0.8
24	53.7 ± 0.5	65.1 ± 0.3	48.5 ± 0.6

^aNot determined.

Table 5.5. Concentrations of Ru measured by ICP-MS in the supernatant from the reaction between complex **2** or **8** and CT-DNA. The reaction was carried out in water, 20 mM NaCl and 2 mM cacodylate, pH 7.4 ± 0.1 , temperature 310K.

Ru in supernatant (μM)		
Time (h)	[(bip)Ru(TsEn)Cl] (8)	[(<i>p</i> -cym)Ru(TsEn)Cl] (2)
Initial (No DNA)	47.6 ± 1.3	81.2 ± 0.5
0.5	48.2 ± 0.9	81.6 ± 1.6
1	44.9 ± 1.5	76.7 ± 1.0
2	47.7 ± 1.3	77.6 ± 1.0
3	46.1 ± 0.4	77.0 ± 0.3
4	46.1 ± 0.6	78.8 ± 0.7
5	44.3 ± 2.4	74.9 ± 1.4
6	45.8 ± 0.9	76.8 ± 1.0
7	44.0 ± 1.3	75.6 ± 0.3
18	47.3 ± 0.8	75.8 ± 2.2
27	46.5 ± 1.6	81.1 ± 0.6

Thermal stability of CT-DNA

The melting curve for CT-DNA (100 μ M) in the presence of complexes **2** or **8** (33.3 μ M, 5 % v/v acetonitrile/water) was recorded. CT-DNA was prepared in cacodylate buffer (2 mM, pH 7.4) and NaCl (20 mM). A decrease in the melting temperature of 4-5 degrees was observed. Exact T_m values are listed in Table 5.6.

Experiments performed in cacodylate buffer (2 mM, pH 7.4) and 2 mM NaCl result in a 3-5 degrees decrease of the melting temperature compared to the DNA. Exact T_m values are depicted in Table 5.6.(Figure 5.6).

Table 5.6. Melting temperature (T_m) of CT-DNA in the presence of **RM175**, complex **2** or complex **8** (ratio 1:3, complex:DNA). The reaction was carried out in cacodylate buffer (2 mM, pH 7.4). The samples were incubated for 2 h at 310 K.

Complex	[NaCl]	T_m (K)	ΔT_m^a
-	20 mM	332.3 \pm 1.0	-
RM175	20 mM	340.2 \pm 0.6	7.9**
2	20 mM	327.5 \pm 0.7	4.9**
8	20 mM	328.1 \pm 0.8	4.2**
-	2 mM	322.7 \pm 1.3	-
RM175	2 mM	336.9 \pm 0.8	14.0**
2	2 mM	320.3 \pm 1.6	2.4
8	2 mM	318.7 \pm 1.3	4.0*

^a variation in melting temperature between free DNA and DNA in the presence of the corresponding complex. * 95 % statistically different from free DNA using a T test analysis.
** 91 % statistically different from free DNA using a T test analysis

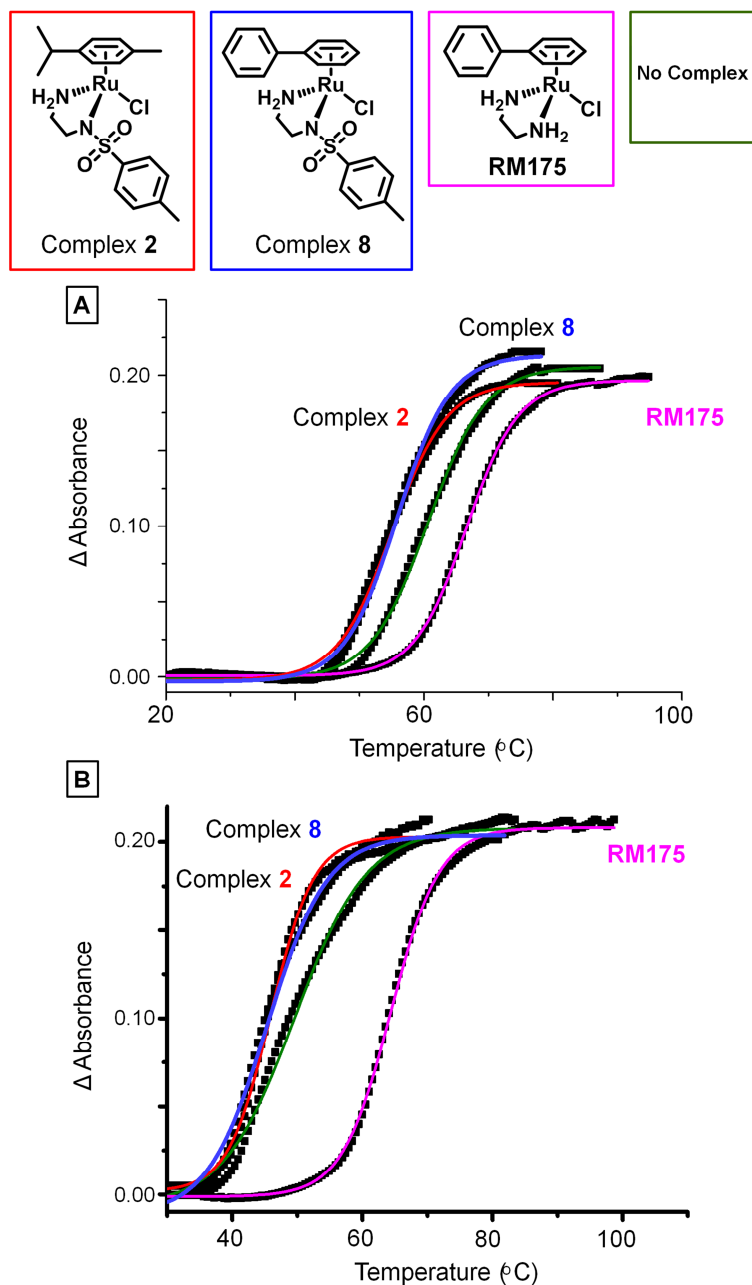


Figure 5.6. Comparison of CT-DNA melting curves in the absence and presence of complex $[(\text{bip})\text{Ru}(\text{en})\text{Cl}]^+$ (**RM175**), $[(p\text{-cym})\text{Ru}(\text{TsEn})\text{Cl}]$ (**2**) and $[(\text{bip})\text{Ru}(\text{TsEn})\text{Cl}]$ (**8**); ratio 1:5 (DNA:complex). (A) 2 mM cacodylate buffer and 20 mM NaCl (B) 2 mM cacodylate buffer and 2 mM NaCl.

Conformational changes of CT-DNA

Conformational changes in DNA when interacting with complexes [(*p*-cym)Ru(TsEn)Cl] (**2**) and [(bip)Ru(TsEn)Cl] (**8**) were studied by CD using solutions of CT-DNA (1 mM) in buffer (2 mM, pH 7.4) and NaCl (20 mM) with different concentrations of complex (ratios 3:1, 5:1, 10:1, 20:1 and 40:1 DNA:Complex). No changes or very small changes were observed in the CD spectra after incubation at 310 K for 24 h using complex **2**, Figure 5.7.

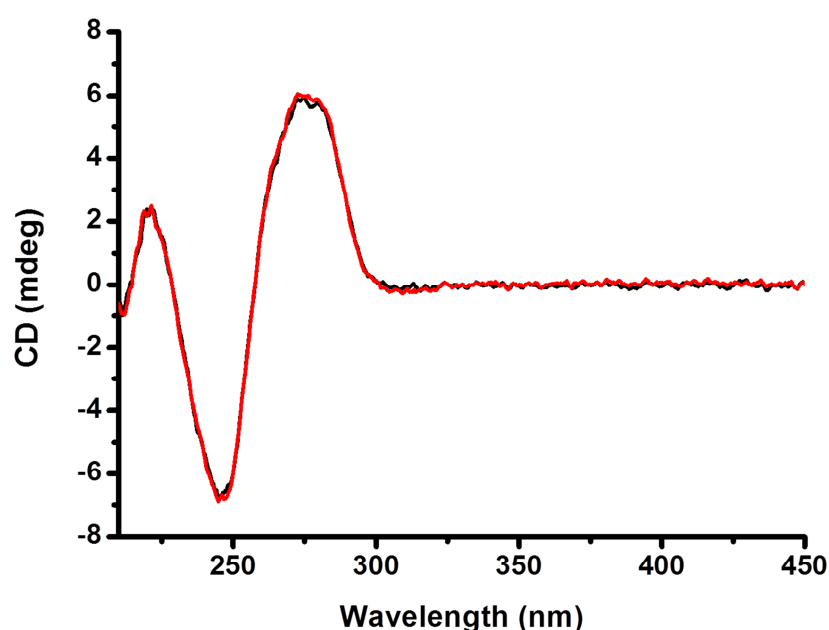


Figure 5.7. Circular dichroism spectra of CT-DNA (1 mM) in red and CT-DNA (1 mM)/complex **2** (ratio 3:1) in black. Both spectrum were recorded under the same conditions, using (A) cacodylate buffer (2 mM, pH 7.4) and NaCl (20 mM) at 298 K, (B) PBS buffer (2 mM, pH 7.4) and NaCl (20 mM).

For complex [(bip)Ru(TsEn)Cl] (**8**), a decrease on the negative band (260 nm) of the CD spectrum, and an increase on the positive band (275 nm) was observed in addition to a small shift of the band (*ca.* 9 nm). Induced bands due to the complex are observed between 350 and 425 nm. Changes in the CD spectra with different concentration of complex can be observed in Figure 5.8.

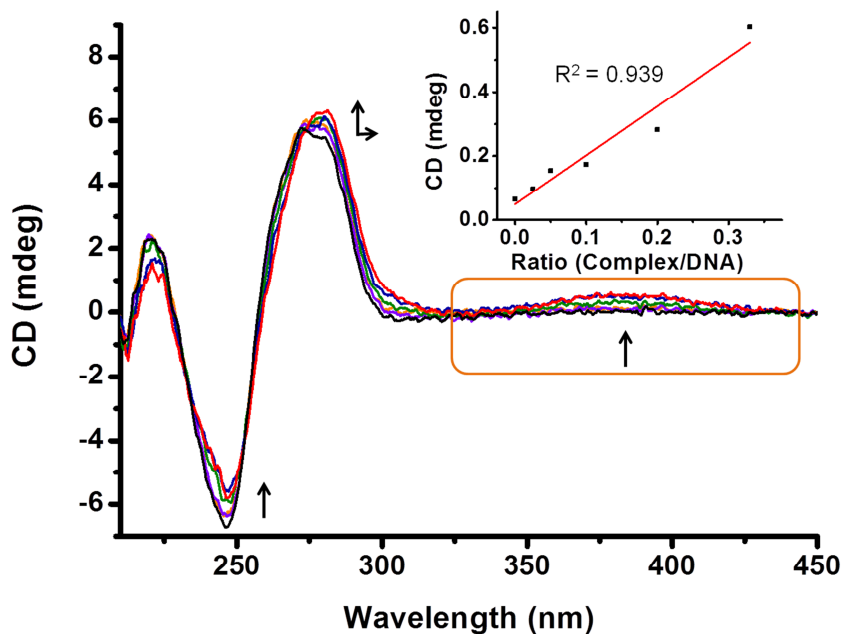


Figure 5.8. Circular dichroism spectra of CT-DNA (1 mM) titration with complex [(bip)Ru(TsEn)Cl] (**8**) (ratios 3:1, 5:1, 10:1, 20:1 and 40:1 DNA:Complex). All the experiments were recorded under the same conditions; using (A) cacodylate buffer (2 mM, pH 7.4) and NaCl (20 mM) at 298 K. Intensity of the induction band at 390 nm was plotted against Ru/DNA ratio.

Linear dichroism spectra of CT-DNA on adding complex **8** were recorded with different concentrations of complex (ratios 3:1, 5:1, 10:1, 20:1 and 40:1). A very small decrease in the signal at 190 and 260 nm was observed. An experiment with CT-DNA after addition of 1 mol equiv. of complex **8** was recorded, weak induction bands are observed after subtracting the signal of CT-DNA. (Figure 5.9).

LD spectra of a solution containing complex $[(p\text{-cym})\text{Ru}(\text{TsEn})\text{Cl}]$ (**2**) and CT-DNA were also recorded, showing similar results as the experiments with complex $[(\text{bip})\text{Ru}(\text{TsEn})\text{Cl}]$ (**8**) (Figure 5.10).

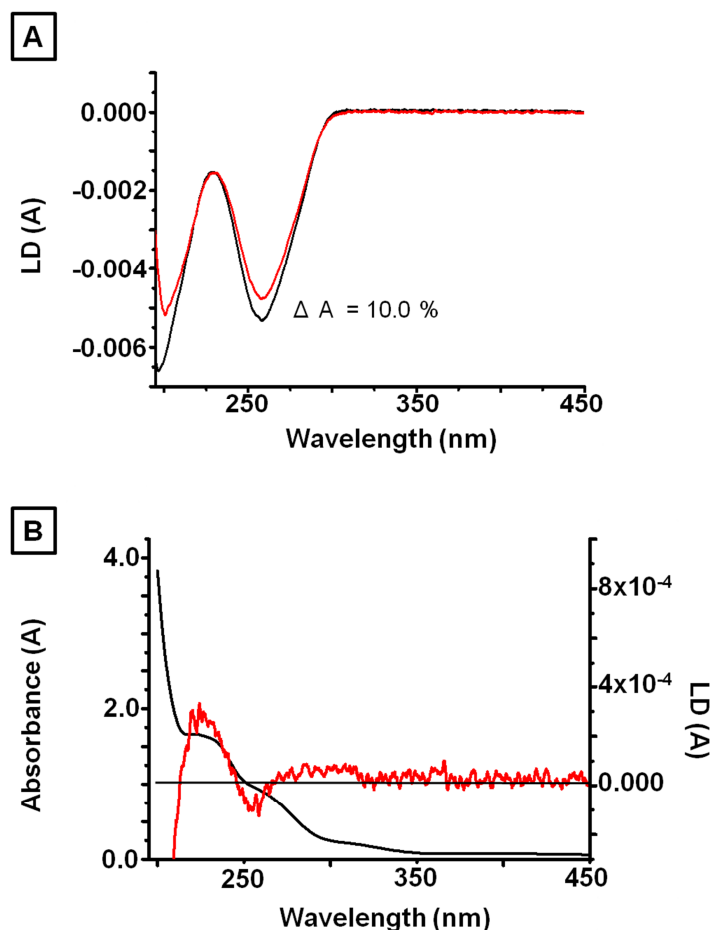


Figure 5.9. Reaction between CT-DNA and complex $[(\text{bip})\text{Ru}(\text{TsEn})\text{Cl}]$ (**8**) (mol. ratio 1:1) 2 mM cacodylate buffer (pH 7.4) and 20 mM NaCl. (A) LD spectra of CT-DNA (black) and CT-DNA/complex **8** (red). (B) Induced LD signal from complex **8** (red) and UV spectrum of complex **8**.

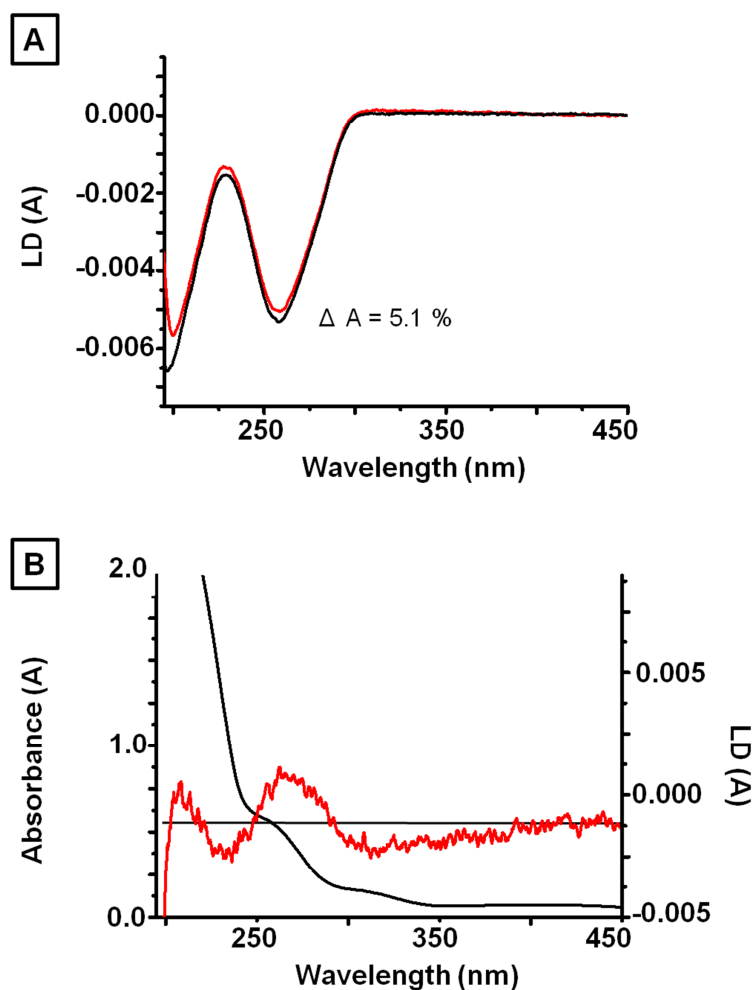


Figure 5.10. Reaction between CT-DNA and complex $[(p\text{-cym})\text{Ru}(\text{TsEn})\text{Cl}]$ (**2**) (mol. ratio 1:1) in 2 mM cacodylate buffer (pH 7.4) and 20 mM NaCl. (A) LD spectra of CT-DNA (black) and CT-DNA/complex **2** (red). (B) Induced LD signal from complex **2** (red) and UV spectrum of complex **2**.

5.1.3. Discussion

DNA is believed to be the main target for $[(\text{bip})\text{Ru}(\text{en})\text{Cl}]^+$ (**RM175**).²³⁻²⁵ Due to the structural similarity of the complexes **1-3**, **5**, **8**, **11**, **13** and **16** with **RM175**, the possibility of DNA being a target was investigated.

5.1.3.1. Interactions with nucleobases

Initially, model nucleobases, 9-ethylguanine and 9-methyladenine, were reacted with complexes **1-3**, **5**, **8**, **11**, **13** and **16** in D₂O, 310 K and pH* 7.2 ± 0.1. The binding of the complexes to 9-EtG or 9-MeA was monitored by ¹H-NMR spectroscopy. Peaks for the 9-EtG adducts were observed by the time the first spectrum was recorded (< 10 min after mixing, Figure 5.3), but no change in the NMR spectrum after 24 h was observed, indicating that the equilibrium was reached rapidly. The peak corresponding to H₈ of coordinated 9-EtG is shifted down field by 0.04-0.8 ppm with respect to the H₈ peak of free 9-EtG (Table 5.1), a chemical shift behaviour typical of [(η⁶-arene)Ru(*N,N'*)Cl].²⁶ Calculated binding constants of the complexes with 9-EtG by NMR were between 40 and 450 mM⁻¹. The binding constants of the complexes are in the same range as that from the ethylenediamine complex [(bip)Ru(en)Cl]⁺ (K_{DNA}= 60.26 mM⁻¹).²⁷ The calculated binding constants are relatively high, which suggests that binding to DNA is possible, similar to [(bip)Ru(en)Cl]⁺.^{12, 13} High resolution mass spectra was recorded to confirm the formation of [(η⁶-arene)Ru(XEn)(9-EtG)]⁺. Binding of complexes **1-3**, **5**, **8**, **11**, **13** and **16** with 9-MeA was also investigated, although no reaction was detected by ¹H-NMR.

It is well established that N7 of guanine (G) is the preferred nucleotide binding site for many transition metals ions.^{12, 13, 27-31} Furthermore, strong and selective binding to N7 of 9-EtG, has been observed for [(η⁶-arene)Ru(en)Cl]⁺.^{12, 13} A pH* titration of [(*p*-cym)Ru(TsEn)(9-EtG)]⁺ was used to confirm that the complex binds to N7. A plot of the chemical shift of H₈ from bound 9-EtG (Figure 5.5), versus pH* gave a pK_a* of 8.77, which can be attributed to the deprotonation of N1 from coordinated 9-EtG and therefore we conclude that the binding of complex **2** to 9-EtG occurs though N7.³² The selectivity of these Ru(II) complexes for N7 of 9-EtG is not surprising, since similar behaviour has been previously described for [(η⁶-arene)Ru(en)Cl]⁺, and many Ru(II) arene complexes.

5.1.3.2. Interaction with CT-DNA

To study the interactions of complexes of the type $[(\eta^6\text{-arene})\text{Ru}(\text{XEn})\text{Cl}]$ (X = mono-sulfonamide) with DNA, two complexes were chosen as models. Complex **2**, $[(p\text{-cym})\text{Ru}(\text{TsEn})\text{Cl}]$, was selected due to its good water solubility and the fact that its reactivity has been intensively studied previously in this thesis. However, it has been well reported previously that complexes containing extended arenes can intercalate DNA, in addition of other interactions; therefore, complex **8**, $[(\text{bip})\text{Ru}(\text{TsEn})\text{Cl}]$, has also been used for these studies.³³

Stock solutions of complex **2** and **8** (0.7 mM in 5 % acetonitrile/water) were prepared and aliquots of μL were added to a solution of CT-DNA in water, 2 mM cacodylate buffer and 20 mM NaCl or water, 2 mM cacodylate buffer and 2 mM NaCl. The reaction mixture was incubated at 310 K, while aliquots of 300 μL were taken at different intervals during a period of 27 h. The DNA was then precipitated by addition of ethanol (700 μL , final concentration 70 % v/v). The Ru complexes which are strongly bound to CT-DNA (coordination) will precipitate together with the DNA upon addition of ethanol, and, therefore the ruthenium concentration in the supernatant should decrease. However, no changes in the Ru concentration could be detected by ICP-MS which suggest no strong interaction between the complexes and the DNA. These results are in disagreement with those previously obtained when reacting the complexes with 9-EtG and 9-MeA. Strong binding constant does not always correlate with strong DNA binding, probably due to the bulk of the *NN'* chelating ligand. In addition to the fact that DNA nucleobases are more hindered than the model 9-EtG or 9-MeA, due to the double helix backbone.

Thermal stability of CT-DNA

The melting temperature of CT-DNA in the presence and absence of complex [(*p*-cym)Ru(TsEn)Cl] (**2**) or [(bip)Ru(TsEn)Cl] (**8**) were determined by UV-Vis (Table 5.6). Higher melting temperature indicates increased stabilization of the DNA which is usually the effect of DNA-intercalators, or complexes coordinated to the nucleobases.³⁴ Per contra, destabilization of the DNA could translate in a decrease of the melting temperature, which could be the case of groove binding.

The melting temperature of CT-DNA in the presence of complex **RM175** was determined as a control. In agreement with the literature,²² an increase in the melting temperature of CT-DNA (14 degrees) was observed after addition of **RM175**, when the reaction was carried out in 2 mM NaCl and 2 mM cacodylate buffer. The increase is due to Ru binding to DNA as well as intercalation.²² However, upon increasing the chloride concentration by *ca.* 10 x times (20 mM NaCl) the melting temperature of CT-DNA in the presence of **RM175**, increases only by 7°. This effect has previously been reported and it is attributed to the partial inhibition of hydrolysis, and, therefore, inhibition of coordination to DNA.^{22, 35}

Experiments performed in the presence of complex **8**, when using 2 mM cacodylate buffer and 2 mM NaCl, show a 4 degrees decrease in the melting temperature. Furthermore, when increasing the salt content by *ca.* 10 times (20 mM NaCl) to inhibit hydrolysis, a 4 degrees decrease of the melting temperature can still be observed. Similar results were obtained when using complex **2**. These experiments support the results obtained on previous experiments, since a decrease on the melting temperature does not agree with coordination to DNA. Per contra, the decrease in the melting temperature, indicates that the complex destabilises CT-DNA, which could be due to electrostatic interactions or groove binding. Interestingly, increasing concentration of NaCl does not have a major influence on the

reaction. Hence, the possibility of electrostatic interactions has been discarded, since higher ionic strength stabilized DNA and should weaken the effect of the complex.

Conformational changes of CT-DNA

Circular dichroism is a common technique to study conformational changes in chiral systems, and is often used to study DNA interactions with metal complexes. CT-DNA is a chiral macromolecule, so changes induced by metal complexes are easily detected. Furthermore, strong binding of a metallodrug to DNA can induce chirality on the metal complex, generating a CD signal.³⁶

In order to have a more clear idea on the type of interaction and the effect of complexes **2** and **8** on CT-DNA, CD spectra of DNA with different concentrations of complex were recorded. Reaction between complex **8** and CT-DNA in water, 2 mM cacodylate buffer and 20 mM NaCl, resulted in the shifting of the CD signals (9 nm), in addition to a slight increase of the positive band at 280 nm and a small decrease of the band at 250 nm. A new band was also observed between 350-450 nm, and its intensity increased with the level of DNA ruthenation (Figure 5.8). These change indicates that complex **8** binds strongly to DNA, and possibly, induces slight conformational changes. However, it is not clear if the changes on the CD spectrum are due to alterations in the DNA conformation in addition to the induced signals from the complex. By analogy with the changes in CD obtained by reacting CT-DNA with [(bip)Ru(en)Cl]⁺ (**RM175**), it is reasonable to suggest that complex **8** binds to double helical DNA, and generates slight conformational changes.²² Furthermore, the induction bands from the complex, seem to be related to the presence of the extended arene, probably due to intercalation into the DNA.^{13,22}

Interaction between complex **2** and CT-DNA was also studied by CD, although no changes could be observed in the spectrum (Figure 5.7). The CD results obtained for complex

[(*p*-cym)Ru(TsEn)Cl] (**2**), suggest that the conformational changes induced on DNA are different from those induced by [(bip)Ru(TsEn)Cl] (**8**). The different behaviour when using the arene *p*-cym or bip can also be observed with the ethylenediamine analogues.²²

Flow linear dichroism is a technique used to study the structure and relative orientation of a molecule. The spectra obtained are the result of the difference in absorption of parallel and perpendicular polarized light to an orientation axis. The technique has been used to study interactions between DNA and ligands or metal complexes.³⁶

In a typical spectrum of CT-DNA, negative bands at 260 and 190 nm can be observed. These bands correspond to the absorbance of DNA bases which are oriented with an angle of 80° from the DNA backbone. An increase on the LD absorbance at 260 nm is indicative of more stiff or rigid DNA.³⁶ Per contra, a decrease on the LD absorbance at 260 nm is a response to the loss of linearity and orientation, in general, due to curling, bending or aggregation of DNA.³⁶

Intercalating molecules are typically responsible for and increase the absorbance at 260 nm, as a consequence of the loss of flexibility and the increase in the linearity of the DNA strings. Furthermore, intercalating molecules bind to DNA in a specific orientation, and therefore, induced bands due to intercalator absorbance can be observed.³⁶ Groove binding molecules, on the other hand, induce bending curling and aggregation on the DNA, and therefore a decrease on the absorbance at 260 nm. Similar to the case with intercalators, the binding is generally oriented and induction bands can be observed.³⁶

A series of LD experiments were performed using complex **2** and **8**. In both cases, interaction with DNA shows a slight decrease in the intensity of the LD signal. Those changes are probably due to the complexes binding in the minor groves of DNA, and the nucleic acid chain bending or aggregating.²² However, the effect of the Ru(II) complexes on

the DNA is remarkably weak, suggesting that the complex does not have a great affinity for DNA. Subtraction of the LD absorbance of CT-DNA for the spectra obtained when reacting with the complexes, gave induced spectra which can be overlapped with the corresponding UV spectrum of the complex, although, the induced bands are very weak.

With all of the information obtained previously we can postulate that complexes **2** and **8** have the ability to interact with DNA. However, the interaction is very weak. The complexes do not coordinate directly to DNA, but probably by binding to the minor grooves. Comparing with the ethylenediamine complexes we can predict that compound **8** probably binds to the groove generating bending or aggregation of DNA but also intercalates through the biphenyl arene.²²

5.1.4. Conclusions

In this section, the ability of complexes of the type $[(\eta^6\text{-arene})\text{Ru}(\text{XEn})\text{Cl}]$ (X = mono-sulfonamide) to bind selectively to 9-ethylguanine though the N7 was demonstrated. Binding constants for the binding to 9-EtG (mM) are of the same order of magnitude as for complex $[(\text{bip})\text{Ru}(\text{en})\text{Cl}]^+$ (60.3 mM). Such binding constants indicate that complexes **2** and **8** have an ability to bind 9-EtG, and possibly, DNA. However, coordination with DNA does not occur, probably due to sterically effects. DNA melting temperatures show that the complexes interact with DNA and destabilize its structure, which indicates that intercalation and coordination are not the main binding mode of the Ru(II) complexes to DNA. Instead, groove binding seems more plausible. Interestingly, complex $[(p\text{-cym})\text{Ru}(\text{TsEn})\text{Cl}]$ (**2**) and $[(\text{bip})\text{Ru}(\text{TsEn})\text{Cl}]$ (**8**) have similar effects on the DNA. On the other hand, complex **RM175**, stabilizes the DNA (Δ melting temperature = +14 degrees), which is in concordance with the compound coordinating DNA, reported previously.³⁷

Complex **8** seems to affect the conformation of the DNA slightly, probably through a certain degree of intercalation of the biphenyl unit into the nucleobases. Finally, LD experiments demonstrate that both complexes, **2** and **8**, are capable of bending or aggregating DNA, probably through groove binding.

Complexes **2** and **8** interact weakly with DNA. Furthermore, the complexes react in a very different manner than their analogous ethylenediamine complexes, such as **RM175**, which coordinates directly to DNA and stabilises its structure.

More studies are necessary to assess the relevance of this interaction and if those complexes can target DNA. However, DNA as a target seems improbable since the interactions with DNA are not strong.

5.2. Glutathione (GSH)

5.2.1. Introduction

Glutathione (GSH) is a tri-peptide (γ -L-glutamate-L-cysteineyl-glycine) present in cells (Figure 5.11). GSH exists in two different forms, oxidized (GSSG) and reduced (GSH). Under normal conditions, the GSH concentrations in mammalian cells are between 5 and 10 mM, with the reduced GSH predominating over the oxidized form.³⁸ Although GSH is synthesized in the cytosol, it is distributed to different intracellular organelles. In addition to the cytosolic pool, GSH is mainly found in the endoplasmic reticulum, nucleus, and mitochondria. Each organocell GSH pool is relatively independent. At physiological pH, glutathione has a negative charge since the two carboxylic acids ($pK_{a1} = 2.12$, $pK_{a2} = 3.59$) are deprotonated while the amine ($pK_a = 8.75$) is found in the protonated form.

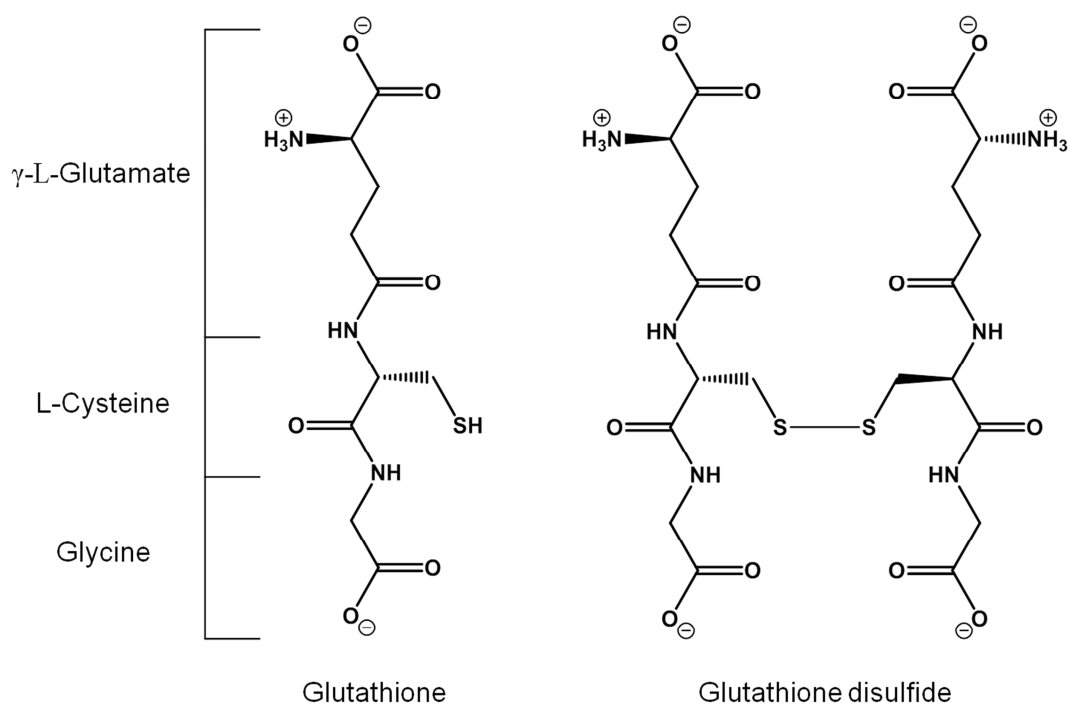


Figure 5.11. Structure of glutathione (GSH) and glutathione disulfide (GSSG) at pH 7.4

The glutathione couple (GSH/GSSG) is a critically important redox player together with other redox active couples. GSH acts as an antioxidant which prevents damage caused by reactive oxygen species (ROS) and reactive nitrogen species (RNS). Under normal conditions, when a cell is not stressed, the processes that generate ROS are well counterbalanced by antioxidant systems, with the GSH couple often considered to be the main defence system.^{38,39}

GSH can also act as a scaffold to transport some toxins outside the cell for later disposal from the body. Many toxic metabolites are produced as side-products of the normal cellular metabolism. Those metabolites can then react with GSH via some enzymatic reaction or in some cases with GS[•] radicals formed from reactions with ROS. Those GS-X adducts are then excreted from the cell. Most glutathione S-conjugates are metabolized outside the cell to the corresponding *N*-acetyl cysteine S-conjugates and excreted through the urine and bile. γ -L-glutamate and glycine residues are usually recovered.^{38, 39} Both GSH and GSSG generated in the liver, circulate in the blood stream and are used to supply other organs. GSH is then used to detoxify injurious external agents from epithelial cells that contact with the exterior, such as intestine and lungs. Finally, this detoxification method is also applied in the case of external toxins, as in the case of some anticancer drugs. When complexes with similar reactivity as cisplatin enter the cell and hydrolyse, they can react with nucleophiles such as GSH. Adducts of GSH with the complexes (GS-X) are formed readily due to the high concentration of GSH in the cytosol and the function of some enzymes such as glutathione-S-transferase. Then, GS-X adducts are transported to the outside of the cell. Cisplatin-resistant cells have increased the levels of GSH and enzymes that catalyse GS-X formation.⁴⁰

The role of GSH is not only as an antioxidant or detoxifying agent, but it is also involved in many other metabolic processes (such as storage and transport of nitric oxide, participation in the metabolism of estrogens, leukotrienes, and prostaglandins, the reduction

of ribonucleotides to deoxyribonucleotides, the maturation of iron-sulfur clusters of diverse proteins and it is involved in the operation of certain transcription factors).³⁸

Due to the importance of GSH in controlling high levels of oxidative stress, it is not surprising that it had become a possible target for cancer therapy. Furthermore, GS⁻ adducts are not always excreted from the cell. On the other hand, depletion of GSH might enhance the cytotoxic activity of other anticancer drugs such as cisplatin.⁴¹

In this section, reaction of GSH and GSSG with the complex [(*p*-cym)Ru(TsEn)Cl] (**2**) are studied as a model for the complexes of this type.

5.2.2. Experimental

5.2.2.1. Materials

The ruthenium(II) complex [(*p*-cym)Ru(TsEn)Cl] (**2**) was synthesised as described in Chapter 3. Trifluoroacetic acid (TFA), glutathione reduced (GSH) and glutathione oxidized (GSSG) were obtained from Sigma-Aldrich. Potassium hydroxide, sodium chloride and perchloric acid were obtained from Fisher Scientific. Non-dried solvents were obtained from Fisher Scientific. The solvents used for HPLC and LC-MS were purchased from Fisher Scientific. D₂O (99.9 % D) for NMR spectroscopy was purchased from Sigma-Aldrich.

5.2.2.2. Interaction with GSH

A stock solution of complex **2** (1.4 mM) in D₂O was prepared and 300 μL added to a 5 mm diameter NMR tubes containing 300 μL of a GSH solution (14 mM, ratio 1:10 complex to GSH). The pH* of the reaction mixture was adjusted to 7.2 ± 0.1 and the reaction monitored by ¹H NMR spectroscopy. ¹H NMR spectra were recorded at 310 K during a period of 24 h on a Bruker AV III 600 spectrometer.

The experiment was repeated using a different concentrations of GSH, ratios 1:3, 1:2.5, 1:2 and 1:1 complex:GSH. The pH* of the reaction mixture was also adjusted to 7.2 ± 0.1 and the reaction monitored by ^1H NMR spectroscopy. ^1H NMR spectra were recorded at 310 K during and at 24 h on a Bruker DRX 500 spectrometer.

A NMR tube containing complex **2** and GSH in D_2O (ratio 1:10) was also prepared under a nitrogen atmosphere (oxygen free). The pH* was adjusted to 7.2 ± 0.1 and the reaction monitored for a period of 24 h at 310 K on a Bruker AV III 600 spectrometer.

5.2.2.3. Identification of species

A reaction mixture of complex **2** with GSH in a molar ratio of 1 to 3 was prepared by adding 1 mL of solution of the complex (1.4 mM) and 1 mL of a solution GSH (2.1 mM), both solutions previously adjusted to pH 7.2 ± 0.1 using KOH and HClO_4 . The reactions were incubated at 310 K for 24 h. HPLC analysis on the reaction mixture was performed in order to adjust the gradient and separate all the product peaks HPLC experiment were performed in collaboration with Prof. Socorro P. Murdoch.

The column used for HPLC and LC-MS was an Agilent ZORBAX Eclipse Plus C-18 (250 x 4.6 mm, 5 μm pore size, PJS-44). The mobile phases were A: water (HPLC grade, Aldrich) containing 0.1 % trifluoroacetic acid, and B: acetonitrile (HPLC grade, Aldrich) containing 0.1% trifluoroacetic acid. Gradients in Table 5.7. The flow rate was 1 mL min^{-1} , wavelength of detection 254 and 210 nm with the reference wavelength at 510 nm.

Table 5.7. HPLC and LC-MS gradients for the separation of the products from the reaction of complex **2** with GSH. Total run of 60 min.

Time (min)	% of B (acetonitrile, 0.1 % TFA)
0	2
10	12
15	15
20	20
25	20
30	50
50	50
60	2

A reaction following the same procedure as that described above was carried out (1:3 mol equiv. complex:GSH). An aliquot of 0.5 mL was removed from the reaction mixture and frozen at times 0, 1, 4, 7 and 12 h. The samples were later analyzed by LC-MS.

In order to obtain mass spectra with higher resolution, a freshly prepared sample of the reaction after incubation 12 h was analysed by LC-HRMS, using a Dionex Ultimate 3000 with a VWD detector coupled to a Bruker MaXis UHR-ESI-TOF mass spectrometer.

5.2.3. Results

5.2.3.1. Interaction with glutathione (GSH)

A stock solution of complex **2** in D₂O was added to a NMR tube containing a solution of GSH (ratio 1:10 complex:GSH) at pH* 7.2 ± 0.1. ¹H NMR spectra were recorded at 310 K over 10 hours (Figure 5.12). The reaction was complete with 100 % conversion of the complex by the time the first NMR spectrum was recorded (< 10 min). A small shift of the resonances corresponding to the TsEn ligand (*N*-(2-aminoethyl)-4-toluensulfonamide) was observed (*ca.* 0.02 and 0.06 ppm), which correspond to free ligand. Two sets of peaks for the *p*-cym bound to Ru were observed, one of which corresponds to a non-symmetric product (4 peaks corresponding to 4 protons of the *p*-cym unit) and a second one corresponding to a symmetric product (2 peaks corresponding to 4 protons of a *p*-cym unit). 5 % of free *p*-cymene can be observed (7.21 ppm). Finally a new multiplet at 3.15 ppm was observed. The integral of the multiplete was that of 1.75 – 2.5 protons per proton corresponding to the aromatic TsEn ligand. However, precise integration was not possible. ¹H NMR spectrum over time (*ca.* 10 h) did not show any change. No formation of GSSG could be detected after 10 h reaction.

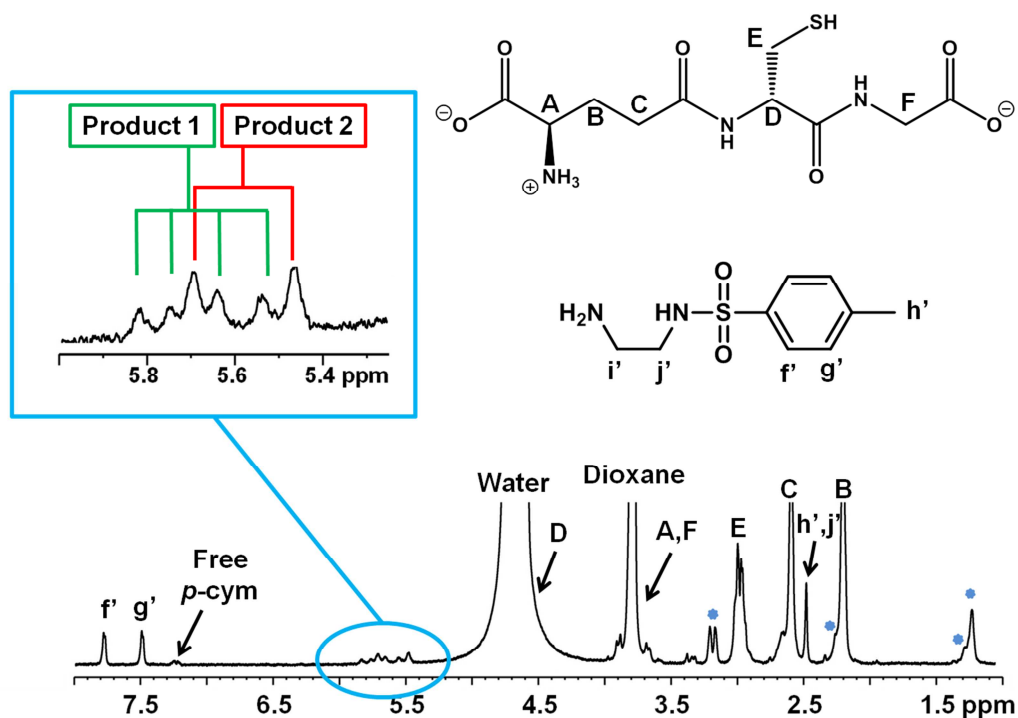


Figure 5.12. ^1H NMR (600 MHz) spectrum of the reaction between complex **2** and 10 mol equiv. of GSH. The pH^* was adjusted to 7.2 ± 0.1 and the spectra recorded at 310 K within 10 min of mixing. The blue dots correspond to new peaks probably due to GS^- in product 1 or product 2. Unreacted GSH can be observed;

A series of experiments using complex **2** and different concentrations of GSH (ratio 1:3, 1:2.5, 1:2 and 1:1) were carried out. The results are similar to those described above. 100 % of the GSH reacted with complex **2** in less than 10 min at 310 K, pH^* 7.2 ± 0.1 . No further reaction was observed in 10 h after the first ^1H NMR spectrum was recorded.

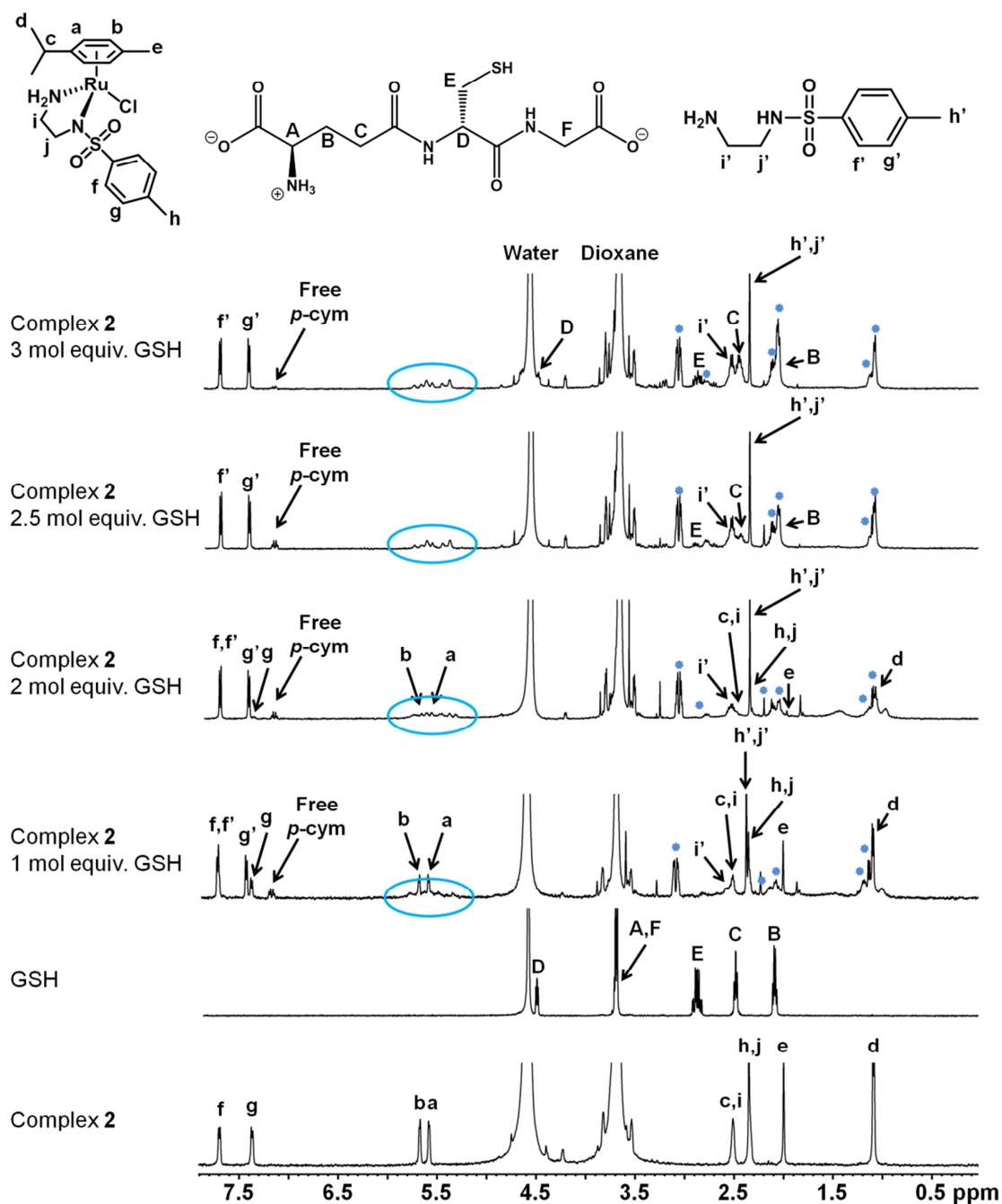


Figure 5.13. ^1H NMR (500 MHz) spectra of the reaction between complex **2** and GSH. The pH^* was adjusted to 7.2 ± 0.1 and the spectra recorded at 310 K within 10 min of mixing. The blue dots correspond to new peaks. Zoom of the peaks between 5 and 7 ppm is depicted in figure 5.14. In the first spectrum, 3 mol equiv. of GSH were used, peaks corresponding to free GSH are observed. In fourth spectrum, 1 mol equiv. of GSH was used, Peaks corresponding to free GSH can not be observed, however, signals from the intact complex can be assigned.

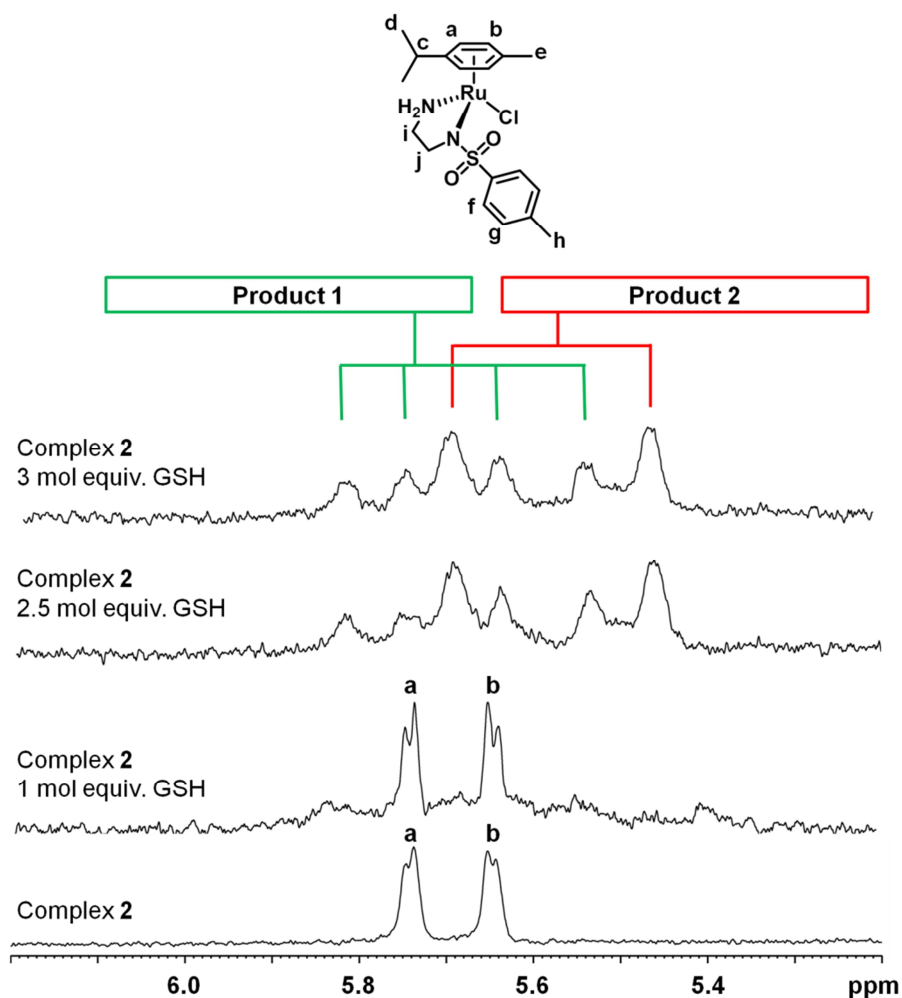


Figure 5.14. ¹H NMR (500 MHz) spectra, between 5 and 7 ppm, of the reaction between complex **2** and GSH. The pH* was adjusted to 7.2 ± 0.1 and the spectra recorded at 310 K within 10 min of mixing. In the first spectrum, 3 mol equiv. of GSH were used, peaks corresponding to two different products can be observed, one being symmetrical and another non-symmetrical. In the third spectrum, 1 mol equiv. of GSH was used, peaks corresponding to complex **2** can be observed in addition to some peaks corresponding to the different products from the reaction.

A stock solution of complex **2** in D₂O was added to a NMR tube containing a solution of GSH (ratio 1:10 complex:GSH) at pH* 7.2 ± 0.1 . The reaction was prepared under nitrogen and the NMR tube filled with nitrogen before sealing. ¹H NMR spectra were

recorded at 310 K over a period of 10 hours. ^1H NMR spectra show the same results obtained previously for the reaction containing oxygen (air).

5.2.3.2. Identification of species by LC-MS

A reaction of complex **2** (0.4 mM) with 3 mol equiv. of GSH (1.2 mM) was carried out in H_2O , pH adjusted to 7.2 ± 0.1 . Samples were diluted to working concentrations with double distilled water. HPLC analysis was performed and the gradient optimised in order to separate the different species. At time < 10 min, six main peaks are observed. At time 12 h, three extra peaks appeared. Freshly prepared samples were then analysed by LC-MS using the gradient previously optimised (Figure 5.15).

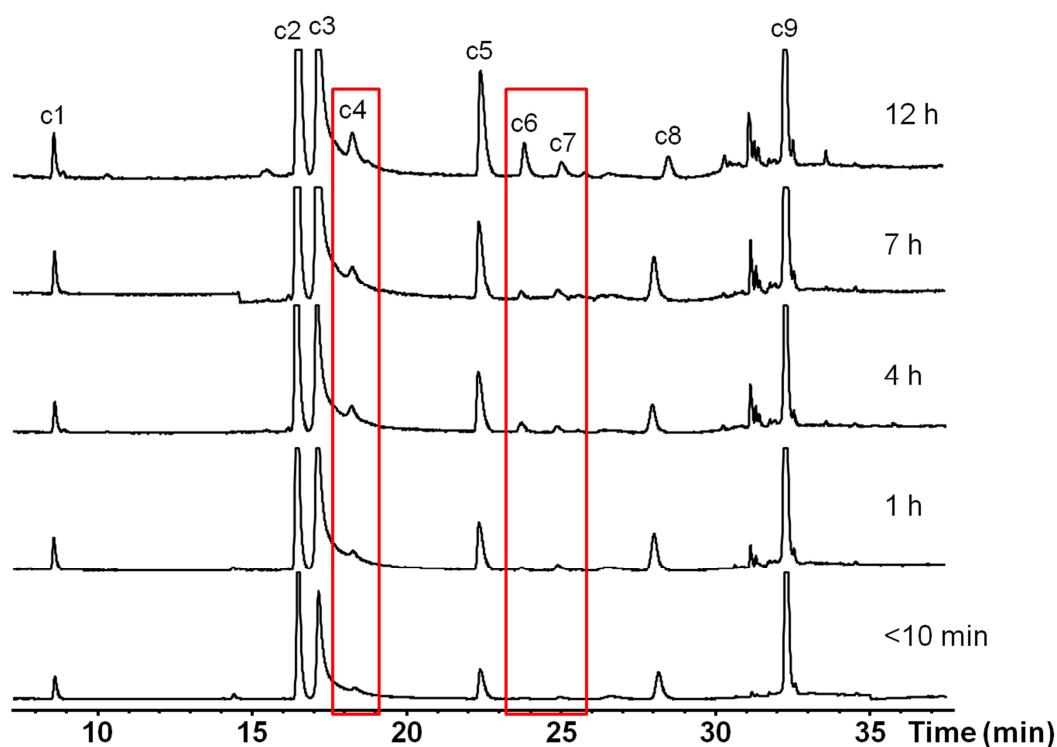


Figure 5.15. HPLC chromatogram, monitored at $\lambda = 254$ nm, for the reaction between complex **2** and 3 mol equiv. of GSH. The reaction was performed in H_2O , 310 K and pH 7.2 ± 0.1 . The sample was analysed at times <10 min, 1, 4, 7 and 12 h. See assignments in Table 5.8.

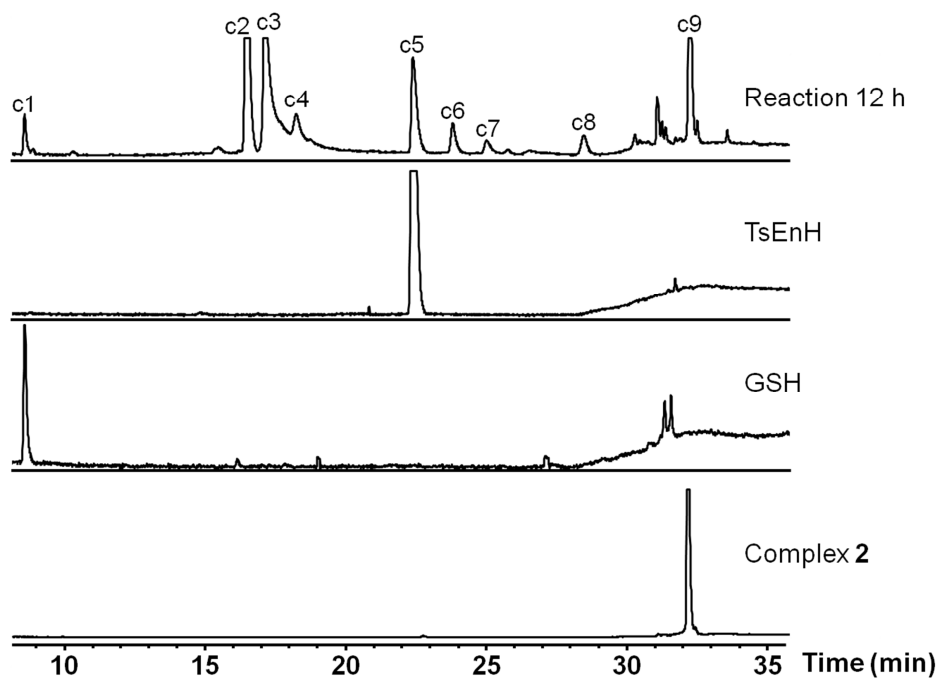


Figure 5.16. HPLC chromatogram, monitored at $\lambda = 254$ nm, of complex **2**, GSH, free ligand (TsEnH) and the reaction mixture after incubating complex **2** with 3 mol equiv. GSH for 12 h at 310 K and pH 7.2. For assignments see Table 5.8.

Table 5.8. Assignment of the species detected by the LC-MS from the reaction of complex [(*p*-cym)Ru(TsEn)Cl] (**2**) and GSH (ratio 1:3, respectively). The reaction was performed in H₂O, at 310 K and pH 7.2 ± 0.1. The wavelength of detection was λ = 254 nm (see Figure 5.15). The red boxes show the peaks that grow over time.

Peak	Retention time (min)	Observed m/z	Assignment Calc. m/z
c1^a	8.6	613.0	GSSG + 3 H ⁺ m/z = 613.2
		308.0	GSH + 2 H ⁺ m/z = 308.1
c2	16.5	693-694 ^b	[((<i>p</i> -cym) ₂ Ru ₂ (μ-GS) ₃)+4H ⁺ m/z = 695.6
c3	17.1	542.0	{(<i>p</i> -cym)Ru(GS)}+H ⁺ m/z = 542.1
c4	18.3	846-849 ^b	{(<i>p</i> -cym)Ru(GS) ₂ }+3H ⁺ m/z = 849.2
c5^a	22.4	215.4	[TsEnH] + H ⁺ m/z = 215.1
c6	23.8	475.3	Unknown
c7	25.0	475.3	Unknown
c8	28.5	475.3	Unknown
c9^a	32.2	449.0	[M-Cl] ⁺ m/z = 449.1

^a peaks assigned by comparison with the controls. GSH, free ligand TsEnH and complex **2**. ^b The resolution is too low and the peak is not clear.

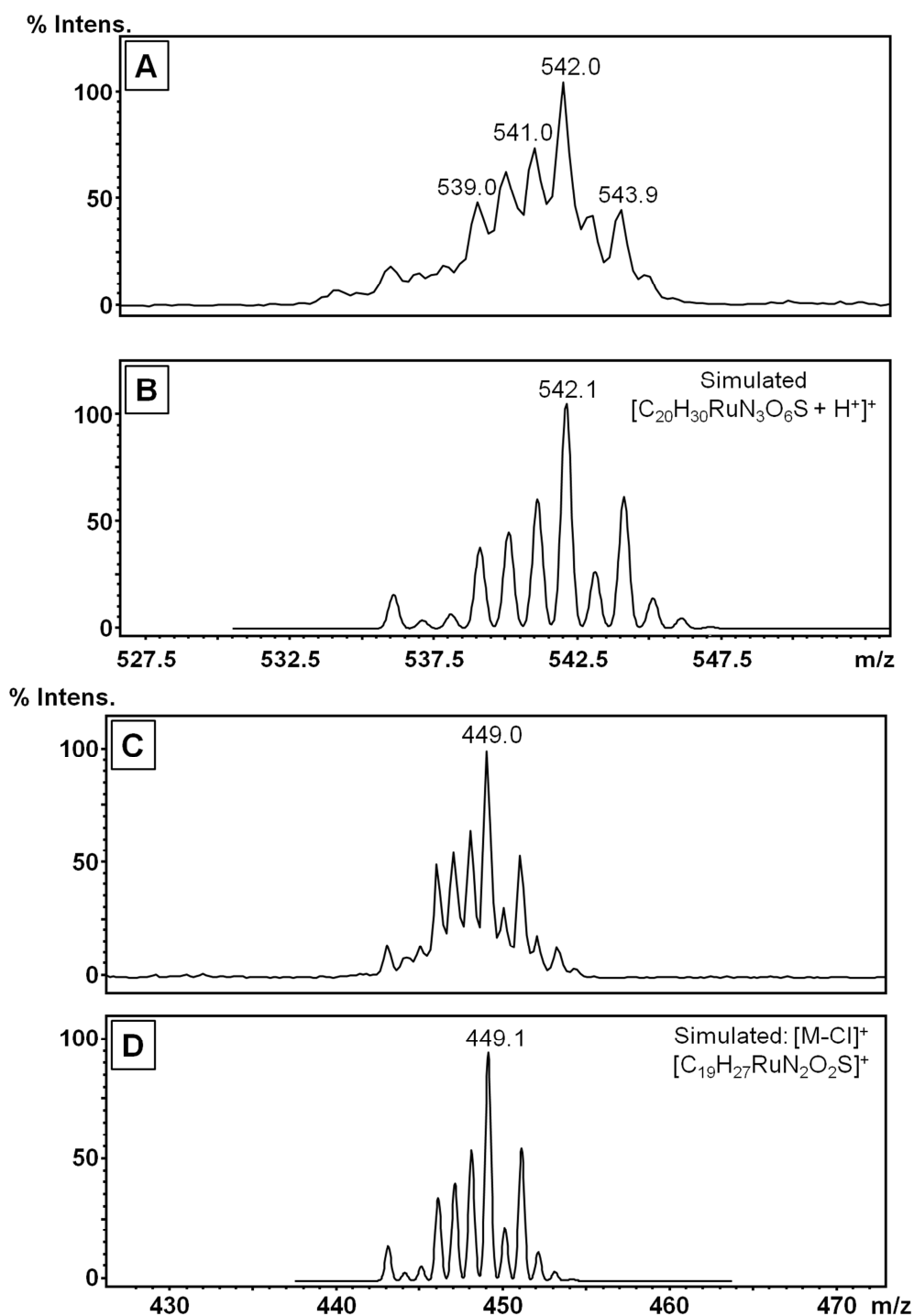


Figure 5.17. Mass spectra of the species (A) c3 ($m/z = 542.1$) and (C) c9 ($m/z = 449.1$) detected at time = 12 h from the reaction of complex $[(p\text{-cym})Ru(TsEn)Cl]$ (**2**) and GSH (ratio 1:3, respectively). The reaction was performed in H_2O at 310 K and $pH\ 7.2 \pm 0.1$. The species are assigned to $\{[(p\text{-cym})Ru(GS)]\} + H^+$ and $[(p\text{-cym})Ru(TsEn)]^+$, respectively. Simulated spectra (B) and (D) are shown under the experimental data.

In order to obtain better resolution in the mass spectra for the peaks c2 and c4, and be able to assign the main product, LC-HRMS was performed. For this experiment, complex **2** and 3 mol equiv. of GSH were incubated at 310 K and pH 7.2 ± 0.1 for 12 h. The column used was an Agilent Eclipse plus C18 (1.8 μm 2.1 x 100 mm), shorter than that used in the previous experiments. The retention time was now halved and some peaks overlapped with each other.

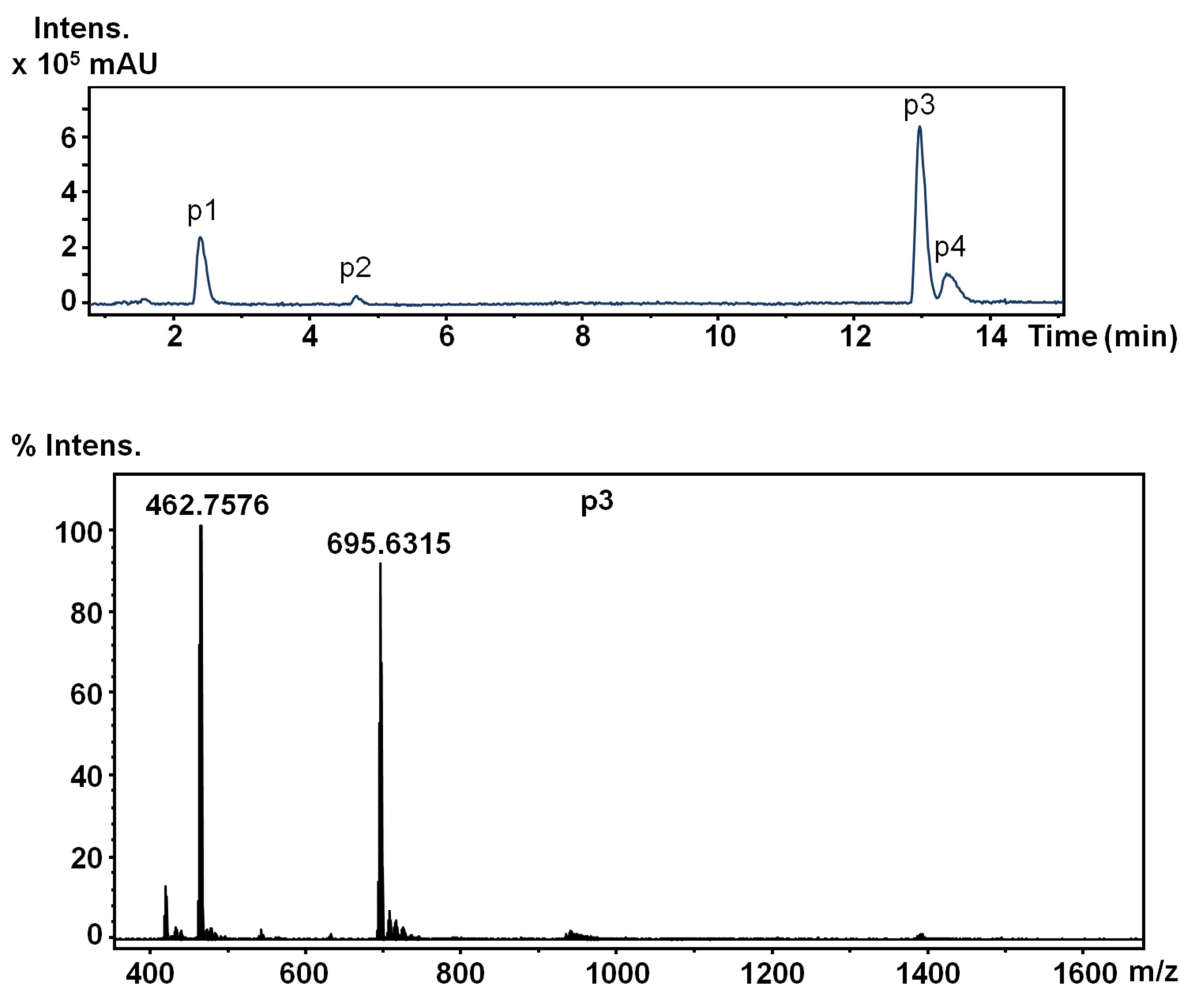


Figure 5.18. (A) HPLC chromatogram at $\lambda = 210$ nm and (B) high resolution mass spectra of the reaction between complex **2** and GSH. The experiment was carried out in H₂O, 310 K and pH 7.2 ± 0.1 and LC-HRMS recorded in a Dionex Ultimate 3000 with a VWD detector coupled to a Bruker MaXis UHR-ESI-TOF mass spectrometer. See assignments in Table 5.9.

Table 5.9. Assignment of the peaks in the chromatogram obtained from LC-HRMS for the reaction of complex **2** and 3 mol equiv. of GSH in H₂O, 310K and pH 7.2 ± 0.1. For chromatogram see Figure 5.18.

Peak	Retention time (min)	Observed m/z	Assignment Calc. m/z
p1	2.4	308.0897	GSH m/z = 308.0911
p2	4.7	613.1586	GSSG m/z = 613.1519
p3	12.9	695.6315	$[(p\text{-cym})_2\text{Ru}_2(\mu\text{-GS})_3]^{2-} + 4\text{H}^+$ m/z = 695.6322
		464.0904	$[(p\text{-cym})_2\text{Ru}_2(\mu\text{-GS})_3]^{2-} + 5\text{H}^+$ m/z = 464.0905
p4	13.3	215.0845	$[\text{TsEnH}] + \text{H}^+$ m/z = 215.0849

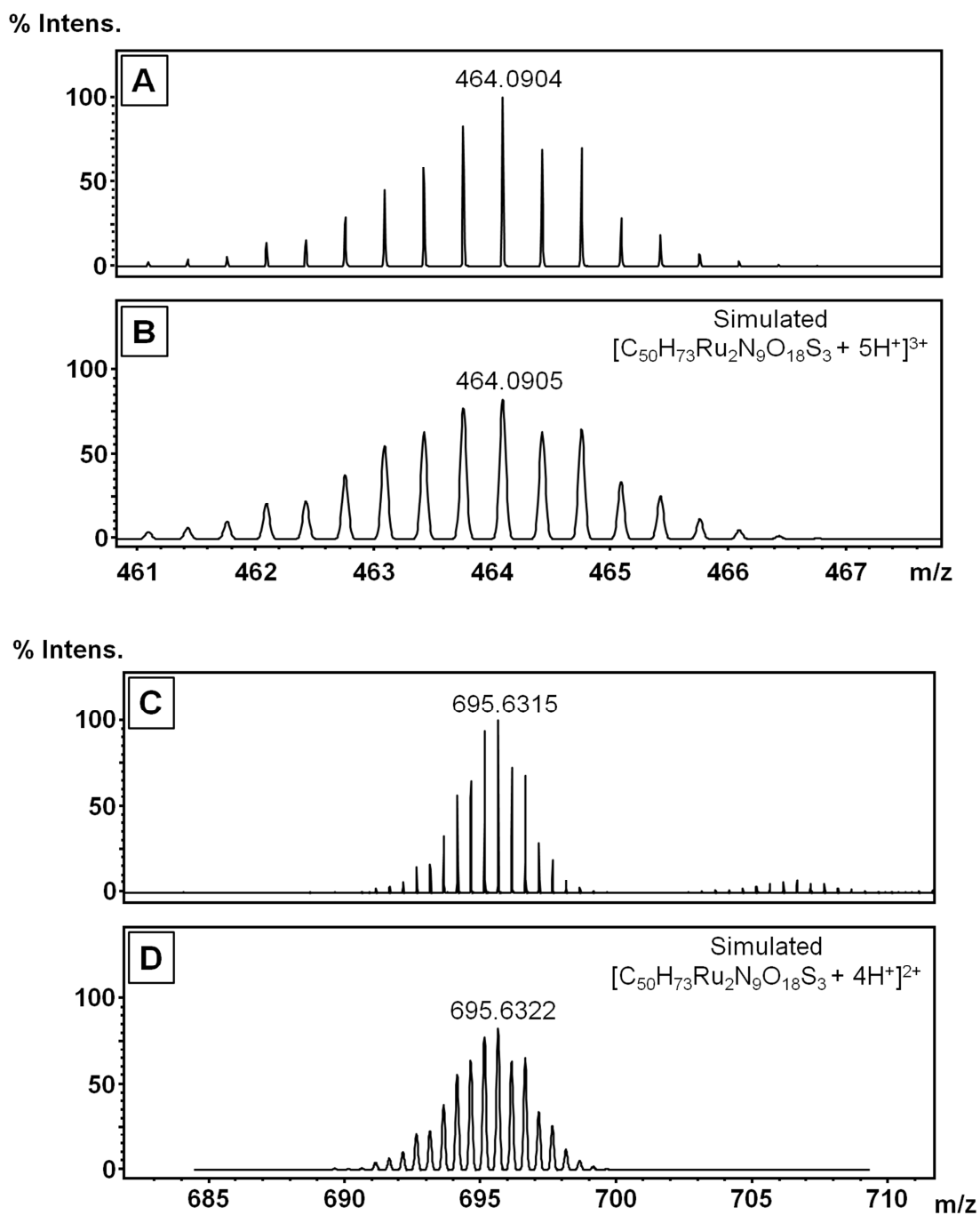


Figure 5.19. High resolution mass spectra, recorded on a Bruker MaXis UHR-ESI-TOF mass spectrometer, of the product p3 from the reaction between complex **2** and GSH in H₂O, 310 K and pH 7.2 ± 0.1 (see Figure 5.18). The peaks are assigned to (A) $[(p\text{-cym})_2Ru_2(\mu\text{-GS})_3] + 4H^+)^{2+}$ and (C) $[(p\text{-cym})_2Ru_2(\mu\text{-GS})_3] + 5H^+)^{3+}$. Simulated spectra (B) and (D) are shown under the experimental data.

5.2.4. Discussion

Many platinum drugs such as cisplatin and carboplatin react with GSH to form GS-Pt adducts which are excreted from the cell.³ Other metallodrugs containing gold(I), bismuth(III), tellurium(IV) or rhenium(V) also display a high affinity for nucleophilic S such as cysteine.⁴² In particular, ruthenium complexes have been shown to react with cysteine-containing proteins and peptides readily. RAPTA complexes, for example, have been shown to potentially inhibit glutathione-S-transferase by binding to the cysteine in the active center,⁴³ as well as other cysteine-containing proteins,^{42, 44} or peptides like glutathione.⁴⁵ Other ruthenium complexes such as KP1019 are known to react with biological reductants such as glutathione. $[(\eta^6\text{-arene})\text{Ru}(\text{azpy})\text{I}]^+$ (azpy = *N,N*-dimethylphenyl- or hydroxyphenyl-azopyridine) complexes undergo activation by ligand reduction and appears to act as a catalyst to oxidise GSH.^{35, 46} $[(p\text{-cym})\text{RuCl}(o\text{-pda})]^+$ (*o*-pda = *o*-phenylenediamine) undergoes ligand-based oxidation and hydrolysis. Interestingly, glutathione can reduce the complex which is oxidized readily by oxygen.⁴⁷ $[(p\text{-cym})\text{Ru}(\text{en})\text{Cl}]^+$ have been shown to bind to serum Cys34 of albumin and induce oxidation.¹³ Other ethylenediamine ruthenium derivatives have been shown to oxidize glutathione to its sulfenato analogue then bind to DNA.¹⁵ Glutathione has also been shown to facilitate binding to N7 guanine in DNA for $[(\eta^6\text{-arene})\text{Ru}(\text{en})\text{Cl}]^+$ complexes after binding to the complex and being oxidised.¹⁶ In this section, the interaction of glutathione with complex **2** was studied.

A first set of experiments using complex **2** and a large excess of GSH was followed by ¹H-NMR. All the spectral changes occurred within the first 10 min. A new peak (multiplet) at 3.15 ppm which was identified as a new signal for the protons from cysteine (CH₂) of bound glutathione (GS⁻). The resonances for the non-cysteine protons of bound GSH overlap with those from free GSH. The reaction between complex **2** and different concentrations of GSH

was followed by ^1H NMR to be able to assign all the peaks of bound GSH when all GSH has reacted (Figure 5.13).

Release of the TsEn ligand is evident from comparison of the ^1H -NMR spectrum of the free ligand with that of the reaction mixture (Figure 5.13 and Figure 5.15).

The peaks corresponding to the *p*-cym arene split into two different sets. Both *p*-cym types are bound to the ruthenium centre as can be seen by the chemical shift (5-6 ppm). Integration of the *p*-cym peaks and the new peak corresponding to the cysteine of the GSH adduct, gives a ratio 1:3.5 *p*-cym:GSH.

Based on the NMR data, the complex undergoes ligand substitution, losing the TsEnH ligand, to form two different species containing GSH, however more analysis is needed to elucidate their nature.

The reaction between complex **2** and GSH (ratio 1:3, pH 7.2 ± 0.1 , 310 K) was analyzed by HPLC and LC-MS. HPLC chromatograms were recorded at times < 10 min, 1, 4, 7 and 12 h. Six main peaks were observed at < 10 min (Figure 5.15). At times 1, 4, 7 and 12 h, three additional peaks appeared and increased in intensity (Figure 5.15).

The analysis of the chromatogram recorded at < 10 min indicates that the Ru(II) complex undergoes ligand substitution in the presence of GSH. A peak corresponding to the TsEnH ligand was observed with a retention time of 22.4 min. Mono-GSH adduct $\{(p\text{-cym})\text{Ru}(\text{GS})\}$ (peak at 17.2 min, $m/z = 542$) and a di-GS dimer $[\{(p\text{-cym})\text{Ru}\}_2(\mu\text{-GS})_3]^{2-}$ (peak at 16.5 min, $m/z = 695.6$) are formed. (Figure 5.15, Figure 5.17, Table 5.8). The exact mass of the peak at 16.5 min (m/z 695.6322) was obtained by high resolution analysis in LC-HRMS. The peak at 28.5 min could not be identified, however, the isotopic pattern shows that it does not contain ruthenium. (Figure 5.18, Figure 5.19, Table 5.9)

The analysis of the chromatogram recorded at time 12 h suggest that $[(p\text{-cym})\text{Ru}]_2(\mu\text{-GS})_2(\text{GS})_2]^{4-}$ might be formed, slowly, over time (peak at 18.3 min, $[(p\text{-cym})\text{Ru}]_2(\mu\text{-GS})_2(\text{GS})_2] + 5\text{H}^+$ $m/z = 849.2$). However, the resolution of the mass spectrum was too poor for confirmation. Two new unidentified peaks which do not contain ruthenium appeared at 23.8 and 25.0 min.(Figure 5.15, Figure 5.17, Table 5.8)

These results are significantly different from those obtained with the analogous ethylenediamine complexes $[(\eta^6\text{-arene})\text{Ru}(\text{en})\text{Cl}]^+$ at pH 7. Complex $[(\text{bip})\text{Ru}(\text{en})\text{Cl}]^+$ (**RM175**) has been shown to react readily with GSH to form the GSH adduct $[(\text{bip})\text{Ru}(\text{en})(\text{GS})]$ which later is converted to $[(\text{bip})\text{Ru}(\text{en})(\text{GS}(\text{O}))]$ by oxidation of the bound GSH in the presence of oxygen. The sulfenato complex can then react with DNA. When the reaction is performed under inert atmosphere, the oxidation of the GS^- does not occur, however the GS^- adduct is still the main product.¹⁵

Instead, the reaction of complex **2** with GSH resembles more that of complex **RM175** when at pH 3. In such a case, the formation of $\{(\text{bip})\text{Ru}(\text{GS})\}$ and the Ru(II) dimer $[(\text{bip})\text{Ru}]_2(\mu\text{-GS})_3]^{2-}$ are observed. However, in contrast with the reaction between **RM175** and GSH, no oxidation of the GS^- in $\{(p\text{-cym})\text{Ru}(\text{GS})\}$ to the sulfenato adduct $[(p\text{-cym})\text{Ru}(\text{GS}(\text{O}))]$ were observed over a period of 12 h using complex **2**^{15, 48}

Based on the analysis by ^1H NMR and LC-MS, the reaction of GSH with complex **2** at 310 K and pH 7.2 ± 0.1 leads to the formation of $\{(p\text{-cym})\text{Ru}(\text{GS})\}$ and a Ru(II) dimer with three GS^- bound through a sulfur bridge $[(p\text{-cym})\text{Ru}]_2(\mu\text{-GS})_3]^{2-}$. $\{(p\text{-cym})\text{Ru}(\text{GS})\}$ could arise from fragmentation of a ruthenium dimer containing only two GS^- $[(p\text{-cym})\text{Ru}]_2(\mu\text{-GS})_2\text{Cl}_2]^{2-}$.

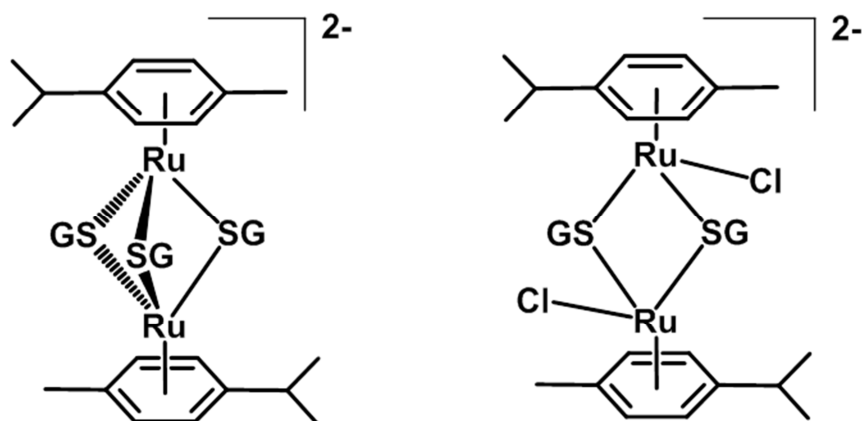


Figure 5.20. Proposed structures for the products from reaction of complex **2** with GSH

Recently, Süß-Fink *et al.* has reported the synthesis and biological activity of a series of ruthenium dimers containing two or three thiolato bridges. It was shown that complexes of the type $[(p\text{-cym})\text{Ru}]_2(\mu\text{-SR})_3^+$ ($\text{SR} = \text{SPh}$, $\text{SC}_6\text{H}_4\text{-}p\text{-tBu}$, $\text{SC}_6\text{H}_4\text{-}p\text{-CH}_3$) are highly cytotoxic toward human ovarian cancer cells, with IC_{50} values in the nanomolar range, among the most active arene ruthenium complexes evaluated.⁴⁹⁻⁵¹ The neutral ruthenium dimers of the type $[(p\text{-cym})\text{Ru}]_2(\mu\text{-SR})_2\text{Cl}_2$ ($\text{R} = \text{CH}_2\text{Ph}$, $\text{CH}_2\text{C}_6\text{H}_4\text{-}p\text{-tBu}$) were found to be less cytotoxic than $[(p\text{-cym})\text{Ru}]_2(\mu\text{-SR})_3^+$.⁵² These ruthenium dimers containing three thiolato bridges have been shown to catalyse the oxidation of GSH to GSSG, but such redox reactions does not seem to be involved in the mechanism of action since the Rh(III) and Ir(III) Cp* analogues show similar IC_{50} values but do not show any catalytic activity.⁵³

Complex $[(p\text{-cym})\text{Ru}]_2(\mu\text{-GS})_3^{2-}$, generated *in situ* through the reaction of complex **2** with GSH, has a similar structure and characteristics as those described by Süß-Fink *et al.*,⁵⁴ suggesting that this complex could display some antiproliferative activity.

5.2.5. Conclusions

The reaction of complex [(*p*-cym)Ru(TsEn)Cl] (**2**) with GSH at pH 7.2 ± 0.1 and 310 K was studied in this section. ^1H NMR data show the formation of 2 different *p*-cym containing molecules, and the release of the TsEn ligand (TsEnH). LC-MS data, also shows the formation of TsEnH, in addition to two main Ru(II) products, $[[(\textit{p}\text{-cym})\text{Ru}]_2(\mu\text{-GS})_3]^{2-}$ and $\{(\textit{p}\text{-cym})\text{Ru}(\text{GS})\}$. No further spectral changes were observed by ^1H NMR after the initial spectrum was recorded. However, the formation of a third Ru(II) species was observed by LC-MS over a period of 12 hours, but it could not be identified due to the low resolution of the mass spectrum. The reaction of complex **2** with GSH resembles that of **RM175**, $[(\text{bip})\text{Ru}(\text{en})\text{Cl}]^+$, when at pH 3.^{15, 48}. Interestingly, the formation of $[[(\textit{p}\text{-cym})\text{Ru}]_2(\mu\text{-GS})_3]^{2-}$ was now achieved under biological relevant conditions suggesting that the ligand TsEn is more labile than *ethylenediamine* (en).

Recently, Süß-Fink *et. al.* reported a series of complexes of the type $[[(\textit{p}\text{-cym})\text{Ru}]_2(\mu\text{-SX})_3]^+$ (SX = sulphur containing molecule) which display very high antiproliferative activities (0.12 - 1.7 μM).^{53, 54} $[[(\textit{p}\text{-cym})\text{Ru}]_2(\mu\text{-GS})_3]^{2-}$, products of the reaction between GSH and complex **2**, show similar structure to that described by Süß-Fink, and therefore, it is possible such dimers play an important role in the low IC_{50} of complex **2** ($13.6 \pm 0.6 \mu\text{M}$).

5.3. References

- (1) Rosenberg, B.; Van Camp, L.; Trosko, J. E.; Mansour, V. H. *Nature* **1969**, *222*, 385-386.
- (2) Rosenberg, B.; Van Camp, L.; Krigas, T. *Nature* **1965**, *205*, 698-699.
- (3) Shen, D.-W.; Pouliot, L. M.; Hall, M. D.; Gottesman, M. M. *Pharmacol. Rev.* **2012**, *64*, 706-721.
- (4) Sancho-Martínez, S. M.; Prieto-García, L.; Prieto, M.; López-Novoa, J. M.; López-Hernández, F. J. *Pharmacol. Ther.* **2012**, *136*, 35-55.
- (5) Boulikas, T. *Cancer Therapy* **2007**, *5*, 351-376.
- (6) Todd, R. C.; Lippard, S. J. *Metallomics* **2009**, *1*, 280-291.
- (7) Kelland, L. *Nature Rev. Cancer* **2007**, *7*, 573-584.
- (8) Zhu, G.; Song, L.; Lippard, S. J. *Cancer Res.* **2013**, *73*, 4451-4460.
- (9) Geldmacher, Y.; Oleszak, M.; Sheldrick, W. S. *Inorg. Chim. Acta.* **2012**, *393*, 84-102.
- (10) Pizarro, A. M.; Sadler, P. J. *Biochimie* **2009**, *91*, 1198-211.
- (11) García-Ramos, J. C.; Galindo-Murillo, R.; Cortés-Guzmán, F.; Ruiz-Azuara, L. *J. Mex. Chem. Soc.* **2013**, *57*, 245-259.
- (12) Chen, H.; Parkinson, J. A.; Morris, R. E.; Sadler, P. J. *J. Am. Chem. Soc.* **2003**, 173-186.
- (13) Chen, H.; Parkinson, J. A.; Parsons, S.; Coxall, R. A.; Gould, R. O.; Sadler, P. J. *J. Am. Chem. Soc.* **2002**, *124*, 3064-3082.
- (14) Habtemariam, A.; Melchart, M.; Fernandez, R.; Parsons, S.; Oswald, I. D. H.; Parkin, A.; Fabbiani, F. P.; Davidson, J. E.; Dawson, A.; Aird, R. E.; Jodrell, D. I.; Sadler, P. J. *J. Med. Chem.* **2006**, *49*, 6858-6868.
- (15) Wang, F.; Xu, J.; Habtemariam, A.; Sadler, P. J. *J. Am. Chem. Soc.* **2005**, *127*, 17734-17743.
- (16) Wang, F.; Xu, J.; Wu, K.; Weidt, S. K.; Mackay, C. L.; Langridge-Smith, P. R. R.; Sadler, P. J. *Dalton Trans.* **2013**, *42*, 3188-3195.

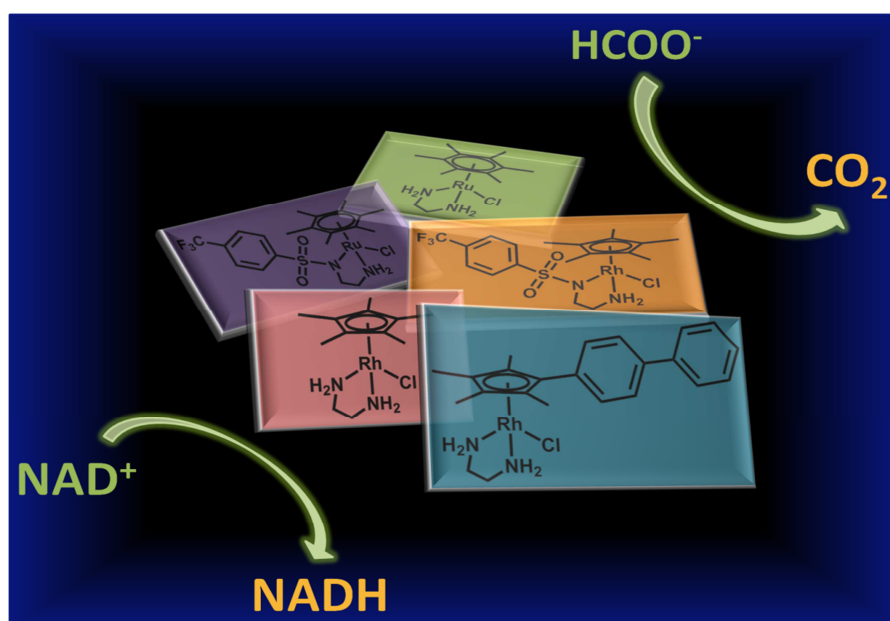
- (17) Bugarcic, T.; Nováková, O.; Halámiková, A.; Zerzánková, L.; Vrána, O.; Kaspárková, J.; Habtemariam, A.; Parsons, S.; Sadler, P. J.; Brabec, V. *J. Med. Chem.* **2008**, *51*, 5310-9.
- (18) Aird, R. E.; Cummings, J.; Ritchie, A. A.; Muir, M.; Morris, R. E.; Chen, H.; Sadler, P. J.; Jodrell, D. I. *Brit. J. Cancer* **2002**, *86*, 1652 - 1657.
- (19) Wang, F.; Chen, H.; Parsons, S.; Oswald, I. D. H.; Davidson, J. E.; Sadler, P. J. *Chem. Eur. J.* **2003**, *9*.
- (20) Melchart, M.; Habtemariam, A.; Parsons, S.; Sadler, P. J. *J. Inorg. Biochem* **2007**, *101*, 1903-1912.
- (21) Peacock, A. F. A.; Melchart, M.; Deeth, R. J.; Habtemariam, A.; Parsons, S.; Sadler, P. J. *Chem. Eur. J.* **2007**, *13*, 2601 - 2613.
- (22) Novakova, O.; Chen, H.; Vrana, O.; Rodger, A.; Sadler, P. J.; Brabec, V. *Biochemistry* **2003**, *42*, 11544-11554.
- (23) Nazarov, A. A.; Hartinger, C. G.; Dyson, P. J. *J. Organomet. Chem.* **2014**, *751*, 251-260.
- (24) Ang, W. H.; Casini, A.; Sava, G.; Dyson, P. J. *J. Organomet. Chem.* **2011**, *696*, 989-998.
- (25) Gasser, G.; Ott, I.; Metzler-Nolte, N. *J. Med. Chem.* **2010**, *54*, 3-25.
- (26) Fernandez, R.; Melchart, M.; Habtemariam, A.; Parsons, S.; Sadler, P. J. *Chem. Eur. J.* **2004**, *10*, 5173 - 5179.
- (27) Peacock, A. F. A.; Habtemariam, A.; Moggach, S. A.; Prescimone, A.; Parsons, S.; Sadler, P. J. *Inorg. Chem.* **2007**, *46*, 4049-4059.
- (28) van Rijt, S. H.; Peacock, A. F. A.; Johnstone, R. D. L.; Parsons, S.; Sadler, P. J. *Inorg. Chem.* **2009**, *48*, 1753-62.
- (29) Peacock, A. F. A.; Habtemariam, A.; Fernández, R.; Walland, V.; Fabbiani, F. P. A.; Parsons, S.; Aird, R. E.; Duncan, I.; Sadler, P. J. *J. Am. Chem. Soc.* **2006**, *128*, 1739-1748.
- (30) Melchart, M.; Habtemariam, A.; Parsons, S.; Moggach, S. A.; Sadler, P. J. *Inorg. Chim. Acta.* **2006**, *359*, 3020-3028.

- (31) Liu, H.-K.; Berners-Price, S. J.; Wang, F.; Parkinson, J. A.; Xu, J.; Bella, J.; Sadler, P. J. *Angew. Chem. Int. Ed.* **2006**, *45*, 8153-8156.
- (32) Kampf, G.; Kapinos, L. E.; Griesser, R.; Sigel, H. *J. Chem.Soc., Perkin Trans.* **2002**, *2*, 1320-1327.
- (33) Liu, H.-K.; Sadler, P. J. *Acc. Chem. Res.* **2011**, *44*, 349-359.
- (34) Kelly, J. M.; Tossi, A. B.; McConnell, D. J.; OhUigin, C. *Nucleic Acids Res.* **1985**, *13*, 6017-6034.
- (35) Pizarro, A.; Habtemariam, A.; Sadler, P. In *Medicinal Organometallic Chemistry*; ed.; Springer Berlin Heidelberg: **2010**; 21-56.
- (36) Dafforn, T.; Norden, B.; Rodger, A. *Linear Dichroism and Circular Dichroism*; 1st edition ed.; The Royal Society of Chemistry: Cambridge, UK, **2011**.
- (37) Novakova, O.; Kasparikova, J.; Bursova, V.; Hofr, C.; Vojtiskova, M.; Chen, H.; Sadler, P. J.; Brabec, V. *Chem. Biol.* **2005**, *12*, 121-129.
- (38) Lushchak, V. I. *J. amino acids* **2012**, *2012*, 1-26.
- (39) Franco, R.; Cidlowski, J. A. *Cell Death Differ.* **2009**, *16*, 1303-1314.
- (40) Chen, H. H. W.; Kuo, M. T. *Met. Based. Drugs* **2010**, 1-7.
- (41) Abdalla, M. Y. *Jordan J. Biol. Sci.* **2011**, *4*, 119-124.
- (42) Fricker, S. P. *Metallomics* **2010**, *2*, 366-377.
- (43) Ang, W. H.; De Luca, A.; Chapuis-Bernasconi, C.; Juillerat-Jeanneret, L.; Lo Bello, M.; Dyson, P. J. *ChemMedChem* **2007**, *2*, 1799-1806.
- (44) Casini, A.; Hartinger, C. G.; Nazarov, A. A.; Dyson, P. In *Medicinal Organometallic Chemistry*; 1st ed.; Springer Berlin Heidelberg, **2010**; 57-80.
- (45) Hartinger, C. G.; Casini, A.; Duhot, C.; Tsybin, Y. O.; Messori, L.; Dyson, P. J. *J. inorg. Biochem.* **2008**, *102*, 2136-2141.

- (46) Dougan, S. J.; Habtemariam, A.; McHale, S. E.; Parsons, S.; Sadler, P. J. *Proc. Natl. Acad. Sci. U. S. A.* **2008**, *105*, 11628-33.
- (47) Bugarcic, T.; Habtemariam, A.; Deeth, R. J.; Fabbiani, F. P. A.; Parsons, S.; Sadler, P. J. *Inorg. Chem* **2009**, *48*, 9444-9453.
- (48) Wang, F.; Weidt, S.; Xu, J.; Mackay, C. L.; Langridge-Smith, P. R.; Sadler, P. J. *Am. Soc. Mass. Spectrom.* **2008**, *19*, 544-549.
- (49) Chérioux, F.; Therrien, B.; Süß-Fink, G. *Inorg. Chim. Acta.* **2004**, *357*, 834-838.
- (50) Giannini, F.; Furrer, J.; Ibao, A.-F.; Süß-Fink, G.; Therrien, B.; Zava, O.; Baquie, M.; Dyson, P.; Štěpnička, P. *J. Biol. Inorg. Chem.* **2012**, *17*, 951-960.
- (51) Giannini, F.; Paul, L. E. H.; Furrer, J.; Therrien, B.; Süß-Fink, G. *New. J. Chem* **2013**, *32*, 3503-3511.
- (52) Ibao, A.-F.; Gras, M.; Therrien, B.; Süß-Fink, G.; Zava, O.; Dyson, P. J. *Eur. J. Inorg. Chem.* **2012**, *2012*, 1531-1535.
- (53) Gupta, G.; Garci, A.; Murray, B. S.; Dyson, P. J.; Fabre, G.; Trouillas, P.; Giannini, F.; Furrer, J.; Süß-Fink, G.; Therrien, B. *Dalton Trans.* **2013**, *42*, 1547-15463.
- (54) Dyson, P. J.; Gras, M.; Ibao, A. F.; Süß-Fink, G.; Therrien, B.; Zava, O. Medicaments based on dinuclear arene ruthenium complexes comprising bridging thiolato, selenolato or alkoxo ligands. Patent N. US20130172408 A1, Jul 4., **2013**.

Chapter 6

Rhodium(III) half-sandwich complexes for the catalytic reduction of NAD^+



6. Rhodium(III) half-sandwich complexes for the catalytic reduction of NAD⁺

6.1. Introduction

Ruthenium(II) catalysts of the type $[(\eta^6\text{-arene})\text{Ru}(\text{XEn})\text{Cl}]$ where XEn = *N*-(2-aminoethyl)-4-Nitrobenzenesulfonamide (NbEn), *N*-(2-aminoethyl)-4-(trifluoromethyl)benzenesulfonamide (TfEn), *N*-(2-aminoethyl)-4-toluenesulfonamide (TsEn), or *N*-(2-aminoethyl)methylenesulfonamide (MsEn), and $\eta^6\text{-arene}$ = *p*-cymene, biphenyl, hexamethylbenzene or benzene have been studied in Chapter 3 for the transfer hydrogenation reactions of NAD⁺ using sodium formate as a hydride source to obtain 1,4-NADH. The biological use of those complexes was also investigated, showing that the complex can affect the ratio of NAD⁺ to NADH in a catalytic manner. This chapter will attempt to improve the catalytic activity of those complexes by changing the Ru(II) metal centre to Rh(III).

In the field of transfer hydrogenation, half-sandwich Ru(II), Rh(III) and Ir(III) catalysts have been very successful.¹⁻⁴ Within those, ruthenium complexes hold a prominent position partly explained by the tendency of the catalysts to be less reactive than rhodium or iridium, in many cases allowing higher regio- and chemo-selectivity. On the other hand, Rh-based catalysts have also been intensively studied,^{5,6,7,8} showing in many cases increased activities, yet, the high activity might correlate with a loss of chemo- and enantio-selectivity in some cases. Nevertheless, ultimately, their catalytic activity and enantio-selectivity depend on the choice of appropriate chiral ligands, the substrate, the hydride donor and the conditions of the reaction.^{6, 9-17}

The Rh(III)-based analogues of Noyori's type catalysts $[(Cp^*)Rh(TsDPEN)Cl]$ (where TsDPEN = (1*S*,2*S*)-*N*-(*p*-toluensulfonyl)-1,2-diphenylethylenediamine) have been reported to reduce imines with higher activity and enantio-selectivity than the ruthenium analogues.^{14,18} In contrast, the catalytic activities of those complexes towards simple ketones have been shown to be lower than for Ru(II) complexes.¹⁹ On the other hand, better activity and enantio-selectivity was shown when reducing chlorinated ketones with the Rh(III) catalysts in comparison with the Ru(II) analogues.^{1,6,14} Interestingly, the use of $[(Cp^*)Rh(TsDPEN)Cl]$ gave rise to higher catalytic activities with good enantio-selectivity for the reduction of a wide range of ketones compared with the ruthenium analogues when used in aqueous media.^{1,20}

For the catalytic regeneration of NADH a library of Rh(III) complexes of the type $[(Cp^*)Rh(N,N')Cl]^+$, where *N,N'* is phenantroline, bipyridyne and derivatives, has been synthesized by Stekhan and Štrěpnička (Table 6.1).²¹⁻²⁴ Those complexes were mainly synthesized in order to regenerate the cofactor NADH necessary for the enzymatic reduction of alcohols. Rh(III) complexes have shown, in general, higher turnover frequencies compared with their Ru(II) analogues and other ruthenium complexes (*ca.* 0.0053 to 10 h⁻¹).²¹⁻²³ The results in the literature show that higher activities can be achieved by using Rh(III) instead of Ru(II) complexes.

Table 6.1. Turnover frequencies of some of the Rh(III) catalysts synthesized by Stekhan and Štrěpnička. (a) 5 M sodium formate, 0.38 mM NAD⁺, 0.025 mM complex, temp. 311 K, phosphate buffer pH 7. (b), 350 mM sodium formate, 8 mM NAD⁺, 0.008 mM complex, temp. 340 K, phosphate buffer pH 7. ²¹⁻²⁴

Compound	TOF (h ⁻¹)
[(Cp*)Rh(bipy)Cl] ⁺	77.5 ^a
[(Cp*)Rh(phen)Cl] ⁺	70.9 ^a
[(Cp*)Rh(4,4'-dimethylbipy)Cl] ⁺	76.4 ^a
[(Cp*)Rh(bipy)Cl] ⁺	875 ^b
[(Cp*)Rh(phen)Cl] ⁺	2000 ^b
[(Cp*)Rh(nitrophen)Cl] ⁺	1740 ^b

In this chapter, the synthesis of a series of organometallic rhodium (III) complexes of the type [(Cp^x)Rh(*N,N'*)Cl] is described, where Cp^x = pentamethylcyclopentadienyl (Cp*), 1-phenyl-2,3,4,5-tetramethylcyclopentadienyl (Cp^xPh) or 1-biphenyl-2,3,4,5-tetramethylcyclopentadienyl (Cp^xPhPh), and *N,N'* = ethylenediamine (en) or *N*-(2-aminoethyl)-4-(trifluoromethyl)benzenesulfonamide (TfEn) as bidentate ligands. The turnover frequencies for the reduction of NAD⁺ under biological relevant conditions and using sodium formate as a hydride source were determined. The catalytic cycle was investigated and compared with their Ru(II) analogues and the [(Cp*)Rh(bipy)Cl] complex reported previously by Fish *et al.*²⁵⁻²⁹

6.2. Experimental

6.2.1. Materials

The Rh(III)-arene precursor dimers $[(Cp^x)RhCl_2]_2$ where the Cp^x is pentamethylcyclopentenyl (Cp^*), 1-phenyl-2,3,4,5-tetramethylcyclopentenyl (Cp^xPh) or 1-biphenyl-2,3,4,5-tetramethylcyclopentenyl (Cp^xPhPh) were prepared following literature methods,³⁰ as was the ligand *N*-(2-aminoethyl)-4-(trifluoromethyl)benzenesulfonamide (TfEnH).³¹ Ethylenediamine (en) was purchased from Sigma-Aldrich and freshly distilled prior to use. Magnesium sulphate, ammonium hexafluorophosphate, silver nitrate, potassium hydroxide, sodium chloride, perchloric acid and hydrochloric acid were obtained from Fisher Scientific. DMSO-*d*₆, MeOD-*d*₄, D₂O, (CD₃)₂CO-*d*₆ and CDCl₃ for NMR spectroscopy were purchased from Sigma-Aldrich and Cambridge Isotope Labs Inc. Non-dried solvents used in syntheses were obtained from Fisher Scientific and Prolabo.

6.2.2. Synthesis and characterisation of the complexes³²

$[(Cp^*)Rh(en)Cl]PF_6$ (17). $[(Cp^*)RhCl_2]_2$ (51.3 mg, 83.0 μ mol) was placed in a round-bottom flask to which dichloromethane (50 mL) was added. Upon the addition of ethylenediamine (9.88 mg, 0.16 mmol, 11 μ l) the solution turned bright yellow. The solution was stirred under nitrogen overnight, after which the solvent was removed on the rotary evaporator to afford a light yellow powder. The crude product was redissolved in methanol and filtered. An excess of ammonium hexafluorophosphate (257.5 mg) was then added and the solution stored in the freezer. Bright yellow crystals were collected. Yield: 42.3 mg (78.3 %). ¹H NMR (400 MHz, CDCl₃): δ_H 5.91 (s, 2H), 3.05 (s, 2H), 2.88 (s, 2H), 2.74 (s, 2H), 1.90 (s, 15H). Anal: Calc for C₁₂H₂₃ClF₆N₂PRh C: 27.91, H: 4.61,

N: 6.21; Found C: 28.11, H: 4.81, N: 5.95. ESI-MS: Calc for $C_{12}H_{23}ClN_2O_2Rh$ (M)⁺ 333.0 *m/z* found 333.0 *m/z*.

[(Cp*Ph)Rh(en)Cl]PF₆ (18). Complex **18** was obtained following the method described above for complex **17** using the dimer [(Cp^xPh)RhCl₂]₂ (50.5 mg, 68.0 μmol). Recrystallisation from methanol resulted in bright yellow crystals. Yield: 31.7 mg (59.0 %). ¹H NMR (400 MHz, CDCl₃): δ_H 7.49 (m, 5H), 5.59 (s, 2H), 3.11 (s, 2H), 3.02 (s, 2H), 2.76 (s, 2H), 2.05 (s, 6H), 1.91 (s, 6H). Anal: Calc for C₁₇H₂₅ClF₆N₂PRh C: 37.76, H: 4.66, N: 5.18; Found C: 37.02, H: 4.67, N: 5.26. ESI-MS: Calc for C₁₇H₂₅ClN₂Rh (M)⁺ 395.0 *m/z* found 395.0 *m/z*.

[(Cp^xPhPh)Rh(en)Cl]PF₆ (19). Complex **19** was obtained following the method described above for complex **17** using the dimer [(Cp^xPhPh)RhCl₂]₂ (51.6 mg, 57.6 μmol). Recrystallisation from methanol resulted in bright yellow crystals. Yield: 47.7 mg (54.2 %) ¹H NMR (400 MHz, CDCl₃): δ_H 7.69 (d, 2H, J = 8.4 Hz), 7.60 (m, 4H), 5.49 (t, 2H, J = 7.5 Hz), 7.41 (t, 1H, J = 7.5), 5.59 (s, 2H), 3.14 (s, 2H), 3.03 (s, 2H), 2.79 (s, 2H), 2.07 (s, 6H), 1.97 (s, 6H). Anal: Calc for C₂₃H₂₉ClF₆N₂PRh C: 44.79, H: 4.74, N: 4.54; Found C: 43.98, H: 4.65, N: 4.54. ESI-MS: Calc for C₂₃H₂₉ClN₂Rh (M)⁺ 471.1 *m/z*, found 471.1 *m/z*.

[(Cp*)Rh(TfEn)Cl] (20). [(Cp*)RhCl₂]₂ (49.7 mg, 80.4 μmol) and *N*-(2-aminoethyl)-4-(trifluoromethyl)benzenesulfonamide (TfEnH) (53.5 mg, 19.9 mmol) were dissolved in dichloromethane (25 mL). The reaction was then stirred under nitrogen atmosphere overnight. The solution was placed in a separating funnel and washed with brine, the organic layer separated and dried over MgSO₄ and filtered. The solution was concentrated *in vacuo* and the product obtained recrystallised from methanol to afford an orange powder. Yield: 40.3 mg (46.4 %). ¹H NMR (400 MHz, CDCl₃): δ_H 8.00 (d, 2H, J = 8.1 Hz), 7.54 (d, 2H, J = 8.1 Hz), 3.19 (s, 2H), 2.60 (s, 3H), 1.71 (s, 15H). Anal: Calc for C₁₉H₂₅ClF₃N₂O₂RhS C: 42.20,

H: 4.66, N: 5.18; Found C: 41.92, H: 4.36, N: 5.01. ESI-MS: Calc. for $C_{19}H_{25}ClF_3N_2O_2RhS$ (M-Cl)⁺ 505.0 *m/z*, found 505.0 *m/z*.

6.2.3. Aqueous Solution Chemistry

Aquation of the chlorido complexes

Solutions of complexes **17-20** (1.4 mM, in D₂O) were prepared and ¹H NMR spectra recorded every 5 min for a period of 12 h. ¹H NMR spectra were recorded at 310 K on a Bruker AV III 600 spectrometer (¹H = 600 MHz) using 5 mm diameter NMR tubes. All data processing was carried out using Topspin 2.1. ¹H NMR chemical shifts were internally referenced to TMS *via* 1,4-dioxane in D₂O ($\delta = 3.75$).

An aqueous solution of the chlorido complex **17-20** (1.4 mM) was treated with silver nitrate (1 mol equiv.) and stirred overnight at room temperature. ¹H NMR spectra were recorded after filtration of the samples through Celite to remove the silver chloride salt formed.

Acidity of the Ru-H₂O bond and pK_a determination

Changes in the chemical shifts of the methyl protons of the Cp^x ligand in the aqua adducts for complexes **17-20** with the pH* (pH not corrected for deuterium) over a range from 2 to 12 were followed by ¹H NMR spectroscopy. Solutions of KOH or HClO₄ in D₂O were used to adjust the pH*. ¹H-NMR spectra were recorded at 298 K on a Bruker AV III 600 spectrometer (¹H = 600 MHz) using 5mm diameter tubes. The data were fitted to the Henderson–Hasselbalch equation using Origin 7.5.

6.2.4. Reduction of NAD⁺

Complexes **17-20** were dissolved in D₂O (1.4 mM, 4 mL) in a glass vial. Aqueous solutions of sodium formate (35 mM, 4 mL) and NAD⁺ in D₂O (7 mM, 2 mL) were also prepared and incubated at 310 K. In a typical experiment, an aliquot of 200 μL from each solution were added to a 5 mm NMR tube. (Final concentrations for complexes **17-19** = 0.44 mM, for NAD⁺ = 2.2 mM and for sodium formate = 11.02 mM; molar ratio 1:5:25). Experiments performed with complex **20** were performed at a lower concentration of NAD⁺ due to the lower catalytic activity, in that case 200 μL of the formate solution and complex solution were added to a 5 mm NMR tube containing 80 μL of NAD⁺ solution and 120 μL of D₂O (Final concentrations for complex **20** = 0.44 mM, for NAD⁺ = 0.88 mM and for sodium formate = 11.02 mM; molar ratio 1:2:25). The pH* of the solution mixture was adjusted to 7.2 ± 0.1 bringing the total volume to 0.635 mL ¹H NMR spectra were recorded at 310 K every 162 s until the completion of the reaction.

6.2.5. Mechanistic studies

A set of experiments were performed to elucidate the catalytic cycle of the complexes described above. All the experiments were performed with complex **17** (1.4 mM, D₂O).

6.2.5.1. Rate-limiting step

Reduction of NAD⁺ using complex **17** and deuterio-formate (25 mol equiv.) was followed by ¹H NMR. The procedure for the kinetic experiment is described in section 6.2.4

6.2.5.2. Dependence on NAD⁺ and formate concentrations

The turnover frequencies of the reduction reaction of NAD⁺ using complexes **17** or **20** and formate (25 mol equiv.) were calculated following the same procedure described in section 6.2.4. The reaction was studied using different concentrations of NAD⁺ (1, 2, 3, 4 and 6 mol equiv.).

A second series of experiments using different concentrations of sodium formate (2, 5, 10, 25, 50, 100, 200 and 1000 mol equiv.) and a constant concentration of NAD^+ (2 mol equiv.) was also performed.

6.2.5.3. Transfer hydrogenation reaction with 1,4-NADH as hydride source

Oxidation of 1,4-NADH (400 μL , 1.4 mM) in D_2O by complex **17-20** was studied by ^1H NMR. The pH^* of the reaction mixture was adjusted to 7.2 ± 0.1 and the experiment performed at 310 K.

6.2.5.4. pH dependence

Optimum pH range for the catalytic process was studied in a series of experiments following the same procedure described in section 6.2.4. Each experiment was performed at a different pH^* over a range from 6 to 10. The pH^* of the reaction was adjusted using deuterated aqueous solutions of KOD and DClO_4 .

6.2.6. Antiproliferative activity

The antiproliferative activity of complexes **17-20** was determined in A2780 ovarian cancer cell lines. IC_{50} values were calculated following the procedure described in Chapter 2. SRB assay was used to determine cell viability. IC_{50} values were determined as duplicates of triplicates in two independent set of experiments.

Cell viability assays with complexes **17-20** in combination with sodium formate were carried out in A2780 ovarian cancer cells. These experiments were carried out as described in Chapter 2 with the following modifications: a fixed concentration of each Rh(III) complex equal to 150 μM was used with co-administration of three different concentrations of sodium formate (0.5, 1 and 2 mM).

6.3. Results

6.3.1. Synthesis and characterization

Rh(III) complexes **17-20** were synthesised (Figure 6.1) using a similar procedure. Typically, the ligand (2 - 2.5 mol equiv.), was added to a dichloromethane solution of the rhodium dimer, $[(Cp^x)RhCl_2]_2$ and the reaction mixture stirred under an N_2 atmosphere. The details for individual reactions are described in the experimental section. All the synthesized complexes were characterized by elemental analysis (CHN), mass spectrometry (ESI-MS) and 1H NMR spectroscopy.

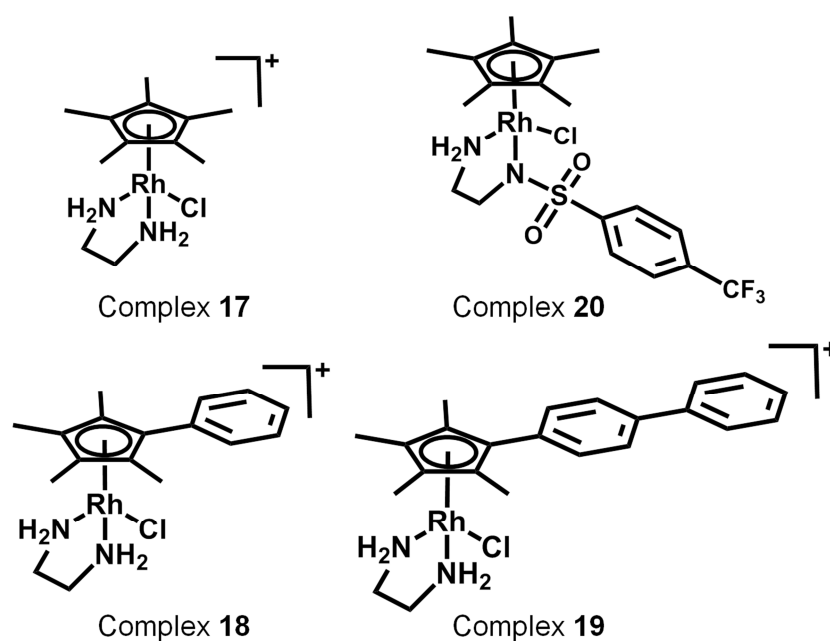


Figure 6.1. Structures of the complexes studied in this work.

6.3.2. Aqueous solution chemistry

Aquation of complexes **17-20** was followed by 1H NMR over a period of 12 h. No apparent changes were observed by 1H NMR. Spectra were compared to that of the aqua adduct formed by reaction of the corresponding complex with silver nitrate (1 mol equiv.).

The rate of aquation of complexes **17-20** was too fast to be determined by ^1H NMR, however the peaks were assigned to the aqua adducts of the complexes.

Changes in the ^1H NMR chemical shifts of the arene protons from the aqua adduct of complexes **17-20** were followed by changing the pH^* ranging from 2 to 12. The data were fitted to the Henderson–Hasselbalch equation. pK_a^* values for complexes **17-20** are shown in table 6.1. (Figure 6.2).

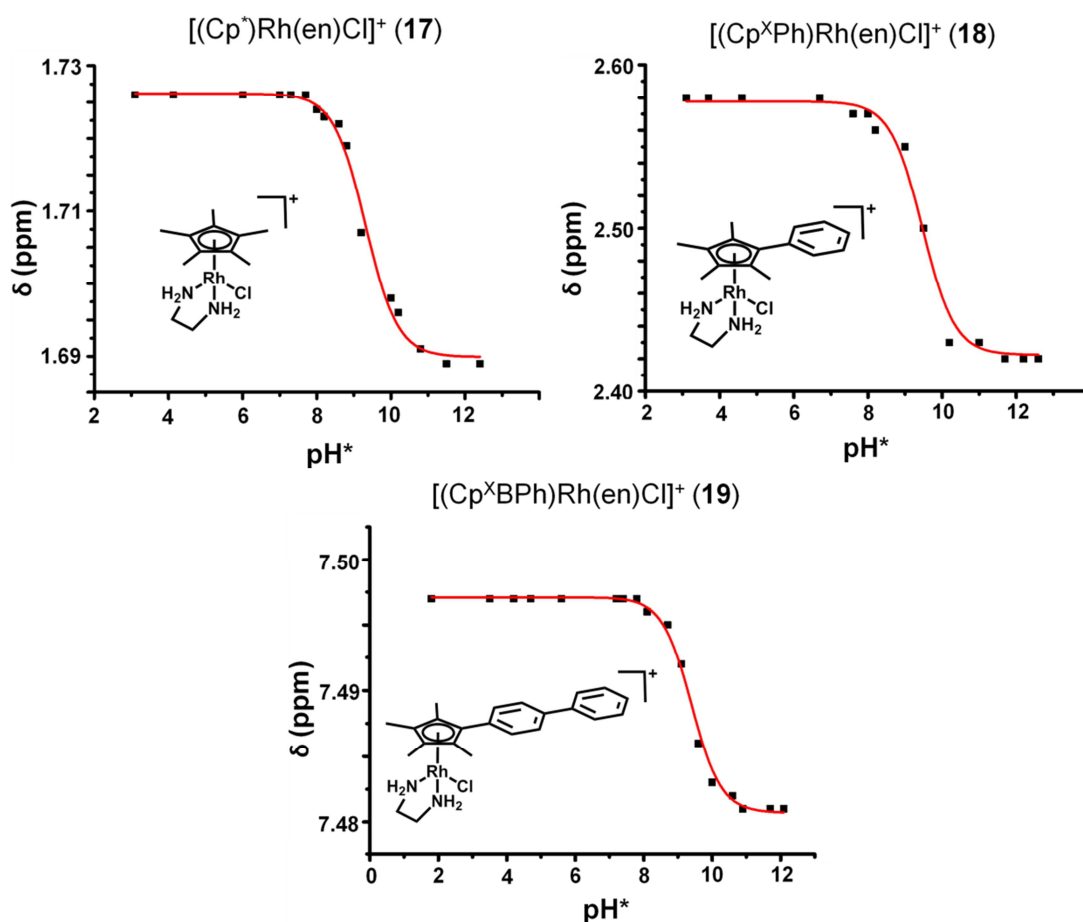


Figure 6.2. Dependence of the chemical shift of the protons in the arene rings of complexes **17-20** on the pH^* . The red lines represent computer fits to the Henderson-Hasselbalchequation.

Table 6.2. pK_a^* values for the aqua adducts of complexes **17-20** at 298 K.

Compound	pK_a^*
$[(Cp^*)Rh(en)Cl] PF_6$ (17)	9.31 ± 0.06
$[(Cp^*Ph)Rh(en)Cl] PF_6$ (18)	9.44 ± 0.08
$[(Cp^*PhPh)Rh(en)Cl] PF_6$ (19)	9.40 ± 0.04

6.3.3. Kinetics of transfer hydrogenation reactions

Catalytic transfer hydrogenation to nicotinamide adenine dinucleotide (NAD^+) in aqueous media using complexes **17-20** as catalyst and formate as hydride source (25 mol equiv.) was studied by 1H NMR at 310 K and pH^* 7.2 ± 0.1 . Spectra were recorded every 162 s until completion of the reaction. The turnover frequency (TOF) for the reactions was determined as described in the experimental section.

Table 6.3. Turnover frequencies for transfer hydrogenation reactions using catalysts **17-20**.

Complex	Cp^x	NN' ligand	TOF (h^{-1}) D_2O
Complex 17	Cp^*	en	7.50 ± 0.06
Complex 18	Cp^xPh	en	19.65 ± 0.01
Complex 19	Cp^xPhPh	en	24.19 ± 1.03
Complex 20	Cp^*	TfEn	4.12 ± 0.01

The turnover frequencies showed a marked dependence on the substituents in Cp^x (Table 6.3), the TOF increasing in the order $Cp^xPhPh > Cp^xPh > Cp^*$. $[(Cp^xPhPh)Rh(en)Cl]$

PF₆ (**19**), with a TOF of 24.19 h⁻¹, was the most active. The reaction was regioselective giving 1,4-NADH in 100 % yield when using complex **19**, similar regioselectivity was achieved when performing the reaction with complex **17** and **18** (99 %).

When comparing the ethylenediamine complex with the complex containing the sulphonamide ligand, the catalytic activity decreases. A decrease in the regioselectivity of the reaction when using complex **20** was also observed with a 7.5 % of 1,6-NADH produced.

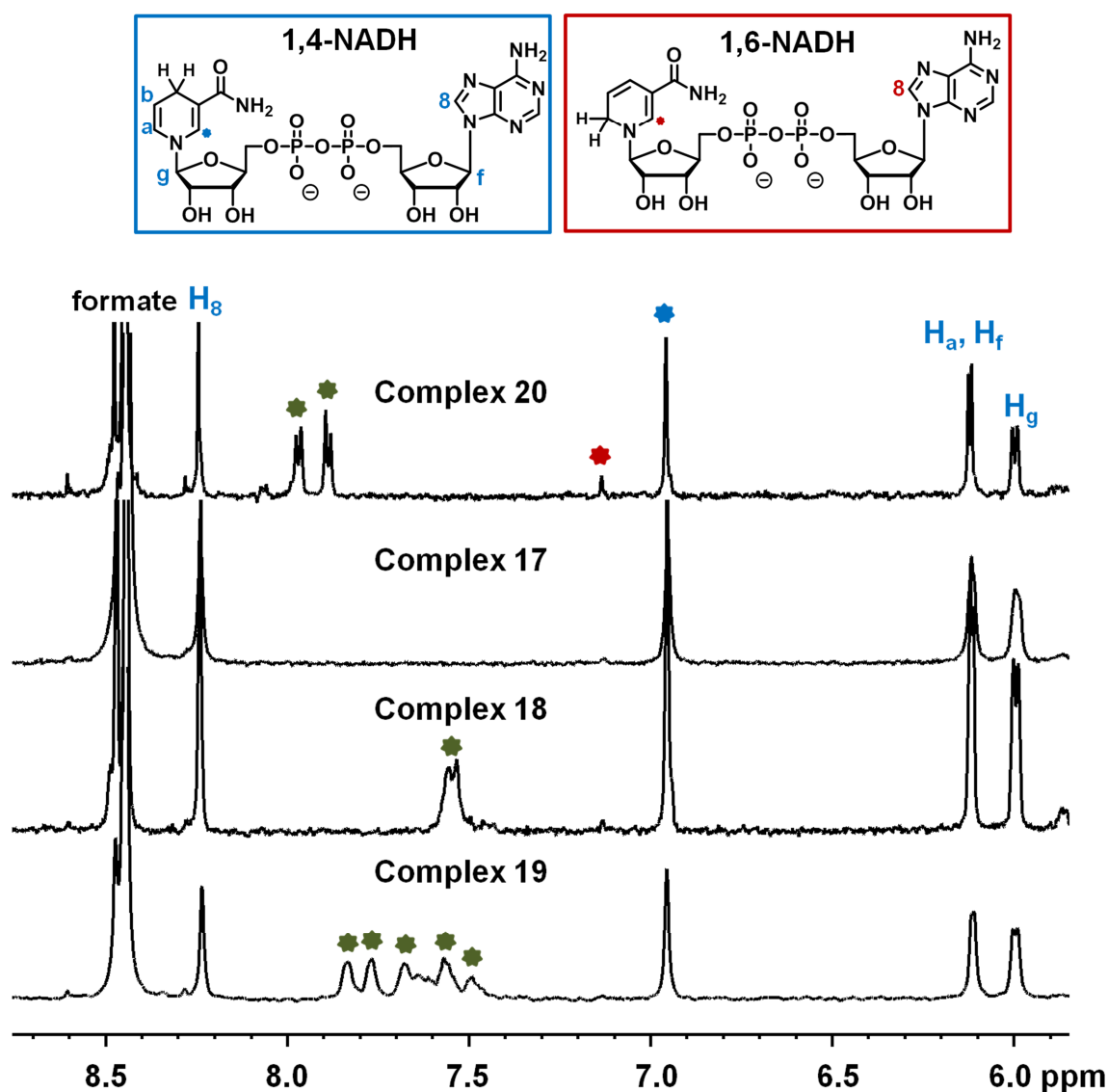


Figure 6.3. ¹H NMR spectra after reduction of the NAD⁺ using catalyst **17-20** and formate as a hydride source. The experiment was performed in D₂O at pH* 7.2 ± 0.1 and temperature 310K. **Green** = Complex, **Blue** = 1,4-NADH and **Red** = 1,6-NADH.

6.3.4. Mechanistic studies

Kinetic isotope experiments (KIE) were performed using complex **17** and deuterio-formate (25 mol equiv.) for the reduction of NAD^+ . The turnover frequency determined using deuterio-formate was $2.32 \pm 0.34\text{h}^{-1}$. The turnover frequency was 3.6 times lower than that obtained using formate (7.50h^{-1}) as the hydride source.

Three experiments were performed using complex **17**, sodium formate and NAD^+ with ratio of 1:25:X, respectively, where $X = 5, 7.5$ and 10 mol equiv. Unchanged turnover frequency (7.50h^{-1}) was obtained when changing the concentration of NAD^+ .

A second series of experiments with complex **17**, sodium formate and NAD^+ in the ratio 1:x:5, respectively, where $x = 5, 10, 25, 50$ or 100 mol equiv. of formate were performed. An important effect due to the concentration of formate can be observed (Figure 6.4).

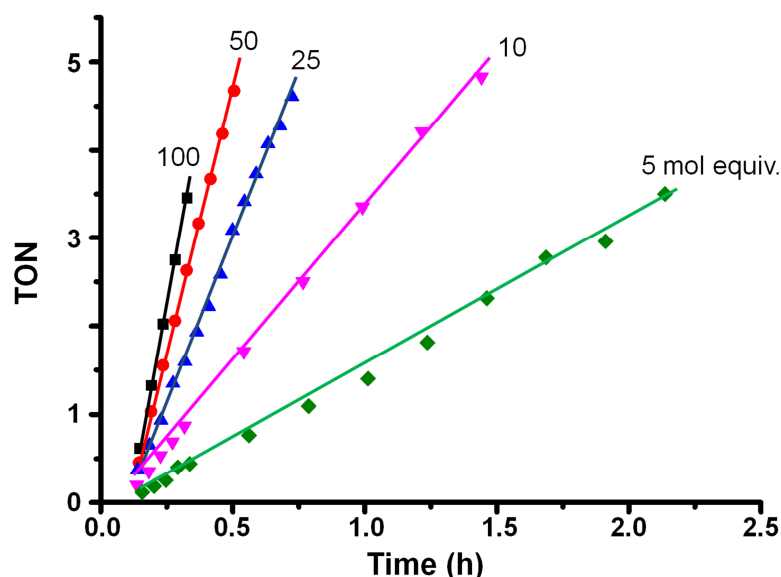


Figure 6.4. Plot of the turnover number against time for the reduction of NAD^+ by complex **17** using formate as a hydride source (ratio 5:1:x, $x = 5, 10, 25, 50$ or 100 mol equiv. respectively. $\text{pH}^* 7.2$, temperature 310K , solvent D_2O). Time is referenced to the mixing time.

Typical Michaelis-Menten behaviour is apparent from a plot of turnover frequency versus formate concentration (Figure 6.5).³³ Thus, from the double-reciprocal (Figure 6.6) the Michaelis constant ($K_M = 54.16 \text{ mM}$) and the maximum turnover frequency ($\text{TOF}_{\text{max}} = 41.49 \text{ h}^{-1}$) were determined.

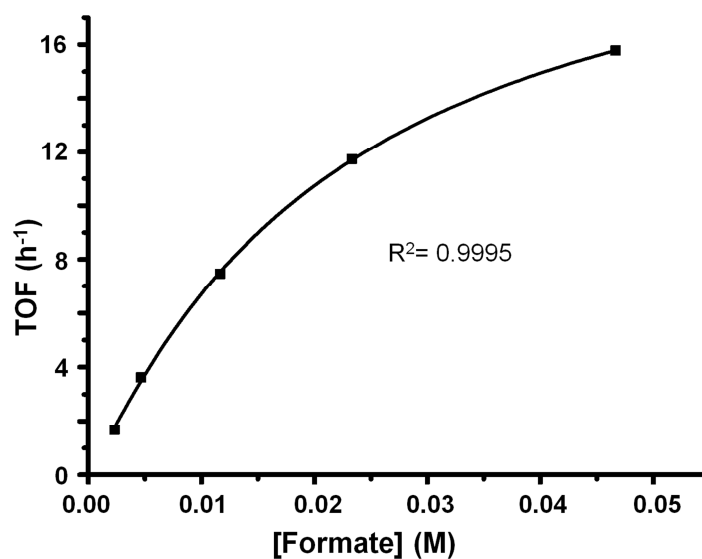


Figure 6.5. Plot of the TOF against the formate concentration, for the reduction of NAD^+ in the presence of different formate concentrations, catalyzed by complex $[(\text{Cp}^*)\text{Rh}(\text{en})\text{Cl}]^+$ (**17**).

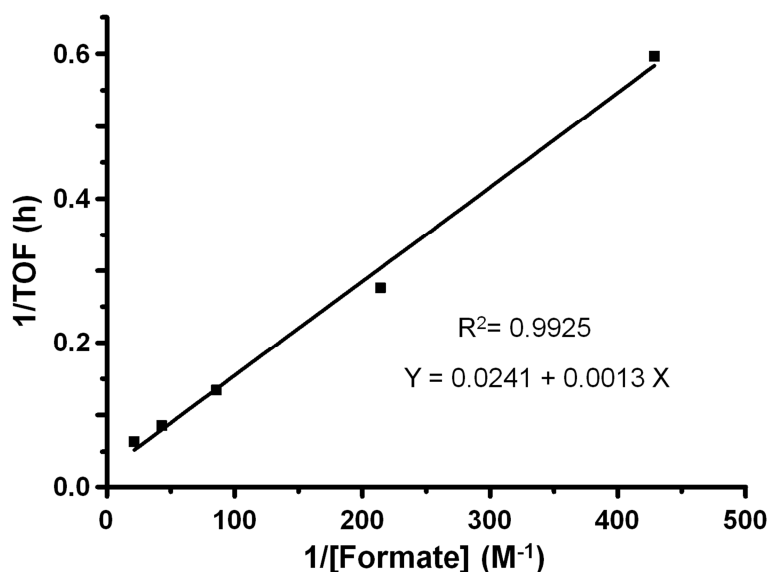


Figure 6.6. A plot of the reciprocal of the TOF against that of formate concentration, for the reduction of NAD^+ in the presence of different mol equiv. of formate, catalyzed by complex **17**. For a reaction following Michaelis-type kinetics, $\text{TOF}^{-1} = (K_M / \text{TOF}_{\text{max}})(1/[\text{S}]) + (1/\text{TOF}_{\text{max}})$ and K_M and TOF_{max} can be obtained from the gradient and y intercept, respectively.

Maximum TOF and Michaelis constant for complex $[(\text{Cp}^*)\text{Rh}(\text{TsEn})\text{Cl}]$ (**20**) were calculated by performing a series of experiments with different concentrations of sodium formate (10, 25, 50, 100 or 500 mol equiv.). Similarly to the behaviour of complex **17**, from the plot of TOF vs concentration of formate, a typical Michaelis-Menten behaviour was obtained. From the double-reciprocal (Figure 6.7) the Michaelis constant ($K_M = 108.37 \text{ mM}$) and the maximum turnover frequency ($\text{TOF}_{\text{max}} = 37.24 \text{ h}^{-1}$) were calculated.

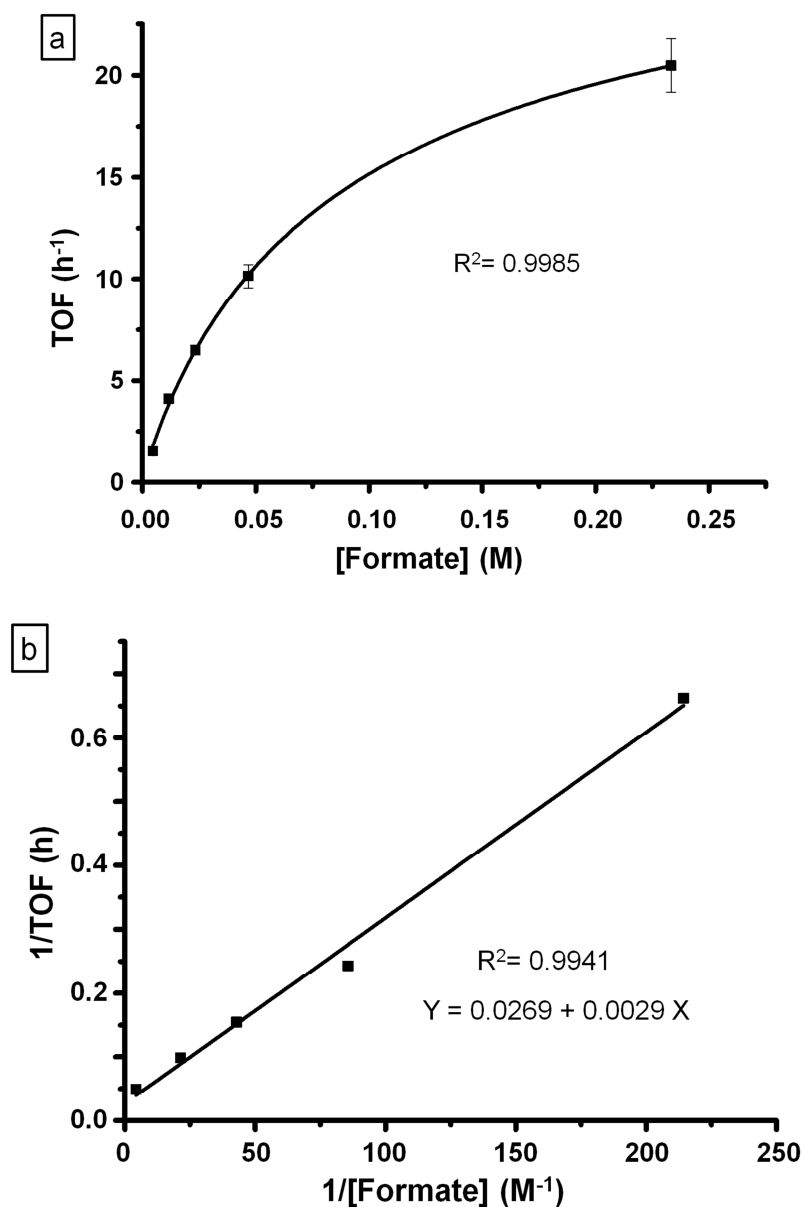


Figure 6.7. Determination of maximum turnover frequency and Michaelis constant for the reduction of NAD^+ using complex **20** and sodium formate (a) Plot of the TOF against the formate concentration, $\text{TOF} = \text{TOF}_{\text{max}} [\text{S}]/(\text{K}_{\text{M}} + [\text{S}])$. (b) Plot of the reciprocal of the TOF against that of formate concentration, $\text{TOF}^{-1} = (\text{K}_{\text{M}}/\text{TOF}_{\text{max}})(1/[\text{S}]) + (1/\text{TOF}_{\text{max}})$.

The pH^* dependence of the catalytic reaction (from pH^* 4 to 10) was also investigated *via* a series of experiments using complex **17**, sodium formate and NAD^+ (ratio 1:25:2, respectively) in D_2O . A dependence on pH^* was observed. The highest TOF (7.5 h^{-1}) was achieved at pH^* 7.3, however the turnover frequencies between pH 6 - 8 are similar. A decrease in the catalytic activity was observed when the pH^* is higher than 9 (Figure 6.8).

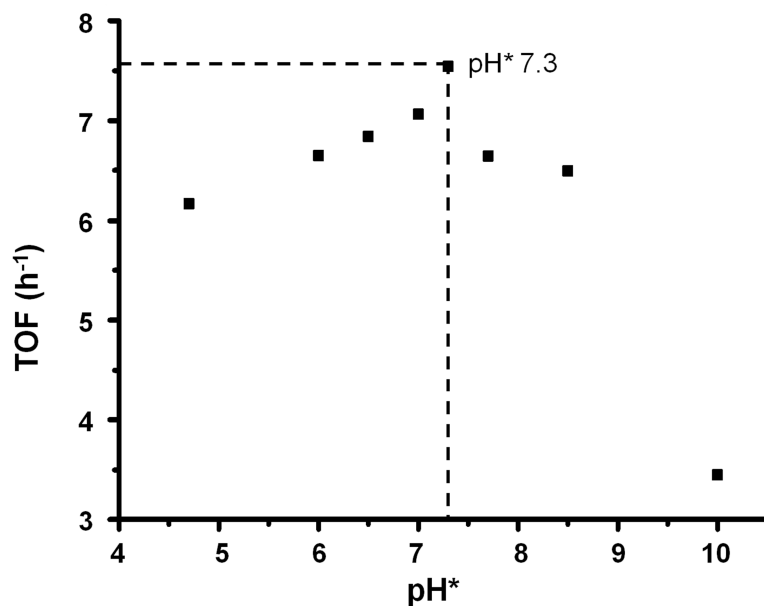


Figure 6.8. Dependence of turnover frequency on the pH^* for the reduction of NAD^+ by complex **1** using formate as a hydride source (mol ratio 5:1:25, respectively, 310 K in D_2O). Maximum turnover frequency achieved at pH 7.3 ± 0.1 .

6.3.5. Cancer cell growth inhibition

The IC_{50} values for the Rh(III) complexes **17**, **18**, **19** and **20** against A2780 human ovarian cancer cells were determined and are listed in Table 6.4. The complexes were found to be inactive against A2780 up to a maximum concentration tested ($> 100 \mu\text{M}$).

Table 6.4. IC₅₀ values for [(Cp*)Rh(en)Cl]⁺ (**17**), [(Cp^xPh)Rh(en)Cl]⁺ (**18**), [(Cp^xPhPh)Rh(en)Cl]⁺ (**19**) and [(Cp*)Rh(TfEn)Cl] against A2780 human ovarian cancer cells

Compound	IC ₅₀ (μM)
Complex 17	>100
Complex 18	>100
Complex 19	>100
Complex 20	>100

Cell survival experiments with complexes **17**, **18**, **19** and **20** upon addition of formate at concentrations of 0.5, 1 and 2 mM were determined (Figure 6.9).

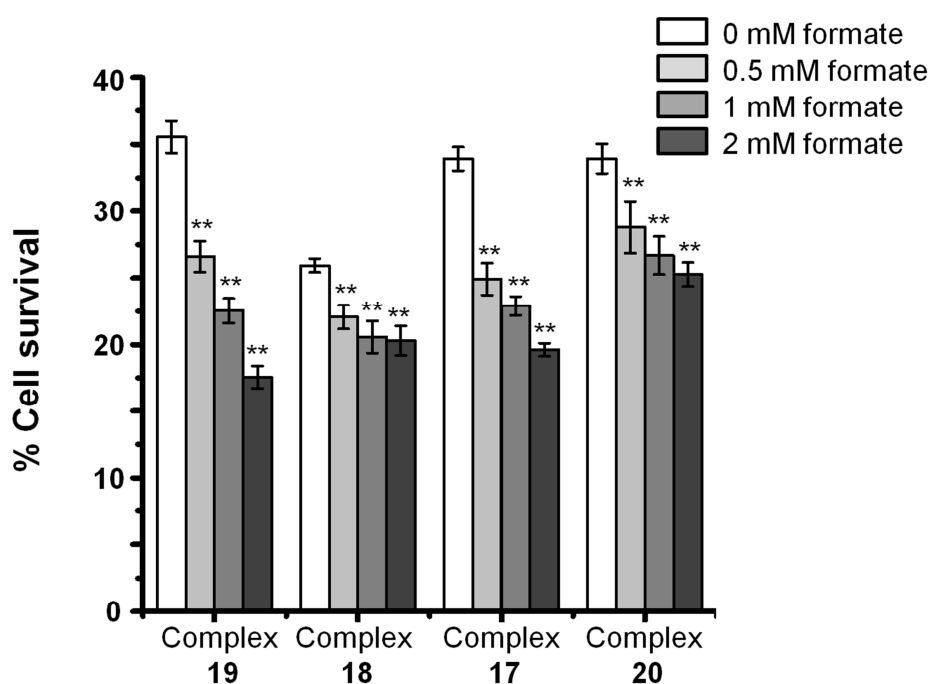


Figure 6.9. Cell survival of A2780 human ovarian cancer cells when treated with complex **17**, **18**, **19** or **20** upon addition of sodium formate at 0.5, 1 or 2 mM concentrations

An increase of the antiproliferative activity of the four Rh(III) complexes upon addition of formate can be observed. The strongest effect was achieved with complex $[(\text{Cp}^x\text{PhPh})\text{Rh}(\text{en})\text{Cl}]^+$ (**19**) with a decrease of cell survival of up to 15 %.

6.4. Discussion

6.4.1. Structures of the complexes

The aim of this chapter was to improve the catalytic activity of the Ru(II) complexes studied for the reduction of NAD^+ using sodium formate as a hydride source. For that purpose, Rh(III) complexes with the same structure to that of the ruthenium complexes $[(\eta^6\text{-arene})\text{Ru}(\text{XEn})\text{Cl}]$ were synthesised. However, the oxidation state Rh(III) cannot be stabilized by electron deficient η^6 -arenes, therefore the more electron rich pentamethylcyclopentadienyl (Cp^*) was used. N-(2-aminoethyl)-4-(trifluoromethyl)benzenesulfonamide (TfEn), the bidentate ligand which showed the highest catalytic activity for ruthenium complexes, was selected for the synthesis of complex **20**.



Complex	Metal	R ₁	R ₂	Arene or Cp ring
RM175	Ru	H	H	biphenyl
Complex 2	Ru		-	<i>p</i> -cymene
Complex 3	Ru		-	<i>p</i> -cymene
Complex 17	Rh	H	H	Cp*
Complex 18	Rh	H	H	Cp ^x Ph
Complex 19	Rh	H	H	Cp ^x PhPh
Complex 20	Rh		-	Cp*

Figure 6.10. Ru(II) and Rh(III) complexes studied in this thesis for the transfer hydrogenation reduction of NAD⁺ using sodium formate as a hydride source.

On the other hand, the analogous ethylenediamine complex [(Cp*)Rh(en)Cl]⁺ (complex **17**) was also synthesized as a model to compare with complex [(Cp*)Rh(TsEn)Cl] (complex **20**). However, complex **17** is more relevant with respect to this project due to higher TOF and increased region-selectivity.

The catalytic activity of complexes of the type $[(\text{Cp}^x)\text{M}(\text{N},\text{N}')\text{X}]$ can be tuned by changing the chelating ligand (N,N') or the Cp^x ring. Recently, a series of iridium complexes containing Cp^x rings with aromatic rings as substituent has been reported.³⁴⁻³⁶ Those complexes have been shown to have good catalytic properties towards transfer hydrogenation.³⁷ In order to improve the catalytic activity of $[(\text{Cp}^*)\text{Rh}(\text{en})\text{Cl}]^+$ (**17**), complexes containing Cp^xPh (**18**) or Cp^xPhPh (**19**) have been synthesized.

6.4.2. Hydrolysis of chlorido complexes and acidity of the aqua complexes

Aquation of the complexes **17-20** in D_2O (1.4 mM) was confirmed by comparing the ^1H NMR spectra of the D_2O solution of the complexes and the solutions obtained after removal of the chloride by reaction with silver ions (AgNO_3). Complexes **17-20** show fast hydrolysis at 310K, reaching equilibrium by the time the first ^1H NMR was recorded (< 6 min). Furthermore, 100% conversion of the chlorido complex to the aqua adduct was achieved. Consequently the turnover frequency for the transfer hydrogenation is not affected by the use of the chlorido complex instead of the aqua adduct.

pH^* titrations of the complexes **17-19** were performed so that the nature of the complexes (aqua or hydroxo adduct) could be determined at pH 7.2. Similar to the ruthenium complexes described previously, the pK_a^* values determined for the Rh complexes **17-19** are between 9 and 10. As a result the complexes exist predominantly as aqua adducts at pH close to 7.4 (Table 6.2).

Table 6.5. Summary of the behaviour of ruthenium and rhodium complexes in aqueous media.

Compound	Hydrolysis rate ^b	Extent of hydrolysis ^b	pK _a [*]
[(bip) Ru (en)Cl] ⁺ (RM175)	Fast-moderate ^a	76.2 % ^a	7.71 ^a
[(Cp*) Rh (en)Cl] ⁺ (17)	Very fast	100 %	9.31
[(Cp*Ph) Rh (en)Cl] ⁺ (18)	Very fast	100 %	9.44
[(Cp*PhPh) Rh (en)Cl] ⁺ (19)	Very fast	100 %	9.40
[(<i>p</i> -cym) Ru (TfEn)] (3)	Very fast	100 %	9.71
[(Cp*) Rh (TfEn)Cl] (20)	Very fast	100 %	ND

^a references 38 and 39, hydrolysis rate constant: $1.24 \cdot 10^{-3} \text{ s}^{-1}$; ND = not determined; ^b 1.4 mM, 310 K.

6.4.3. Kinetics of transfer hydrogenation reactions

The turnover frequency (TOF) for the reduction of NAD⁺ using complexes **17-19** and formate as a hydride source were determined at biological relevant conditions (310 K, pH* 7.2 ± 0.1). A general tendency in which the more electron-withdrawing Cp^x ring leads to higher catalytic activity (Table 6.6) was observed. Accordingly, the complex [(Cp^xPhPh)Rh(en)Cl]⁺ show the highest activity followed by complex [(Cp^xPh)Rh(en)Cl]⁺ and, in turn, all of them are more active than [(Cp*)Rh(en)Cl]⁺. In contrast with the results obtained with complexes [(η⁶-arene)Ru(XEn)Cl], the increase on the steric hindrance does not have a dramatic effect on the turnover frequency for the Rh(III) complexes.

An improvement of 7 to 24 x times was achieved when using Rh(III) complexes **17-19** compared with [(hmb)Ru(en)Cl]⁺. (Table 6.6).

Table 6.6. Summary of TOFs of Ru(II) and Rh(III) complexes for reduction of NAD⁺ using formate as a hydride source at 310 K and pH* 7.4.

Complex	TOF (h ⁻¹)
[(hmb)Ru(en)Cl] ⁺	0.85 ^a
[(Cp*)Rh(en)Cl] ⁺ (17)	7.50
[(Cp ^x Ph)Rh(en)Cl] ⁺ (18)	19.65
[(Cp ^x PhPh)Rh(en)Cl] ⁺ (19)	24.19
[(Cp*)Rh(TfEn)Cl] ⁺ (20)	4.12
[(bn)Ru(TfEn)Cl] ⁺ (12)	6.62

^a reference 33.

When performing the catalytic reaction with complex **20**, the turnover frequency (TOF = 4.12 h⁻¹) determined was 2x times lower than that obtained for complex [(Cp*)Rh(en)Cl]⁺ (**17**) (TOF = 7.5 h⁻¹). The use of the chelating ligand *N*-(2-aminoethyl)-4-(trifluoromethyl)benzenesulfonamide (TfEn) instead of ethylenediamine (en) has been shown to enhance the catalytic activity of Ru(II) compounds (Table 6.6). Nevertheless Rh(III) compounds exhibit the opposite effect.

Comparing the catalytic activity of complex **20** with the ruthenium complexes [(η⁶-arene)Ru(TfEn)Cl], Rh(III) is similar to the Ru(II). This is not completely unexpected, as a decrease in the catalytic activity when using the rhodium analogues of Noyori's catalysts

[(Cp*)Rh(TsDPEN)Cl] instead of the ruthenium catalyst for the transfer hydrogenation of some ketones has been reported.⁴⁰

Several other Ru, Rh and Ir complexes have previously been reported to catalyze the regioselective reduction of NAD⁺ to 1,4-NADH using formate as a hydride source.^{21, 22, 41, 42} The complexes used in this work show a low TOF when compared with other [(Cp*)Rh(*N,N'*)Cl] (*N,N'* = ethylenediamine, bipyridyl, phenantroliidyl or dipyridylamine) (*ca.* Up to 2000 h⁻¹).^{21, 22, 41} Nonetheless, the improvement of the catalytic activity compared with the ruthenium complexes described in Chapter 3 is remarkable. (Table 6.6)

6.4.4. Mechanism of the catalytic reduction of NAD⁺

In this section, the catalytic cycle for the transfer hydrogenation reaction using the complex [(Cp*)Rh(en)Cl]⁺ (**17**) as a catalyst is investigated. For that purpose a series of four experiments were performed and the results are compared to those obtained for the same reaction using the complex [(*p*-cym)Ru(TsEn)Cl] (**2**).

Reduction of NAD⁺ using sodium deuterio-formate (DCOO⁻) and complex **1** (ratio 5:25:1 NAD⁺:formate:complex) was studied, the turnover frequency determined was 3.6 times smaller than that with obtained using protiated formate (HCOO⁻). The difference in the turnover frequency between the two reactions suggests that the rate-limiting step of the reaction is the hydride transfer.

The factors that might influence the reaction rate were also investigated in a series of experiments where the concentration of the different reagents was varied. No significant alterations in the rate were observed (TOF= 7.50) when the NAD⁺ concentration was changed from 5 to 7.5 or 10 mol equiv. The unchanged turnover frequency implies that the reaction rate does not depend on the NAD⁺ concentration. However when the experiments were

performed with different concentrations of the hydride source (sodium formate) the reaction rate decreased, suggesting that formate is involved in the reaction rate (Figure 6.7).

Plotting the turnover frequency against formate concentration, shows a typical Michaelis-Menten behaviour.^{33,26,43} The maximum turnover frequency calculated from the double reciprocal of TON vs formate concentration for complex **17** gave a $\text{TOF}_{\text{max}} = 41.49 \text{ h}^{-1}$, about 28 x higher than that previously determined for the ethylenediamine complex $[(\text{hmb})\text{Ru}(\text{en})\text{Cl}]^+$ ($\text{TOF}_{\text{max}} = 1.46 \text{ h}^{-1}$).³³ In comparison with the complex $[(p\text{-cym})\text{Ru}(\text{TsEn})\text{Cl}]$ (**2**) ($\text{TOF}_{\text{max}} = 6.9 \text{ h}^{-1}$) the turnover frequency is about 6x times higher.

A set of experiments using NAD^+ , sodium formate and complex **20** in a ratio 2:x:1 (x = 10, 25, 50, 100 or 500 mol equiv.) were recorded, and the maximum turnover frequency ($\text{TOF}_{\text{max}} = 37.2 \text{ h}^{-1}$) and the Michaelis-Menten constant ($K_M = 108.4 \text{ mM}$) calculated.

Table 6.7. Summary of TOF_{max} and K_M values determined for the reduction of NAD^+ using formate as a hydride source and Ru(II) or Rh(III) complexes. Temperature 310 K, pH* 7.4.

Complexes	$\text{TOF}_{\text{max}} (\text{h}^{-1})$	$K_M (\text{mM})$
$[(\text{hmb})\text{Ru}(\text{en})\text{Cl}]^+$	1.5 ^a	58 ^a
$[(\text{Cp}^*)\text{Rh}(\text{en})\text{Cl}]^+$ (17)	41.5	41.5
$[(\text{Cp}^*)\text{Rh}(\text{TfEn})\text{Cl}]^+$ (20)	37.2	108.4
$[(p\text{-cym})\text{Ru}(\text{TsEn})\text{Cl}]$ (2)	6.9	42.1

^a reference 33.

The Michaelis constant for complex **20** ($K_M = 108.4$ mM) indicates a weak affinity for formate compared to complexes $[(Cp^*)Rh(en)Cl]^+$ ($K_M = 41.5$ mM), $[(hmb)Ru(en)Cl]^+$ ($K_M = 58$ mM)³³, and $[(p-cym)Ru(TsEn)Cl]$ (42.1 mM). However, it has stronger affinity for formate than $[(Cp^*)Rh(bipy)H_2O]^{2+}$ ($K_M = 140$ mM).⁴³ On the other hand the maximum turnover frequency ($TOF_{max} = 37.2$ h⁻¹) of the reaction indicated an increase in the catalytic activity compared to $[(hmb)Ru(en)Cl]^+$ ($TOF_{max} = 1.46$ h⁻¹)³³ or $[(p-cym)Ru(TsEn)Cl]$ (6.9 h⁻¹) but lower catalytic activity compared with the complex $[(Cp^*)Rh(en)Cl]^+$ ($TOF = 41.5$ h⁻¹). The maximum turnover frequency of the Rh(III) complexes is higher than that from the Ru(II) analogues which might result in an improvement on the catalytic activity in cells due to the high concentrations of formate used (2 mM sodium formate in the media), however complex **20** shows a much lower affinity for formate which could indicate that the catalyst will be poisoned more readily. Overall, the use of Rh(III) based systems allowed us to increase the efficiency of the transfer hydrogenation reaction.

Finally, the possibility of the reverse reaction, where 1,4-NADH is oxidized to NAD⁺ was studied.⁴⁴ Experiments employing 1,4-NADH as the hydride source were attempted, however no formation of the hydride adduct or NAD⁺ could be detected after 10 h using 0.4 mM complex, 0.8 mM 1,4-NADH at 310K and pH* 7.4.

With the data obtained, the catalytic cycle proposed is the same than that for the ruthenium complex $[(p-cym)Ru(TsEn)Cl]$.

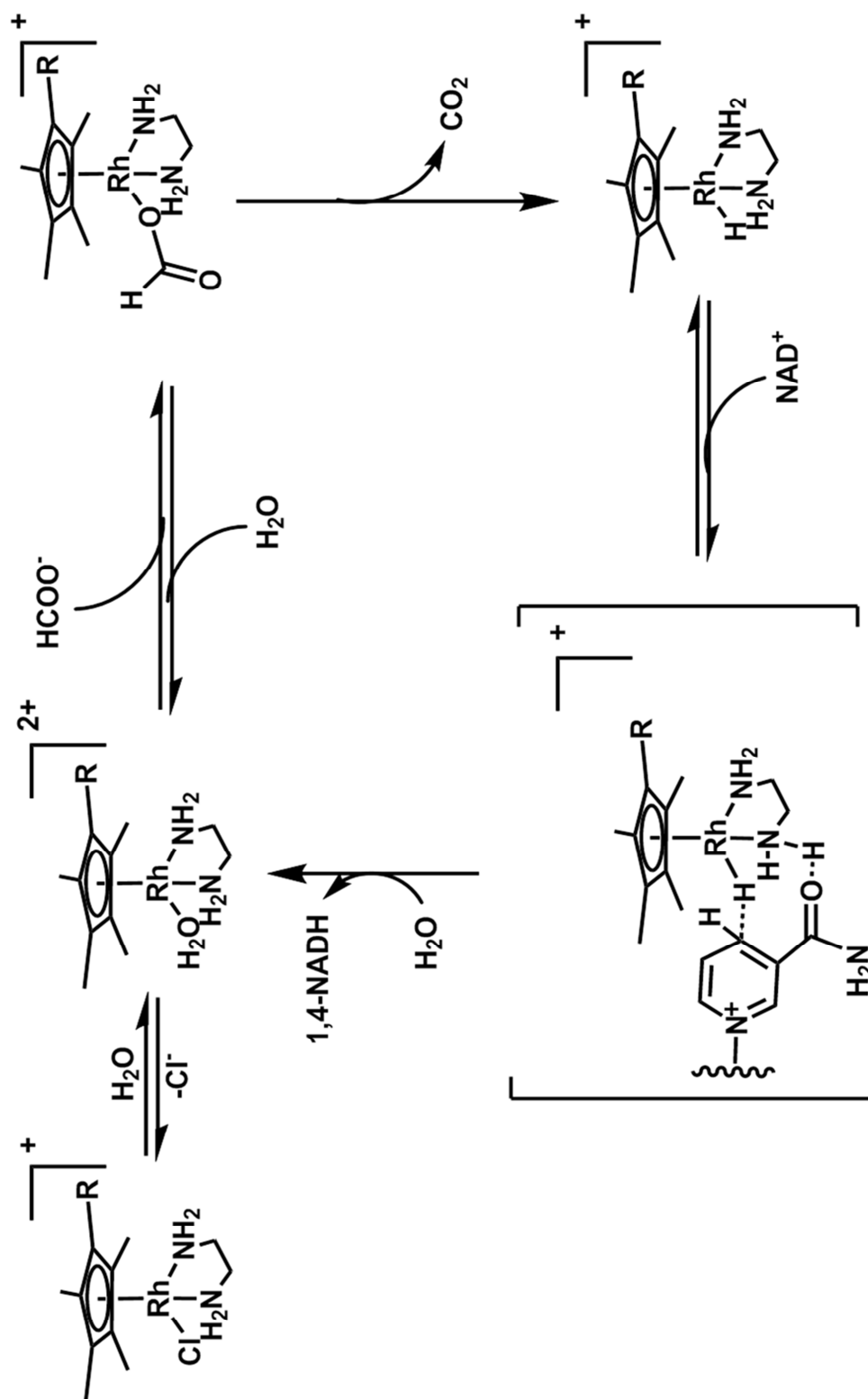


Figure 6.11. Proposed catalytic cycle for complexes of the type $[(Cp^x)Rh(en)Cl]^+$ based on that proposed in Chapter 3

The last experiment performed was to determine the optimum pH and the possibility of using those complexes under biological conditions. The maximum activity for complex **17** was observed at pH* 7.3 (Figure 6.8). However the TOF obtained was very similar in a range of pH between 5 and 9. At higher pH* the concentration of OH⁻ inhibits the reaction due to the formation of Rh(III)-OH.

Table 6.8. Comparison the catalytic cycles of ruthenium and rhodium complexes.

	[(<i>p</i> -cym) Ru (TsEn)Cl]	[(Cp*) Rh (en)Cl] ⁺
	(2)	(17)
Hydrolysis	Fast	Fast
Rate-limiting step	Hydride formation	Hydride formation
NAD⁺ concentration dependence	No	No
Formate concentration dependence	Yes	Yes
Optimum pH*	7.2 ± 0.1	7.3 ± 0.1
Reaction with 1,4 NADH	No	No

6.4.5. Cancer cell growth inhibition

Rh(III) complexes **17**, **18**, **19** and **20** were found to be inactive against A2780 up to a maximum concentration tested (> 100 μM) (Table 6.4).

Cell survival with complexes **17** - **20** upon addition of formate at concentrations of 0.5, 1 and 2 mM was determined (Figure 6.9). The complexes show a decrease in cell survival upon addition of formate. Taking into consideration the high excess of formate

compared to the complexes, and the fact that higher concentrations of formate gave lower cell survival, it can be assumed that the complex reacts catalytically with formate. This behaviour was also observed in Chapter 4 when using Ru(II) complexes.

As discussed previously, the catalytic activity of the complexes of the type $[(Cp^x)Rh(en)Cl]$ ($Cp^x = Cp^*, Cp^xPh$ and Cp^xPhPh) depends strongly on the Cp^x ring. The catalytic activity decreases in the order $Cp^xPhPh > Cp^xPh > Cp^*$. However, this trend cannot be observed in cells. Complex $[(Cp^xPh)Rh(en)Cl]^+$ (**18**) show the smaller improvement after addition of formate, followed by $[(Cp^*)Rh(en)Cl]^+$ and $[(Cp^xPhPh)Rh(en)Cl]^+$.

Despite the higher catalytic activity of the Rh(II) complexes **17-20** compared with the Ru(II) complexes studied in Chapter 3 and 4, the improvement on the antiproliferative activity of the Rh(III) complexes is not as drastic as in the case of the Ru(II) analogues. The Rh(III) complexes are probably poisoned more easily than the Ru(II) due to the higher reactivity of the Rh metal centre.

6.5. Conclusions

In this chapter, a series of water-soluble Rh^{III} half-sandwich complexes of the type [(Cp^x)Rh(*N,N'*)(Cl)], where *N,N'* is ethylenediamine (en) or *N*-(2-aminoethyl)-4-(trifluoromethyl)benzenesulfonamide (TfEn), have been synthesized for the first time. These complexes are analogous of [(η⁶-arene)Ru(en)Cl]⁺, previously studied in our group, and [(η⁶-arene)Ru(TfEn)Cl], studied in Chapter 3. The change of the metal centre from Ru(II) to Rh(III) was carried out to test the hypothesis that a higher reaction rate might be achieved by using Cp^{*}Rh(III) systems, rather than arene Ru(II) compounds.

Here, It has been demonstrated that the Rh(III) complexes synthesized are capable of carrying out transfer hydrogenation reactions for the reduction of NAD⁺ using formate as a hydride donor and under physiological relevant conditions (310 K, pH* 7.4). However, reduction of NAD⁺ using complex **20** leads to a turnover frequency of 4.12 h⁻¹, displaying no improvement compared to the Ru(II) arene analogues (6.62 h⁻¹ for [(bn)Ru(TfEn)Cl]). On the other hand, turnover frequency values for complexes **17-19** (7.50, 19.65 and 24.19 h⁻¹ respectively) are up to two order of magnitude higher than those for [(hmb)Ru(en)Cl]⁺ (0.85 h⁻¹).

The nature of the Cp^x ring significantly influences the catalytic activity, [(Cp^xPhPh)Rh(en)Cl]⁺ (**19**) (TOF = 24.2 h⁻¹) being the most active compound, while the activity decreases in the order [(Cp^xPhPh)Rh(en)Cl]⁺ > [(Cp^xPh)Rh(en)Cl]⁺ > [(Cp^{*})Rh(en)Cl]⁺.

Mechanistic studies in those new systems were carried out in order to determine a plausible catalytic cycle. Fast hydrolysis of the complexes was observed by ¹H NMR. pK_a* values (*ca.* 9-10) indicate that the Rh(III) complexes remain in their aqua form instead of the hydroxo. The rate-limiting step was identified as the hydride formation. The reaction with

complex $[(Cp^*)Rh(en)(Cl)]^+$ (**17**) showed a dependence of the reaction rate on the formate concentration but not on NAD^+ concentration. No reaction between complex **17-20** and 1,4-NADH was detected after 10 h. Optimum pH* for the reaction with complex **17** was found to be (7.3 ± 0.1) which is close to physiological pH. Those results indicate a similar cycle to the one proposed for their Ru(II) arene analogues.

The maximum turnover frequency of complexes **17** and **20** indicates (41.5 and 37.2 h^{-1} , respectively) an important improvement on the catalytic activity at high concentrations of formate compared with that of the Ru(II) analogues (6.9 h^{-1}), even for complex $[(Cp^*)Rh(TfEn)Cl]$ (**20**). This improvement on the maximum turnover frequency is expected to translate in a significant enhancement of the antiproliferative activity when the complexes are used in combination with high concentrations of formate.

Cell survival experiments showed an increase on the antiproliferative activity of the Rh(III) complexes in combination with formate. However, the improvement on the activity of Rh(III) complexes with formate is much lower than in the case of Ru(II) complexes. Rh(III) metal centres, being more reactive than Ru(II) are more likely to be poisoned. Therefore, it is concluded that Ru(II) complexes containing XEn ligands (XEn = TsEn, TfEn, MsEn or NbEn) are more suitable for catalytic reactions in cells than the Rh(III) studied in this chapter.

6.6. References

- (1) Wu, X.; Wang, C.; Xiao, J. *Plat. Met. Rev.* **2010**, *54*, 3-19.
- (2) Ogo, S.; Matsumoto, T.; Robertson, A. *Dalton Trans.* **2011**, *40*, 10304-10310.
- (3) Gladiali, S.; Alberico, E. *Chem. Soc. Rev.* **2006**, *35*, 226-236.

- (4) Brandt, P.; Andersson, P. G.; Backvall, J.; Samec, J. S. M. *Chem. Soc. Rev.* **2006**, *35*, 237-248.
- (5) Wu, J.; Wang, F.; Ma, Y.; Cui, X.; Cun, L.; Zhu, J. *Chem. Commun.* **2006**, 1766-1768.
- (6) Matharu, D. S.; Martins, J. E. D.; Wills, M. *Chem. Asian J.* **2008**, *3*, 1374-1383.
- (7) Al-Salim, T.; Hadi, J. S.; Al-Nasir, E. A.; Hassen, M. A. *J. Sci. Res.* **2010**, *2*, 501-511.
- (8) Ward, T. R. *Acc. Chem. Res.* **2011**, *44*, 47-57.
- (9) Zhou, Y.; Lu, S.; Chen, Q.; Wang, D. *Chem. Rev.* **2012**, *112*, 2557-2590.
- (10) Xue, D.; Chen, Y. C.; Chui, X.; Wang, Q. W.; Zhu, J.; Deng, J. G. *J. Org. Chem.* **2005**, *70*, 3584-3591.
- (11) Noyori, R. *Angew. Chem. Int. Ed* **2002**, *41*, 2008-2022.
- (12) Meuzelaar, G. J.; van Vliet, M. C. A.; Maat, L.; Sheldon, R. A. *Eur. J. Org. Chem* **1999**, 2315-2321.
- (13) Karvembu, R.; Prabhakaran, R.; Natarajan, K. *Coord. Chem. Rev.* **2005**, *249*, 911-918.
- (14) Ikariya, T. *Bull. Chem. Soc. Jpn* **2011**, *84*, 1-16.
- (15) Gladiali, S.; Mestroni, G. In *Transition metals for organic synthesis*; ed.; Wiley-VCH: Germany, **1998**; *2*, 97-117.
- (16) Bøgevig, A.; Pastor, I. M.; Adolfsson, H. *Chem. Eur. J.* **2004**, *10*, 294-302.
- (17) Blacker, A. J.; Ikariya, T. *Acc. Chem. Res.* **2007**, *40*, 1300-1308.
- (18) Baker, D. C.; Mao, J. *Org. Lett.* **1999**, *1*, 841-843.
- (19) Murata, K.; Ikariya, T.; Noyori, R. *J. Org. Chem.* **1999**, *64*, 2186-2187.
- (20) Cross, D. J.; Kenny, J. A.; Houson, I.; Campbell, L.; Walsgrove, T.; Wills, M. *Tetrahedron: Asymmetry* **2001**, *12*, 1801-1806.
- (21) Canivet, J.; Süß-Fink, G.; Štěpnička, P. *Eur. J. Inorg. Chem.* **2007**, 4736-4742.
- (22) Haquette, P.; Talbi, B.; Barilleau, L.; Madern, N.; Fosse, C.; Salmain, M. *Org. Biomol. Chem.* **2011**, *9*, 5720-5727.

- (23) Hildebrand, F.; Kohlmann, C.; Franz, A.; Lütz, S. *Adv. Synth. Catal* **2008**, *350*, 909-918.
- (24) Ruppert, R.; Herrmann, S.; Steckhan, E. *Chem. Commun.* **1988**, 1150-1151.
- (25) Lutz, J.; Hollmann, F.; Ho, T. V.; Schnyder, A.; Fish, R. H.; Schmid, A. *J. Organomet. Chem.* **2004**, *689*, 4783-4790.
- (26) Lo, H. C.; Leiva, C.; Buriez, O.; Kerr, J. B.; Olmstead, M. M.; Fish, R. H. *Inorg. Chem.* **2001**, *40*, 6705-6716.
- (27) Lo, H. C.; Fish, R. H. *Angew. Chem. Int. Ed.* **2002**, *41*, 478-481.
- (28) Leiva, C.; Lo, H. C.; Fish, R. H. *J. Organomet. Chem.* **2010**, *695*, 145-150.
- (29) Buriez, O.; Kerr, J.; Fish, R. *Angew. Chem. Int. Ed.* **1999**, *38*, 1997-2000.
- (30) Bjorgvinsson, M.; Halldorsson, S.; Arnason, I.; Magull, J.; Fenske, D. *J. Org. Chem.* **1997**, *544*, 207-215.
- (31) Tan, J.; Tang, W.; Sun, Y.; Jiang, Z.; Chen, F.; Xu, L.; Fan, Q.; Xiao, J. *Tetrahedron* **2011**, *67*, 6206-6213.
- (32) Garcia, G.; Sanchez, G.; Romero, I.; Solano, I.; Santana, M. D.; Lopez, G. *J. Organomet. Chem.* **1991**, *408*, 241-246.
- (33) Yan, Y. K.; Melchart, M.; Habtemariam, A.; Peacock, A. F.; Sadler, P. J. *J. Biol. Inorg. Chem.* **2006**, *11*, 483-488.
- (34) Hearn, J. M.; Romero-Canelón, I.; Qamar, B.; Liu, Z.; Hands-Portman, I.; Sadler, P. J. *ACS Chemical Biology* **2013**, *8*, 1335-1343.
- (35) Liu, Z.; Habtemariam, A.; Pizarro, A. M.; Clarkson, G. J.; Sadler, P. J. *Organometallics* **2011**, *30*, 4702-4710.
- (36) Liu, Z.; Habtemariam, A.; Pizarro, A. M.; Fletcher, S. A.; Kisova, A.; Vrana, O.; Salassa, L.; Bruijninx, P. C. A.; Clarkson, G. J.; Brabec, V.; Sadler, P. J. *J. Med. Chem.* **2011**, *54*, 3011-3026.

- (37) Liu, Z.; Deeth, R. J.; Butler, J. S.; Habtemariam, A.; Newton, M. E.; Sadler, P. J. *angew. Chem. Int. Ed* **2013**, *52*, 4194-4197.
- (38) Wang, F.; Habtemariam, A.; van der Geer, E. P. L.; Fernández, R.; Melchart, M.; Deeth, R. J.; Aird, R.; Guichard, S.; Fabbiani, F. P.; Lozano-Casal, P.; Oswald, I. D. H.; Jodrell, D. I.; Parsons, S.; Sadler, P. J. *Proc. Natl. Acad. Sci. U. S. A.* **2005**, *102*, 18269-18274.
- (39) Wang, F.; Chen, H.; Parsons, S.; Oswald, I. D. H.; Davidson, J. E.; Sadler, P. J. *Chem. Eur. J.* **2003**, *9*, 5810-5820.
- (40) Murata, K.; Ikariya, T.; Noyori, R. *J. Org. Chem.* **1999**, *64*, 2186-2187.
- (41) Hildebrand, F.; Kohlmann, C.; Franz, A.; Lütz, S. *Advanced Synthesis & Catalysis* **2008**, *350*, 909-918.
- (42) Liu, Z.; Romero-Canelón, I.; Qamar, B.; Hearn, J. M.; Habtemariam, A.; Barry, N. P. E.; Pizarro, A. M.; Clarkson, G. J.; Sadler, P. J. *Angew. Chem. Int. Ed.* **2014**, *53*, 3941-3946.
- (43) Steckhan, E.; Herrmann, S.; Ruppert, R.; Dietz, E.; Frede, M. *Organometallics* **1991**, *10*, 1568-1577.
- (44) Betanzos-Lara, S.; Liu, Z.; Habtemariam, A.; Pizarro, A. M.; Qamar, B.; Sadler, P. J. *Angew. Chem. Int. Ed.* **2012**, *51*, 3897-3900.

Chapter 7

Conclusions

Future Work



7. Conclusions and future work

The aim of the project was primarily concerned with the design of catalytic organometallic ruthenium/rhodium complexes with the ability to reduce nicotinamide adenine dinucleotide via transfer hydrogenation. These complexes can then be used to perform the catalytic reaction in cancer cells, aiming to deplete the levels of NAD^+ thereby effecting the disruption of the homeostasis and eventual death of cancer cells.

7.1. Conclusions

7.1.1. Chapter 3: Ruthenium(II) arene complexes for the catalytic reduction of NAD^+

For the purpose of this thesis, Noyori's catalyst ($[(\eta^6\text{-arene})\text{Ru}(\text{TsDPEN})\text{Cl}]$, Figure 7.1) was selected as a structural model for the design of effective catalysts for transfer hydrogenation reactions. The Noyori catalyst has been successfully used for transfer hydrogenation of different substrates, such as ketones, imines and $\text{C}=\text{C}$ double bonds.¹ Furthermore, the catalyst was stable and highly active in aqueous media.² However, the design of the original Noyori catalyst (Figure 7.1) was directed towards asymmetric catalysis in organic solvents.³ For that reason, the chelating ligand contains two chiral carbons with a phenyl substituent, which confers the catalyst with enantioselectivity. The high enantioselectivity of these catalysts due to the lipophilic phenyl groups, is, however in detriment of the solubility in water. Given that enantioselectivity is not a requirement in NAD^+/NADH catalysis, avoiding chiral centres offers a plausible strategy for the design and synthesis of a more water soluble derivative of Noyori's catalyst (Figure 7.1). Furthermore,

reduction of different substrates could be performed using sodium formate as the hydride source, which is non-toxic to cells up to relatively high concentrations (< 7 mM), and could be used in combination with the drug.^{2, 4}

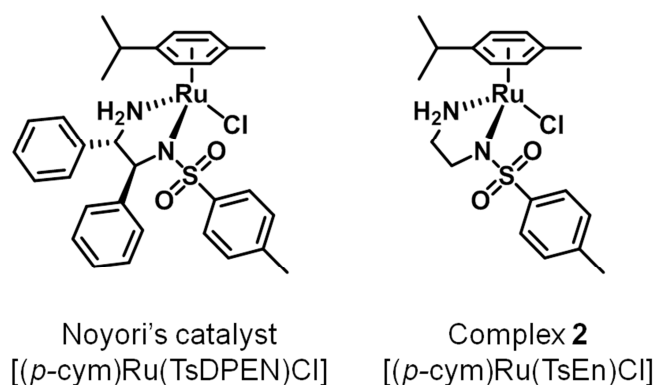


Figure 7.1. Structures of Noyori's catalyst and complex 2.

A series of arene Ru(II) complexes of the type $[(\eta^6\text{-arene})\text{Ru}(N,N')\text{Cl}]$ containing the modified Noyori's chelating ligand (N,N') were synthesised. Catalytic reduction of NAD^+ was then studied using spectroscopic methods, using the complexes and 25 mol equivalents of sodium formate as a hydride source. In order to perform the experiments with more relevant conditions to our final aim, the reduction of NAD^+ was performed in water, adjusting the pH* to 7.4 and keeping the temperature at 310 K. Comparison of the TOF of the complexes with different arene but the same ligands show a defined trend where a decrease on the catalytic activity of the complexes follows the order $\text{bn} > \text{bip} > p\text{-cym} > \text{hmb}$. Comparison of the TOF using different chelating ligands was also performed with the trend $\text{TfEn} > \text{TsEn} > \text{MsEn}$ where the ligand TfEn contains the most electron-withdrawing substituent group in the sulphonamide while MsEn contains the less electron-withdrawing group. Complex (**12**) $[(\text{bn})\text{Ru}(\text{TfEn})\text{Cl}]$ was found to be the most active with a TOF of 10.4 h^{-1} .

The catalytic cycle of this type of complexes was studied using complex $[(p\text{-cym})\text{Ru}(\text{TsEn})(\text{Cl})]$ (**2**). The effects of the concentration of substrate and hydride source (sodium formate) on the reaction rate has been determined for complex **2**. Isotopic effect studies implicates $[(\eta^6\text{-arene})\text{Ru}(N,N')(\text{H})]$ formation as the rate-limiting step. The dependence of the reaction rate for complex $[(p\text{-cym})\text{Ru}(\text{TsEn})]$ (**2**) on the solvent and pH* were also investigated. The complexes showed a strong effect in the catalytic activity due to different solvents. The optimum pH* was found at 7.6.

7.1.2. Chapter 4: Performing transfer hydrogenation reactions in cancer cells

The more soluble and active compounds were selected from the series of complexes synthesised (chapter 3) for *in cellulo* experiments with A2780 ovarian cancer cells. In an ideal situation, the catalysts would be non-cytotoxic or moderately cytotoxic, but, upon addition of the hydride source (formate) the complexes will be highly cytotoxic. The complexes tested, displayed moderate antiproliferative activity with IC₅₀ values between 11.4 and 21.2 μM . Still, upon addition of formate, the antiproliferative activity of the complexes was potentiated, achieving lower IC₅₀ values. Cell survival experiments show that complexes $[(p\text{-cym})\text{Ru}(\text{MsEn})\text{Cl}]$ (**1**) and $[(p\text{-cym})\text{Ru}(\text{TsEn})\text{Cl}]$ (**2**) display the higher increase of the antiproliferative activity. An IC₅₀ of 1 μM , comparable to the clinically used cisplatin (1.2 μM), was achieved with complex (**2**) upon addition of 2 mM formate. A control experiment with cells treated only with increasing concentrations of formate had no effect on cell survival, showing that the increase in the proliferative activity is not due to the formate alone but as a result of the reaction between formate and the complex. Cellular accumulation experiments proved that cells treated with formate and complex accumulate as much ruthenium as the cells treated only with the complex. , experiments using acetate instead of

formate were also carried out, showing that no potentiation can be achieved. Acetate is a carboxylate similar to formate but which does not have the capability to act as a hydride donor. These experiments suggest that transfer hydrogenation reactions in cells can be achieved.

Determination of the NAD^+ and NADH levels in cells was also carried out. A decrease on the concentration of NAD^+ can be observed while the concentration of NADH increases. Interestingly, this trend changes after 12 hours of drug exposure, probably due to poisoning of the catalyst.

7.1.3. Chapter 5: Interactions of half sandwich Ru(II) mono-sulfonamide complexes with DNA and GSH

Chapter 5 was concerned with the study of the interactions between the Ru(II) complexes synthesized in Chapter 3 and DNA or GSH. DNA was studied as a possible target for the complexes since the analogues ethylenediamine compounds ($[(\text{bip})\text{Ru}(\text{en})\text{Cl}]^+$ **RM175**) have been shown to target DNA.^{5, 6} However, and despite the structural similarities with their ethylenediamine analogues, complexes $[(p\text{-cym})\text{Ru}(\text{TsEn})\text{Cl}]$ **2** and $[(\text{bip})\text{Ru}(\text{TsEn})\text{Cl}]$ **8** display very weak affinity for CT-DNA. Binding kinetics experiments, melting temperature and circular and linear dichroism were used. Complexes **2** and **8** were shown to weakly interact with CT-DNA through groove binding, but no coordination or intercalation could be proven.

GSH is a tripeptide that is found in cells at concentrations of up to 10 mM. Some of the more important functions of the GSH are as an antioxidant and as a detoxifying agent.^{7, 8} GSH is known to react with some metal-based drugs such as cisplatin.⁹ The GS^- -M adducts are then excreted from the cells. The interaction between GSH and the Ru(II) complexes of

the type $[(\eta^6\text{-arene})\text{Ru}(\text{en})\text{Cl}]^+$ has also been studied. Interestingly, these en complexes were shown to react with GSH to form a GS^- adduct, which later undergoes ligand based oxidation to form sulfenato-GS. Finally, the Ru(II) complex undergoes ligand substitution and binds DNA.^{6, 10} In this section of Chapter 5, It has been demonstrated that the complexes $[(\eta^6\text{-arene})\text{Ru}(\text{XEn})\text{Cl}]$ ($\text{X} = \text{Ms}, \text{Ts}, \text{Tf}$ and Nb , see Chapter 3 for structures) react readily with GSH. However, instead of forming mono GS^- adducts, the reaction generates a Ru dimer containing three GS^- units. Ru(II) dimers containing three $\mu\text{-SR}$ bridges have been previously shown to display antiproliferative activity towards cancer cells.¹¹⁻¹⁴ Therefore, there is a possibility that the *in situ* GS^- -Ru dimer is the active form of the complex, and is responsible for the moderate IC_{50} values obtained in Chapter 4.

7.1.4. Chapter 6: Rhodium(III) half-sandwich complexes for the catalytic reduction of NAD^+

In Chapter 6, a series of Rh(III) complexes, containing either ethylenediamine or the modified Noyori's chelating ligand, were synthesized and studied. The aim was to develop more active catalysts which, in combination with formate, could improve the antiproliferative activity of the complexes even more than was possible with Ru(II) complexes. The Rh(III) complexes were shown to reduce NAD^+ catalytically in the presence of formate, achieving TOF up to 3.5 times higher than the Ru(II) analogues. The catalytic cycle and optimum conditions for these catalysts was also studied. Despite the increased catalytic activity achieved by using a Cp^xRh system, the compounds were shown to achieve lower potentiation when tested in cells. Possibly, this is because the Rh(III) complexes can react with GSH and other biomolecules more readily than the Ru(II) analogues.

7.2. Future work

In this section, the following steps for the completion of this project and some new areas of investigation will be described.

7.2.1. New ligands for increased solubility

Increasing water solubility: it has been shown that complexes containing *o*-terphenyl as a η^6 -arene display very good catalytic activity, however the water solubility of the complexes is a major drawback. In order to improve the water solubility of these complexes, new chelating ligands containing a functional group that may confer improved water solubility without a detrimental effect on the activity of the complexes could be synthesised (Figure 7.2).¹⁵

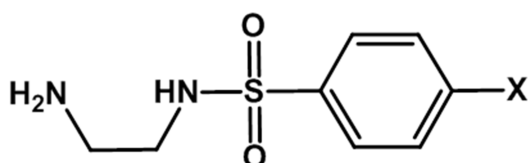


Figure 7.2. General structure of the chelating ligand. X = sulfonic, hydroxyl, carboxylate or phosphonate.

In fact the addition of some electron-withdrawing groups, such as sulfonic acid, may even help to improve the catalytic activity of the complexes. It has been shown in Chapter 3 that more electron withdrawing groups correlate with more active complexes.

7.2.2. Increasing the stability of the catalysts

In order to improve the stability of the type of catalysts described in this thesis, a series of tethered complexes can be synthesised. Wills *et al.* have reported the synthesis and catalytic activity of a series of tethered Noyori's type complexes which have displayed very good enantioselectivity, conversions and catalytic activity.¹⁶⁻²⁰ These types of complex

contain an η^6 -arene unit which is bound to the chelating Noyori-type ligand. The complexes benefit from increased stability towards ligand substitution of the chelating ligand (Figure 7.3).

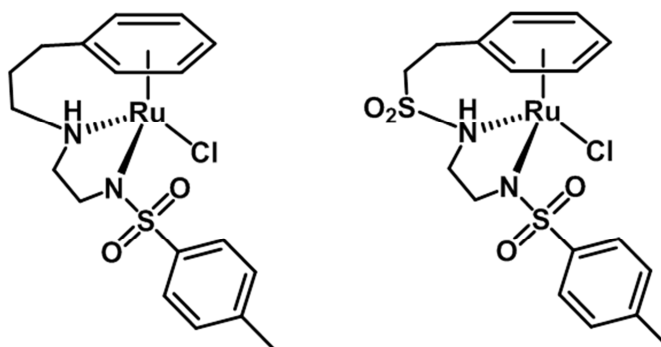


Figure 7.3. Tethered complexes.

7.2.3. Controlling the hydrolysis and selectivity of the complexes

The antitumor activity of many metal based drugs results from the activation through hydrolysis. The labile aqua adducts can bind or coordinate specific targets. However, the indiscriminate uptake of metallodrugs in cells leads to poor selectivity and severe toxicity. These drawbacks have motivated the synthesis of new metallodrugs which can be activated by light.²¹⁻²³

The complexes synthesised in Chapter 3 have been shown to hydrolyse readily. In order to control the hydrolysis, a series of compounds containing pyridine type monodentate ligands could be synthesised. Using such ligands the hydrolysis of the compounds could be blocked. However upon light irradiation of the complexes, induce the monodentate ligand substitution.²¹ However, to be able to photoactivate the complexes, it might be necessary to work with conjugated chelating ligands.^{21, 22, 24, 25}

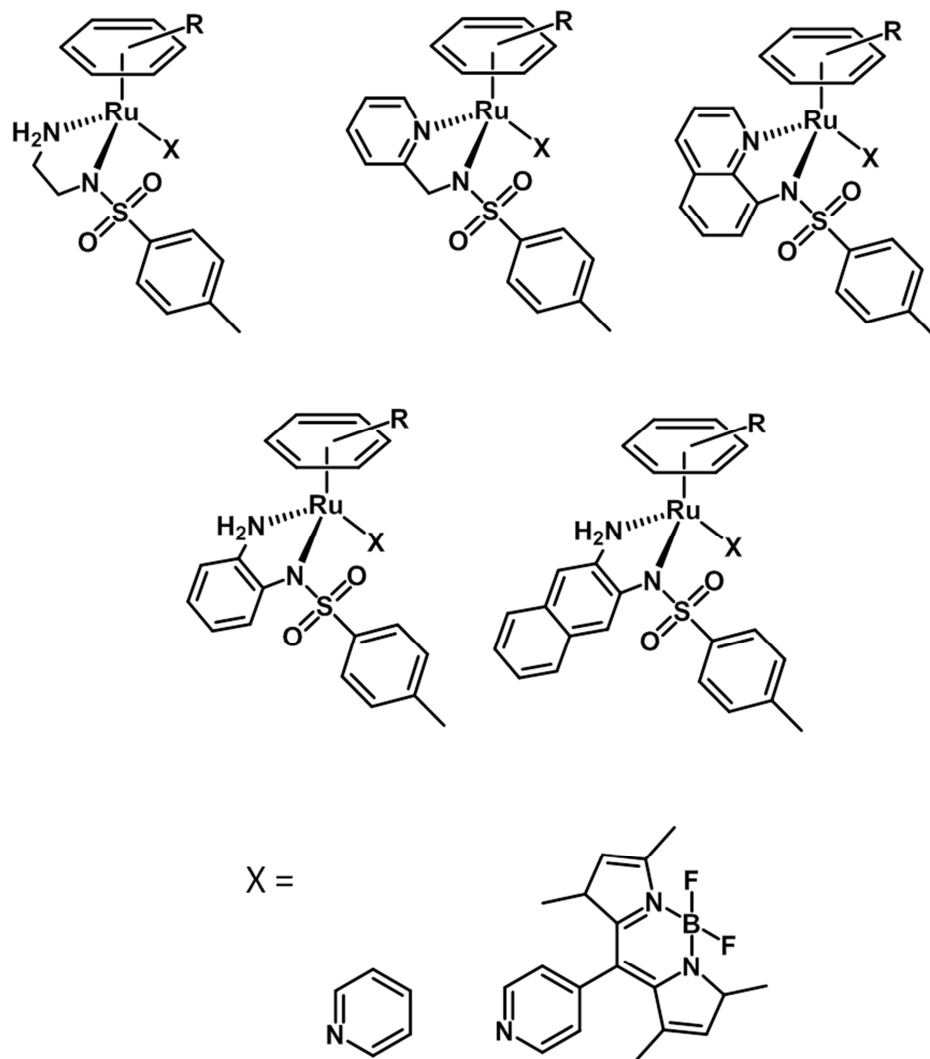


Figure 7.4. Series of compounds containing py or BODIPY as a monodentate ligand.

Some Ru(II) half sandwich complexes containing pyridine as a monodentate ligand, have been previously shown to be activated by light irradiation.²¹ However, In order to achieve deeper tissue penetration long wavelengths (λ 650-900 nm) of irradiation are more suitable than those necessary for the activation of pyridine containing complexes. For this reason a long wavelength absorbing chromophore (BODIPY) could be used as an optimum monodentate ligand.²²

7.2.4. Cell studies

Study the selectivity of the complexes towards cancerous cells. For that purpose, A set of experiments with MRC5 human fetal lung fibroblast cells could be performed using complex [(*p*-cym)Ru(TsEn)Cl] (**2**) in combination with formate. The antiproliferative activity of this type of complexes towards A2780c cisplatin resistant ovarian cancer cells could also be tested.

7.2.5. Reactions with GSH

In order to investigate whether the complexes discussed in this thesis react with GSH, to form an active Ru(II) dimer, a series of experiments in co-administration with L-BSO (Figure 7.5) could be carried out. L-Buthionine sulfoximine (L-BSO), is a small organic molecule that is able to inhibit the enzyme γ -glutamylcysteine synthetase. This enzyme is involved with the synthesis of GSH. As a consequence of treatment with L-BSO, a significant decrease on the intracellular levels of GSH can be observed. L-BSO can be administered in high doses, increasing ROS levels and inducing apoptosis.²⁶ However, low doses of L-BSO have been used to reduce levels of GSH in cells and increase sensitivity of some metal based drugs that are detoxified by GSH. Interestingly, a reduction of GSH of up to 40 % has been shown to be safe with no apoptosis induced.²⁶⁻²⁸

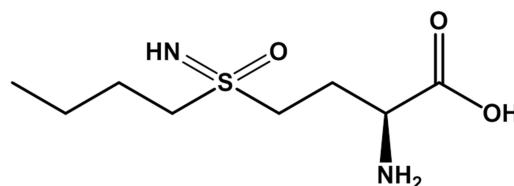


Figure 7.5. L-Buthionine sulfoximine.

7.2.6. Reactions between Rh(III) complexes and GSH

The possibility of Rh(III) catalysts being poison more readily than the Ru(II) analogues has been discussed previously in Chapter 6. However, no experimental evidence was provided. In order to confirm the hypothesis, reaction between GSH and the Rh(III) complexes could be carried out.

7.3. References

- (1) Gladiali, S.; Alberico, E. *Chem. Soc. Rev.* **2006**, *35*, 226-236.
- (2) Wu, X.; Li, X.; Hems, W.; King, F.; Xiao, J. *Org. Biomol. Chem.* **2004**, *2*, 1818-1821.
- (3) Shohei Hashiguchi, A. F., Karl-Josef Haack, Kazuhiko Matsumura, Takao Ikariya, Ryoji Noyori *Angew. Chem. Int. Ed* **1997**, *36*, 288-290.
- (4) Hanzlik, R. P.; Fowler, S. C.; Eells, J. T. *Drug Metab. Dispos.* **2005**, *33*, 282-286.
- (5) Aird, R. E.; Cummings, J.; Ritchie, A. A.; Muir, M.; Morris, R. E.; Chen, H.; Sadler, P. J.; Jodrell, D. I. *Brit. J. Cancer* **2002**, *86*, 1652 - 1657.
- (6) Wang, F.; Xu, J.; Wu, K.; Weidt, S. K.; Mackay, C. L.; Langridge-Smith, P. R. R.; Sadler, P. J. *Dalton Trans.* **2013**, *42*, 3188-3195.
- (7) Armstrong, J. S.; Steinauer, K. K.; Hornung, B.; Irish, J. M.; Lecane, P.; Birrell, G. W.; Peehl, D. M.; Knox, S. J. *Cell Death Differ.* **2002**, *9*, 252-263.
- (8) Lushchak, V. I. *J. Amino Acids* **2012**, *2012*, 1-26.
- (9) Chen, H. H. W.; Kuo, M. T. *Met. Based. Drugs* **2010**, 1-7.
- (10) Wang, F.; Xu, J.; Habtemariam, A.; Sadler, P. J. *J. Am. Chem. Soc.* **2005**, *127*, 17734-17743.
- (11) Chérioux, F.; Therrien, B.; Süß-Fink, G. *Inorg. Chim. Acta.* **2004**, *357*, 834-838.

- (12) Giannini, F.; Furrer, J.; Ibao, A.-F.; Süß-Fink, G.; Therrien, B.; Zava, O.; Baquie, M.; Dyson, P.; Štěpnička, P. *J. Biol. Inorg. Chem.* **2012**, *17*, 951-960.
- (13) Giannini, F.; Paul, L. E. H.; Furrer, J.; Therrien, B.; Süß-Fink, G. *New. J. Chem* **2013**, *32*, 3503-3511.
- (14) Ibao, A.-F.; Gras, M.; Therrien, B.; Süß-Fink, G.; Zava, O.; Dyson, P. J. *Eur. J. Inorg. Chem.* **2012**, *2012*, 1531-1535.
- (15) Bubert, C.; Blacker, J.; Brown, S. M.; Crosby, J.; Fitzjohn, S.; Muxworthy, J. P.; Thorpe, T.; Williams, J. M. J. *Tetrahedron Lett.* **2001**, *42*, 4037-4039.
- (16) Soni, R.; Jolley, K. E.; Clarkson, G. J.; Wills, M. *Org. Lett.* **2013**, *15*, 5110-5113.
- (17) Hannedouche, J.; Clarkson, G. J.; Wills, M. *J. Am. Chem. Soc.* **2004**, *126*, 986-987.
- (18) Hayes, A. M.; Morris, D. J.; Clarkson, G. J.; Wills, M. *J. Am. Chem. Soc.* **2005**, *127*, 7318-7319.
- (19) Morris, D. J.; Hayes, A. M.; Wills, M. *J. Org. Chem.* **2006**, *71*, 7035-7044.
- (20) Matharu, D. S.; Morris, D. J.; Clarkson, G. J.; Wills, M. *Chem. Commun.* **2006**, 3232-3234.
- (21) Betanzos-Lara, S.; Salassa, L.; Habtemariam, A.; Sadler, P. J. *Chem. Commun.* **2009**, 6622-6624.
- (22) Zhou, Q.-X.; Lei, W.-H.; Hou, Y.-J.; Chen, Y.-J.; Li, C.; Zhang, B.-W.; Wang, X.-S. *Dalton Trans.* **2013**, *42*, 2786-2791.
- (23) Pizarro, A.; Habtemariam, A.; Sadler, P. In *Medicinal Organometallic Chemistry*; ed.; Springer Berlin Heidelberg: **2010**; 21-56.
- (24) Macías, B.; García, I.; Villa, M. a. V.; Borrás, J. n.; Castiñeiras, A.; Sanz, F. *Polyhedron* **2002**, *21*, 1229-1234.
- (25) Darbre, T.; Dubs, C.; Rusanov, E.; Stoeckli-Evans, H. *Eur. J. Inorg. Chem.* **2002**, *2002*, 3284-3291.

(26) Abdalla, M. Y. *Jordan J. Biol. Sci.* **2011**, *4*, 119-124.

(27) Trachootham, D.; Zhang, W.; Huang, P. In *Drug Resistance in Cancer Cells*; ed.; Springer US: **2009**; 137-175.

(28) Marengo, B.; De Ciucis, C.; Verzola, D.; Pistoia, V.; Raffaghello, L.; Patriarca, S.; Balbis, E.; Traverso, N.; Cottalasso, D.; Pronzato, M. A.; Marinari, U. M.; Domenicotti, C. *Free Radical Biol. Med.* **2008**, *44*, 474-482.

Conferences and meetings attended

Soldevila, J.J.; Bruijninx, P.C. A.; Romero-Canelón, I.; Habtemariam, A.; Sadler, P. J.; Design of catalytic anticancer drugs: NADH regeneration by Ru(II) half-sandwich; *1st International Symposium on Functional Metal Complexes that Bind to Biomolecules*, **2013**, P-38 (Poster)

Soldevila, J.J.; Bruijninx, Pieter C. A.; Habtemariam, Abraha; Sadler, P. J.; NADH Regeneration by Ru(II) Half Sandwich Complexes containing Monotosylated Ethylenediamine Chelating Ligands; *A Joint Meeting of Dalton Division Interest Groups: Inorganic Chemistry*, **2012**, P-106 (Poster)

Soldevila, J.J.; Bruijninx, Pieter C. A.; Habtemariam, Abraha; Sadler, P. J.; NADH Regeneration by Ru(II) Half Sandwich Complexes containing Monotosylated Ethylenediamine Chelating Ligands; *XXV International Conference on Organometallic Chemistry*, **2012**, P-213 (Poster)

Soldevila, J.J.; Bruijninx, Pieter C. A.; Habtemariam, Abraha; Sadler, P. J.; NADH Regeneration by Ru(II) Half Sandwich Complexes containing Water Soluble Monotosylated Ethylenediamine Chelating Ligands; *11th International Symposium on Applied Bioinorganic Chemistry*, **2011**, P-156 (Poster)

Soldevila, J.J.; Bruijninx, Pieter C. A.; Habtemariam, Abraha; Sadler, P. J.; Regeneration of NADH by Ru(II) Half Sandwich Complexes; *5th EuCheMS conference on Nitrogen Ligands*, **2011**, P-141 (Poster)

Publications

“Fabrication of crystals from single metal atoms”. N.P.E. Barry, A.Pitto-Barry, A.M. Sanchez, A.P. Dove, R.J. Procter, J.J. Soldevila-Barreda, N. Kirby, I. Hands-Portman, C.J. Smith, R.K. O’Reilly, R. Beanland, and P.J. Sadler, *Nature Comms.* **2014**,

“Improved Catalytic Activity of Ruthenium–Arene Complexes in the Reduction of NAD⁺” J.J. Soldevila-Barreda; P.C.A. Bruijninx; A. Habtemariam; G.J. Clarkson; R.J. Deeth; P.J. Sadler, *Organometallics*, **2012**, *31*, 5958-5967.

Patent

“Novel Iridium/Rhodium anti-cancer compounds”. Liu, Z.; Soldevila, J.J.; Pizarro, A.M.; Habtemariam, Abraha; Sadler, P. J.;**2011**, PCT/GB2011/000776